Universitat Autònoma de Barcelona

PERFORMANCE, MONITORING AND MODELING OF HYDROGENOTROPHIC SULFATE REDUCTION: A STUDY IN A GAS-LIFT BIOREACTOR

David Camilo Cueto Ferreira

Universitat Autònoma de Barcelona

Escola d'Enginyeria

Deparament d'Enginyeria Química, Biològica i Ambiental

PERFORMANCE, MONITORING AND MODELING OF HYDROGENOTROPHIC SULFATE REDUCTION: A STUDY IN A GAS-LIFT BIOREACTOR

PhD thesis
PhD Program in Environmental Science and Technology

David Camilo Cueto Ferreira

Supervised by:

Dr. David Gabriel Buguña, Dr. Juan Antonio Baeza, Dra. Maria del Mar Baeza

Academic tutor:

Doctor David Gabriel Buguña

September 2022

GENOCOV
Departament d'Enginyeria Química,
Biològica i Ambiental
Escola d'Enginyeria
Universitat Autònoma de Barcelona
Barcelona, Spain

DAVID GABRIEL BUGUÑA, full professor from the Departament d'Enginyeria Química, Biològica i Ambiental of the Universitat Autònoma de Barcelona, JUAN ANTONIO BAEZA LABAT, full professor from the Departament d'Enginyeria Química, Biològica i Ambiental of the Universitat Autònoma de Barcelona, and MARIA DEL MAR BAEZA LABAT, associate professor from the Departament de Química of the Universitat Autònoma de Barcelona

CERTIFY:

That the engineer DAVID CAMILO CUETO FERREIRA has carried out under our supervision the research work entitled "Performance, monitoring and modeling of hydrogenotrophic sulfate reduction: a study in a gas-lift bioreactor", which is presented in this report, and it constitutes his thesis to obtain the Degree of Doctor in Environmental Science and Technology from the Universitat Autònoma de Barcelona.

To whom it may concern and may record it for the appropriate purposes, we present this thesis to the Escola de Doctorat of the Universitat Autònoma de Barcelona, signing this certificate at

Bellaterra (Cerdanyola del Vallès), September 2022

Dr. David Gabriel Buguña Dr. Juan Antonio Baeza Labat Dra. Maria del Mar Baeza Labat

The world ain't all shine and rainbows

…

And I don't care how tough you are

It will beat you to your knees and keep you there permanently if you let it

You, me, or nobody is gonna hit as hard as life

But it ain't about how hard you hit

It's about how hard you can get hit and keep moving forward

How much you can take and keep moving forward

That's how winning is done

Stallone, S (Director). (2006). Rocky Balboa [Film]. MGM

Dedicatoria

A la memoria de mi padre,

Tu partida fue un choque fuerte y difícil de afrontar
Me hizo repensar si realmente había valido la pena tanto tiempo lejos de casa
Fue precisamente tu legado, tu ejemplo, tus enseñanzas, lo que me ayudó a sobreponerme y seguir adelante

A mi madre,

Gracias por tu entrega abnegada e incansable. Tu amor incondicional. Tu nobleza. Tu gran corazón.
Gracias por dulcificar mi espíritu rebelde. Nos has llevado lejos.

«Optimista, positivo y triunfador. Dispuesto a alcanzar el éxito y la felicidad»

Edinson Cueto Quintero

Acknowledgment

Als meus supervisors David, Juan y Mireia

M'emporto un exemple extraordinari de vosaltres. La dedicació, ajuda constant i motivació que m'han brindat, espero posar en pràctica el dia que estigui a la vostra posició.

Estic profundament agraït per la paciència i tot el suport.

El David que va iniciar aquesta aventura és molt diferent del que l'acaba. Tinc molt per millorar, però molt del que he après, els dec en gran mesura a vosaltres.

Moltes gràcies per tot.

To my colleagues and friends

I have been lucky for all the people I could meet and learn from along this PhD journey.

I want to express my gratitude to:

All members of GENOCOV group, from whom I learned so much.

All members from the Department of Chemical, Biological and Engineering, ICTA and the Chemical Department at Autonomous University of Barcelona that helped me in many ways to achieve this goal.

A mi esposa

Sara, gracias por acompañarme en este camino. Gracias a la vida que permitió juntar nuestros caminos y seguir tantas aventuras. Gracias por las alegrías y las tristezas.

Que la vida nos regale lo que soñamos, y que nos de la fuerza de enfrentar lo que nos hará madurar.

Sin ti no hubiera sido posible.

Te amo.

A mi familia en Colombia

Todo mi agradecimiento a mis hermanos: Tomás, Alicia, Jorge y Jose. Cada uno ha aportado alegría a mi vida. A mi madre por todo el amor. Ustedes han sido mi gran motivación, más aún cuando decidí irme a Barcelona en busca de esta meta.

A minha família na Portugal

Obrigado à minha família em Portugal

João, David, Maria José, estou profundamente grato por todo o apoio que vocês nos deram. Obrigado pela ginjinha, o beirão e as tardes de policiais com a Maria José. Obrigado por me ensinar a amar os gatos.

Obrigado à Teresa e ao Manuel por todo o carinho e pelos belos momentos. Foram um grande apoio.

Obrigado à Cila, aos avós e a todos. Sou eternamente grato por todo o amor.

Obrigado aos gatos, Kalimero, Bolinhas, Barbie, Lulu, Poirrot, Princesa, Pepita. Á Boneca, por entrar nas nossas vidas, pouco a pouco, e ensinar-me a amar. E agora, sentir a sua falta, a gata mais furiosa e fofa.

Thesis abstract

Sulfur is an abundant element on earth that is essential for living beings. It is present in many different forms due to the wide range of oxidation states. Some of these sulfur forms represent an environmental concern as they are largely emitted to the environment due to different anthropogenic activities. This is the case of sulfur dioxide that is mainly emitted from fossil fuels combustion, and amongst its associated problems are the acid rain and the formation of particulate pollutants.

Therefore, different strategies have been developed to treat sulfur dioxide such as flue gas desulfurization processes that can achieve removal efficiencies over 95%. The large formation of gypsum and other operational challenge has enhanced the development of other technologies based on biological process. This is the case of the SONOVA/ENSURE process that aims at treating the flue gas emissions targeting sulfur recovery that could allow its valorization in other economic sectors. It consists of three global steps: gases absorption, biological conversions, and elemental sulfur recovery. This thesis focused on the biological step and, particularly, on the sulfate reduction to sulfide, using H_2 as electron donor and CO_2 as carbon source. Some challenges of this process are the low growth rate of hydrogenotrophic sulfate reducing microorganisms (H2-SRB), the H_2-competition of these microorganisms with homoacetogens, and the low H_2 solubility. In that sense, this study was developed in three main facets: 1) experimental evaluation of the biological sulfate reduction, 2) implementation of a sulfide online-monitoring system (S-OMS), and 3) mathematical modeling of the biological sulfate reduction.

For the experimental study of the biological sulfate reduction, preliminary experiments were performed to enhance the hydrogenotrophic sulfate reduction using an inoculum from a full-scale UASB reactor that treated sulfate-rich wastewater from a pulp and paper factory. The microbial community was enriched in H2-SRB through sequential operation of two stirred-tank reactors (STR) and a gas-lift reactor (GLR) fed with H_2 and CO_2. Preliminary gas-liquid mass transfer characterization was done in the GLR by determining the overall H_2-mass transfer coefficient. From the H2-SRB enrichment experiments, methane production was avoided but low sulfate reduction was obtained. Therefore, the GLR was set up in a sequential batch operation aiming at increasing the sulfate reduction rate (SRR).

The sequential batch operation was evaluated in 60 batch cycles at different sulfate loading rates (SLR). Methane production was not detected, and acetate was produced when the SLR was low; thus, an optimal and stable operation was achieved at a SLR of 902 mg $S\text{-}SO_4^{2-}$ L^{-1} d^{-1} with a 93±7 % (w/w) sulfate removal efficiency.

The implementation of a S-OMS was made by three main steps: 1) system manufacturing, 2) analytical characterization, and 3) demonstration of its utility by monitoring a sulfidogenic reactor. The analytical system showed that it can measure total dissolved sulfide (TDS) in a range of 1.5 to 30400 mg TDS L^{-1}, and the repeatability and reproducibility tests showed a suitable RSD in the range 1.8-5.3 %. The results of the GLR monitoring for nine cycles showed that the S-OMS measurements correlated satisfactorily with measures from commercial sulfide ion selective electrode.

The last step of this thesis consisted in the development, calibration, and validation of a mathematical model to describe the GLR operation. Maximum specific growth rate for H2-SRB ($\mu_{max.SRB}$), active fraction of H2-SRB (acf_{SRB}) and H_2S-inhibition constant for H2-SRB (k_i) were the parameters selected from a sensitivity analysis, and then, they were adjusted to obtain the best model description of the experimental sulfate data. The adjusted parameters with confidence interval were $\mu_{max.SRB}$ = 0.53±0.02 d^{-1}, acf_{SRB} = 0.200±0.003 and k_i = 100±7 mg $S\text{-}H_2S$ L^{-1}. A set of data of the GLR operation was used for model validation of sulfate, TDS, and acetate. A statistical analysis showed good results for sulfate and acetate with less accuracy for TDS that was explained from the large experimental deviations of TDS values.

As a part of the model validation, different simulations were performed to evaluate the model predictions under different operational scenarios. These simulations showed that sequential batch operation with shorter cycle duration or higher liquid volume exchange could improve the specific sulfate reduction rate (s-SRR) and thereby, less solid would be accumulated without affecting the SRR. It also predicted that the system could operate in continuous mode with SRR comparable to the sequential batch operation and higher s-SRR.

Overall, the selection and growth of H2-SRB and the maximization of the SRR through a sequential batch operation was demonstrated together with a good description of the experimental values through a mathematical model. Also, a good approach was achieved for the implementation of a S-OMS for the real-time monitoring of sulfide concentration.

Resumen de la tesis

El azufre es un elemento abundante en la tierra que es esencial para los seres vivos. Está presente en muchas formas debido a la amplia gama de estados de oxidación. Algunas de estas formas de azufre representan una preocupación ambiental ya que se emiten en grandes cantidades al medio ambiente debido a diferentes actividades antropogénicas. Este es el caso del dióxido de azufre que se emite principalmente por la combustión de combustibles fósiles y, entre sus problemas asociados, se encuentran la lluvia ácida y la formación de material particulado.

Por lo tanto, se han desarrollado diferentes estrategias para tratar el dióxido de azufre, como los procesos de desulfuración de gases de combustión que pueden lograr eficiencia de eliminación superior al 95%. La gran producción de yeso y otros retos operacionales han promovido el desarrollo de otras tecnologías basadas en procesos biológicos. Este es el caso del proceso SONOVA/ENSURE, que tiene como reto el tratamiento de las emisiones de gases de combustión con el objetivo de la recuperación de azufre lo que podría permitir su valorización en otros sectores económicos. Consta de tres etapas globales: absorción de gases, conversiones biológicas y recuperación de azufre elemental. Esta tesis se centró en la etapa biológica y, en particular, en la reducción de sulfato a sulfuro utilizando H_2 como donador de electrones y CO_2 como fuente de carbono. Algunos desafíos de este proceso son la baja velocidad de crecimiento de los microorganismos sulfato reductores hidrogenotróficos (H2-SRB), la competencia por H_2 de estos microorganismos con los homoacetógenos y la baja solubilidad del H_2. En este sentido, el presente trabajo se desarrolló en tres facetas principales: 1) evaluación experimental de la reducción biológica de sulfato, 2) implementación de un sistema de monitorización en línea de sulfuro (S-OMS), y 3) modelación matemática de la reducción hidrogenotrófica de sulfato.

Para el estudio experimental de la reducción biológica de sulfato, se realizaron experimentos preliminares utilizando un inóculo de un reactor UASB a gran escala que trataba aguas residuales ricas en sulfato de una fábrica de pulpa y papel. La población microbiana se enriqueció en H2-SRB mediante la operación secuencial de dos reactores de tanque agitado (STR) y un reactor gas-lift (GLR) alimentados con H_2 y CO_2. De forma preliminar, se realizó la caracterización de la transferencia de materia gas-líquido en el GLR mediante la determinación de los coeficientes globales de transferencia de materia de H_2. En los experimentos de enriquecimiento de H2-SRB se evitó la producción de metano, pero se obtuvo una baja

reducción de sulfato. Con el objetivo de aumentar la velocidad de reducción de sulfato (SRR), el GLR se configuró posteriormente en una operación secuencial por lotes.

La operación secuencial por lotes se evaluó en 60 ciclos a diferentes velocidades de carga de sulfato (SLR). No se detectó producción de metano y se produjo acetato cuando el SLR era bajo; de esta forma, se logró una operación óptima y estable a un SLR de 902 mg $S\text{-}SO_4^{2-}$ L^{-1} d^{-1} con una eficiencia de eliminación de sulfato de 93±7 % (p/p).

La implementación del S-OMS se realizó en tres pasos principales: 1) fabricación del sistema, 2) caracterización analítica y 3) demostración de su utilidad mediante el monitoreo de un reactor sulfidogénico. El sistema analítico demostró que puede medir sulfuro total disuelto (TDS) en un intervalo de 1.5 a 30400 mg TDS L^{-1}, y las pruebas de repetibilidad y reproducibilidad mostraron una adecuada desviación estándar relativa (RSD) en el intervalo 1.8-5.3 %. Los resultados del GLR monitorizando nueve ciclos mostraron que las mediciones del S-OMS se correlacionaron satisfactoriamente con las medidas de un electrodo selectivo de iones de sulfuro comercial.

El último paso de esta tesis consistió en el desarrollo, calibración y validación de un modelo matemático para describir la operación del GLR. La velocidad específica máxima de crecimiento para H2-SRB ($\mu_{max.SRB}$), la fracción activa de H2-SRB (acf_{SRB}) y la constante de inhibición de H_2S (k_i) fueron los parámetros seleccionados mediante un análisis de sensibilidad, y luego se ajustaron para obtener la mejor descripción por el modelo de los datos experimentales de sulfato. Los parámetros ajustados con intervalo de confianza fueron $\mu_{max.SRB}$ = 0,53±0,02 d^{-1}, acf_{SRB} = 0,200±0,003 y k_i = 100±7 mg $S\text{-}H_2S$ L^{-1}. Se utilizó un conjunto de datos de la operación GLR para la validación del modelo de sulfato, TDS y acetato. Un análisis estadístico mostró buenos resultados para sulfato y acetato con menor precisión para TDS, lo que se explica por las grandes desviaciones experimentales de los valores de TDS.

Como parte de la validación del modelo, se realizaron diferentes simulaciones para evaluar las predicciones del modelo bajo diferentes escenarios operativos. Estas simulaciones mostraron que la operación secuencial por lotes con una duración de ciclo más corta o un mayor intercambio de volumen de líquido podría mejorar la velocidad específica de reducción de sulfato (s-SRR) y, por tanto, menos sólido se acumularía sin afectar la SRR. También predijo que el sistema podría operar en modo continuo con SRR comparable a la operación secuencial

por lotes y mayor s-SRR.

En general, se demostró la selección y el crecimiento de H2-SRB y la maximización de la SRR a través de una operación secuencial por lotes junto con una buena descripción de los valores experimentales a través de un modelo matemático. Asimismo, se logró una buena aproximación para la implementación de un S-OMS para el monitoreo en tiempo real de la concentración de sulfuro.

Resum de la tesi

El sofre és un element abundant a la terra que és essencial per als éssers vius. És present en moltes formes a causa de l'àmplia gamma d'estats d'oxidació. Algunes d'aquestes formes de sofre representen una preocupació ambiental ja que s'emeten en grans quantitats al medi ambient a causa de diferents activitats antropogèniques. Aquest és el cas del diòxid de sofre que s'emet principalment per la combustió de combustibles fòssils i, entre els problemes associats, hi ha la pluja àcida i la formació de material particulat.

Per tant, s'han desenvolupat diferents estratègies per tractar el diòxid de sofre, com els processos de dessulfuració de gasos de combustió que poden assolir eficiències d'eliminació superiors al 95%. La gran producció de guix i d'altres reptes operacionals ha promogut el desenvolupament d'altres tecnologies basades en processos biològics. Aquest és el cas del procés SONOVA/ENSURE, que té com a repte el tractament de les emissions de gasos de combustió amb l'objectiu de la recuperació de sofre que podria permetre'n la valorització en altres sectors econòmics. Consta de tres etapes globals: absorció de gasos, conversions biològiques i recuperació de sofre elemental. Aquesta tesi es va centrar en l'etapa biològica i, en particular, en la reducció de sulfat a sulfur utilitzant H_2 com a donador d'electrons i CO_2 com a font de carboni. Alguns reptes d'aquest procés són la baixa velocitat de creixement dels microorganismes sulfat reductors hidrogenotròfics (H2-SRB), la competència per H_2 d'aquests microorganismes amb els homoacetògens i la baixa solubilitat de l'H_2. En aquest sentit, aquest estudi es va desenvolupar en tres facetes principals: 1) avaluació experimental de la reducció biològica de sulfat, 2) implementació d'un sistema de monitorització en línia de sulfur (S-OMS), i 3) modelització matemàtica de la reducció hidrogenotròfica de sulfat.

Per a l'estudi experimental de la reducció biològica de sulfat, es van fer experiments preliminars utilitzant un inòcul d'un reactor UASB a gran escala que tractava aigües residuals riques en sulfat d'una fàbrica de polpa i paper. La població microbiana es va enriquir en H2-SRB mitjançant l'operació seqüencial de dos reactors de tanc agitat (STR) i un reactor gas-lift (GLR) alimentats amb H_2 i CO_2. De manera preliminar, es va realitzar la caracterització de la transferència de matèria gas-líquid al GLR mitjançant la determinació dels coeficients globals de transferència de matèria de H_2. Als experiments d'enriquiment de H2-SRB es va evitar la producció de metà, però es va obtenir una baixa reducció de sulfat. Per tal d'augmentar la

velocitat de reducció de sulfat (SRR), el GLR es va configurar posteriorment en una operació seqüencial per lots.

L'operació seqüencial per lots es va avaluar en 60 cicles a diferents velocitats de càrrega de sulfat (SLR). No es va detectar producció de metà i es va produir acetat quan el SLR era baix; d'aquesta manera, es va aconseguir una operació òptima i estable a un SLR de 902 mg $S\text{-}SO_4^{2-}$ L^{-1} d^{-1} amb una eficiència d'eliminació de sulfat de 93±7% (p/p).

La implementació de l'S-OMS es va fer en tres passos principals: 1) fabricació del sistema, 2) caracterització analítica i 3) demostració de la seva utilitat mitjançant el monitoratge d'un reactor sulfidogènic. El sistema analític va demostrar que pot mesurar sulfur total dissolt (TDS) en un interval de 1.5 a 30.400 mg TDS L^{-1}, i les proves de repetibilitat i reproductibilitat van mostrar una adequada desviació estàndard relativa (RSD) en el interval 1.8-5.3%. Els resultats del GLR monitoritzant nou cicles van mostrar que els mesuraments de l'S-OMS es van correlacionar satisfactòriament amb les mesures d'un elèctrode selectiu d'ions de sulfur comercial.

L'últim pas d'aquesta tesi va consistir en el desenvolupament, el calibratge i la validació d'un model matemàtic per descriure l'operació del GLR. La velocitat específica màxima de creixement per a H2-SRB ($\mu_{max.SRB}$), la fracció activa de H2-SRB (acf_{SRB}) i la constant d'inhibició de H2S (k_i) van ser els paràmetres seleccionats d'una anàlisi de sensibilitat, i després es van ajustar per obtenir la millor descripció pel model de les dades experimentals de sulfat. Els paràmetres ajustats amb interval de confiança van ser $\mu_{max.SRB}$ = 0,53±0,02 d^{-1}, acf_{SRB} = 0,200±0,003 i k_i = 100±7 mg $S\text{-}H_2S$ L^{-1}. Es va fer servir un conjunt de dades de l'operació GLR per a la validació del model de sulfat, TDS i acetat. Una anàlisi estadística va mostrar bons resultats per a sulfat i acetat amb menys precisió per a TDS, el que s'explica per les grans desviacions experimentals dels valors de TDS.

Com a part de la validació del model, es van fer diferents simulacions per avaluar les prediccions del model sota diferents escenaris operatius. Aquestes simulacions van mostrar que l'operació seqüencial per lots amb una durada de cicle més curta o un intercanvi més gran de volum de líquid podria millorar la velocitat específica de reducció de sulfat (s-SRR) i, per tant, menys sòlid s'acumularia sense afectar la SRR. També va predir que el sistema podria operar de manera continuada amb SRR comparable a l'operació seqüencial per lots i més s-SRR.

En general, es va demostrar la selecció i el creixement de H2-SRB i la maximització de la SRR mitjançant una operació seqüencial per lots juntament amb una bona descripció dels valors experimentals mitjançant un model matemàtic. Així mateix, es va aconseguir una bona aproximació per a la implementació d'un S-OMS per al monitoratge en temps real de la concentració de sulfurs.

List of abbreviations

μ_{max}	Maximum specific growth rate
$\mu_{max.hAC}$	Maximum specific growth rate for homo-AC
$\mu_{max.SRB}$	Maximum specific growth rate for H2-SRB
[AC]	Acetate concentration in the GLR
$[C]_{g,bag}$	H_2 concentration in the bag connected to the reactor headspace to replace the liquid volume removed during the reactor partial draining
$[C]'_{g,to}$	Concentrations of model components in the gas phase at the beginning of a batch
$[C]_{to}$	Concentrations of model components in the liquid phase at the beginning of a batch, determined from equation 7.9 (for soluble components) and equation 7.10 (for particulate components)
$[C_i]$	Concentration of model components in the liquid phase
$[C_i]_g$	Concentration of model components in the gas phase
$[H_2]_g$	H_2 concentration in the gas phase of the GLR
$[H_2]_l$	H_2 concentration in the liquid phase of the GLR
$[H_2]_{sat}$	H_2 saturation concentration in the liquid phase
[H2-SRB]	H2-SRB concentration in the GLR
[homo-AC]	Homo-AC concentration in the GLR
$[S\text{-}H_2S]_g$	Hydrogen sulfide concentration in the gas phase
$[S\text{-}SO_4^{2-}]$	Sulfate concentration in the GLR
$[S\text{-}SO_4^{2-}]_{added}$	Expected sulfate initial concentration for a batch in the GLR
$[S\text{-}SO_4^{2-}]_{end}$	Sulfate concentration at the end of a batch in the GLR
$[S\text{-}SO_4^{2-}]_{to}$	Real sulfate initial concentration for a batch in the GLR
[TDS]	Concentration of TDS in the GLR
$\Delta[S\text{-}SO_4^{2-}]$	Difference of sulfate concentrations at the beginning and end of a batch in the GLR
Δ[TDS]	Difference of TDS concentrations at the end and beginning of a batch in the GLR
acf_{SRB}	Active fraction of H2-SRB

ac-SLR	Accumulated volumetric sulfate loading rate
ADM1	Anaerobic digestion model No. 1
AnMBR	Anaerobic membrane reactor
BES	2-Bromoethanesulfonate
b_{hAC}	Maximum specific decay rate for homo-AC
b_{SRB}	Maximum specific decay rate for H2-SRB
$C_i(\theta)$	Model sulfate concentration evaluated at the optimal parameters
COD	Chemical oxygen demand
COD-Acetate	COD equivalent to acetate
$COD_{s,dis}$	Dissolved COD in the discharge supernatant
COD-Solids	COD equivalent to solids
$COD_{t,dis}$	Total COD in the discharge supernatant
COD-TDS	COD equivalent to TDS
COD-Unidentified	Soluble COD equivalent to unidentified components
CPE	Co-polyester
CSTR	Continuous stirred-tank reactor
D_{H2}	Diffusivity coefficient for H_2
$d_{H2\|SRB}$	Volumetric decay rate for H2-SRB
D_{H2S}	Diffusivity coefficient for H_2S
d_{hAC}	Volumetric decay rate for homo-AC
E_c	Electromotive force
ENSURE	Enhanced treatment of flue-gases in multistage bioscrubbers towards sulfur recovery
$E_{reference}$	Potentiometric response of the reference electrode
EV	Liquid exchange volume
$E_{working}$	Potentiometric response of the working electrode
F	Faraday constant
F_g	Gas-inlet flowrate

F_l	Liquid flowrate for a continuous operation
FGD	Flue-gas desulfurization
FIA	Flow injection analysis
FIM	Fisher information matrix
F_{obj}	Objective function for the minimization algorithm of the model calibration
f_{sed}	Particulate fraction loss in the sedimentation step
G_i	Generation/consumption term for the mathematical model
GLR	Gas-lift reactor
H2-SRB	Hydrogenotrophic sulfate reducing microorganisms
H_2S-stripping	Percentage of sulfide stripping
H_{H2}	Henry coefficient for H_2
H_{H2S}	Henry coefficient for H_2S
homo-AC	Homoacetogenic microorganisms
HRT	Hydraulic residence time
IoA	Index of agreement
$J(\theta)$	Residual error function
$k_{H2.hAC}$	H_2 half-saturation constant for homo-AC
$k_{H2.SRB}$	H_2 half-saturation constant for H2-SRB
k_i	H_2S-inhibition constant for H2-SRB
K_La	Overall mass transfer coefficient
K_La_{H2}	Overall H_2-mass transfer coefficient
K_La_{H2S}	Overall H_2S-mass transfer coefficient
k_{ST}	Sulfate half-saturation constant for H2-SRB
LOC	Lab on a chip
LOD	Limit of detection
LR	Linear range
ME	Model efficiency
MM	Mineral medium

N	Number of experimental data used in the model calibration
ORP	Oxidation-reduction potential
p	Number of parameters estimated in the model calibration
P_{H2}	Hydrogen partial pressure
pKa1	First acid dissociation constant for H_2S
pKa2	Second acid dissociation constant for H_2S
Qi	Inverse of the covariance matrix
R	Universal gas constant
r_{hAC}	Volumetric growth rate for homo-AC
$r_{H2\|SRB}$	Volumetric growth rate for H2-SRB
RSD	Relative standard deviation
$r_{t.H2}$	Volumetric H_2 gas-liquid mass transfer
$r_{t.H2S}$	Volumetric H_2S gas-liquid mass transfer
S^0	Elemental sulfur
S^{2-}-ISE	Commercial sulfide ion selective electrode
S_{added}	Concentration of soluble components in the MM
SAOB	Sulfide antioxidant buffer
SD	Standard deviation
SEM	Scanning electron microscopy
SEM-EDX	Energy dispersive X-ray
S_{end}	Concentrations of soluble components at the end of a batch in the GLR
S'_{end}	Concentrations of soluble components in the GLR at the end of the sedimentation period
SIA	Sequential injection analysis
SLR	Volumetric sulfate loading rate
SOB	Sulfide oxidizing microorganisms
Sol_{dis}	Solid concentrations in the discharge supernatant
Sol_{end}	Solid concentrations at the end of a batch
S-OMS	Sulfide online-monitoring system

SONOVA	Development of an integral process for the treatment of SO_x and NO_x contaminants generated in flue-gases aiming at its valorization
SRB	Sulfate reducing microorganisms
SRR	Volumetric sulfate reduction rate
SRR_{max_th}	Maximum and theoretical SRR in the GLR
S_{to}	Initial concentrations of soluble components (TDS and sulfate) for a batch in the GLR
STR	Stirred-tank reactor
Sulfate-RE	Sulfate removal efficiency
T	Temperature
t_c	Batch duration in the GLR
TDS	Total dissolved sulfide
TSS	Total suspended solids
UASB	Upflow anaerobic sludge blanket reactor
V	GLR liquid volume during batch
V	Parameters-covariance matrix
V'	GLR liquid volume during sedimentation period
VFA	Volatile fatty acids
V_g	Gas volume of the GLR setting
V_s	Volume of sulfide standard added for the standardization of S^{2-}-ISE
V_{sed}	Volume of GLR culture medium removed for sedimentation
V'_{sed}	Volume of settled sludge after sedimentation
VSS	Volatile suspended solids
VSS_{dis}	VSS concentration in the discharge supernatant
VSS_{end}	VSS concentration in the end of a batch in the GLR
V_t	Volume of Pb^{2+} standard titrated during the standardization of the S^{2-}-ISE
VSS loss	Percentage of VSS lost respecting the total VSS mass in the V_{sed} for the sedimentation step
$Y_{AC\|H2}$	Mass yield coefficient of acetate and H_2

$Y_{hAC\|H2}$	Mass yield coefficient of homo-AC and H_2
$Y_{SRB\|H2}$	Mass yield coefficient of H2-SRB and H_2
$Y_{ST\|H2}$	Mass yield coefficient of sulfate and H_2

TABLE OF CONTENTS

Thesis abstract…… VII

Resumen de la tesis…… IX

Resum de la tesi……...XII

List of abbreviations…… XV

CHAPTER 1. MOTIVATIONS, OBJECTIVES, AND THESIS OVERVIEW…… 1

1.1. MOTIVATIONS……..3

1.2. OBJECTIVES……..4

1.2.1. General objectives……..4

1.2.2. Specific objectives……4

1.3. THESIS OVERVIEW……..6

CHAPTER 2. INTRODUCTION…… 9

2.1. CHAPTER OUTLINE……11

2.2. RESEARCH INTEREST…… 11

2.2.1. Sulfur cycle on earth: geochemical and anthropogenic contributions……...11

2.2.2. The SO_2 environmental concern……14

2.3. TECHNOLOGIES AVAILABLE TO COPE WITH SO_2 ENVIRONMENTAL PROBLEMS…… 15

2.3.1. Conventional flue gases treatment……15

2.3.2. Biological treatment of SO_2……...16

2.4. INTEGRATED TREATMENT OF SO_2 AND NOX FOR SULFUR RECOVERY……22

2.4.1. SONOVA/ENSURE process……22

2.4.2. Literature reports related to the SONOVA process……...24

CHAPTER 3. MATERIALS AND METHODS……..29

3.1. GLR CONFIGURATION……31

3.2. COMPOSITION OF SOLUTIONS…… 32

3.3. ANALYTICAL METHODS……...33

CHAPTER 4. PRELIMINARY EXPERIMENTS FOR THE SULFATE REDUCTION STUDY…… 39

4.1. CHAPTER OUTLINE…… 41

4.2. INTRODUCTION……...42

4.3. BIOMASS GROWTH AND SELECTION…… 43

4.3.1. Setup of reactors A and B…… 43

4.3.2. Results of sulfate consumption and biomass growth for the operations of reactors A and B……46

4.4. PRELIMINARY EXPERIMENTS IN THE GLR: ABIOTIC TESTS AND INOCULATION FOR KINETIC STUDY……48

4.4.1. GLR setup……... 48

4.4.2. Assessment of the liquid-gas mass transfer in the GLR……... 50

4.4.3. GLR inoculation and start-up for biomass growth and sulfate reduction enhancement……..55

4.4.4. Characterization of H2-SRB kinetic and microbial diversity identification…….57

4.4. MAIN CONCLUSIONS……. 65

CHAPTER 5. STUDY OF THE SULFATE REDUCTION IN A SEQUENTIAL BATCH OPERATION……67

5.1. CHAPTER OUTLINE…… 69

5.2. EXPERIMENTAL LAYOUT…….70

5.2.1. Process setup and analytical tools……. 70

5.2.2. Operating conditions of the sequential batch operation under different SLR…...73

5.3. PERFORMANCE OF THE SEQUENTIAL BATCH OPERATION OF THE GLR UNDER DIFFERENT SLR…… 76

5.3.1. Sulfate reducing activity throughout the sequential batch operation…… 76

5.3.2. Acetate and COD distribution in the effluent……... 80

5.3.3. Microbial diversity along the sequential batch operation……. 82

5.4. DISCUSSION……. 83

5.4.1. Analysis of the reactor performance throughout the sequential batch operation..83

5.4.2. Analysis of the stable conditions for the sulfate reduction: stage VIII……. 89

5.5. MAIN CONCLUSIONS……. 94

CHAPTER 6. DEVELOPMENT OF A SULFIDE ONLINE-MONITORING SYSTEM FOR SULFIDOGENIC REACTORS…….. 97

6.1. CHAPTER OUTLINE…… 99

6.2. INTRODUCTION……...99

6.3. EXPERIMENTAL LAYOUT……101

6.3.1. Experimental setup of the sulfide online-monitoring system……... 101

6.3.2. Design of the 3D-microdevice for sulfide measurement…….. 104

6.3.3. Preparation of the analytical measurement system and response evaluation……105

6.3.4. Validation of the sulfide online-monitoring system……..106

6.4. MANUFACTURE AND CHARACTERIZATION OF THE SULFIDE ONLINE-MONITORING SYSTEM…….. 107

6.4.1. Microdevice manufacture……..107

6.4.2. Preparation and morphological characterization of the Ag/Ag_2S-working electrode…… 109

6.4.3. Evaluation of the working range of the sulfide online-monitoring system……...109

6.4.4. Repeatability study of the sulfide online-monitoring system……. 112

6.4.5. Reproducibility study of the sulfide online-monitoring system……..113

6.5. VALIDATION OF THE SULFIDE ONLINE-MONITORING SYSTEM WITH THE GLR OPERATION…… 114

6.6. DISCUSSION OF THE ANALYTICAL RESULTS OF THE NOVEL SULFIDE ONLINE-MONITORING SYSTEM…….. 115

6.7. MAIN CONCLUSIONS……. 117

CHAPTER 7. MATHEMATICAL MODELING OF THE BIOLOGICAL SULFATE REDUCTION……... 119

7.1. CHAPTER OUTLINE…… 121

7.2. INTRODUCTION……...121

7.2.1. Mathematical modeling: an optimization tool for experimental design and process scale-up…… 121

7.3. MATHEMATICAL MODEL DESCRIPTION…….. 123

7.3.1. Definition of the mathematical model for a single batch in the GLR……... 124

7.3.2. Sensitivity analysis to identify the most sensitive parameters of the mathematical model…….. 131

7.3.3. Mathematical model calibration and validation…… 132

7.3.4. Model simulation under different influent and operational conditions……. 136

7.4. RESULTS OF THE SENSITIVITY ANALYSIS: IDENTIFICATION OF THE MOST INFLUENTIAL PARAMETERS OVER MODEL OUTPUTS……. 137

7.5. RESULTS OF MODEL CALIBRATION AND VALIDATION…….. 139

7.5.1. Model calibration: optimal parameters and minimization algorithm…… 139

7.5.2. Mathematical model validation and calibration: data comparison and statistical analysis…….. 141

7.6. ANALYSIS OF THE OPTIMAL PARAMETERS $\mu_{max.SRB}$ AND k_i: COMPARISON WITH LITERATURE REPORTS……... 148

7.7. MODEL EVALUATION FOR DIFFERENT OPERATIONAL CONDITIONS….. 150

7.8. MAIN CONCLUSIONS……. 154

CHAPTER 8. OVERALL CONCLUSIONS……...157

8.1. OVERALL CONCLUSIONS……. 159

8.2. FUTURE WORK…… 160

REFERENCES……163

APPENDIX…….. 183

Appendix A. Technical sheet of the GLR dimensions……...185

Appendix B. Calibration of the commercial S^{2-}-ISE and sulfide distribution……... 188

Appendix C. Kinetic, stoichiometric, and physicochemical parameters……191

Appendix D. 3-D printing setting for the microdevice manufacture……. 193

Appendix E. Calibration of the S-OMS for the different analytical and monitoring experiments…….. 194

CHAPTER 1
MOTIVATIONS, OBJECTIVES, AND THESIS OVERVIEW

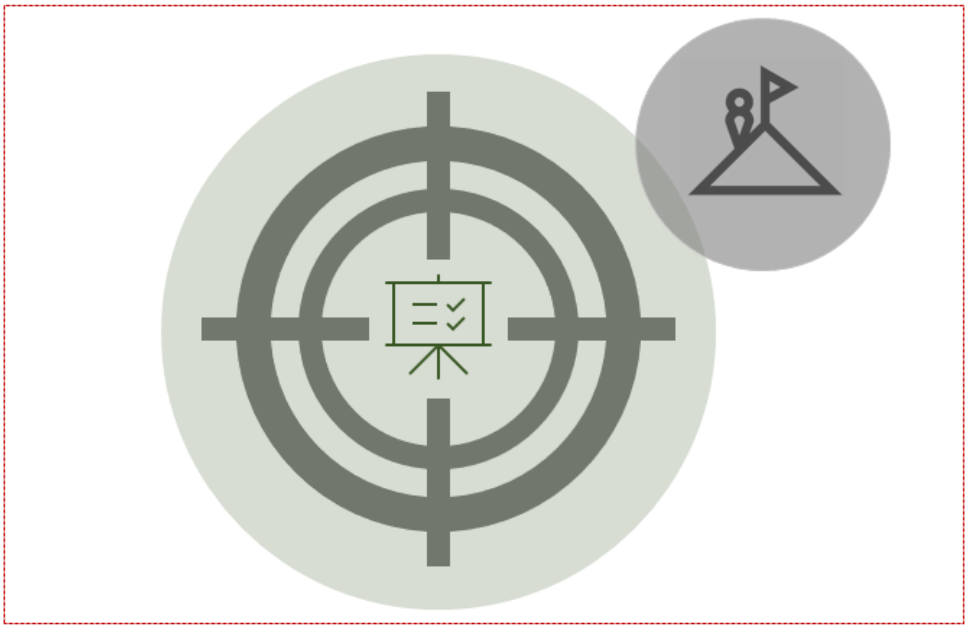

1.1. MOTIVATIONS

This work has been developed in the Research Group on Biological Treatment and Valorization of Liquid and Gas Effluents (GENOCOV*) of the Department of Chemical, Biological and Environmental Engineering at the Autonomous University of Barcelona. The research was developed under a global process that aimed at treating flue-gases towards the recovery of elemental sulfur as a potential value-added product. This global process has been developed in two different projects funded by the Spanish government: 1) Development of an integral process for the treatment of SO_x and NO_x contaminants generated in flue-gases aiming at its valorization (SONOVA, for its acronym in Spanish) with reference CTQ2015-69802-C2-1-R, and 2) Enhanced treatment of flue-gases in multistage bioscrubbers towards sulfur recovery (ENSURE) with reference RTI2018-099362-B-C21.

The SONOVA and the ENSURE projects have been established in three main steps: 1) gases absorption, 2) biological treatment, which consists of biological sulfate reduction to sulfide and the partial oxidation of sulfide to elemental sulfur, and 3) sulfur recovery. Overall, it is intended to treat the SO_x and NO_x contaminants with the recovery of a potential value-added product (elemental sulfur) that can be used in different industrial sectors. These projects were also focused on the biofilm characterization, sulfate and sulfide monitoring, and the biological activity and microbial diversity study.

The sulfate reduction step was studied in two other PhD thesis in the GENOCOV group with remarkable results, in which sulfate reduction was studied heterotrophically using an upflow anaerobic sludge blanket (UASB) reactor fed with crude glycerol as carbon source and electron donor. In the thesis presented herein, the sulfate reduction was studied autotrophically using H_2 (as electron donor) and CO_2 (as carbon source) in a gas-lift reactor (GLR) and a sulfide online-monitoring system (S-OMS) was developed to measure sulfide production in sulfidogenic reactors. In that order, this work was divided into three main topics: 1) the experimental study of the sulfate reduction in a H_2/CO_2-fed GLR, 2) the development and implementation of a S-OMS to monitor sulfide concentration in the GLR, and 3) the definition, calibration, and validation of a mathematical model for the characterization of the biological sulfate reduction in the GLR.

*www.genocov.com

1.2. OBJECTIVES

1.2.1. General objective

To evaluate experimentally and by simulation the hydrogenotrophic sulfate reduction in a lab-scale gas-lift reactor for the treatment of sulfate-rich wastewaters produced in the flue-gases scrubbing processes.

Description: The experimental evaluation aims at enhancing the hydrogenotrophic sulfate reducing activity in a gas-lift reactor (GLR) and the development and validation of a S-OMS. The development of a mathematical model is indented to describe the sulfate reducing process in the GLR by defining the processes required and estimating the most sensitive parameters.

1.2.2. Specific objectives

1. **To enrich the hydrogenotrophic sulfate reducing biomass in two lab-scale stirred tank reactors and a gas-lift reactor.**

   Description: As the inoculum was taken from a full-scale UASB reactor rich in heterotrophic and methanogenic microorganisms, the first goal was to cultivate the inoculum and the augmentation of the hydrogenotrophic sulfate reducing activity.

   The experiments developed to accomplish this objective are detailed in Chapter 4.

2. **To enhance the hydrogenotrophic sulfate reducing activity in the gas-lift reactor operated in a sequential batch mode.**

   Description: Based on the preliminary experiments to grow and select the hydrogenotrophic sulfate reducing biomass, the reactor was setup as a sequential batch reactor to improve the biomass retention and therefore maximize the volumetric sulfate reduction rate.

   The experiments performed to accomplish this objective are described in Chapter 5.

3. **To develop a sulfide online-monitoring system to measure total dissolved sulfide in sulfidogenic reactors.**

   Description: A S-OMS was proposed to allow the characterization of sulfide production in sulfidogenic reactors. This goal was targeted in the following steps: 1) manufacturing of a microfluidic device for potentiometric measurement of TDS; 2) an evaluation of the analytical efficacy of the S-OMS through working range determination, repeatability, and reproducibility tests; and 3) validation of the S-OMS with real-time operation of the sulfidogenic GLR.

   The experiments performed to accomplish this objective are described in Chapter 6.

4. **To propose a mathematical model for the description of the biological sulfate reduction process in the GLR.**

   Description: The development of a mathematical model is proposed to describe the biological sulfate reduction in the GLR operated as a sequential batch reactor. The following steps are proposed to accomplish this goal: 1) to perform a sensitivity analysis to identify the most sensitive parameter; 2) the calibration of the most influential parameters to fit the mathematical model to the experimental data; 3) to determine the confidence interval of the parameters subjected to optimization; 4) the validation of the mathematical model with experimental data; and 5) the use of the model to predict the system behavior for different influent sulfate concentration and operational conditions.

   The results of the mathematical model are described in Chapter 7.

1.3. THESIS OVERVIEW

As this research focuses on the study of sulfate reduction, the manufacture of a S-OMS, and the development of a mathematical model to describe the sulfate reduction activity in the reactor, this work was accomplished following the procedure detailed in Figure 1.1. The experimental study of the sulfate reduction was divided into two main steps that are explained in Chapter 4 and 5. The first part is discussed in Chapter 4 and consisted in preliminary experiments for the biomass growth and selection of sulfate reducing microorganism that were performed in two lab-scale stirred tank reactors (STR) and in a GLR; in the latter, abiotic tests were evaluated to characterize the H_2 gas-liquid mass transfer before the inoculation. The second part is discussed in Chapter 5 and consisted in evaluating and enhancing the volumetric sulfate reduction rate (SRR) in a sequential batch operation of the GLR with sludge recovery, where stages with different sulfate loading rates (SLR) were explored to analyze the sulfate conversion to sulfide and acetate production.

In parallel to the sulfate reduction study, the S-OMS was developed in three main steps that are explained in Chapter 6: 1) the manufacture of a microdevice for potentiometric measurement of TDS, 2) the evaluation of the analytical accuracy through determination of working range for TDS measurement, and characterization of the analytical method from repeatability and reproducibility experiments, and 3) the validation of the S-OMS by measuring the sulfide production in the GLR operation explained in Chapter 5.

After the GLR operation as a sequential batch reactor, a mathematical model was developed to describe the sulfate reduction process. This model is presented in Chapter 7 and consisted in the definition of a mathematical model considering two biological process (sulfate reduction and acetate production) and two physical process (H_2 and H_2S gas-liquid mass transfer), then a local sensitivity analysis was performed to identify the most sensitive parameters that were further used to calibrate the model with experimental data. The precision of the parameter was determined by its confidence interval estimation through the Fisher Information Matrix (FIM). Then, part of the experimental data was used to validate the model and the accuracy of the model prediction was measured by different statistical tests. The last step of the mathematical model consisted in evaluating different operational scenarios to explore the predicted system behavior. Finally, the general conclusions of this research are detailed in Chapter 8.

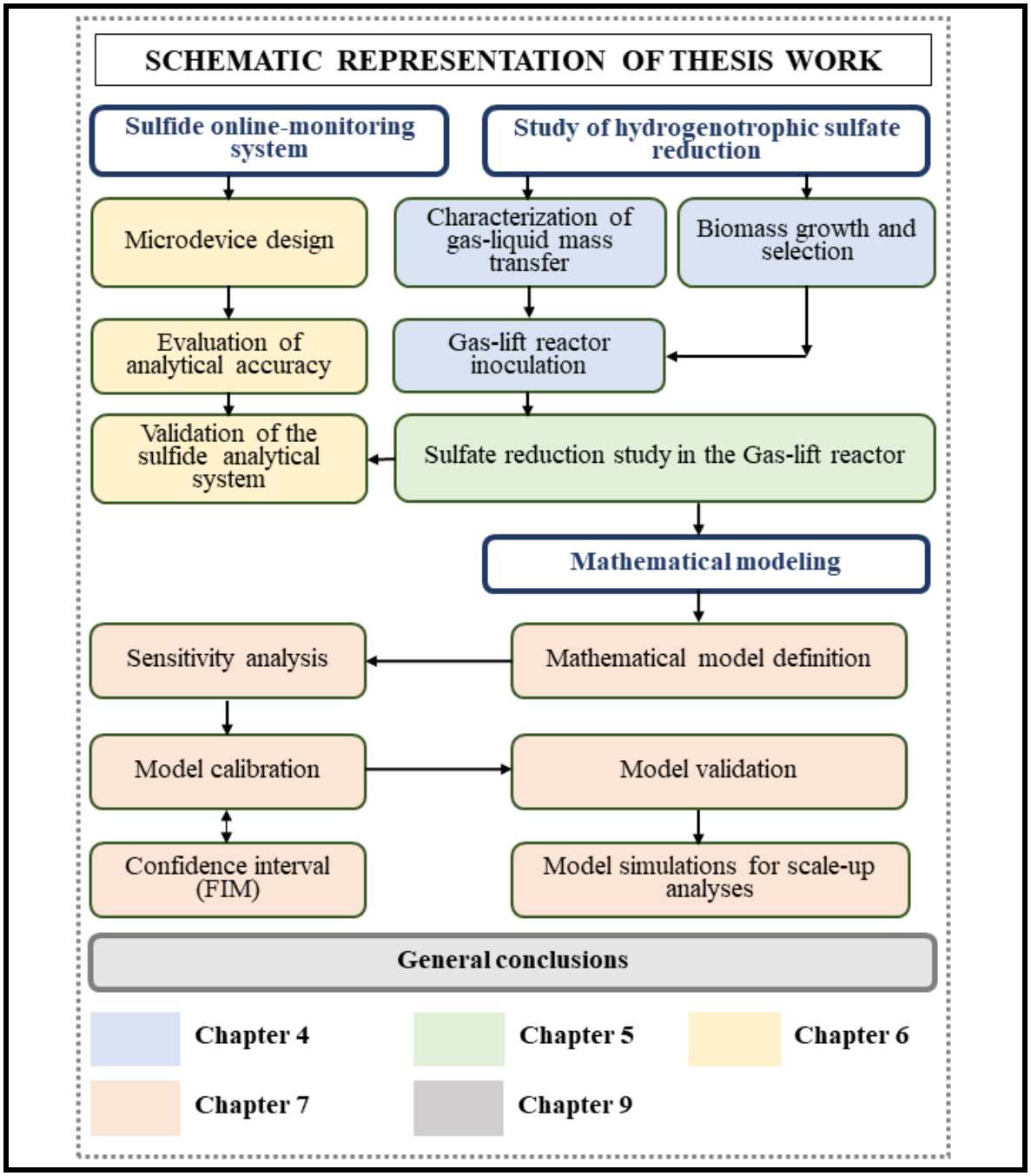

Figure 1.1. Schematic representation of the thesis work. The routes to accomplish the four specific goals of the thesis: the hydrogenotrophic sulfate reduction growth, the study in the GLR, the sulfide online-monitoring system, and the mathematical modeling.

CHAPTER 2
INTRODUCTION

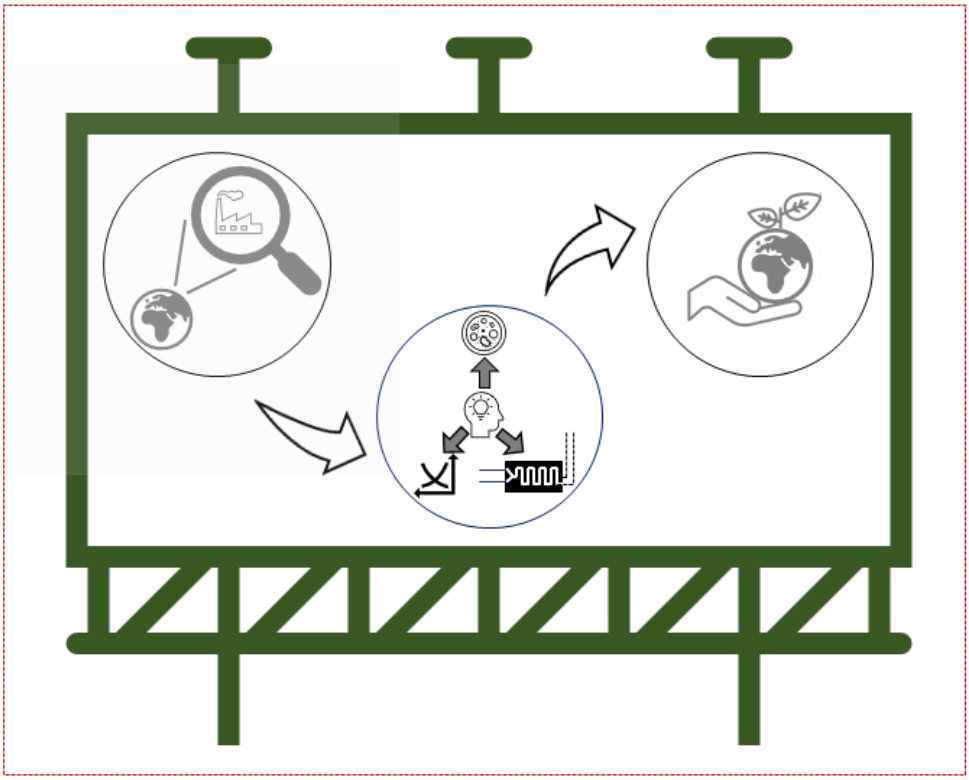

2.1. CHAPTER OUTLINE

The aim of this work is to perform a study for the biological treatment of sulfate-rich wastewaters, with special interest to those that are produced in the scrubbing processes applied to the sulfur recovery from SO_2-containing gases. Sulfur dioxide is worldwide emitted from different anthropogenic activities such as electricity and heat production, commercial/household heating, industrial/construction activities, and petroleum refining and storage, where the largest emissions are mainly generated in the fossil fuel combustion processes.[1–4] The latter are complex as they can be composed mainly by CO_2, SO_2, NO_x, and in minor quantities chlorides and trace metals, where all of them are of deep concern.[5–7]

The environmental problem derived from SO_2 emissions have been studied for years, forcing the development of international agreements to enhance the treatment of SO_2-containing off-gases and the use of more sustainable energy sources. It was the case in 1979 of the first international convention on long-range transboundary air pollution, in which it was recognized the environmental problem associated to the anthropogenic emissions of contaminants to the atmosphere.[8,9] From there, different technologies have been developed to mitigate this environmental problem, and even when there has been significant improvement, the problem is still worrisome.[10]

Herein, the study is focused on the biological treatment of previously captured SO_2, and in that order, in section 2.2, it is introduced the environmental problem that this research copes, based on the earth sulfur cycle and the environmental concern of some sulfur compounds. In section 2.3, the technologies developed as an economical and sustainable alternative and their limitations for the treatment of SO_2 contaminant are presented and divided as conventional technologies and biotechnologies. In section 2.4, the analysis of integrated treatment of SO_2 and NO_x with sulfur valorization, where the SONOVA process is explained, and some relevant advances reported in the literature are discussed.

2.2. RESEARCH INTEREST

2.2.1. Sulfur cycle on earth: geochemical and anthropogenic contributions

Sulfur cycle on earth is as represented in Figure 2.1 (adapted from Muyzer et al.[11]). Sulfur is the 10th most abundant element on earth and the highest sulfur reservoirs are in the

lithosphere with around $2 \cdot 10^{10}$ megatons (Mt) and in the hydrosphere with around $1.3 \cdot 10^{9}$ Mt. It is an essential element for life but due to the wide range of oxidation states (-2, 0, +2, +4, +6) sulfur is complex and can be present in different forms that are harmful for the environment. Sulfur is present in the atmosphere and biosphere with minor quantities of around 5 and 3 Mt, respectively.[12] It is present in nature mainly in form of pyrite (FeS_2) and gypsum ($CaSO_4$), which are predominant forms in lithosphere. The emissions to the atmosphere in form of SO_2 and H_2S are mainly due to volcanic eruptions and pyrite-rich sediments,[11] as shown in Figure 2.1. The biosphere sulfur cycle is characterized by diverse microorganisms that obtain energy from oxidized and reduced sulfur forms, such as the sulfur oxidizers (SOB) and the sulfate reducers (SRB),[13] and plants that uptake sulfate (SO_4^{2-}) from soil. Similarly, organic matter decomposition and flux of sulfur from the atmosphere contribute to sulfur deposition back to soil and waterbodies.[11] In the atmosphere, H_2S is easily oxidized to SO_2, which can end up as sulfuric acid (H_2SO_4) that can be deposited in rains or dried depositions as sulfate.[14]

There are also significant anthropogenic sulfur emissions that contribute to the sulfur global balance. Human activities related with mining, fossil fuel combustion, industrial/construction activities, petroleum refining and storage, and inappropriate treatment of wastewaters can trigger significant sulfur release to the atmosphere and to natural waterbodies.[1–4,15]

With respect to the global flux of sulfur, Jones et al.,[12] reported a sulfur flux inventory naturally emitted to the atmosphere of 20 to 53 Mt S per year, in which SO_2 is the major contributor to this emission through volcanic eruptions. Meanwhile, the anthropogenic sulfur flux in form of SO_2 was estimated in around 48.5 Mt S per year in 2010, and its highest pick emission was in the 1980's with SO_2 flux over 60 Mt S per year.[16] It has also been reported that fossil fuel combustion is responsible for around 90% of anthropogenic SO_2 emissions. Additionally, the main economic sectors that are responsible for the high SO_2 emissions to the atmosphere are the power industry, transportation, and buildings according to the International Energy agency.[17]

Other human activities such as brackish industries, textile, pulp & paper factories, tannery and mining cause other sulfur contamination that produce wastewater and sewage disposal into waterbodies and lands of around 50 Mt S per year.[15]

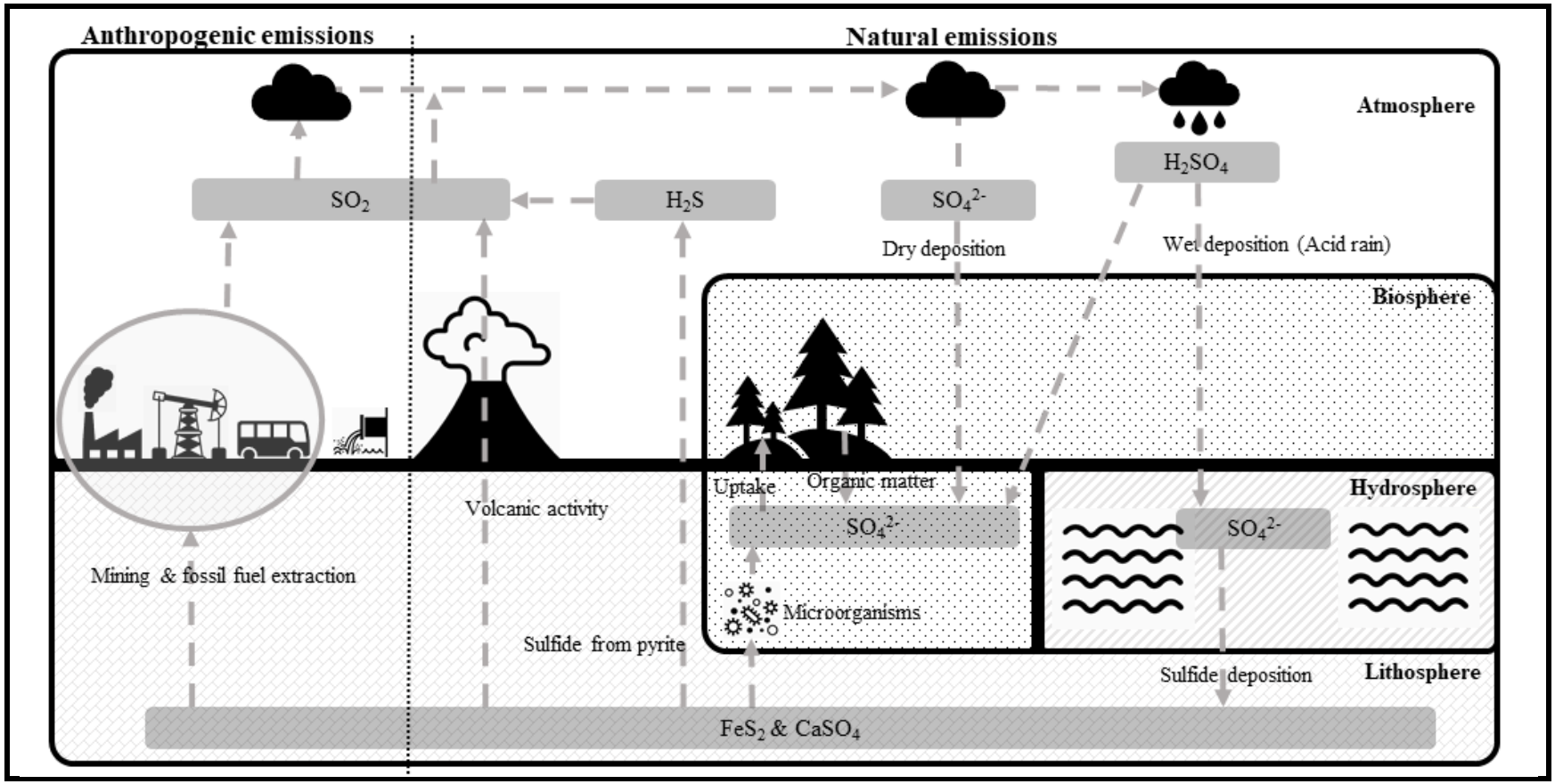

Figure 2.1. Natural and anthropogenic sulfur cycle. Sulfur uptake by microorganism and plants from biosphere. It is mainly disposed to atmosphere through volcanic activity and minor release of H_2S from pyrite sediments also takes place. Mining and fossil fuel burning are the main human sources of SO_2 emission while some wastewaters contribute to sulfur disposal in ecosystems. This Figure was adapted from Muyzer et al.[11]

Overall, the total amount of anthropogenic sulfur emissions significantly exceeds the natural sulfur fluxes, raising concern regarding proper treatment to avoid its associated environmental problem. Particularly, SO_2 emissions to the atmosphere are similar and sometimes higher than natural emissions, increasing the environmental problems associated to the disposal of this compound to the atmosphere.

2.2.2. The SO_2 environmental concern

SO_2 is a contaminant that gets into the air for the anthropogenic activities mentioned above. In the air and in the presence of water, SO_2 can form sulfurous acid (H_2SO_3) that can be further oxidized to sulfuric acid (H_2SO_4) in the present of oxygen (O_2).[2] These compounds can cause acid rains that affect aquatic and land ecosystems and are corrosive to steel and other construction materials.[2,12,18] The dissociated form of sulfuric acid (sulfate) can have a dehydration and laxative effect at high concentrations (over 200 mg L^{-1}) over human beings and animals when drinking.[19,20]

Moreover, direct exposure to SO_2 can cause skin burns and acute respiratory problems in adults and children.[21,22] In fact, the maximum SO_2 concentrations for short period of time (less than 1 hour) is 100 ppm, and concentrations over 400 ppm can cause respiratory problems in short time.[23]

Also, SO_2 in the atmosphere can produce smog and sulfate aerosols that act as secondary particulate pollutants. The latter is also dangerous for human beings and can affect solar radiation by heating or cooling the atmosphere depending on the aerosols source and properties.[12,18,24]

2.2.3. The H_2S environmental concern

H_2S is a colorless gas with a strong odor, inflammable, toxic by inhalation.[14,25] It is detectable for human smell at concentrations between 0.0005 and 0.3 ppm, and due to its toxicity, the sulfide concentration for 24 hours exposure shall be below 0.1 ppm to avoid acute respiratory problems, while concentrations between 1000 to 2000 ppm can cause death in minutes.[26] It can be found in natural gas, biogas, syngas and landfill gas, etc., as a problematic and an undesirable product that must be treated.[27] Additionally, incorrect

treatment of wastewater such as those coming from the textile, paper industries and acid mine drainage can trigger high disposal of H_2S, which is a problem for ecosystem by depletion of O_2 concentrations due to oxidation or by direct toxicity to living beings.[14,28]

Apart from the H_2S environmental and toxicity problems, H_2S is also concerning in some industrial processes due to its sour corrosion capacity. In fact, it is estimated that H_2S causes 40% of pipelines deterioration in the oil and gas industry.[29] Corrosion in industrial processes is not only a matter of cost and economically investments. Pipeline destruction has led to the spilling of raw materials that can harness environment. A remarkable case was the North Sea pipeline leakage due to corrosion in 2011 that spilled around 200 tons of oil in the sea.[29]

2.3. TECHNOLOGIES AVAILABLE TO COPE WITH SO_2 ENVIRONMENTAL PROBLEMS

2.3.1. Conventional flue gases treatment

Flue gases are normally treated through flue gas desulfurization (FGD) processes, which have been proven economically feasible. This process consists of absorbing SO_2, with limestone ($CaSO_3$) as absorbent, in a scrubber.[30] Particularly, wet FGDs are widely applied due to its large efficiency with 90% of worldwide implementation,[31] and this system can achieve removal efficiencies over 95%.[32] The global reactions taking place in a wet FGD unit process are the following:

$$CaCO_{3(s)} + SO_{2(g)} + 2H_2O_{(aq)} \rightarrow CaSO_3 \cdot 2H_2O_{(aq)} + CO_{2(g)} \qquad \text{Equation 2.1}$$

$$CaSO_3 \cdot 2H_2O_{(aq)} + \frac{1}{2}O_{2(g)} \rightarrow CaSO_4 \cdot 2H_2O_{(aq)} \qquad \text{Equation 2.2}$$

This process is normally performed at pH between 5 to 6,[30] and release CO_2 (Equation 2.1). Complete oxidation to produce gypsum (Equation 2.2) is desired as it can be reutilized in cement production, wallboard manufacturing and agriculture. Just in United States, 59 Mt of FGD by-products were generated in 2014 from which 49% were reused mainly in wallboard production[33]. In the case of Europe, report for E15 countries for 2016 shows that 34 Mt of desulphurization contaminant were generated, among that, 10 Mt were gypsum

from which 75% was reused.[34]

Overall, FGD has major disadvantages that limit gypsum production and reutilization such as 1) corrosion of scrubber vessels and erosion are important and extended problems,[35] 2) partial oxidation of limestone decreases gypsum production and increase accumulation of $CaSO_3 \cdot 2H_2O$, 3) highly pure limestone is needed as impurities limit gypsum reutilization,[30] and 4) the large production of FGD-derived gypsum surpasses its demand forcing to dispose great quantities in landfills.[32,36]

Other FGD processes are implemented with the use of sodium alkali (NaOH) with removal efficiencies over 95%. In this case, sulfate-rich wastewater with sulfate concentrations than can go up to 6700 mg $S\text{-}SO_4^{2-}$ L^{-1} can be generated.[20] These sulfate-rich effluents demands a treatment before disposal, as it can be reduced to H_2S under anoxic conditions.

Sulfate-rich effluents can be treated with different technologies such chemical, physical, and microbial processes. Chemical precipitation is an alternative to remove sulfate, but it demands large chemical agents and high investment in operational units is needed for solid separation and disposal. Physical separation such as membrane filtration and ion exchange can be applied to treat sulfate-rich effluents with high removal efficiencies, but they have high economical cost associated.[19]

2.3.2. Biological treatment of SO_2

Biological treatment of sulfate-rich effluents consists of the use of specific microorganisms that can oxidize or reduce sulfur species for energy production. This technology represents an economical alternative with low waste generation, yet, the selection of proper electron donor may be a drawback in term of process and cost depending on the system.[4,19,37,38]

The biological treatment of sulfate-rich effluents represents a feasible alternative from the economic and technical perspectives.[36] Therefore, the mechanisms of the biological treatment of sulfate-rich effluents and the nowadays biotechnologies are discussed in this section.

Microbial sulfur cycle

Sulfur plays an important role in living beings and is the sixth most abundant element in microbial life.[39] Sulfur is used in assimilatory processes mainly by prokaryotes, plants, and fungi, in which sulfur uptake is performed to synthesize organic compounds such as amino-acids, proteins, enzymes and fats. As seen in Figure 2.2, sulfur is used by microorganisms in assimilatory pathway for the synthesis of amino-acids such as cysteine and methionine, through reduction of SO_4^{2-} and partial formation of $S_2O_3^{2-}$ and S^0.[40] Meanwhile, sulfur is used in dissimilatory processes by eubacteria and archaea, in which sulfur species can be used as electron acceptor by SOB or donor by SRB for energy production.[11,13,36,41,42]

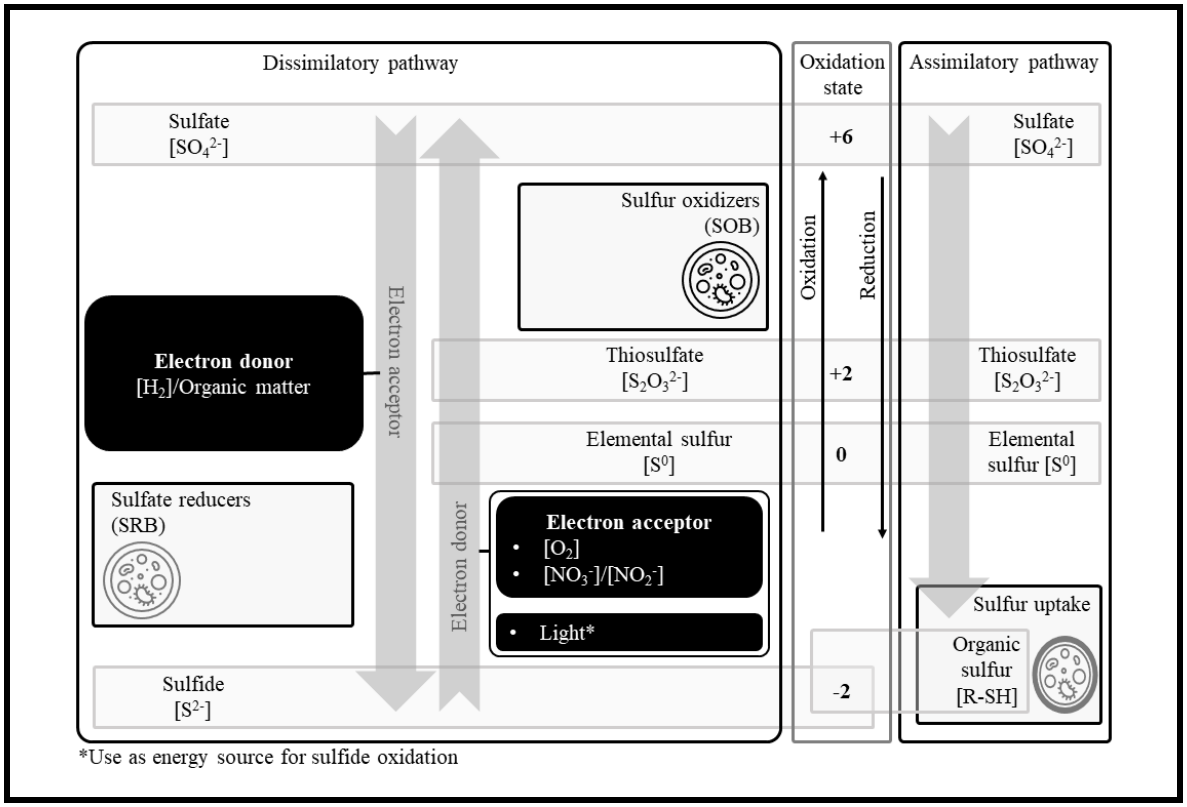

Figure 2.2. Microbial sulfur cycle. In dissimilatory pathways, SRB obtains energy from reduction of sulfate to hydrogen sulfide and SOB obtain energy from oxidation of sulfide and other partially oxidized species, e.g., S^0 and $S_2O_3^{2-}$. Assimilatory pathways are characterized by sulfate reduction to form sulfide organic compounds.

The energy use depends on the oxidation state that can go from the most oxidized form, SO_4^{2-}, to the most reduced form, S^{2-}, with oxidation states of +6 and -2, respectively. The sulfur oxidation/reduction pathway has intermediate states that allow the formation of ions and compounds, from which the most abundant are sulfur dioxide (SO_2), hydrogen sulfide

(H_2S), elemental sulfur (S^0), thiosulfate ($S_2O_3^{2-}$), sulfite (SO_3^{2-}) and sulfate (SO_4^{2-}).[43]

SOB can grow in a temperature range of 4 to 90 ºC and a pH range of 1 to 9;[13] they can obtain energy from the oxidation of sulfur species, e.g., HS^- or $S_2O_3^{2-}$, where the chemo-lithotrophic oxidation takes place with O_2 or NO_3^-/NO_2^- as electron acceptors, while phototrophic SOB need light to oxidize sulfide and reduce CO_2 to build up carbon blocks.[13]

Meanwhile, SRB can grow autotrophically or heterotrophically, in a temperature range of 0 to 100 ºC and pH range of 3 to 9.8,[36] and use sulfate as electron acceptor and a range of electron donors from H_2 to organic compounds such as lactate, pyruvate and other short-chain fatty acids.[11] Additionally, some SRB can oxidize acetate to CO_2 and are known as complete oxidizers.[4,11,36]

The range of electron donors that SRB can use to produce energy is one of the reasons of its easy proliferation under anaerobic environments,[4] and as these compounds are also used by other microorganisms to grow, the thermodynamic and kinetic properties play important roles in the routes of substrate and products in mixed culture bioprocesses,[11] like UASB reactors for the treatment of wastewaters.[44] This is also important in the treatment of sulfate-rich effluents where electron donor and/or carbon source are lacking, as it is the case of the wastewaters produced in the scrubbing of flue-gases.[4,36]

Some of the main sulfate reduction reactions catalyzed by SRBs are gathered in Table 2.1. Sulfate can be reduced with the use of volatile fatty acids (VFA) such as acetate ($C_2H_3O_2^-$), propionate ($C_3H_5O_2^-$), butyrate ($C_4H_7O_2^-$), and lactate ($C_3H_5O_3^-$). In the case of H_2, inorganic carbon source can be supplied by CO_2 for the microbial growth, and H_2 represents a highly beneficial alternative in terms of thermodynamics, as more energy is released from its reaction (Equation 2.3).[11]

Beyond the electron donors shown in Table 2.1, other organic sources have been proven as feasible electron donors and carbon sources in the treatment of sulfate-rich wastewaters.[36,37,45] Yet, for many of them, the biological sulfate reduction takes place after hydrolysis and fermentative processes, normally ending up in the VFAs shown in Table 2.1.[4,11]

From the stoichiometry (Equation 2.3 to 2.7), the corresponding substrate/sulfate mass ratios, in g substrate g^{-1} $S\text{-}SO_4^{2-}$, are 0.3, 1.8, 3.0, 5.4, and 5.6 for hydrogen, acetate, propionate, butyrate and lactate, respectively, meaning that less hydrogen is consumed per

mass unit of sulfate reduced.

Additionally, the autotrophic sulfate reduction with H_2 and CO_2 exhibits less microbial competition than heterotrophic growth and higher kinetic affinity for hydrogen,[46] which is an important parameter as due to the H_2 low solubility,[47] H_2 is normally a limiting substrate.[48]

Table 2.1. Kinetic reactions taking place in most common dissimilatory sulfate reduction process performed by SRB using hydrogen, acetate, propionate, butyrate, and lactate as electron donors.[11,13]

	$\Delta G^{o'}$ [kJ/reaction]	
$SO_4^{2-} + 4H_2 + H^+ \rightarrow HS^- + 4H_2O$	-151.9	Equation 2.3
$SO_4^{2-} + C_2H_3O_2^- \rightarrow 2HCO_3^- + HS^-$	-47.6	Equation 2.4
$\frac{3}{4}SO_4^{2-} + C_3H_5O_2^- \rightarrow C_2H_3O_2^- + HCO_3^- + \frac{3}{4}HS^- + \frac{1}{4}H^+$	-37.7	Equation 2.5
$\frac{1}{2}SO_4^{2-} + C_4H_7O_2^- \rightarrow 2C_2H_3O_2^- + \frac{1}{2}HS^- + \frac{1}{2}H^+$	-27.8	Equation 2.6
$\frac{1}{2}SO_4^{2-} + C_3H_5O_3^- \rightarrow C_2H_3O_2^- + HCO_3^- + \frac{1}{2}HS^-$	-80.2	Equation 2.7

These thermodynamic and stochiometric advantages of hydrogen over other substrates in Table 2.1 have been extended for scale-up processes where economic feasibility have been proven,[37] and in many cases, large sulfate reduction loads have been obtained using syngas as H_2 and carbon sources.[36,49]

When there are only H_2, CO_2 and sulfate, SRB must compete for H_2 and CO_2 with hydrogenotrophic methanogens and homo-acetogens.[48] For these two latter, the reactions take place as shown in Equations 2.8 and 2.9 (Table 2.2). These two processes also provide lower energetic gain than the autotrophic SRB (Equation 2.3), while all these processes consume protons (H^+), which means that their microbial activities will tend to raise the pH.

Biotechnological applications

There are different biotechnologies that have been implemented in full-scale processes aiming at treating diverse sources of sulfate-rich effluents. Some remarkable technologies to treat sulfate-rich effluents are the THIOPAQ^{TM} process that can treat acid mine drainage and metallurgical wastewaters.[11,36] The THIOPAQ^{TM} process aims at reducing sulfate to sulfide autotrophically and then, sulfide is further precipitated with heavy metals. In this case, the heavy metals are necessary and limit the process applications to the wastewater mentioned above.

Table 2.2. Kinetic reactions performed by hydrogenotrophic methanogens and homo-acetogenic microorganisms.[11]

	$\Delta G^{\circ'}$ [kJ/reaction]	
$HCO_3^- + 4H_2 + H^+ \rightarrow CH_4 + 3H_2O$	-104.9	Equation 2.8
$HCO_3^- + 4H_2 + H^+ \rightarrow C_2H_3O_2^- + 4H_2O$	-56.5	Equation 2.9

Also, integrated process for sulfate reduction, autotrophic denitrification, and nitrification (SANI) can be applied for the treatment of diverse sulfate-laden streams with low ratio of sulfate to chemical oxygen demand (COD).[36,50] This process consists in the integration of heterotrophic sulfate reduction with autotrophic denitrification (reduction of nitrate with sulfide oxidation), and finally ammonia is autotrophically oxidized to nitrate. The three microbial activities integrated in the SANI process allowed to reduce sludge production in 90% and save 35 % energy.[50]

Other applications that aim at treating flue-gases in an integrated absorption/biological process to elemental sulfur (S^0) recovery can achieved removal efficiencies over 90%.[11] The absorption of SO_2 can be done with alkaline solutions according to Equations 2.10 and 2.11. Then, sulfate can be reduced with the use of an external carbon and electron donor source according to Equation 2.12 and 2.13. Finally, sulfide is partially oxidized to elemental sulfur (S^0) (Equation 2.14) that can be recovered for further exploitation in other industrial process such metal bioleaching, industry of sulfuric acid production, fertilizers production in agriculture sector, among other applications.[13]

$$SO_2 + OH^- \rightarrow HSO_3^-$$ Equation 2.10

$$HSO_3^- + 0.5O_2 \rightarrow SO_4^{2-} + H^+$$ Equation 2.11

$$HSO_3^- + 6e^- \rightarrow HS^- + 3H_2O$$ Equation 2.12

$$SO_4^{2-} + 8e^- \rightarrow HS^- + 3H_2O + OH^-$$ Equation 2.13

$$HS^- + 0.5O_2 \rightarrow S^0\downarrow + OH^-$$ Equation 2.14

The sulfate reduction step can be applied in anaerobic upflow blanket reactors (UASB) with the need of an external organic matter source. This process is favored at mesophilic conditions and due to the granular-type sludge, short hydraulic residence time (HRT) with large volumetric sulfate reductions rates (SRR) can be obtained. In fact, it can be applied to diverse sulfate-rich wastewater, yet, CH_4 production is one drawback of this process.[45,51,52]

An alternative for the sulfate reduction step is the autotrophic sulfate reduction using H_2 and CO_2 as electron donor and carbon sources, respectively, and can be implemented in gas-lift reactors (GLR).[49,53,54] As mentioned above, this configuration has the advantage that the microbial proliferation is limited to three autotrophic processes: hydrogenotrophic sulfate reduction, hydrogenotrophic methane production and homoacetogenesis.[46]

Regarding the sulfide oxidation step, it can be performed in stirred-tank reactors (STR) using oxygen or nitrate as electron acceptors, where sulfur production can be enhanced by supplying ideal ratios of oxygen/sulfide or nitrate/sulfide.[15] Also, oxidation-reduction potential (ORP) of -400 mV[55] and -380 mV[56] have been reported ideals for the maximization of elemental sulfur production.

2.4. INTEGRATED TREATMENT OF SO_2 AND NO_X FOR SULFUR RECOVERY

2.4.1. SONOVA/ENSURE process

Worldwide discussions about coping environmental concern and depletion of raw materials have led the development of diverse ways of structuring economic sectors. These concerns result from the severe impact on earth that are caused by the high rate of commodities consumption and environmental contamination associated to the fast-growing world population. In fact, worldwide discussions have taken place since 1987, when the World Commission on Environment and Development reported the need of development sustainable processes so that all economic sectors can grow with no restrictions.[57,58] Thus, the sustainable way to build processes is called a circular economy, which is defined by the United Nations as follows:[59] "The circular economy is a new and inclusive economic paradigm that aims to minimize pollution and waste, extend product lifecycles, and enable broad sharing of physical and natural assets. It strives for a competitive economy that creates green and decent jobs and keeps resource use within planetary boundaries." This definition implies that commodities and all industrial processes have to be developed mimicking natural cycles,[60] which means that it should be intended to valorize residues into products that can be reused, and mitigate contaminants as much as possible.

Therefore, the concern related about the flue-gases emissions can be coped with the development of technologies that can integrate the valorization of these residues. This is the concept from which the SONOVA/ENSURE process was developed. It aims at treating flue-gases as shown in the schematic representation of Figure 2.3.

The SONOVA process consists in 3 global steps for the integrated treatment of SO_2 and NO_x gases aiming at recovering elemental sulfur as a value-added product, which has gained interest in recent years.[11,36,56] The treatment of flue-gases (SO_2 and NO_x) consists of a two-step physical-chemical capture of SO_2 and NO_x gases. Then, the biological process is divided in two parts, the first part aims at reducing sulfate and the second part aims at oxidizing sulfide to elemental sulfur. Finally, the third global step consists in recovering the elemental sulfur for its further exploitation as a value-added product. Herein, it is also intended to study the biofilm characteristics in the biological step, the monitoring of sulfate and hydrogen sulfide production, the biological activity, and the microbial diversity.

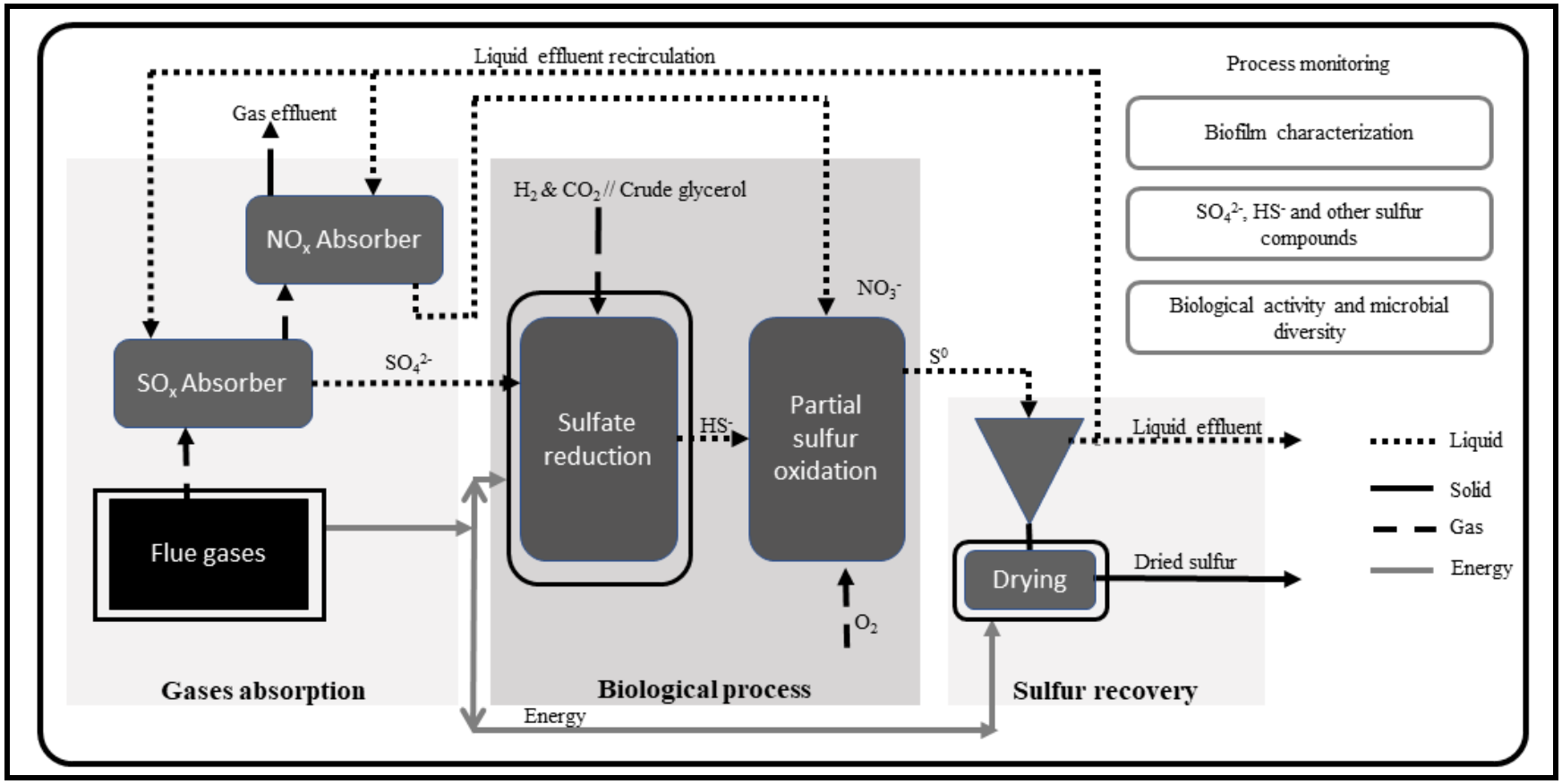

Figure 2.3. SONOVA process for the treatment of flue gases. The process is divided into three main steps, the gases absorption where NO_x and SO_x gases are transferred to the liquid phase, the biological treatment of SO_4^{2-} and NO_3^- that is performed in 2 steps and the recovery of sulfur as a potential value-added product.

2.4.2. Literature reports related to the SONOVA process

Flue-gases absorption

From the flue-gases absorption, some advances have been made by Guimerà et al.,[6] in which the SO_2 and NO_x captures were studied obtaining removal efficiencies of 98.9 and 55.9 % (w/w), respectively. For the first step, the SO_2 conversion in the liquid phase proceeds as described by Equations 2.10 and 2.11.

Also, $NaHCO_3$ was used to mimic liquid effluent from the first and second biological step (Figure 2.3) as these are alkaline components characterized in these effluents. The use of $NaHCO_3$ allowed SO_2 removal over 80 % (w/w).

Meanwhile, the main NO_x species are nitrogen monoxide (NO) and nitrogen dioxide (NO_2). In this step NO needs to be oxidized to NO_2 and $KMnO_4$ was found by Guimerà et al.,[6] as a suitable oxidation and adsorption agent with removal efficiency between 50 to 60 % (w/w).

Biological sulfate reduction

From the biological process, a sulfate reduction study was carried out by Fernandez-Palacios et al.,[45] in a UASB reactor using crude glycerol as carbon source and electron donor. It was obtained a SRR of 4.3 g $S\text{-}SO_4^{2-}$ L^{-1} d^{-1} at a COD/$S\text{-}SO_4^{2-}$ ratio of 5.4 g O_2 g^{-1} S with a sulfate removal efficiency (Sulfate-RE) of 94 % (w/w). Nevertheless, CH_4 was detected in small fraction 2.5% (V/V) of the gas outlet and acetate was highly accumulated in the effluent with concentrations of up to 340 mg L^{-1}.

Remarkable results have also been reported for autotrophic sulfate reduction. Syngas has been studied in a biofilm GLR fed with syngas as CO_2 and H_2 source, and SRR of 5 g $S\text{-}SO_4^{2-}$ L^{-1} d^{-1} was obtained.[53] Also, direct feeding of H_2/CO_2 was reported in a biofilm GLR with SRR of 6 g $S\text{-}SO_4^{2-}$ L^{-1} d^{-1}.[49] Yet, biofilm formation of H2-SRB is challenging as it has been reported in some works, where culture with only suspended biomass was obtained with SRR (in g $S\text{-}SO_4^{2-}$ L^{-1} d^{-1}) of 0.2[61] and 0.3.[54]

Biological sulfide oxidation and recovery

Regarding the biological sulfide oxidation, characterization of SOB kinetic parameters

for aerobic and anoxic growth with the aid of mathematical modeling has been reported. It was the case of the estimation of sulfur oxidation routes in SOB through respirometry experiments, where kinetic parameters of SOB were determined and maximum intracellular S^0-accumulation was found to be 25.6 % (w/w).[62] Also, elemental sulfur (S^0) production has been proven as a viable alternative with sulfide conversion to S^0 of 86 % (w/w) for volumetric sulfide loading rate of 0.6 g S L^{-1} d^{-1}.[56]

The anoxic sulfide oxidation with autotrophic denitrification has been characterized through mathematical modeling calibration of experimental data, and it has been reported that sulfide and nitrite have a substrate inhibition effect for microbial growth at concentrations of 33 mg N-NO_2^- L^{-1} and 78 mg S-H_2S L^{-1}.[63] Thus, acclimation study has been performed to increase SOB resistance to nitrite inhibition, and it was achieved an SOB culture able to resist nitrite concentration of 150 mg N-NO_2^- L^{-1}. In that order, optimal sulfide oxidation with autotrophic denitrification has been reported at 35 ºC and pH between 7.5 and 8.[64]

Meanwhile, the sulfide oxidation with denitrification has been studied for production of nitrite for an anammox process. It was reported by Polizzi et al.,[65] who studied the sulfide oxidation with partial denitrification to nitrite for the further supply of nitrite to an anammox process, and it was obtained a conversion of NO_3^- to NO_2^- of 95 % (w/w) for sulfide loading rate of 0.1 g S L^{-1} d^{-1} and nitrate loading rate of 0.2 g N-NO_3^- L^{-1} d^{-1}.

The sulfur recovery step was evaluated by Mora et al.,[38] in the study of jar tests in which an optimal result showed S^0 purity of 74.3 % (w/w) with a recovery efficiency of 64.4 % (w/w) that was achieved with the use of coagulant FL4820 at 0.5% dosage. Moreover, this work also explored the three steps of the SONOVA project for a real industrial flue-gas treatment and showed that it is economically feasible.

Development of sulfide online-monitoring systems

Analytical techniques are important for the monitoring of key components that can help to understand process behaviors.[66] Technologies are based on many different physical principles that have evolved along the years.[67] Some of these developments have been focused on the real-time measurement and miniaturization (lab on a chip concept, LOC) of the analytical system for low cost platforms.[68–71] These miniaturized systems can be

developed with aid of 3D-printing and inkjet printing technologies using different analytical techniques as detection system, among which, electrochemical technique have been extensively applied.[72,73]

These systems are of great interest for sulfidogenic reactors, where the sulfide production can inhibit microbial growth and therefore, its monitoring and control are necessary.[11,13,36,74]

In this direction, the development of a sulfide online monitoring system (S-OMS) have been reported based on a 3D-printed sulfide electrode for potentiometric measurement.[75] This system showed a Nernstian response and a working range for total dissolved sulfide (TDS) of 3.2 to 32000 mg TDS L^{-1} with a response time of 8 seconds, demonstrating a good approach for its implementation in the online monitoring of real samples in sulfidogenic reactors. Also, an inkjet-printed sulfide electrode has been reported with a low cost and fast fabrication, showing Nernstian response, a working range of 1 to 1600 mg TDS L^{-1}, and a response time of 2 seconds.[72]

Mathematical modeling of biological process

Mathematical models are important tools for experimental design, process scale-up and optimization.[76] They are developed on a series of steps that requires experimental data for model calibration and validation, model definition that depends on operational setting such as type of reactors and operation, microbial culture and environmental conditions.[44,76]

In the treatment of sulfate-rich effluents, mathematical models have been proposed for the description of experimental process in UASB, GLRs , amongst others.[44] The kinetic of microbial growth can be described by a Monod kinetic that, depending on the hydrogen sulfide concentration, an inhibition term may be including for proper experimental description.[77,78] Overall, anaerobic processes are model through the anaerobic digestion model No. 1 (ADM1) developed by the International Water Association (IWA), in which organic anaerobic degradation steps are included: hydrolysis, acidogenesis, acetogenesis and methanogenesis,[79] and some extensions of this model have been reported to include the biological sulfate reduction.[77,78,80]

Model development for sulfate reduction processes have been mainly implemented for heterotrophic cultures and using ADM1. It was the case of Barrera et al.,[77] who modeled an

UASB reactor treating high strength sulfate wastewater and was able to determine kinetic parameters of SRB with some deviations of model with respect to experimental data.

Additionally, Zhou et al.,[52] studied a crude glycerol fed UASB reactor treating sulfate through batch tests to discover the biological mechanisms that governed the main degradation pathways. It was obtained that glycerol was degraded to 1,3-propanediol, ethanol, formate, propionate, and acetate by fermentative bacteria. Then, these organic compounds, except for acetate, were used by SRB. This explained the reason of why during the UASB reactor operation a large fraction of acetate was accumulated in the effluent.

For autotrophic sulfate reduction, Esposito et al.,[46] developed a mathematical model using parameters from the literature for the simulation and design of a H_2/CO_2 fed GLR, and validation of this model was done by Frunzo et al.[81]

Overall, kinetic parameters for H2-SRB have been estimated through mathematical models of UASB reactors fed with organic matter and using granular biomass, as reported by Alphenaar et al.,[82] Kalyuzhnyi et al.,[83] Federovich et al.,[78] and Omil et al.[84]

CHAPTER 3
MATERIALS AND METHODS

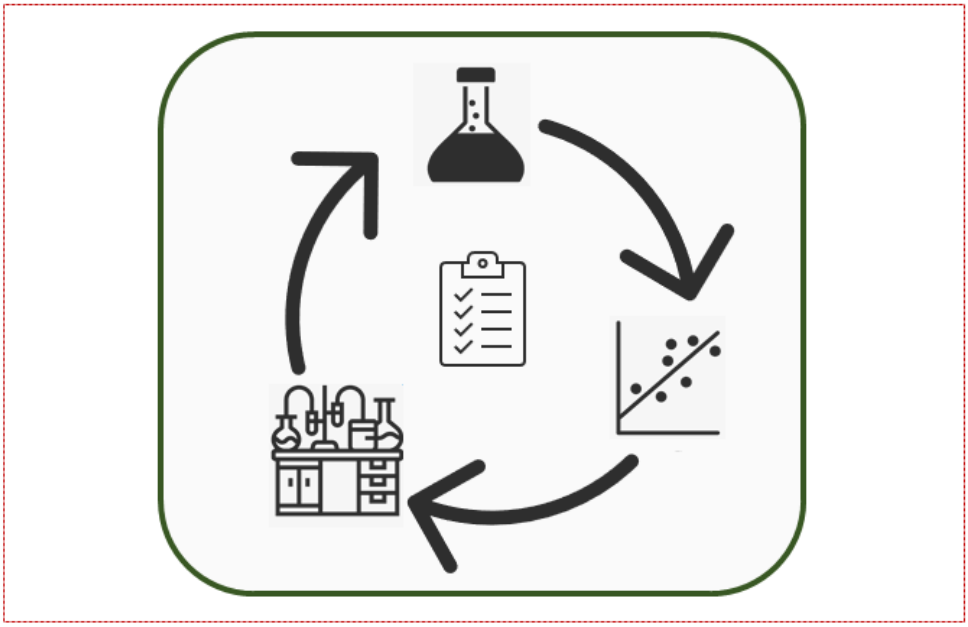

3.1. GLR CONFIGURATION

The GLR had a total volume of 7.09 L with a liquid volume capacity of 6.75 L. It was divided into three main pieces that are separated with dash lines in Figure 3.1 and are defined as follows: the gas-diffusing part, the mixing zone, and the three-phase separator. These pieces had frosted glass joints that, together with silicone gaskets and flange clamps, can be assembled. The inlets/outlets openings can be controlled, i.e., to keep opened or closed, by using screw caps and silicone joints.

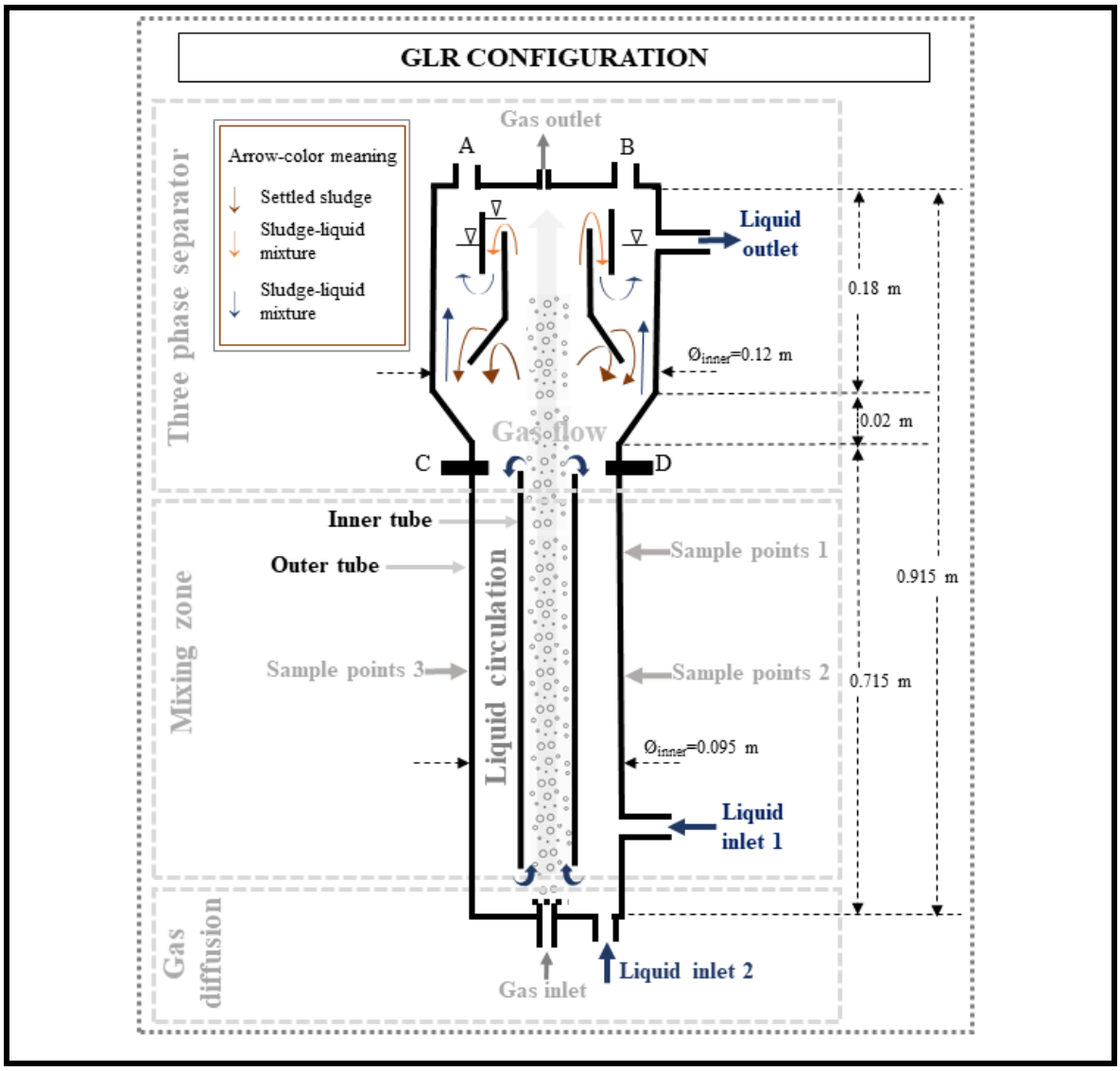

Figure 3.1. The gas-lift reactor (GLR) configuration. The reactor was divided into three main parts: the gas-diffusing part, the mixing zone, and the three-phase separator. The color arrows in the separator represents the liquid-solid-gas routes in the three-phase separator.

As seen in the Figure, the gas-diffusing section was on the bottom and contains a liquid inlet and a gas inlet with a diffuser that was a glass-porous plate. The mixing zone was in the middle and was formed by an inner tube (also called riser), an outer tube (also called downcomer), three sampling points and another liquid inlet. The operation of this zone mimicked a stirred tank reactor (STR) due to the gas-liquid dynamics: bubbled gas in the riser induced a difference in the liquid density that forced the liquid to flow upwards in the riser and downwards in the downcomer.[85] The three-phase separator aimed at separating gas from the liquid while keeping the solid inside the reactor; the color arrows in the three-phase separator indicate the solid-liquid-gas routes and this dynamic is according to the literature.[86,87]

The deflector in the separator aims at retaining solids and conducting gas to the outlet line; while the other tube, i.e., the outer tube in the three-phase separator, helps to settle the denser solids that can rise through the first one.

Finally, the detailed information about the reactor dimensions can be found in the technical sheet of the reactor shown in Appendix A.

3.2. COMPOSITION OF SOLUTIONS

The composition of the mineral medium (MM) used in the sulfate reducing experiments, the sulfide antioxidant buffer (SAOB) and the sulfide-stock solution used to calibrate the sulfide electrodes are all described in this section.

MM composition

The MM was prepared as shown in Table 3.1, and as it has been reported in the literature.[49] The sulfate concentration was prepared according to the experiments; its concentration is specified in the corresponding Chapters. 2-bromoethanesulfonate (BES) was used in some experiments to inhibit methanogenic activity.[88]

MM was also doped with acid trace, alkaline trace and vitamin solutions that were prepared as described in the literaute,[54] and added 10 ml per liter of MM.

Table 3.1. MM composition prepared on tap water.

Compound	Concentration [g L^{-1}]
NH_4Cl	0.3
K_2HPO_4	1
$NaHCO_3$	4
$CaCl_2 \cdot 2H_2O$	0.11
$MgCl_2 \cdot 6H_2O$	0.1
BES	0.12

SAOB solution

The SAOB solution used to measure sulfide was prepared as shown in Table 3.2.

Table 3.2. Concentration of the SAOB solution.

Compound	Concentration [g L^{-1}]
NaOH	80
L(+)-ascorbic acid	34
EDTA	67

Sulfide-stock solution

The sulfide-stock solution was prepared to have a 32 g TDS L^{-1} (TDS: total dissolved sulfide) with a Sodium Sulfide reagent (Sodium sulfide nonahydrate, 98 %, ACROS ORGANICS). It was stored at 4ºC in an amber borosilicate glass bottle.

3.3. ANALYTICAL METHODS

Herein, it is presented the analytical tools and sample preparation applied along the experimental section of the work.

Sample preparation

The samples for the sulfate and acetate quantification were filtered prior measurement with 0.22 µm pore-size hydrophilic polyether-sulfone (PES) filters. Samples were diluted with ultrapure water to have concentration between the calibration ranges and prepared in screw-top transparent-glass 2ml vials (12X32mm, Scharlab).

In the case of total dissolved sulfide (TDS), the samples were always diluted with a total volume of 10 ml from which 5 ml were SAOB and the other 5 ml were the sample or a diluted sample with distilled water. The latter was done to keep always the TDS concentration between the calibration range, and the SAOB in the same dilution that was applied during the calibration. These samples were prepared in 40-ml glass vials (EPA Screw vials, 40-EPAVCSA).

Total chemical oxygen demand (COD_t) was measured with no pretreatment of the sample while for the dissolved COD_s samples were filtered with 0.22 µm pore-size hydrophilic polyether-sulfone (PES) filters.

Gas samples were gathered in a 1-liter Tedlar bag and a gas sampling syringe (Gas syringe A-2, 100-µL RN, 0.029"X0.005"X2", bevel open end, VICI) was used to inject 100-µL of gas sample to the gas chromatography.

Sulfate measurement

Sulfate was measured with an Ion chromatography (Dionex AS-AP, Thermo Scientific) that was calibrated to measure sulfate, thiosulfate, nitrate, and nitrite in a range of 1 to 100 mg L^{-1} (concentration in: $S\text{-}SO_4^{2-}$, $S\text{-}S_2O_3^{2-}$, $N\text{-}NO_3^-$, $N\text{-}NO_2^-$). This equipment had a Dionex IonPacTM AS11-HC-4 µm column (diameter: 2 mm, height: 250 mm, Thermo Scientific) and autosampler (Ultimate 3000 Autosampler) that used potassium hydroxide (Dionex EGC 500 KOH, Thermo Scientific) as eluent with a flowrate of 0.33 mL min^{-1}.

Acetate measurement

Acetate was measured with a high-performance liquid chromatography (Ultimate 3000, Dionex Integrion HPLC, USA) calibrated to measure volatile fatty acids (VFA) in the range of 20 to 1000 mg L^{-1} (concentration in mg L^{-1} of compound: Formate, Acetate, Propionate, Butyrate, Iso-butyrate, Valeric and Iso-valeric). This equipment contained an ICSep ICE-CPREGEL 87H3 column (diameter: 7.8 mm, height:150 mm, Transgenomic, Omaha, NE, USA), a refractive index detector (Waters 2410) with an IR of 1024, and an autosampler (Ultimate 3000 Autosampler). Sulfuric acid (6 mM H_2SO_4) was used as mobile phase with a flow rate of 0.5 mL min^{-1}.

Sulfide measurement

Sulfide in the liquid phase was measured with a commercial sulfide ion selective electrode (S^{2-}-ISE, Orion™ Silver/Sulfide electrode, Thermo Scientific) that used a filling solution of KNO_3 (B optimum results™, Orion 900062, Thermo Scientific) and was connected to a multimeter (SB90M5 Symphony multimeter, VWR) for potentiometer (E_c) recording.

This procedure accounted several steps before measurement. First, a standardization was done to determine the sulfide concentration of a sulfide-stock solution by titrating a 0.1M Pb^{2+} solution (Orion ionplus, Lead Standard 0.1 M Pb^{2+}, Thermo Scientific) in a 0.1-liter beaker containing 30 ml of SAOB and 1 ml of the sulfide-stock solution. Thus, a precipitation reaction proceeded as shown in Equation 3.1. The reaction evolution was tracked by monitoring E_c during titration. The S^{2-}-ISE was connected to a multimeter (SB90M5 Symphony multimeter, VWR) and the membrane side of the electrode was immersed in the solution while E_c was recorded after each lead solution addition. This latter was added by 0.05 ml volume and using a 10-ml burette (A-6054 AFORA 10 ml ± 0.02 ml).

The total sulfide consumption can be accomplished when a sharp increase of E_c takes place, i.e., the highest slope between the increase in E_c and the volume added ($\Delta E_c/\Delta V$).[89] Hence, the sulfide concentration can be estimated from Equation 3.2, where V_t represents the total lead volume titrated, V_s the sulfide volume added (in this case 1 mL), and the sulfide concentration is given in M.

$$S^{2-} + Pb^{2+} \rightarrow PbS\downarrow \qquad \text{Equation 3.1}$$

$$\left[S^{2-}\right] = 0.1\left[\text{M } Pb^{2+}\right]\cdot\frac{V_t[\text{ml}]}{V_S[\text{ml}]} \qquad \text{Equation 3.2}$$

This standardization was used to calibrate the commercial S^{2-}-ISE, and the S-OMS developed in this work that will be explained in Chapter 6.

Finally, the calibration of the commercial electrode was done by the standard addition measurement,[90] which is the appropriate method for an off-line analytical technique (the sulfide addition is detailed in Appendix B) and the analytical response was evaluated from the Nernst Equation.[75,91] The undissociated hydrogen sulfide (H_2S) fraction was determined

from the TDS concentration based on the pH of the samples as detailed in Appendix B.

COD measurement

The COD was measured with COD kits (COD, tube test MR, Lovibond Water Testing) of middle range 0–1500 mg COD L^{-1}, and following the M131 method reported by the supplier,[92] that consisted of adding 2 ml of sample in the COD vial and incubating for 2 hours at 148 ºC. The same procedure must be done with a blank prepared with 2 ml of ultrapure water. After the incubation, the samples were taken outside and cool down to room temperature and then, samples were measured with a photometer that uses LEDs and interference filters (MD 100 COD Instrument, Lovibond Water Testing).

Solid measurement: total suspended solids (TSS) and volatile suspended solids (VSS)

Solids were measured according to the standard methods,[93] where aliquots, herein of 10 ml, were filtered with glass fiber filters (MF-Millipore™ hydrophilic glass fiber Membrane, 0.7 µm pore size, 47 mm diameter, Merck) in a filtration assembly connected to a vacuum pump. Prior and after use, filters were dried in a stove (UF 75, Memmert) at 105ºC to drive off water, and in both cases, filters were weighed with an analytical balance to obtain filter weight w1 and w2, respectively. Afterwards, filters were heated in a Muflle furnace (Model: 12PR/300 serie8B, Hobersal) at 550ºC to drive off volatile solids, and finally ash-carrying filters were weighed to obtained filter weight w3. Before weighing, filters were always cold down in a glass desiccator with silica as drying agent.

TSS was equivalent to the weight difference between w1 and w2, while VSS was equivalent to weight difference between w2 and w3. Concentrations (in mg L^{-1}) were determined from these weights and the volume of aliquot filtered.

Gas composition measurement

The gas phase of reactors used along the experiment was measured to identify the gas composition of CH_4, CO_2, and H_2 and O_2. This was done with a Gas Chromatography (7820A, Agilent Technologies, USA) that had a capillary column (Al_2O_3 PLOT: 50 m, 0.53 mm) and worked at 250 ºC.

DNA extraction and sequencing

DNA extraction and sequencing was done following the protocol already reported in the literature.[56] The MoBio PowerBiofilm™ DNA extraction kit protocol (MoBio Laboratories, Carlsbad, CA, USA) was applied. The quality and quantity of the extracted DNA were measured with a NanoDrop 1000 spectrophotometer (Thermo Fisher Scientific, Waltham, MA, USA) and with a minimal DNA concentration of 5 ng L^{-1}. This samples were stored at -20ºC before sequencing.

Microbial identification was analyzed with the Illumina platform NGS next generation sequencing in the Genomic and Bioinformatics Service of the Autonomous University of Barcelona (UAB, Barcelona, Spain). Fragment of bacterial 16S V4 ribosomal RNA (around 300 bp) was amplified using the primers pair 515F-GTGCCAGCMGCCGCGGTAA and 806R GGACTACHVGGGTWTCTAAT.

CHAPTER 4

PRELIMINARY EXPERIMENTS FOR THE SULFATE REDUCTION STUDY

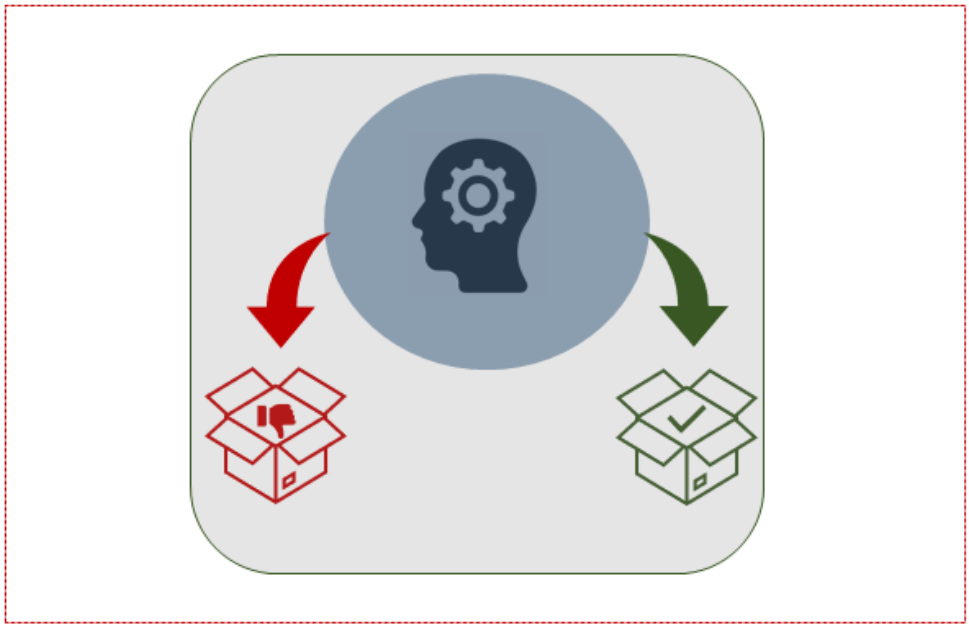

4.1. CHAPTER OUTLINE

As this work aimed at evaluating the autotrophic sulfate reduction using H_2 as electron donor and CO_2 as electron acceptor, this Chapter describes the preliminary experiments performed to grow and select the inoculum. This process is shown in Figure 4.1, in which the initial inoculum was taken from a full-scale UASB reactor that treated pulp & paper wastewaters rich in sulfate and organic compounds. Thus, heterotrophic- and methanogenic-microorganisms were predominant in the microbial community of the inoculum. Therefore, the inoculum was grown to select hydrogenotrophic sulfate reduction microorganisms (H2-SRB) by enrichment of the biomass in stirred-tank reactors (STR) A and B. The initial inoculation was done in Reactor A that had a 1-liter liquid capacity and was followed for 47 days, after which the culture medium was taken to inoculate Reactor B that had a 10-liter liquid capacity and was operated for 48 days. Later, the culture medium was taken from reactor B to start up the GLR.

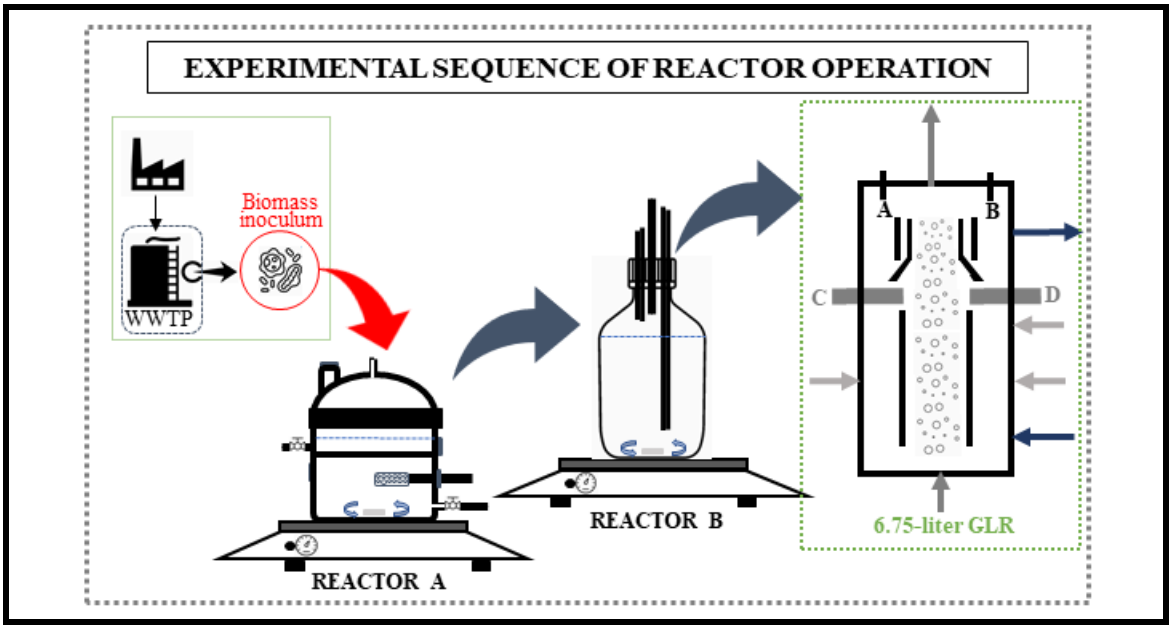

Figure 4.1. Biomass growth and selection. Biomass inoculum was taken from a full-scale UASB reactor that treats wastewater from a pulp & paper factory. Reactor A and B were used for biomass growth and selection, after which culture medium was taken to inoculate the GLR.

Additionally, a set of abiotic experiments, albeit before inoculation, were performed in the GLR to determine the overall H_2-mass transfer coefficient (K_La_{H2}). After inoculation, two preliminary investigations were conducted in the GLR: first, the reactor was inoculated and operated for 88 days in sequential batches to increase biomass density and hydrogenotrophic

sulfate reduction activity; and second, the sulfate reduction activity was examined through batch tests to determine the kinetic parameters and the biofilm activity. Afterwards, and based on these preliminary experiments, the GLR operation was set up to study the sulfate reduction in a sequential batch way with sludge recovery; the latter is the subject of Chapter 5.

Consequently, in this chapter the experiments performed in reactors A and B for biomass growth and selection are explained in section 4.3; then, the sequence of experiments performed in the GLR are presented as follows: 1) the abiotic test to determine the K_La_{H2}, 2) the GLR inoculation, and 3) the biomass characterization through kinetic experiments and microbial identification are all pointed out in section 4.4. Finally, the main conclusions of these results are established in section 4.5.

4.2. INTRODUCTION

Mass transfer limitations are important to choose properly reactor type in any processes. In our case, a literature review was done to consider the kinetic aspects of H2-SRB and the H_2 and CO_2 properties. For H_2-fed reactors, where the influent lacks organic compounds, e.g., wastewater produced in flue-gas scrubbing processes, the main assets of H2-SRB are the thermodynamical advantages of H_2 over other electron donor sources (see Table 2.1 in Chapter 2),[11,13] and the limited growth of heterotrophic microorganisms as readily-degradable organic compounds are hardly present. Nevertheless, substrate competition can take place due to other H_2/CO_2 consumers, such as homo-acetogens and methanogens. In that case, an advantage of H2-SRB is the high H_2-affinity,[4,48] that favors them over homo-acetogens and methanogens under H_2-limiting environment. Hence, H_2/CO_2-fed reactors represent a compelling alternative to the treatment of sulfate-rich and inorganic wastewaters.

On the contrary, the low H_2-solubility[47] is the main drawback of these systems as H_2 normally ends up limiting the sulfate reduction capacity. Consequently, reactor configurations that enhance H_2-mass transfer to the liquid phase are preferably to maximize sulfate reduction; between them, STR and gas-lift reactors (GLR) offer favorable mixing conditions over other conventional reactors, e.g., upflow anaerobic blanket (UASB) or fluidized bed reactors. STR normally describes the best mixing conditions but hinders biomass aggregation, and thence, by hampering solid separation, slow growing microorganisms will seldom proliferate, which means that they demand long hydraulic

retention time (HRT). Meanwhile, GLR normally displays fewer mixing conditions than STR, but can boost biofilm formation, i.e., particle-based biofilm or granulated biomass. Nicolella et al,[94] suggested a threshold value for maximum specific growth rate (μ_{max}) of 2.4 d^{-1}, meaning that STR is preferred for μ_{max} above this threshold value, whilst GLR can be considered in the opposite case. Regarding μ_{max} for H2-SRB ($\mu_{max.SRB}$), different values have been reported, from 0.3 to 5 d^{-1} by Tang et al.,[95] and Kalyuzhnyi et al.,[96] respectively; the former was based on a H_2-fed membrane reactor with no other external electron-donor source, while the latter was estimated from a STR treating organic wastes and thereby a microbial culture rich in heterotrophic microorganisms. Similarly, Esposito et al.,[46] proposed a mathematical model for a H_2/CO_2-fed GLR with a value of 1.1 d^{-1} for the $\mu_{max.SRB}$. Overall, GLR has been used for autotrophic sulfate reduction aiming at favoring the biofilm formation due to growth rates,[54,97,98] but in some cases biofilm activity has not been achieved.[54,61]

4.3. BIOMASS GROWTH AND SELECTION

4.3.1. Setup of reactors A and B

Reactor A consisted in two pieces that were joined with a flange clamp and were assembled as shown in Figure 4.2. This reactor had 4 septa for liquid and gas sampling: S1, S2, S3 and S4. Sampling port S4 had a tube with a gas diffuser that was used to bubble N_2 or H_2. The headspace had an inlet/outlet line that was connected to a 1-liter Tedlar bag (FlexFoil 1-liter Sample Bag SKC) for H_2 filling and to a gas extractor for H_2S stripping (red configuration). Mineral medium (MM) refilling and liquid sampling were done through valve V5, while gas sampling was done from the Tedlar bag.

Regarding the operation, the reactor was placed on a magnetic stirrer at 180 rpm at room temperature (~20°C) and the inoculation was performed with 0.05 liter of inoculum and 0.65 liter of MM containing 100 mg $S\text{-}SO_4^{2-}$ L^{-1}, which resulted in an initial total (TSS) and suspended (VSS) solid concentration of 620 and 414 mg L^{-1}, respectively. MM for this reactor contained 2-bromoethanesulfonate (BES) to inhibit methanogenic activity.[88] The detail information about MM composition is shown in Chapter 3 (section 3.2).

Also, a total of eight feeding cycles were run in a fed-batch way along the culture period. Cycle duration was set between 4 to 10 days according to sulfate consumption. From the second to the last cycle, the setup was done with addition of 0.05 liter of MM, where sulfate

concentration of 900 and 3000 mg $S\text{-}SO_4^{2-}$ L^{-1} was prepared for batches 2 to 4 and 5 to 8, respectively. Lastly, for the last batch, 0.05 liter of MM was added while 0.05 liter of culture medium was removed to keep the liquid level in 1-L.

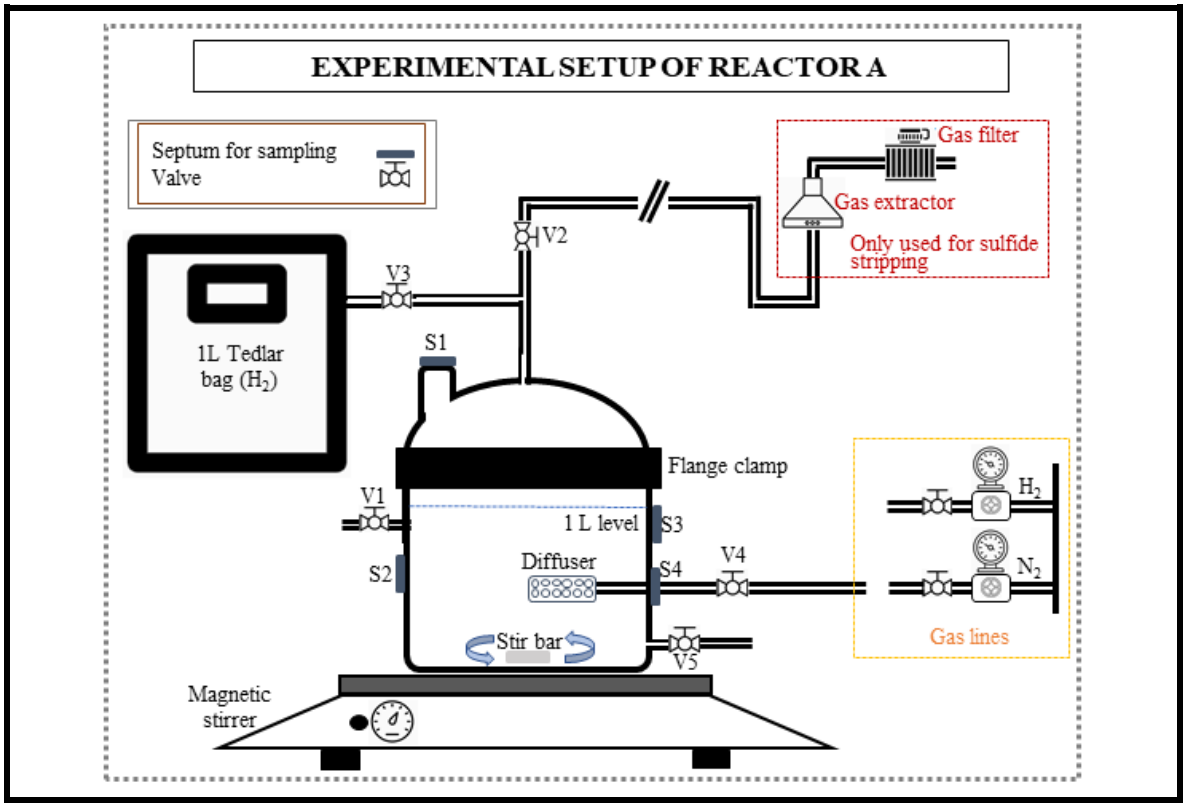

Figure 4.2. Experimental setup of reactor A. This reactor was placed on a magnetic stirrer at 180 rpm. A 1-liter Tedlar bag was filled with H_2 while H_2S stripping was done by bubbling N_2 and using a gas extractor device (red configuration). Gas samples were taken from the Tedlar bag, while liquid samples were taken from V5.

To avoid H_2S accumulation and H_2 limitation along each feeding cycle, H_2S-stripping and H_2-refilling were done as every two days as follows: the 1-liter Tedlar bag was emptied. Next, N_2 and H_2 were bubbled for 10 and 5 minutes, respectively, keeping valve V3 closed and valve V2 opened. Then, the bag was refilled with H_2. Furthermore, liquid samples were taken daily and at the beginning of each batch to track sulfate consumption in an Ion Chromatography (IC), and gas phase was sampled at the end of each batch to measure methane (CH_4) production in a Gas Chromatography (GC). The specifications of the IC and GC are shown in Chapter 3 (section 3.3).

After reactor A operation, 0.9 liters of culture medium were mixed with 4.1 liter of MM containing 500 mg $S\text{-}SO_4^{2-}$ L^{-1} to inoculate reactor B (Figure 4.3). This reactor was a 10-liter

glass bottle that was placed on a magnetic stirrer at 180 rpm and room temperature (~20°C) using a 3-liter Tedlar bag connected on the top for H_2 filling. In that way, the operation was performed in a fed-batch way like in reactor A. It was started up with 5-L and each consecutive feeding cycle was performed with the addition of 0.5 liter of MM with a total of 11 cycles. MM had a sulfate concentration of 2500 and 5000 mg $S\text{-}SO_4^{2-}$ L^{-1} for batches 2 to 9 and 10 to 11, respectively.

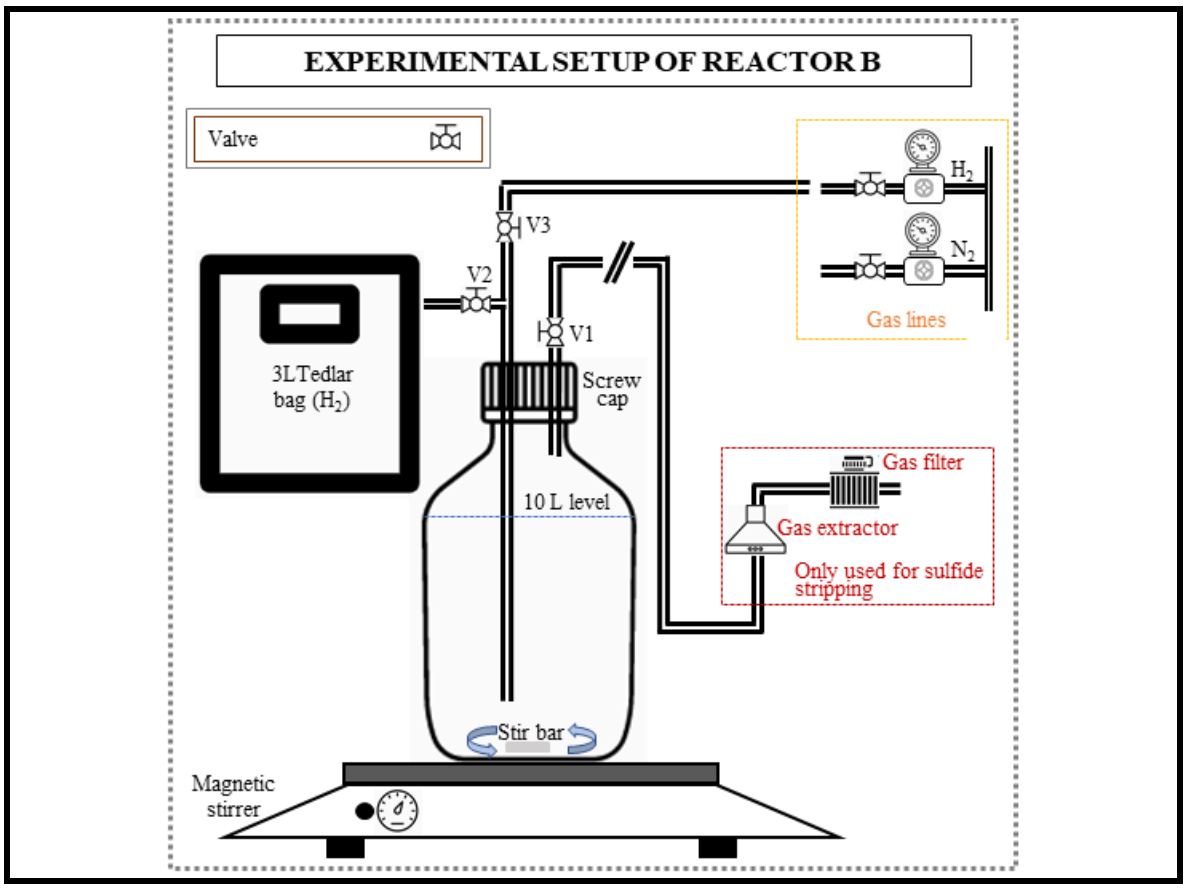

Figure 4.3. Experimental setup of reactor B. The reactor was placed on a magnetic stirrer at 180 rpm. A 3-liter Tedlar bag was filled with H_2 while H_2S stripping was done by bubbling N_2 and using a gas extractor device (red configuration).

Batch duration was set up according to the sulfate consumption, and the experimental operation was done with valve V1 and V3 closed. Also, H_2S-stripping and H_2-refilling were done every 2 days in the following sequence: the 3-liter bag was emptied; then, N_2 and H_2 were bubbled for 10 and 5 minutes, respectively, keeping Valve V2 closed while V1 and V3 opened. Finally, the bag was refilled with H_2. Finally, liquid samples were taken daily and at the beginning of each feeding cycle to track sulfate consumption with an IC; meanwhile, gas

samples were taking at the end of each batch to identify methane production with a GC.

4.3.2. Results of sulfate consumption and biomass growth for the operations of reactors A and B

The performance of reactor A is shown in Figure 4.4 A and B, and the performance of reactor B is shown in Figure 4.4 C and D. In Figures 4.4 A and C are plotted the volumetric sulfate loading rate (SLR), the accumulated sulfate load rate (ac-SLR, which was determined from the real initial sulfate concentration as it was accumulated from previous batches), the volumetric sulfate reduction rate (SRR), and the reactor liquid volume. Figures 4.4 B and D plot the TSS and VSS measured at the end of each batch; all figures are labelled with the same x-title, where batch number and batch duration (in brackets) are assigned.

Herein, the volumetric SLR was determined from the sulfate addition that was explained in section 4.3.1, i.e., it was based on the dilution of the sulfate added and the cycle duration. Meanwhile, the ac-SLR is resulting from the sulfate added and the remaining sulfate from the previous cycles, which means it was determined from the initial sulfate concentration and the batch duration. Furthermore, the SRR was determined from the sulfate consumed and the batch duration. These three variables were pointed out to avoid inaccurate interpretation as the volumetric SRR was higher than the SLR in some cycles due to the sulfate accumulation.

As seen in Figure 4.4A, the SRR in reactor A increased from 11 to 38 mg $S\text{-}SO_4^{2-}$ L^{-1} d^{-1} from the first to the last batch. In addition, VSS kept on an average concentration of 419±11 mg L^{-1} (Fig. 4.4B) with a net increase of 141 mg of VSS while the liquid volume was increased from 0.7 to 1 liter along the 8 batches. Also, H_2 was in an average of 64±12 % V/V while CH_4 was not detected in the gas phase at the end each batch. This could lead to the conclusion that methanogens were inhibited and it was attributed to the addition of BES in the MM, as mentioned in section 4.3.1.

Then, 0.9 liters of culture medium were taken from reactor A after batch eight to inoculate reactor B. In this case, the SRR increased from 5 to 142 mg $S\text{-}SO_4^{2-}$ L^{-1} d^{-1} (Figure 4.4C) and the VSS concentration increased from 68 to 190 mg VSS L^{-1}, with a net gain of 1558 mg VSS. VSS measurement was not available for batches 2, 8 and 10.

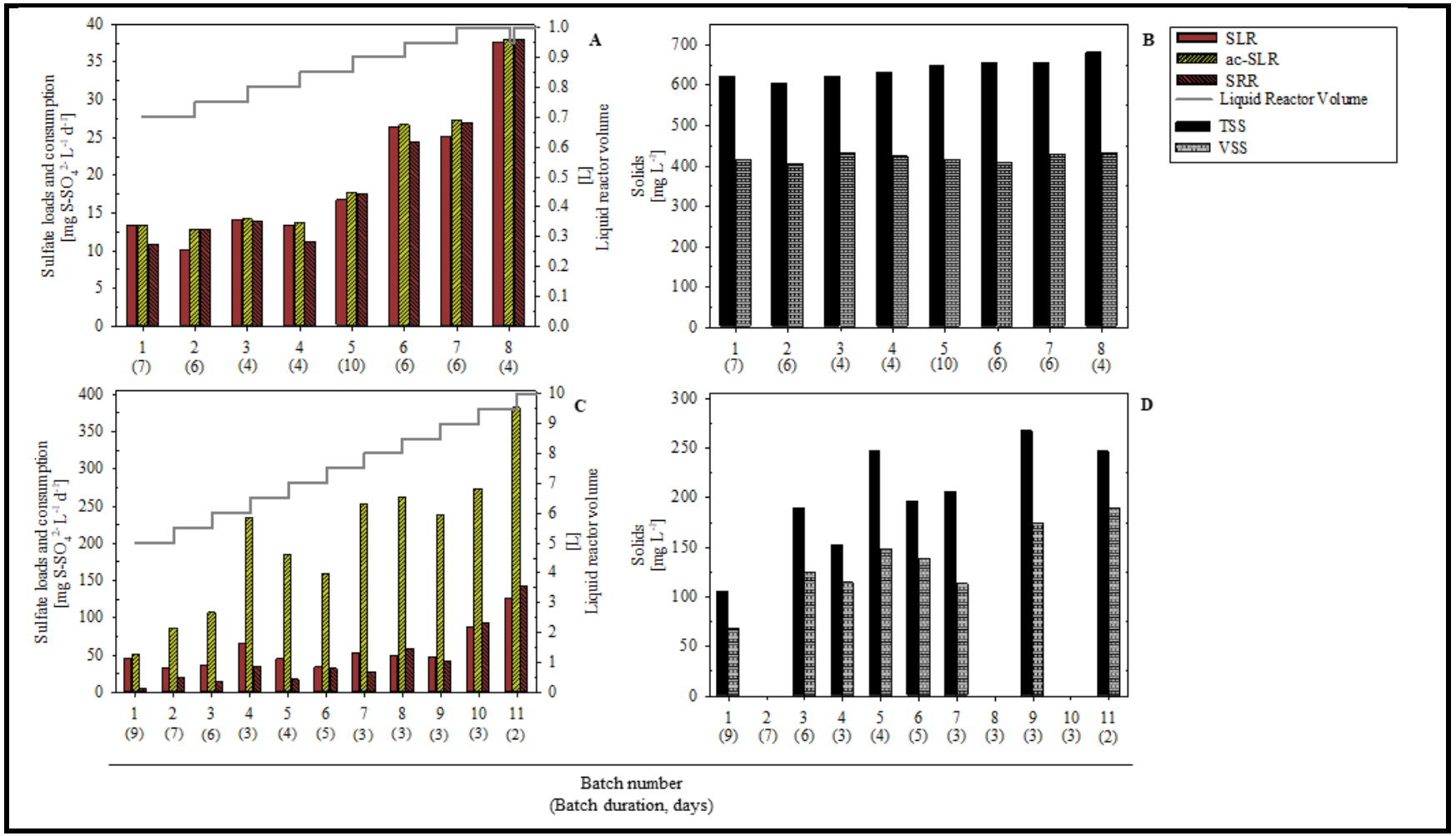

Figure 4.4. Performance of reactor A is shown in Figures A and B, and performance of reactor B is shown in Figures C and D. Figures A and C plot the SLR, the ac-SLR and the SRR on the left y-axis, while the liquid reactor volume is on the right y-axis. Figures B and D plot the TSS and VSS. All Figures are labelled with the same x-title, where there are expressed the batch number and duration (in brackets).

1

Finally, H_2 was in an average of 81±7 % V/V in the gas phase and CH_4 was not identified at the end of each batch, even when no BES was added in the MM, which means that methanogens were completely suppressed from the microbial culture.

After these experiments, 2-L of culture medium were taken from reactor B to inoculate the GLR. But before, the GLR was subjected to abiotic tests to assess liquid-gas mass transfer. For that reason, the abiotic tests will be introduced at first in the next section.

4.4. PRELIMINARY EXPERIMENTS IN THE GLR: ABIOTIC TESTS AND INOCULATION FOR KINETIC STUDY

4.4.1. GLR setup

The experimental setup of the GLR is shown in Figure 4.5. The reactor had CO_2 and H_2 inlet lines connected to two Bronkhorst digital mass flow controllers (DMFC) of 0-15- and 0-50-ml min^{-1}, respectively, and an alternative N_2-inlet line connected to a Bronkhorst mass flow controller of 0-50 L min^{-1}. The latter was only used for the abiotic tests. All mass flow controllers were installed with a ball check valve to avoid reversed flow, and they were connected to a flowmeter power supply (Power Supply +15V dc-2A, IberFluid Instruments SA) and to a computer that had a custom-made software (ADD Control, Labwindows/CVI 2017© National Instruments)[99] that acquires and controls the process variables.

Moreover, the gas line also contained a recirculation with a liquid trap for possible liquid overfilling due to clogging or foam formation. This liquid trap consisted in an empty standard 0.5-liter glass bottle (with a total volume of 0.605 liters) sealed with a screw cap that had two openings, for inlet and outlet. Thus, the total gas volume was 0.94 L. The recirculation and inlet lines were connected to a peristaltic pump (Masterflex, model 77200-60) and this latter to the gas inlet of the GLR. Right after the peristaltic pump, a coalescing filter element was installed to remove liquid droplets (Nylon housing with borosilicate glass filter, 710N-70C Headline Filters). Also, neoprene tubing (Masterflex™ Norprene™ L/S™ Precision Pump Tubing, inner diameter 7.9 mm) was used for gas pumping, while semi-rigid plastic tubing (Nalgene tubing of 5 mm inner diameter) was used for the rest of the gas line.

As seen in Figure 4.5, the gas outlet system included a sulfide trap to avoid hydrogen sulfide emissions and was arranged in two sulfide-capture steps; the first was composed of an impinger where sulfide was bubbled in a 2 M NaOH solution, and the second one

comprised a plastic bottle filled with a symclosene-based (Trichloroisocyanuric acid: $C_3Cl_3N_3O_3$) and granulated solid where the gas had to pass through.

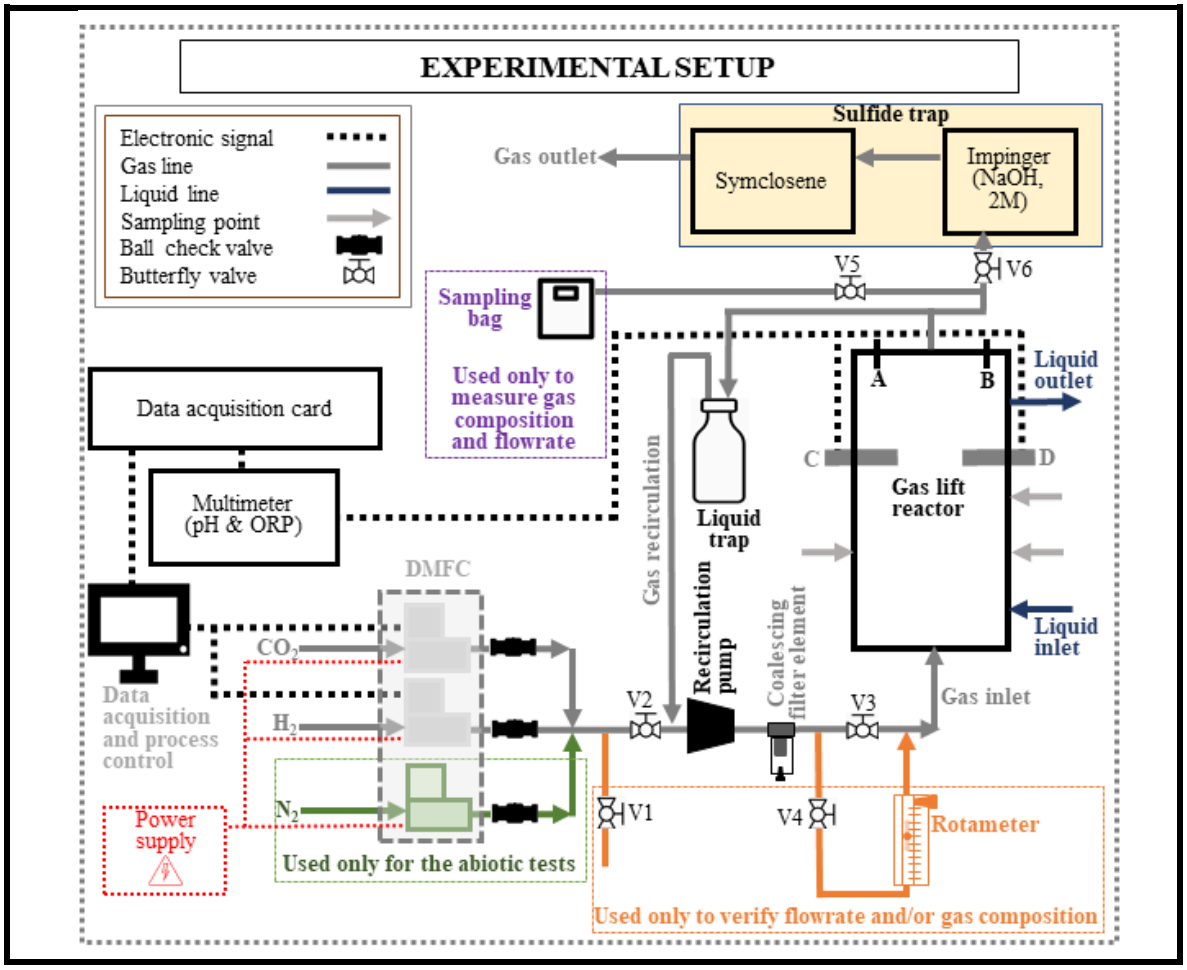

Figure 4.5. Experimental setup of the GLR. The reactor was setup with a H_2 and a CO_2 gas inlet lines using mass flowmeters; an alternative N_2-line for abiotic tests (green configuration); a gas recirculation line coupled with a liquid trap to avoid liquid accumulation in the gas lines; a Tedlar bag for gas sampling (purple configuration); a two-step sulfide trap to avoid H_2S emissions (yellow configuration); and a rotameter to measure total gas flowrate (orange configuration). Data acquisition of online parameters, pH, ORP or dissolved H_2, was used.

Furthermore, the orange configuration in Figure 4.5 was used to measure the gas flowrate and composition after H_2 and CO_2 mixing in the inlet; the purple configuration was used to sample the gas in the outlet. 1-liter Tedlar bag (FlexFoil 1-liter Sample Bag SKC) was used for gas sampling.

Regarding the reactor configuration, it is detailed in Chapter 3 (section 3.1). It had two openings for probe placing (C and D, Figure 4.5), where a pH (CRISON 5333) and oxidation-reduction potential (ORP, CRISON 5353) probes were placed for experiments in the GLR.

Meanwhile, a H_2-probe was only used in the GLR during the abiotic tests as this sensor had interference from H_2S and could be damaged from large H_2S exposure.[100]

The pH- and ORP-probes were connected to a Multimeter (MultiMeter 44 Crison). This latter was connected to a data acquisition card (PCLD-8710, DIN-rail Wiring Terminal Board) mounted in a computer for data logging and processing. The liquid inlet and outlet lines were set up according to the operation type.

Finally, the ADD Control software was used for data logging of pH and ORP, to set up H_2, CO_2 and N_2 flowrates, and to set up the pump cycles in the sulfide online-monitoring experiments (Chapter 6).

4.4.2. Assessment of the liquid-gas mass transfer in the GLR

Experimental layout

The abiotic tests to characterize the gas-liquid mass transfer under different H_2-inlet and gas recirculation flowrates are specified in Table 4.1. A total of nine combinations were evaluated in duplicate, resulting in eighteen abiotic tests. The H_2-inlet flowrates were set up with the H_2-DMFC mentioned in section 4.4.1, while the recirculation flowrates were determined with a rotameter (orange configuration in Figure 4.5) by closing Valve 3 and opening Valve 4, and were obtained from three pump positions, i.e., positions 4, 6, and 8 in Table 4.1, that ranged from a low to high power capacity of the recirculation pump.

These tests were performed with tap water at room temperature (~20°C) and aimed at determining K_La_{H2} through the dynamic gas in-gas out method that has been reported previously;[101] in which H_2 was bubbled until saturation and then, N_2 was bubbled to reach H_2-free water to proceed with the next experiments.

In this case, CO_2-inlet line was closed, while the alternative N_2-line was used in cycle with the H_2-line. Also, the gas line was operated by closing valves 1, 4 and 5 and opening valves 2, 3 and 6 (Figure 4.5), while the liquid inlet and outlet were closed along the experiments. Moreover, a H_2-probe (Unisense H2-NP, hydrogen needle sensor of 6 mm) was used to measure dissolved H_2 online during abiotic tests. The probe was placed in position D (Figure 4.5) with a plastic cover of 9 mm diameter to protect sensor needle from damage and measurement noise due to bubbling. Data was recorded by connecting the probe to a Unisense microsensor multimeter, and the latter to a computer where SensorTrace logger (Unisense

software) was used for probe polarization, calibration, and data logging. As suggested by the H_2-probe supplier,[100] the sensor was polarized at +1000 mV until signal stabilization, i.e., 12 to 15 hours, and then, a two-point calibration was done for hydrogen zero and saturation concentrations. Thus, a 250 mL glass bottle filled with 0.1 liter of tap water (~20°C) was used for the calibration, where zero concentration was determined by recording H_2-probe signal after bubbling N_2 for 15 minutes, while H_2-saturated concentration was obtained after bubbling H_2 until the potentiometric signal was stable.

Table 4.1. Experimental combination of the gas recirculation and the H_2-inlet flowrate set up to determine the global H_2-mass transfer coefficients in the GLR.

Gas in-gas out experimental combination

	Recirculation pump		
	Position 4 [2 L min^{-1}]	Position 6 [2.3 L min^{-1}]	Position 8 [3 L min^{-1}]
Inlet H_2-flowrate [ml H_2 min^{-1}]	10	10	10
	25	25	25
	50	50	50

Then, Equation 4.1, that defines the H_2-mass transfer to the liquid phase,[102] was used to estimate the K_La_{H2} through a custom-made code (developed in Matlab R2021a) that used the function *fminsearch*.

$$\frac{d[H_2]_{liq}}{dt} = K_L a_{H2} \cdot \left([H_2]_{sat} - [H_2]_{liq}\right) \qquad \text{Equation 4.1}$$

In Equation 4.1 the left side represents the rate of H_2-transfer to the liquid phase, in mg H_2 L^{-1} d^{-1}, which depends on the K_La_{H2}, the H_2-saturation concentration $[H_2]_{sat}$, and the hydrogen concentration in the liquid phase $[H_2]_{liq}$. The K_La_{H2} estimation was done with the mathematical integration of Equation 4.1, where $[H_2]_{sat}$ was set as the maximum concentration obtained in each experiment.

Assessment of H_2-mass transfer coefficient

Abiotic tests results are shown in Figure 4.6, where each subplot title labels the gas

recirculation pump position (4, 6 and 8) with the H_2-inlet flowrate (in mL min^{-1}: 10, 25 and 50) set up for the experimental result plotted. Subplots in the same raw share the same y-axis and subplots in the same column share the same x-axis. Besides, the red and blue color graphs represent the first and second repetitions of each experiment, while dotted and line graphs depict the experimental values and the model prediction, respectively.

In terms of the experimental profiles of H_2 concentration, saturation curves described higher deviations in the repetitions of experiments 6-25, 8-10 and 8-25, which could be explained by the fact that in those experiments, the repetitions were carried out in different days; therefore, they were performed with different preliminary calibrations that could have led to different correlation of sensor signal and assigned concentration in the calibration of each repetition due to the intrinsic difficulties of the calibration with H_2 standards. Thus, an error may have been added in the linear correlation between sensor signal and H_2 concentration, but not in the saturation curve profile, as the latter is mainly governed by bubble size, gas hold-up, turbulence and liquid properties.[103] Nevertheless, it does not necessarily mean that the K_La_{H2} estimation may not have errors.

Hence, the estimations of the H_2-mass transfer coefficients, in d^{-1}, are shown in Table 4.2, where experimental repetitions are displayed with the corresponding mean ($\bar{x}$) and standard deviation (SD). For these K_La_{H2} estimation, the error associated with the H_2-probe response time was neglected. This assumption was done from a study reported in the literature that suggests that sensor response time must be lower or equal to $1/K_La_{H2}$ to neglect its error associated in the determination of mass transfer coefficients.[104,105] In this work, if the highest K_La_{H2}, 92.8±4.2 d^{-1} (see Table 4.2) is used as a reference, the resulting threshold value is 0.0108 d (931 s), while the H_2-probe has a response time lower than 10 s.[100] Therefore, it could be considered that the H_2-probe response time does not have influence in the determination of the K_La_{H2}.

Regarding the results, the K_La_{H2} increased when H_2-inlet flowrate was increased for each recirculation rate; these outcomes were unexpected as the H_2-inlet flowrates were significantly lower than the recirculation rates which made difficult to have an impact on the aforenamed parameters that control the resulting K_La_{H2}.

Meanwhile, the K_La_{H2} increased when recirculation rate was increased from 2 to 2.3 L min^{-1} for each H_2-inlet flowrate, but the opposite occurred when recirculation rate was

increased from 2.3 to 3 L min^{-1} (Table 4.2). The former is explained from the fact that an increase in the gas flow rate increases the superficial gas velocity, the liquid circulation in the mixing zone of the reactor and therefore the mass transfer coefficient.[106] Yet, large superficial gas velocity could end up switching the reactor behavior from a well-mixed to a plug-flow hydrodynamic. This has been studied through a hydrodynamic parameter called Bodenstein number (Bo) that depends on the liquid superficial velocity and an axial dispersion coefficient, i.e. the larger the Bo number the higher the plug-flow hydrodynamic,[107] which means that for superficial gas velocity large enough, the liquid superficial velocity increases and also the Bo parameter. As the Bo number relies heavily on the reactor configuration: crossed-sectional area of downcomer and riser, reactor height, size of gas diffusion, mixing zone and three-phase separator, and the gas and liquid superficial rates, a deeper study is needed to fully understand the GLR hydrodynamic.

Table 4.2. Global H_2-mass transfer coefficients (K_La_{H2}, units in d^{-1}). They were determined for three different H_2-inlet flowrates and three different gas recirculation flowrates. Experiments were done in duplicate, and repetitions are labelled as Exp1 and Exp2. The K_La_{H2} mean values with the standard deviation are also shown.

Inlet flowrate	Pump position 4 (2 L min^{-1})			Pump position 6 (2.3 L min^{-1})			Pump position 8 (3 L min^{-1})		
	Exp1	Exp2	Mean	Exp1	Exp2	Mean	Exp1	Exp2	Mean
[mL H_2 min^{-1}]	K_La_{H2} [d^{-1}]								
10	30.8	33	31.9±1.5	41	48.5	44.7±5.3	54	33	43.5±15
25	34.9	36.6	35.8±1.2	73	72.3	72.7±0.5	39.3	52.6	46±9.4
50	46.7	52.1	49.4±3.8	95.8	89.9	92.8±4.2	47.2	64	55.6±12

Besides that, pump position 6 (recirculation flowrate was 2.3 L min^{-1} and H_2-inlet flowrate was 50 ml min^{-1}) were selected for the sulfate reduction study in the GLR as this combination resulted in the highest mass transfer coefficient: 92.8±4.2 d^{-1} (Table 4.2).

Finally, the experimental measurements could have errors associated to the probe signal as the probe supplier warns. These errors are associated to the H_2-probe mounting such as movement, vibration, and electrical/mechanical equipment.[100] Yet, they were not possible to avoid in the GLR setup as the recirculation pump, the flowmeter power supply and other equipment were fundamental to carry out the abiotic experiments.

1

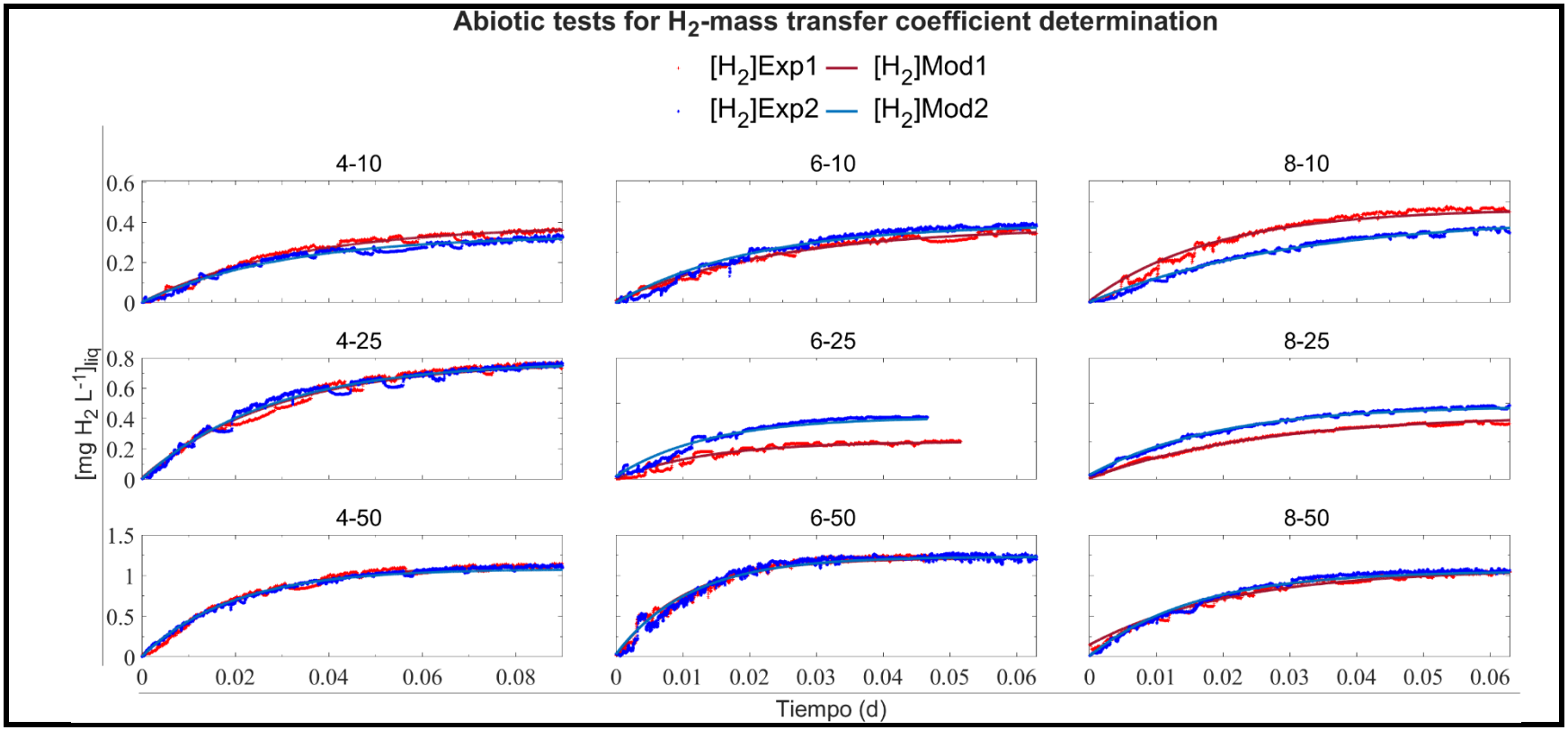

Figure 4.6. Results of the abiotic tests performed in the GLR to determine the K_La_{H2}. A total of 9 different H_2-inlet and gas recirculation combinations were evaluated in duplicate (red and blue figures). The plot subtitles represent recirculation pump position (4, 6, 8, which are equivalent to the flowrates shown in Table 4.1) and H_2-inlet flowrates (in mL min^{-1}: 10, 25, 50). Dotted graphs represent experimental values while line graphs represent model predictions (through K_La_{H2} estimation).

4.4.3. GLR inoculation and start-up for biomass growth and sulfate reduction enhancement

Experimental layout

From the results of the abiotic tests, the H_2-inlet and gas recirculation flowrates were set up to 50 mL min^{-1} and 2.3 L min^{-1}, respectively. The carbon source was supplied at a flowrate of 10 mL CO_2 min^{-1} to mimic typical H_2 and CO_2 fraction in syngas as this latter is a common and feasible residual source used in scale-up processes.[4,11,36] Inoculation was performed with 2 liters of the culture medium of reactor B, which had a sulfate concentration of 480 mg S-SO_4^{2-} L^{-1}, and 4.75 liter of MM containing 100 mg S-SO_4^{2-} L^{-1}. Operation was studied for 3 months in a total of ten batch cycles. From cycles 2 to 10, the same amount of MM added was removed from the reactor culture medium. The addition was as follows: 0.3 and 0.5 liters of MM containing 5000 mg S-SO_4^{2-} L^{-1} were added for batches 2 to 5 and 6 to 7, respectively, while 0.5 liters of MM containing 7000 mg S-SO_4^{2-} L^{-1} were added for batches 8 to 10.

Additionally, three materials were used to evaluate biofilm formation based on the fact that plastic materials,[108] sand,[109] and pumice,[49,110] have been reported in the literature as supporting materials for biofilm formation. Therefore, particle size was classified with testing sieves with diameter of 2.5, 0.7-1.2, 0.3-0.7 mm, respectively, and a total of 150 g of each material were added in the reactor at the inoculation. Regardless the addition of these materials to evaluate the biofilm formation, the latter was not observed in complementary experiments after the three months of operation and therefore it is not covered in this work.

Liquid samples were taken every two days to measure the sulfate concentration in an IC, gas samples were taken once a week to measure the gas composition in a GC, and solids were measured at the end of each batch.

Overall performance of the GLR along the startup period

The results of the GLR operation are shown in Figure 4.7. Figure 4.7A shows the SLR, the ac-SLR, the SRR and the liquid reactor volume, while TSS and VSS are plotted in Figure 4.7B. Both figures share the same x-axis, where cycle number and cycle duration (in brackets) are labelled.

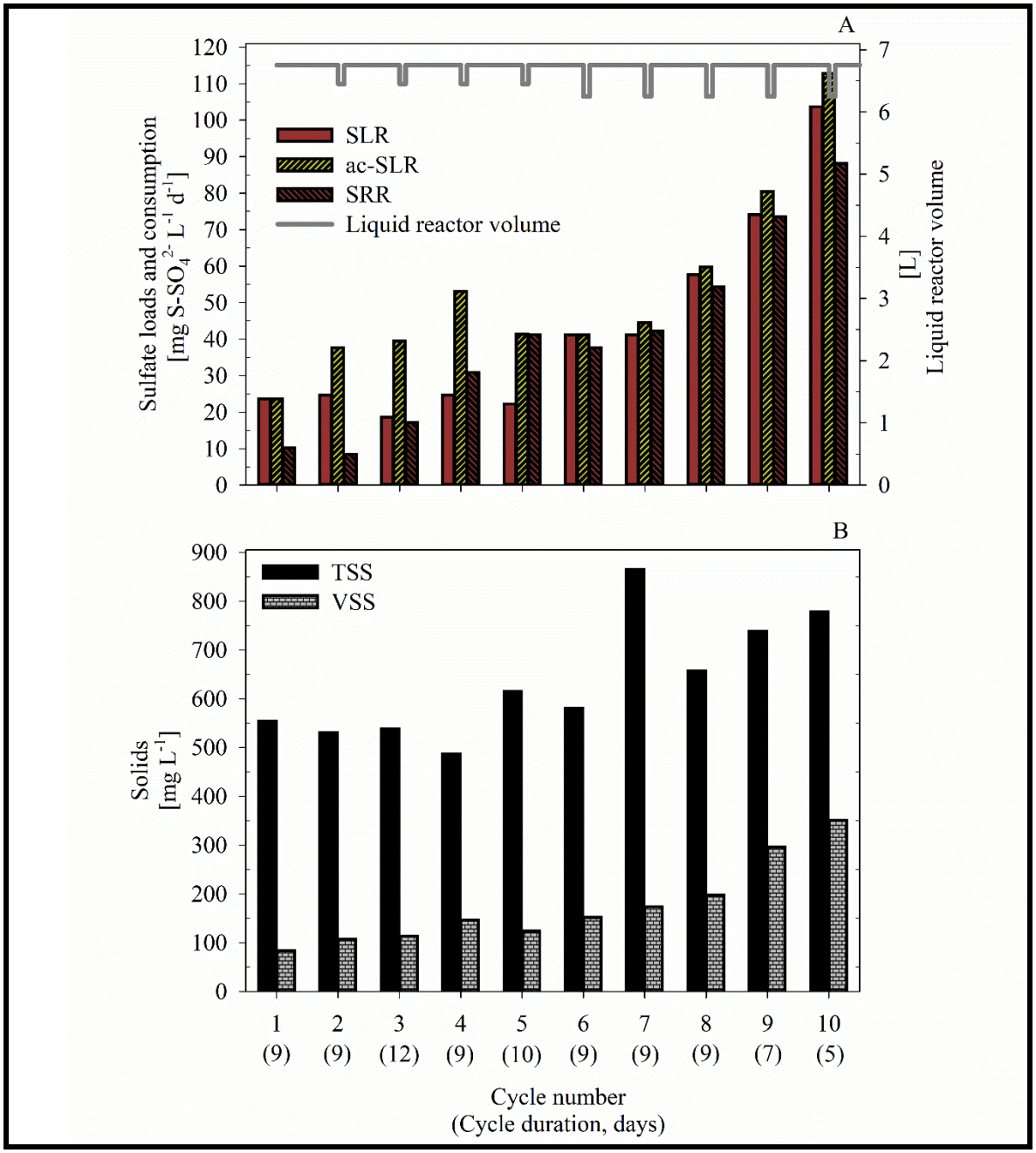

Figure 4.7. Experimental result of the GLR where 10 cycles were performed. In Figure 4.7A, the volumetric SLR, the sulfate accumulated load and the volumetric SRR are plotted on the left y-axis, while liquid reactor volume is plotted on the right y-axis. TSS and VSS are plotted in Figure 4.7B. Both figures shared the same x-axis, where cycle number and duration (in brackets) are labelled.

The SRR increased from 10 to 88 mg SO_4^{2-} L^{-1} d^{-1} (Figure 4.7A), and VSS increased from 80 to 350 mg VSS L^{-1} (Figure 4.7B), from the first to the last batch; also, H_2 concentration was 85±2 % V/V and no CH_4 was identified in the gas phase. The outcome in

terms of the SRR shows that after 88 days of operation in the GLR, the volumetric SRR was lower than the results obtained in the last batch of reactor B. An observed yield defined as the ratio of the added-up mass of total sulfate consumed, in mg $S\text{-}SO_4^{2-}$, and the added-up mass of total VSS produced, in mg VSS, accounted in the whole operation of each reactor can be used to compare the three reactors; this observed yield was 4.9, 8.0 and 8.4, in mg $S\text{-}SO_4^{2-}$ mg^{-1} VSS, for reactors A, B and GLR, respectively. A larger increase in the ratio was obtained from reactor A to reactor B that suggests a H2-SRB selection over other microorganisms; but comparing reactor B and the GLR, it was almost constant. This may indicate that the GLR operation did not show a significantly improvement in terms of H2-SRB selection, and neither in the volumetric SRR. Moreover, these observed yields are significantly lower than the stoichiometric yield of H2-SRB that is 20 mg $S\text{-}SO_4^{2-}$ mg^{-1} VSS.[78] A result that could be due to cell debris accumulation that ended up accounting in the VSS measurement, and/or kinetic activity of other microorganisms.

Another observable aspect between the three reactors operation is the VSS/TSS fraction; while it was 0.66±0.02 and 0.67±0.07 in reactors A and B, respectively, for the GLR this fraction decreased to 0.27±0.1. This reduction is explained from the addition of sand and pumice particles as supporting material to evaluate biofilm formation that increased the non-volatile solid fraction. Nevertheless, biofilm was not observed in related experiments and therefore this part was not covered in this work as mentioned above.

At this point, to have a broader comprehension of the H2-SRB activity, it was decided to characterize the microbial culture through kinetic experiments and microbial diversity identification. These experiments are the scope of the next section.

4.4.4. Characterization of H2-SRB kinetic and microbial diversity identification

Experimental layout

A set of tests were developed to evaluate the kinetic parameters of the H2-SRB, to fully characterize the sulfate reduction activity and to identify the microbial community in the broth culture. The batch experiments performed in the GLR aimed at determining the maximum specific growth rate ($\mu_{max.SRB}$) and the sulfate half-saturation constant (k_{ST}).

A total of nine batch tests were performed in the GLR with the initial sulfate

concentration shown in Table 4.3. Concentrations were set up using different sulfate-stock solutions. The sulfate concentration was measured every 0.5 hours during the first 2.5 hours of each experiment, while the initial sulfate concentration reached through dilution was determined by mass balance. Solids were measured in duplicate after the 2.5 hours of each experiment. Even when sulfate was tracked for the first 2.5 hours, each batch was run until complete sulfate consumption.

Table 4.3. Batch experiments in the GLR to characterize the kinetics of sulfate reducing microorganisms. A total of 12 batches were performed with an initial sulfate concentration shown in the last column.

Batch	Sulfate stock-solutions [mg $S\text{-}SO_4^{2-}\ L^{-1}$]	Volume added [L]	Initial sulfate concentration in the GLR [mg $S\text{-}SO_4^{2-}\ L^{-1}$]
1	250	0.05	2
2	500	0.12	9
3	1250	0.06	11
4	2000	0.085	25
5	2000	0.115	34
6	2000	0.15	44
7	2000	0.22	65
8	5000	0.12	89
9	5000	0.185	137

During these experiments, a pH- and an ORP-probes were placed in position C and D of the GLR (Fig. 4.5) to analyze the sulfate activity with the environmental conditions in the reactor. For the kinetic parameter determination, the SRR in each batch was determined by a linear regression of the sulfate consumption along time, and from there, the specific sulfate reduction rate (s-SRR), i.e., rate of sulfate consumption per VSS in the reactor, was also determined. Then, s-SRR can be mathematically related to the sulfate concentration by the Monod Equation,[111]. Through a custom-made code (developed in Matlab R2021a) that used an *fminsearch* function, the $\mu_{max.SRB}$ and k_{ST} were estimated. No sulfide inhibition was considered as the total dissolved sulfide (TDS) kept below 20 mg TDS L^{-1} during these batches. After these experiments, samples were taken from the suspended broth culture for DNA extraction and sequencing following the protocol already reported in the literature.[56]

The detailed information about this procedure is explained in Chapter 3 (section 3.3).

Kinetic study in the GLR and microbial identification

The results of these batch experiments are shown in Figure 4.8, where the volumetric SRR (Figure 4.8A) and the VSS concentration (Figure 4.8B) per batch are depicted; for both figures the x-axis is shared and labelled with the number of experiments, and this latter was organized in an increasing sulfate concentration evaluated at the beginning of each batch (Table 4.3). The volumetric SRR was determined from a five-point linear regression of the sulfate profile over time. The R-square coefficient of determination (R^2) was always above 0.98.

The results show that the VSS was in an average of 315±14 mg VSS L^{-1} throughout the experiments and for the last four experiments, 6 to 9, where the initial sulfate concentration was evaluated from 44 to 137 mg S-SO_4^{2-} L^{-1} (Table 4.3), the SRR was over 100 mg S-SO_4^{2-} L^{-1} d^{-1}, with an average of 115±16 mg S-SO_4^{2-} L^{-1} d^{-1}. This outcome is higher than the SRR in the last batch cycles of reactor A (Figure 4.4A) and the GLR start-up experiments (Figure 4.7A), but still lower than the SRR in the last batch reactor B (Figure 4.4C). The low sulfate reduction activity can be analyzed from the environmental conditions in the GLR. The pH, ORP and temperature were 7.40±0.05, 199±9 mV and ~20°C, respectively, along the batches. From one side, sulfate reducing microorganisms have been reported to work optimally in a pH range of 6.5 to 8.5,[4,36] indicating that no problem shall be associated to the pH in the GLR. On the other side, optimal temperatures at mesophilic conditions over 32ºC have been reported for sulfate reducing microorganisms (SRB).[36,112] Yet, the easy adaptation of SRB has also been reported with a temperature tolerance between -5 to 75ºC.[36]

Furthermore, this outcome is significantly lower than some remarkable results reported in the literature, as seen in Table 4.4. Van Houten et al., have obtained high volumetric SRR of 3300 and 5000 mg S-SO_4^{2-} L^{-1} d^{-1} using syngas in GLRs, and 6000 mg S-SO_4^{2-} L^{-1} d^{-1} using H_2/CO_2 in a GLR (see Table 4.4). Meanwhile, Bijmans et al,[97] used a GLR and obtained a volumetric SRR of 1600 mg S-SO_4^{2-} L^{-1} d^{-1} using H_2/CO_2 in acidic condition to favor metal sulfides recovery.

On the other hand, Sousa et al.,[54] and Nevatalo et al.,[113] reported values in the order of magnitude of the results in this work (Table 4.4); while the first studied autotrophic sulfate reduction at low temperature, at 9ºC, and halo-alkaline conditions in a GLR to treat sulfate-rich and inorganic streams, the second aimed at treating acid mine drainage streams at low temperatures and pH. Nevertheless, these results are still higher than the obtained in this work. Regarding the ORP, it has not been extensible correlated to predict optimal environmental conditions for biological sulfate reduction. Nevertheless, lower ORP of -220 mV,[114] and -290 mV,[115] have been reported ideal reduction environments for the predominance of sulfate reducing microorganisms.

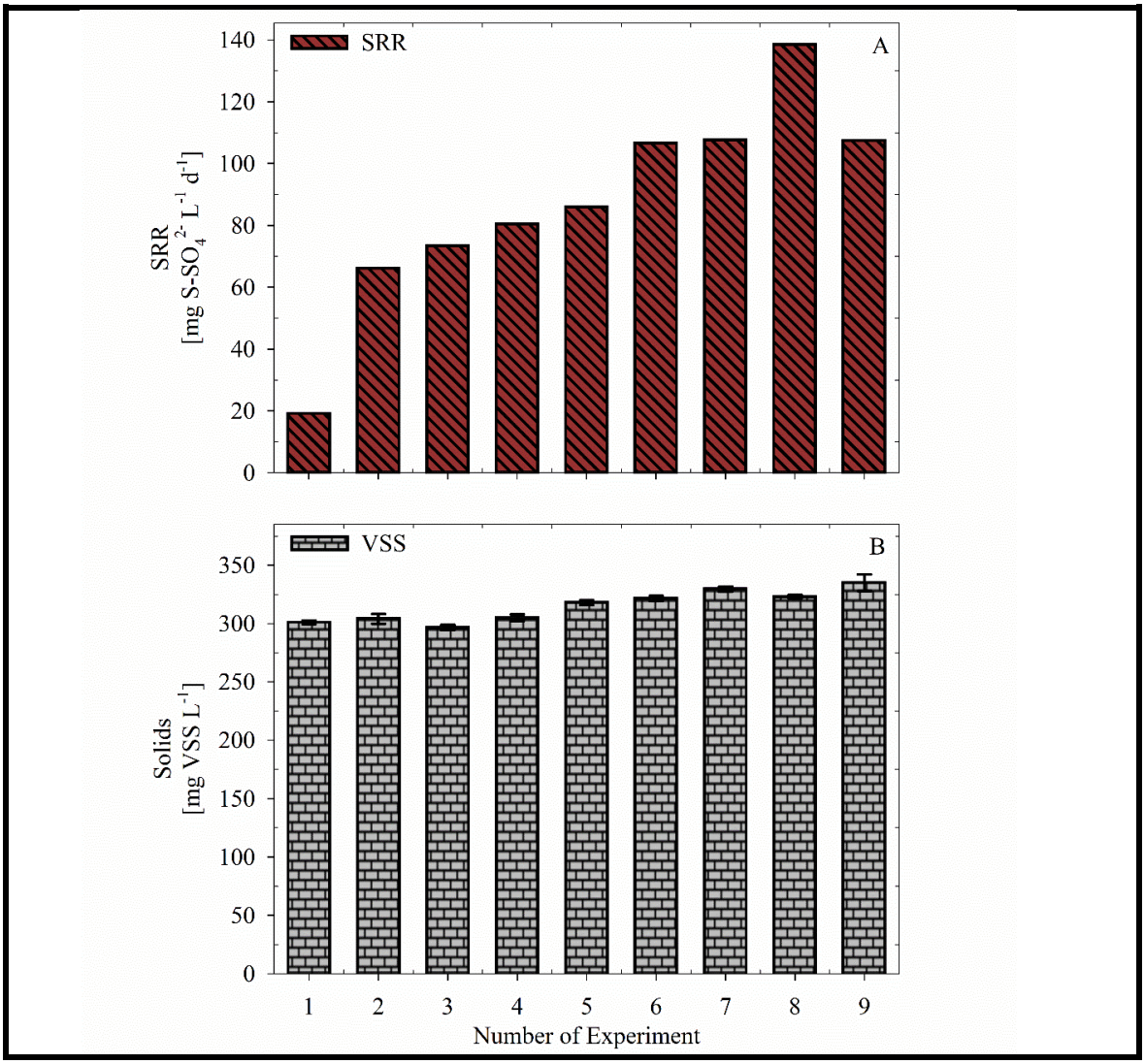

Figure 4.8. Experimental result of the batch tests in the GLR. Figure 4.8A shows the volumetric SRR and Figure 4.8B shows the VSS concentration per batch.

Thus, to analyze if there was a mass transfer limitation, the K_La_{H2} was used as a reference to determine the maximum volumetric hydrogen transfer to the liquid phase and based on the stoichiometry of hydrogenotrophic sulfate reduction (Equation 2.3 of Chapter 2), the maximum and theoretical hydrogenotrophic SRR (SRR_{max_th}) can also be estimated. Therefore, the theoretical and maximum H_2 mass transfer could be estimated when $[H_2]_{liq}$ is zero (from equation 4.1), and considering that the H_2 gas fraction is 0.83, as it is in the gas inlet according to the H_2 & CO_2 flowrates in the GLR (section 4.3.3), and the Henry constant for hydrogen (H_{H2}) at 20ºC is $2.72 \cdot 10^{-4}$, in atm L solution mg^{-1} H_2,[47] the maximum H_2-mass transfer will be 126 mg H_2 L^{-1} d^{-1}, which will be equivalent to a SRR_{max_th} of 504 mg S-SO_4^{2-} L^{-1} d^{-1}, assuming that all hydrogen is consumed by H2-SRB to reduce sulfate. Herein, even when this estimation is done from the assumption of zero hydrogen concentration in the liquid phase and a hydrogen volumetric fraction equal to the gas inlet dilution, it is still useful to set the maximum H_2 mass transfer, as a $[H_2]_{liq}$ higher than zero or the present of other compounds in the gas phase, e.g., H_2S, will both decrease the H_2 mass transfer. Also, the same argument leads to conclude that H_2-mass transfer is not necessary in the maximum value during the GLR operation.

Table 4.4. Remarkable results of the volumetric SRR reported in the literature compared to the results of the GLR in this work.

Feeding source	pH	T [ºC]	Volumetric SRR [mg S-SO_4^{2-} L^{-1} d^{-1}]	Reference
Syngas	7	30	3300	Van Houten et al.,[54]
Syngas	7-7.5	30-35	5000	Van Houten et al.,[116]
H_2/CO_2	7	30	6000	Van Houten et al.,[98]
H_2/CO_2	5	30	1600	Bijmans et al,[97]
H_2/CO_2	9	35	576	Sousa et al.,[54]
H_2/CO_2	7.5	9	200	Nevatalo et al.,[61]
GLR	7.4	20	115±16	This work

Accordingly, H_2-limitaiton was unlikely based on the estimated SRR_{max_th}, the low sulfate reduction rates obtained in the GLR, and the high H2-SRB affinity to H_2.[44] Thence, the analysis was focused on determining the kinetic parameters of H2-SRB in the reactor

based on Equation 4.2, in which hydrogen limitation was not considered, neither H_2S-inhibition as the sulfide concentration in the experiments was always below 20 mg TDS L^{-1}.

Equation 4.2 represents a single Monod kinetic expressed for sulfate consumption; in which, [S- SO_4^{2-}] is the sulfate concentration, in mg S-SO_4^{2-} L^{-1}. $Y_{SRB|H2}$ is the stochiometric yield between H2-SRB and H_2, in mg VSS mg^{-1} H_2, that is 0.34.[96] 4 is the stoichiometric yield between S-ST and H_2, in mg S-ST mg^{-1} H_2, (Equation 2.3 of Chapter 2).[37] Finally, s-SRR is the aforesaid specific sulfate reduction rate, in mg S-ST VSS^{-1} d^{-1}.

$$\text{s-SRR}=\frac{4}{Y_{SRB|H2}}\cdot\mu_{max.SRB}\cdot\frac{[\text{S-SO}_4^{2-}]}{k_{ST}+[\text{S-SO}_4^{2-}]} \qquad \text{Equation 4.2}$$

The s-SRR was determined from the volumetric SRR and VSS measured for each experiment (Figure 4.8A and B). Then, s-SRR was related to the initial sulfate concentration in each batch, as seen in Figure 4.9, to analyze the sulfate affinity and maximum growth rate of the H2-SRB, i.e., estimation of $\mu_{max.SRB}$ and k_{ST}, from the Monod model represented in Equation 4.2, which results are also depicted in Figure 4.9.

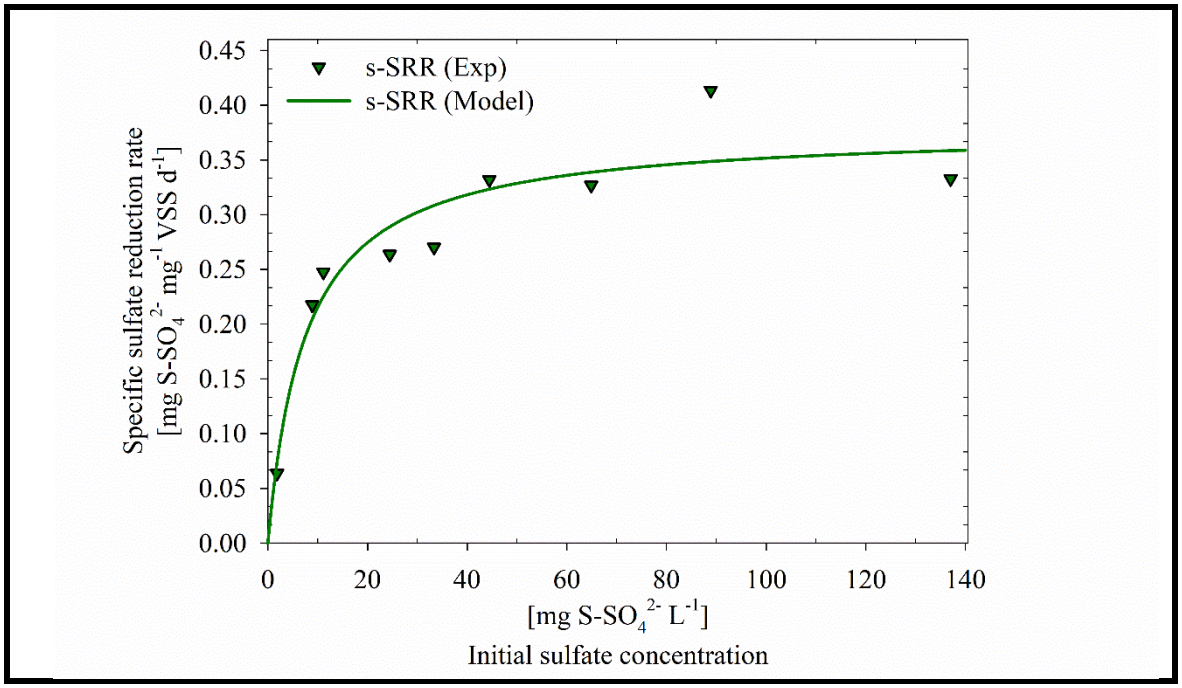

Figure 4.9. Experimental s-SRR and model prediction of s-SRR per initial sulfate concentration in each batch. The inverted triangles represent the experimental values and the solid green line the model estimation.

In Figure 4.9, the experimental and model s-SRR per batch are shown and the adjusted $\mu_{max.SRB}$ and k_{ST} were 0.0325 d^{-1} and 7.6 mg $S\text{-}SO_4^{2-}$ L^{-1}, respectively. The former suggests that for a continuous operation where no solid retention takes place, i.e., equal hydraulic (HRT) and solid retention time (SRT), the duplication time is 31 days, and therefore, the HRT should be higher than this value for the microbial proliferation of H2-SRB. Due to this low $\mu_{max.SRB}$ and as no biofilm formation was observed, the continuous operation was discarded for further experiments.

Other works have reported $\mu_{max.SRB}$ higher than the current estimation, as it is the case of Tang et al.,[95] Spanjers et al.,[77] Kalyuzhnyi et al.,[83] and Federovich et al.,[96]: 0.3, 1.9, 2.8 and 5 d^{-1}, respectively; whereas in the same works, the k_{ST} were: 0.5, 6, 6.4 and 0.3 mg $S\text{-}SO_4^{2-}$ L^{-1}, respectively. Tang et al.,[95] and Federovich et al.,[96] reported high sulfate affinity, while Spanjers et al.,[77] and Kalyuzhnyi et al.,[83] obtained k_{ST} values akin to the k_{ST} of this work. Finally, the kinetic analysis and the environmental conditions can be analyzed together with the microbial distribution obtained from the Illumina test. The results are shown in Figure 4.10, where the taxonomy is displayed in relative abundance (%) of genus level. Also, the exploded slices in the Figure correspond to the identified genus belonging to sulfate reducing, methanogenic, and homo-acetogenic microorganisms.

Results show that five genera that accounted 29.2% of the total identified hits belong to sulfate reducing microorganisms: *Sulfurospirillum*, *Desulfovibrio*, *Desulfocurvus*, *Desulfomicrobium* and *Desulfobulbus*. Meanwhile, 1.4% of the total identified hits belong to the genus *Methanobrevibacter*, which has been classified as hydrogenotrophic methane producers;[117] yet, even when methane was not measured during these kinetic experiments, it was measured for the operation of reactor A and B, and during the inoculation and start-up period of the GLR where methane was not identified (section 4.3.2 and 4.4.3).

Similarly, homo-acetogens of the genus *Acetobacterium* has been detected with a relative abundance of 1.1% of the total identified hits; species of this genus have been reported in H_2/CO_2 fed reactors growing symbiotically with sulfate reducing microorganisms.[118] Nevertheless, as acetate was not measured, the present of the *Acetobacterium* genus in the Illumina results does not imply homo-acetogenic activity.

The Unclassified group accounted for 10.2% where the non-identified hits to the genus level are gathered, while the microorganisms labelled as Others accounted for 11.1%, where

all the genera that accounted less than 1% were included. As mentioned before, CH_4 was not detected in the start-up of the reactor operation (section 4.4.3), while acetate was not measured so far, which suggests, from the first, that some cell debris could arise in the DNA extraction and then in the Illumina results, and from the second, that acetate production shall be quantified.

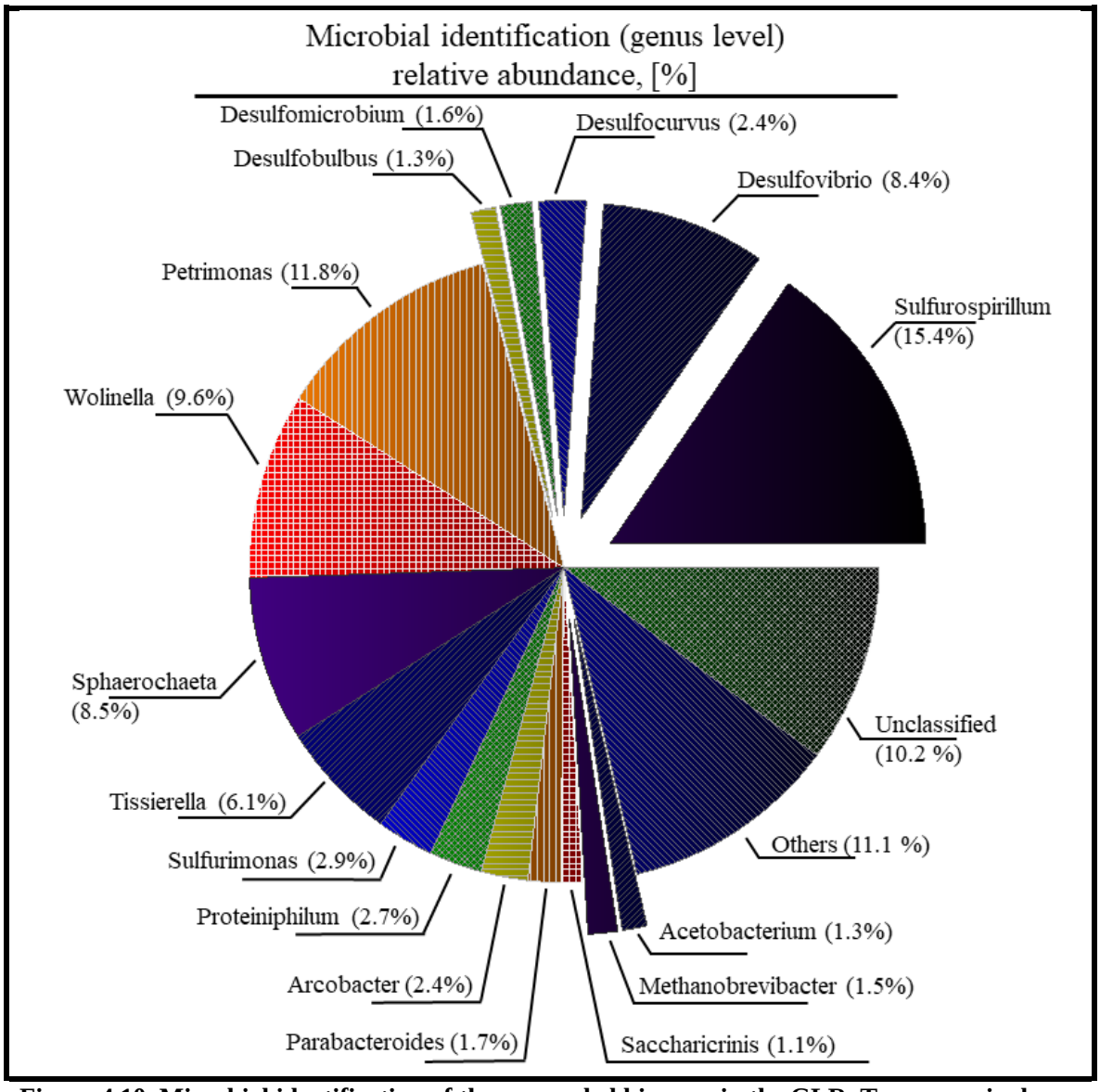

Figure 4.10. Microbial identification of the suspended biomass in the GLR. Taxonomy is shown genus level and the relative abundance in percentage (%). Genus with a relative abundance lower than 1% were accounted as Others and exploded slices represent the identified sulfate reducing, methanogenic and homo-acetogenic microorganisms.

Additionally, the results also show large quantities of fermentative-type microorganisms as it is the case of species from the genus *Petrimonas*,[119,120] *Sphaerochaeta*,[121] *Tissierella*,[122] *Proteiniphilum*,[123]Parabacteroides,[124] and *Saccharicrinis*,[125] with a total relative abundance of 31.9%; meanwhile, a relative abundance of 9.6% of the genus *Wolinolla* was detected, from which species have been reported as non-fermentative microorganism that can reduces fumarate with hydrogen sulfide as electron donor.[126]

Lastly, trace fraction of genus *Sulfurimonas* and *Arcobacter* were detected with a relative abundance of 2.9% and 2.4%, respectively. In that other, species from the genus *Sulfurimonas* can use, as electron donor and acceptor, the couple thiosulfate/nitrate or sulfide/oxygen, in the dissimilatory pathway, but it has been reported to grow with thiosulfate and H_2/CO_2,[127] which is according to the GLR operation; and lastly, species from the genus *Arcobacter* are chemoorganotrophic that can grow aerobically or anaerobically.[128]

Overall, it is important to remark that even when the Illumina test aims at detecting the microbial population, it does not reflect the microbial activity and thereby the microorganisms identified may have not been growing; a perspective that is according with the absence of organic source in the reactor feeding. Therefore, their present can be explained from the sludge source that came from a UASB reactor where fermentative microorganisms are normally present.

4.4. MAIN CONCLUSIONS

The biological sulfate reduction growth with H_2/CO_2 has been done in a biomass enrichment process, using two STRs and a GLR that was previously characterized in terms of the gas-liquid mass transfer. The results suggests that methanogens were fully washed out from the microbial culture that was brought from a CH_4-producing UASB reactor. Even though, the highest SRR was 142 mg $S\text{-}SO_4^{2-}$ L^{-1} d^{-1} achieved in reactor B, in the GLR it was 115±16 mg $S\text{-}SO_4^{2-}$ L^{-1} d^{-1}.

The results in the GLR suggests that the SRR is far from being limited by the H_2-mass transfer, as based on the abiotic tests, the maximum hydrogen transfer is 126 mg H_2 L^{-1} d^{-1}, which is equivalent to a maximum sulfate reduction of 504 mg $S\text{-}SO_4^{2-}$ L^{-1} d^{-1}, for an assumed unique hydrogen consumption by H2-SRB.

Finally, the microbial identification shows a 29.2% relative abundance of identified SRB, and a large fraction of fermentative microorganisms that may be dragged from the inoculum; this could also be the reason of the identified methanogenic and homo-acetogenic microorganisms, but these two latter with a low relative abundance of less than 2% for each case.

The results show that is not feasible to set up the reactor in a continuous operation as it will demand large HRT.

CHAPTER 5

STUDY OF THE SULFATE REDUCTION IN A SEQUENTIAL BATCH OPERATION

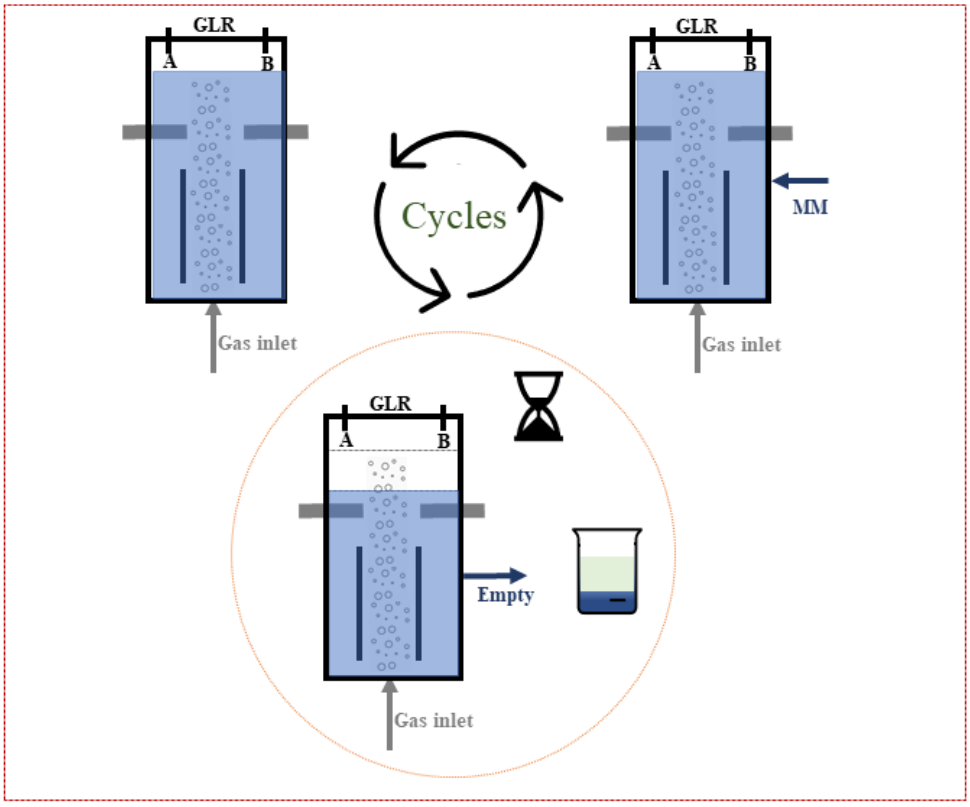

5.1. CHAPTER OUTLINE

The hydrogenotrophic sulfate reduction was studied previously in the two stirred-tank reactors (STRs) and the gas-lift reactor (GLR) as discussed in Chapter 4. Hydrogenotrophic sulfate reducing microorganisms (H2-SRB) were grown and selected in the STRs, after which no CH_4 production was observed. Thus, two set of experiments were performed to increase the volumetric sulfate reduction rate (SRR) and to characterize the process kinetics. The first set of experiments in the GLR in Chapter 4 consisted of a startup period of 10 sequential batches where the SRR increased from 10 to 88 mg SO_4^{2-} L^{-1} d^{-1}. The second set of experiments in the GLR in Chapter 4 showed that the highest SRR was 115±16 mg $S\text{-}SO_4^{2-}$ L^{-1} d^{-1} and the maximum specific growth rate of the H2-SRB ($\mu_{max.SRB}$) was 0.0325 d^{-1}. This means that a hydraulic residence time (HRT) over 31 days would be needed if a continuous operation was intended, since biomass did not granulate in the system and the reactor had no settling unit, i.e., the sludge residence time (SRT) was equal to the HRT. The low sulfate reduction activity in the second set of experiments in Chapter 4 was attributed to the low biomass concentration and the environmental conditions. The pH and the oxidation-reduction potential (ORP) were monitored online, and these parameters were 7.4±0.05 and -199±9 mV, respectively. No problem was associated from the pH as sulfate reducing microorganisms have been reported to work optimally in a pH range of 6.5 to 8.5.[4,36] No extensive evidence was found in the literature about reducing environment to favor sulfate reduction, but the moderate ORP could have been due to traces of O_2 in the reactor.

Therefore, the sulfate reduction is studied in Chapter 5 in the GLR operated as a sequential batch reactor (SBR) with sludge recovery aiming at increasing the SRR. Accordingly, Chapter 5 is organized as follows: a brief presentation in this section 5.1; all the experimental procedures regarding the sequential batch operation are described in section 5.2; the results of the sequential batch operation are provided in section 5.3 in this order: 1) the sulfate reducing activity throughout the sequential batch operation in the GLR, 2) the acetate production and the chemical oxygen demand (COD) distribution in the effluent, and 3) the DNA extraction and microbial population distribution in different stages of the operation. Discussion of the results and their comparison with other literature reports are presented in section 5.4; finally, the general conclusions are established in section 5.5.

5.2. EXPERIMENTAL LAYOUT

5.2.1. Process setup and analytical tools

The sequential batch operation consisted of two main steps in each cycle: the batch operation for the biological sulfate reduction and the sedimentation for solids recovery. The operation comprised batches for sulfate reduction that were set up to last 21 to 22 hours, after which part of the culture medium was taken from the reactor for solids sedimentation as described in Figure 5.1. The reactor was kept at room temperature (~20ºC), pH and ORP were not controlled but monitored online as explained in section 4.4.1. During the batches, liquid samples were taken 2 to 3 times to measure the total dissolved sulfide (TDS) and sulfate. One of these samples at the end of each batch was taken for acetate, total suspended solids (TSS) and volatile suspended solids (VSS) analysis. In Figure 5.1, S_{end} and Sol_{end} represent the concentration of the soluble and solid components at the end of each batch; the former refers to TDS, sulfate ($S\text{-}SO_4^{2-}$) and acetate, while the latter refers to TSS and VSS.

During the reactor partial draining at the end of each batch, a 3-liter tedlar bag filled with H_2 was connected to the headspace of the reactor to fill with H_2 the liquid volume removed, to avoid O_2 leaking inside the reactor. This was done through valve 5 keeping valve 6 closed as seen in Figure 4.5 (Chapter 4). Moreover, the removed liquid was settled outside the reactor to avoid clogging of the glass-porous plate (gas diffuser of the GLR). This step consisted of removing 1.5 or 2.5 liters of the culture medium, V_{sed} in Figure 5.1, from the GLR to settle solids for 2 hours in a flask covered with parafilm to minimize sulfide loss due to volatility and oxygen dissolution. Then, 1 (for V_{sed} equals to 1.5 L) or 2 liters (for V_{sed} equals to 2.5 L) of the supernatant were discharged, and the remaining 0.5 liters of settled sludge, V'_{sed} in Figure 5.1, were mixed with 1 or 2 liters, respectively, of fresh mineral medium (MM) to be finally fed to the reactor to start a new cycle. The MM volume added to the reactor, which was equal to the volume of the discharged supernatant, was the liquid volume exchange (VE). MM contained sulfate and is represented as S_{added} in Figure 5.1.

The solids in the discharged supernatant, represented in Figure 5.1 as Sol_{dis}, were measured to quantify the VSS loss in the sedimentation step. Thus, the fraction of solids lost per cycle was determined from Equation 5.1, where $[VSS]_{dis}$ is the VSS concentration in the Sol_{dis} and $[VSS]_{end}$ is the VSS concentration at the end of the corresponding batch. Solids at

the end of each batch and in the discharged supernatant were measured in duplicate.

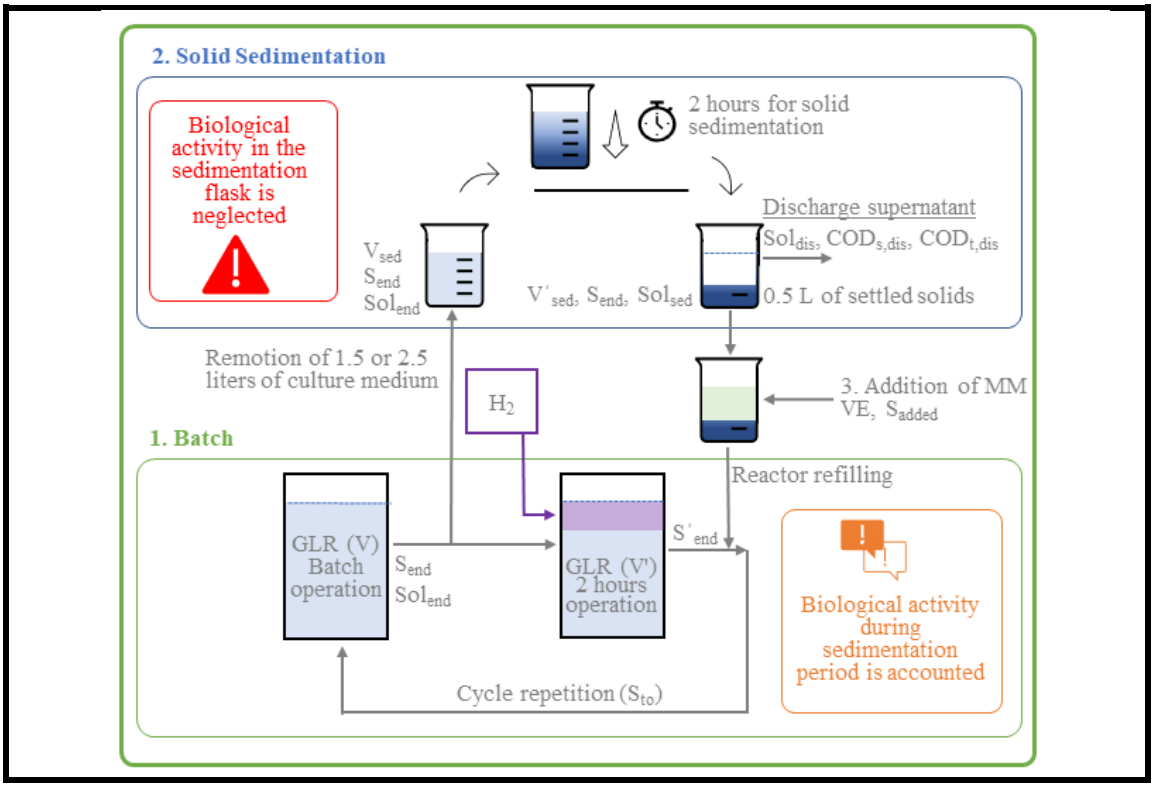

Figure 5.1. Sequential batch operation of the GLR. Reactor cycles were as follows: 1) Batch operation where sulfate reduction was tracked; 2) GLR partial draining to settle solids for 2 hours; and 3) MM refilling to start a new batch. Biological activity during sedimentation period was accounted in the GLR but not in the sedimentation flask.

Additionally, biological activity was not considered in the sedimentation flask and the concentrations of the soluble components at the end of sedimentation in the flask were assumed equivalent to the concentrations at the end of the batch in the GLR. This was proven during the first cycles of the sequential batch operation as the differences in the sulfate and TDS measurements at the end of a cycle and after the sedimentation period were lower than the Ion Chromatography (IC) and the commercial sulfide ion selective electrode (S^{2-}-ISE) errors.

$$\text{VSS loss}=\frac{[\text{VSS}]_{dis}\cdot VE}{[\text{VSS}]_{end}\cdot(VE+0.5L)}\cdot 100,\ [\%] \qquad \text{Equation 5.1}$$

On the contrary, biological activity was considered in the GLR during the sedimentation time as the reactor was continuously fed with H_2 and CO_2 in this period. For that reason, after

the 2 hours sedimentation period, a liquid sample was taken again from the GLR to measure TDS and sulfate, S'_{end} in Figure 5.1. Then, the resulting MM-sludge broth was returned to the reactor to start a new cycle where the initial sulfate and TDS, S_{to} in Figure 5.1, were estimated by dilution using Equation 5.2.

$$S_{to} = \frac{S'_{end} \cdot V' + S_{added} \cdot VE + S_{end} \cdot 0.5}{V} \qquad \text{Equation 5.2}$$

As acetate can be produced by homo-acetogenic microorganisms (homo-AC) from H_2 and CO_2 consumption, an HPLC was used to measure acetate and other volatile fatty acids (formate, propionate, butyrate, iso-butyrate, valeric and iso-valeric). The description of the HPLC analysis is shown in Chapter 3 (section 3.3). The acetate concentration was converted to the theoretical equivalent COD concentration determined from the complete oxidation with oxygen[129] according to its stoichiometric molar ratio of 1.07 g O_2 g^{-1} CH_3COOH (Equation 5.3).

Also, sludge settling could enhance solid accumulation in the reactor, where part of the solids was active biomass while others were inactive biomass that degraded into soluble compounds. This was evaluated from COD measurements from cycle 26 to the end of the operation. The total and dissolved COD in the discharged supernatant, $COD_{t,dis}$ and $COD_{s,dis}$ in Figure 5.1, respectively, were measured to determine the COD distribution of the effluent. These samples were measured with no pretreatment for the $COD_{t,dis}$, while samples were previously filtered with 0.22 µm pore-size hydrophilic polyether-sulfone (PES) filters for the $COD_{s,dis}$ measurement, as it was described in Chapter 3 (section 3.3). Also, the theoretical equivalence of COD and TDS (2 g O_2 g^{-1} S-H_2S) was considered from the complete oxidation with oxygen[129] defined in Equation 5.4. It has been reported that the experimental COD of sulfide accounts for ~87% (w/w) of the theoretical COD due to incomplete oxidation of sulfide during COD tests.[130] Therefore, the TDS/COD equivalence was established considering that the experimental COD accounted for 87% of the real TDS concentration. This TDS-COD conversion was used from cycle 26 to 60 to analyze the COD distribution.

$$CH_3COOH + 2O_2 \rightarrow 2H_2O + 2CO_2 \qquad \text{Equation 5.3}$$

$$H_2S + 2O_2 \rightarrow SO_4^{2-} + 2H^+$$ Equation 5.4

Thus, the COD distribution is herein presented as the acetate equivalent COD (COD-Acetate), the TDS equivalent COD (COD-TDS), the particulate COD (COD-Solids, determined as the difference between $COD_{t,dis}$ and $COD_{s,dis}$), and the unidentified dissolved-components COD (COD-Unidentified, determined as the subtraction of COD-TDS and COD-Acetate to the $COD_{s,dis}$).

Despite methane was not produced in the preliminary experiments (Chapter 4), the gas outlet was sampled once a week to measure the gas composition with gas chromatography (detailed in Chapter 3, section 3.3) as a low fraction of methanogens (1.5% relative abundance) was detected in the DNA sequencing at the end of the preliminary experiments in the GLR (Figure 4.10 of Chapter 4) and the sludge recovery set up for the current experiments could ended up in larger fractions of methanogens in the culture medium, and thereby CH_4 production.

DNA extraction and sequencing of the microbial community were performed in duplicate after cycles 14 and 56. The inoculum was previously sequenced for microbial identification as detailed in Chapter 4 (Section 4.4.4). Results are shown at genus level. For the microbial distribution, the identified hints of microorganisms associated with metabolisms different of homo-acetogenic, methanogenic and sulfate reducing activities, and hints with relative abundance smaller than 1% were clustered in group Others, while the unidentified hints at genus level were gathered as Unclassified.

Finally, all analytical methods and solutions are detailed in Chapter 3.

5.2.2. Operating conditions of the sequential batch operation under different SLR

For the sequential batch operation, the MM was bubbled with N_2 to avoid O_2 in the reactor during the inoculation period and the first 3 cycles, aiming at diminishing the oxygen concentration that would be the reason of the moderate low ORP discussed in Chapter 4 (section 4.4.4). The main information about the sequential batch operation is shown in Table 5.1. Eight different stages were considered for the total of 60 cycles performed as a function of the sulfate concentration in the MM, the VE, the expected initial sulfate concentration

($[S\text{-}SO_4^{2-}]_{added}$) in the GLR, the expected sulfate loading rate (SLR) and the total duration of each stage.

The sequential batch operation was performed with influent sulfate concentrations in the MM that ranged from 3375 to 7500 mg $S\text{-}SO_4^{2-}$ L^{-1} and resulted in SLR between 545 and 2424 mg $S\text{-}SO_4^{2-}$ L^{-1} d^{-1} except for stage V. In the latter, the operation lasted longer and the SLR was decreased. Due to the sulfate accumulation in the reactor, the accumulated sulfate loading rate (ac-SLR), i.e., the load determined from the real initial sulfate concentration $[S\text{-}SO_4^{2-}]_{to}$ in the GLR, was higher during some batches. SLR and ac-SLR were determined from Equation 5.5 and 5.6, respectively, where t_c represents a batch duration in days, and $[S\text{-}SO_4^{2-}]_{end}$ is the sulfate-form sulfur at the end of a batch. Similarly, the SRR was determined from Equation 5.7, and the specific sulfate reduction rate (s-SRR) from Equation 5.8, where $[VSS]_{end}$ is the volatile suspended solid concentration at the end of a batch cycle.

Table 5.1. Sequential batch operation of the GLR. A total of 60 cycles and 8 stages were evaluated with different SLR and were defined from the MM addition and VE.

Stage number	Batch	VE	Sulfate in the MM	SLR	Time
		[L]	[mg $S\text{-}SO_4^{2-}$ L^{-1}]	[mg $S\text{-}SO_4^{2-}$ L^{-1} d^{-1}]	[d]
I	1-3	1	3375	545	0-3
II	4-6	1	5063	818	3-6
III	7-11	1	6750	1091	6-15
IV	12-14	2	3375	1091	15-18
V	15	0.4	0	-	18-23
	16-19	0.4	32000	299±58	23-49
	20	2	5407	161	49-59
	21-25	0.26	16000	368±209	59-71
VI	26-30	2	7500	2424	71-78
VII	31-47	1	7500	1212	78-100
-	48	1	-	-	100-101
VIII	49-60	1	5575	902	101-113

Solid sedimentation was not performed from cycles 15 to 19 and 21 to 25 in which MM pulses of 0.4 and 0.26 liters were added, respectively, with the same volume of culture

medium removed. The sulfate concentration in the MM was 32000 mg $S\text{-}SO_4^{2-}$ L^{-1} for cycles 16 to 19 and 16000 mg $S\text{-}SO_4^{2-}$ L^{-1} for cycles 21 to 25. Sulfate was not added in cycles 15 and 48 as these were set up to reduce the sulfate accumulated in the reactor, and for cycle 20, sedimentation was done with a VE of 2 liters, and a MM sulfate concentration of 5407 mg $S\text{-}SO_4^{2-}$ L^{-1}. Also, samples were taken at the end of cycles 15 to 25 to measure sulfate, while TDS and solids were not monitored during this period.

$$SLR = \frac{[S\text{-}SO_4^{2-}]_{added}}{t_c} \quad \text{Equation 5.5}$$

$$ac\text{-}SLR = \frac{[S\text{-}SO_4^{2-}]_{to}}{t_c} \quad \text{Equation 5.6}$$

$$SRR = \frac{[S\text{-}SO_4^{2-}]_{to} - [S\text{-}SO_4^{2-}]_{end}}{t_c} \quad \text{Equation 5.7}$$

$$s\text{-}SRR = \frac{SRR}{[VSS]_{end}} \quad \text{Equation 5.8}$$

In terms of the GLR performance, the sulfate removal efficiency (Sulfate-RE), and the H_2S-stripping, i.e., the H_2S removed through the gas outlet, were calculated for each batch. Regarding the Sulfate-RE, it was determined from the sulfate consumption per cycle as described in Equation 5.9. Meanwhile, the H_2S-stripping per cycle was determined from Equation 5.10, and it is equivalent to the difference between the sulfate consumption, $\Delta[S\text{-}SO_4^{2-}]$ and the TDS increase, $\Delta[S\text{-}TDS]$.

The sulfate and TDS concentrations are reported in the equivalent sulfur concentration, $S\text{-}SO_4^{2-}$ and S-TDS, so that Equation 5.9 could be valid for the H_2S stripping determination.

$$Sulfate\text{-}RE = \frac{[S\text{-}SO_4^{2-}]_{to} - [S\text{-}SO_4^{2-}]_{end}}{[S\text{-}SO_4^{2-}]_{to}} \cdot 100, \, [\%] \quad \text{Equation 5.9}$$

$$H_2S\text{-}stripping = \frac{\Delta[S\text{-}SO_4^{2-}] - \Delta[S\text{-}TDS]}{\Delta[S\text{-}SO_4^{2-}]} \cdot 100, \, [\%] \quad \text{Equation 5.10}$$

Besides the results that are discussed in this Chapter, TDS was monitored online during stages I to III to validate a novel sulfide online monitoring system (Chapter 6).

5.3. PERFORMANCE OF THE SEQUENTIAL BATCH OPERATION OF THE GLR UNDER DIFFERENT SLR

5.3.1. Sulfate reducing activity throughout the sequential batch operation

The GLR was set up for a sequential batch operation after the kinetic evaluation described in Chapter 4 (section 4.4.4). A 5-day inoculation period was performed as follows. A volume of 3.5 liters of the culture medium was taken from the GLR to settle the solids for 2 hours. Afterwards, 3 liters of supernatant were centrifuged at 6000 rpm (BECKMAN, Avanti^{TM} J-20 Centrifuge), and then, the solids were recovered and mixed with the 0.5 liters of settled solids and 3 liters of fresh MM. The resulting broth was bubbled with N_2 for 15 minutes and returned to the GLR. The initial VSS concentration (173 mg VSS L^{-1}) was determined by dilution based on the concentration in the GLR at the end of the previous operation (335 mg VSS L^{-1}, section 4.4.4). The MM contained 1750 mg S-SO_4^{2-} L^{-1} and after 4 days, as sulfate was consumed, 0.5 liters of MM containing 5000 mg S-SO_4^{2-} L^{-1} were spiked in the reactor with the same amount of culture medium removed. On day 5 after inoculation, sulfate was completely consumed, acetate was not detected, the TDS concentration was 194 mg L^{-1} and TSS and VSS concentrations were 1140±99 and 318±2 mg L^{-1}, respectively. The low VSS/TSS fraction (0.28) was explained by the addition of inorganic packing materials in the preliminary experiments in the reactor (section 4.4.3).

Based on these conditions, the sequential batch operation was started as described in Table 5.1. Results of the sulfate concentration, the sulfate reducing activity, the TDS and solids concentrations are shown in Figure 5.2. The sulfate concentration at the beginning, $[S\text{-}SO_4^{2-}]_{to}$, and end, $[S\text{-}SO_4^{2-}]_{end}$, of each batch are shown in Figure 5.2A, together with the Sulfate-RE that was determined from Equation 5.9. The SLR, the ac-SLR, the SRR and the s-SRR are shown in Figure 5.2B; these parameters were determined as explained in section 5.2.2. The TDS concentrations at the beginning, $[TDS]_{t0}$, and end, $[TDS]_{end}$, of each batch, and the H_2S-stripping, are plotted in Figure 5.2C. The TSS and VSS concentrations at the end of each batch ($[TSS]_{end}$ and $[VSS]_{end}$, respectively), the VE per cycle, and the percentage of VSS loss in the effluent with respect to the total VSS in the sedimentation flask

(determined from Equation 5.1) are shown.

As mentioned in section 5.2.2, TDS and solids were not measured from cycles 15 to 25 and therefore, data from these cycles are not available in Figures 5.2C and 5.2D.

In stage I and II, sulfate did not accumulate in the reactor and the Sulfate-RE was over 95 % from cycle 1 to 5, but it dropped to 77 % in cycle 6. This took place with a raise in the SRR of 531±126 to 770±70 mg $S\text{-}SO_4^{2-}$ L^{-1} d^{-1} from stage I to stage II, while the s-SRR fluctuated in these periods with average rate of 1.6±0.3 mg $S\text{-}SO_4^{2-}$ VSS^{-1} d^{-1}. Meanwhile, TDS started to accumulate in the reactor as it increased from 287 to 621 mg TDS L^{-1} at the end of cycles 1 to 6. A similar trend was observed from the VSS that increased from 318±2 to 495±49 mg VSS L^{-1} at the end of cycles 1 to 6.

From stage III to IV, sulfate started to accumulate in the reactor with a concentration of 1963 mg $S\text{-}SO_4^{2-}$ L^{-1} at the end of cycle 14 while the SLR was stepwise increased (Table 5.1), and therefore, the ac-SLR started to be higher than the SLR; yet the SLR were lower for cycles 7 and 10 as these cycles lasted 2 and 4 days, respectively. This was followed by a decrease in the SRR, except in cycle 8 and 9, from cycle 7 to 14 that was also reflected in the Sulfate-RE (Figure 5.2A). The s-SRR decreased from cycles 6 to 11 but partially recovered from cycles 12 to 14 (Figure 5.2B). TDS accumulation increased until cycle 9 with a concentration of 1095 mg TDS L^{-1}, and then dropped to 322 mg TDS L^{-1} at the end of cycle 14 (Figure 5.2C). Similarly. the VSS concentration in the reactor increased to 610±14 mg VSS L^{-1} at the end of cycle 9, after which it started to decrease until 285±14 mg VSS L^{-1} at the end of cycle 14 (Figure 5.2D). Overall, from cycles 1 to 14, the VSS/TSS fraction was 38±5 %, the ORP -531±32 mV, and the pH raised from 7.4 to 8 from cycle 1 to 10, and then dropped to 7.6 until cycle 14. Sulfate was completely consumed during stage V, cycles 15 to 25, and therefore, the Sulfate-RE was 100%, thus leading to equal SLR, ac-SLR and SRR. The s-SRR, TDS and solids are not reported in this stage as solids and TDS were not measured during these cycles. The normal sequential batch operation including sludge settling was restarted in stage VI, in which the VE was 2 liters and the SLR was raised to 2463±186 mg $S\text{-}SO_4^{2-}$ L^{-1} d^{-1}. In this stage, the SRR increased from 674 to 825 mg $S\text{-}SO_4^{2-}$ L^{-1} d^{-1} while the s-SRR increased from 0.5 to 0.8 mg $S\text{-}SO_4^{2-}$ VSS^{-1} d^{-1}. However, the Sulfate-RE was only 16±7 % due to the sulfate accumulation.

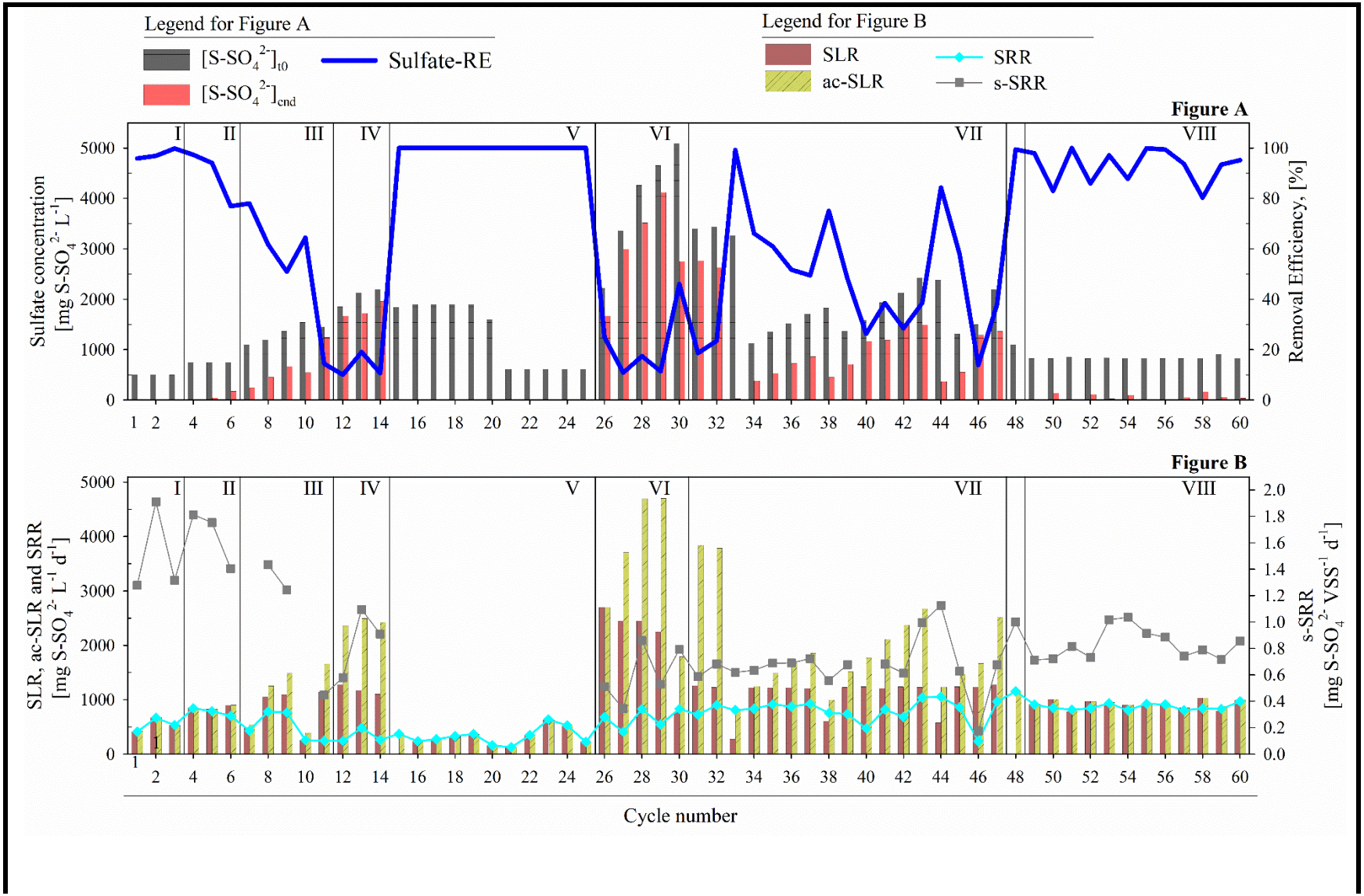
Legend for Figure A
[S-SO4 2-]t0
[S-SO4 2-]cnd
Sulfate-RE
Legend for Figure B
SLR
ac-SLR
SRR
s-SRR
Figure A
Sulfate concentration [mg S-SO4 2- L-1]
Removal Efficiency, [%]
I
II
III
IV
V
VI
VII
VIII
Figure B
SLR, ac-SLR and SRR [mg S-SO4 2- L-1 d-1]
s-SRR [mg S-SO4 2- VSS-1 d-1]
Cycle number

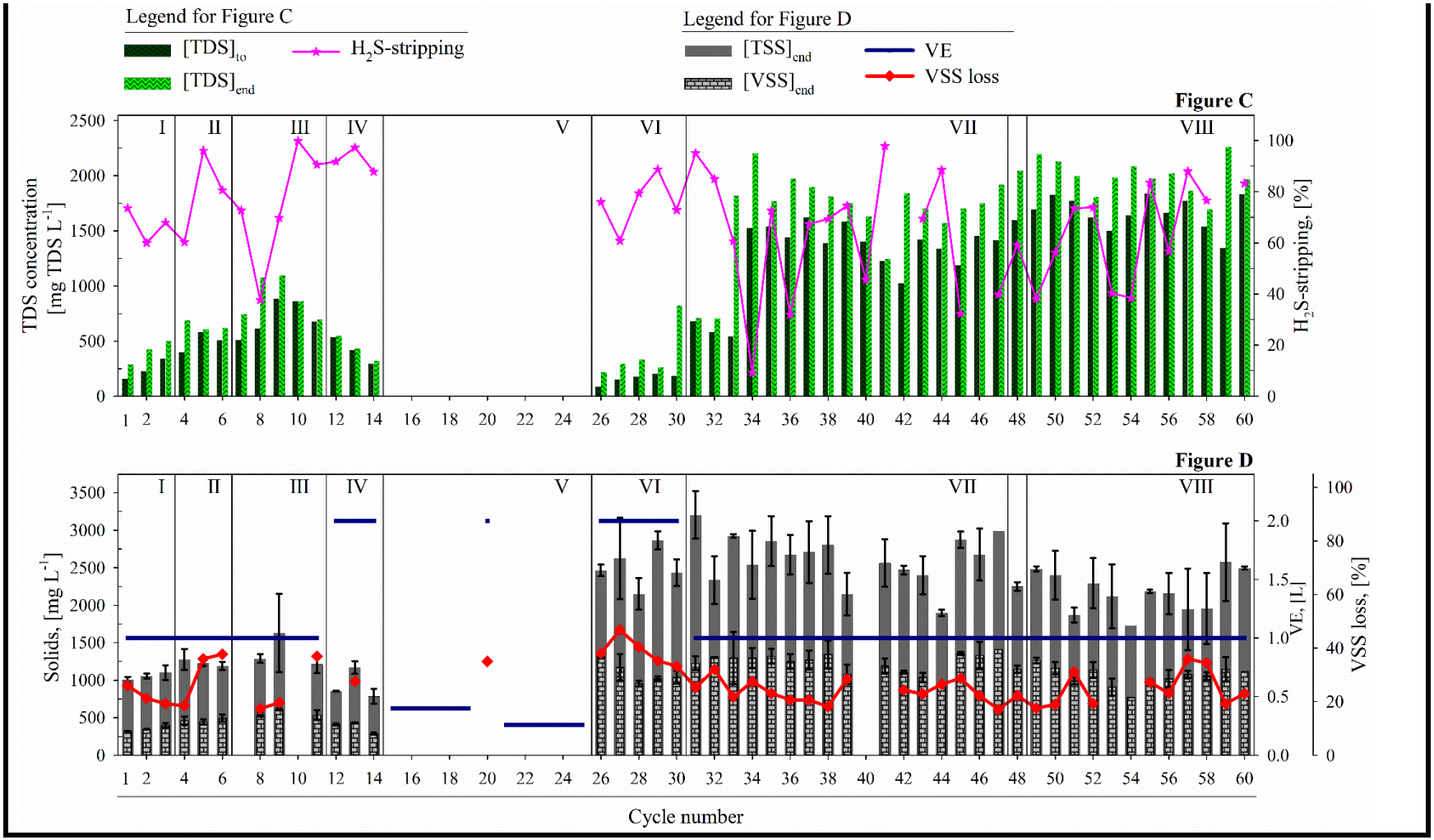

Figure 5.2. Results of the sequential batch operation of the GLR. Figure A: initial and final sulfate concentration per cycle and sulfate removal efficiency. Figure B: SLR, ac-SLR, SRR and s-SRR per cycles. Figure c: initial and final TDS concentrations per cycle. Figure D: solids (TSS and VSS), liquid VE and fraction of VSS loss.

Even though cycle 30 was set up for 3 days aiming at decreasing the sulfate accumulation in the reactor, the sulfate concentration was 2749 mg $S\text{-}SO_4^{2-}$ L^{-1} at the end of this cycle while TDS raised from 185 to 823 mg TDS L^{-1} in cycle 30. Due to the sulfate accumulation in the reactor, the VE was decreased to 1 liter for stage VII. The SRR was high along this stage except for cycles 40 and 46, with an average SRR of 851±109 mg $S\text{-}SO_4^{2-}$ L^{-1} d^{-1}. A similar trend was observed in the s-SRR that was 0.7±0.2 mg $S\text{-}SO_4^{2-}$ VSS^{-1} d^{-1}, also excluding cycle 40 and 46.

As in stage VI, TDS showed a slight increase from cycle 30 to 32 but, as cycle 33 lasted longer (4 days), the TDS largely accumulated in this cycle with a raise from 543 to 1818 mg TDS L^{-1}. From there to the end of stage VII, the TDS concentration was 1772±211 mg TDS L^{-1}. Moreover, the VSS concentration was 1233±133 mg VSS L^{-1} along stage VII, and the VSS/TSS fraction was 47±4 %.

Cycles 33, 38 and 44 were set up to last longer (4, 2 and 2 days, respectively) to decrease the ongoing sulfate accumulation. Since sulfate concentration in the reactor leaned to accumulate from stage III to VII, excluding stage V, meaning that the SLR was always higher than the SRR capacity of the system, cycle 48 was set up with no sulfate addition in the MM to consume the sulfate accumulated in the reactor. Hence, stage VIII was set up with a SLR of 919±78 mg $S\text{-}SO_4^{2-}$ L^{-1} d^{-1}. Sulfate barely accumulated from cycle 49 to 60, the Sulfate-RE was 93±7 %, while the SRR was 861±56 mg $S\text{-}SO_4^{2-}$ L^{-1} d^{-1} and the s-SRR was 0.8±0.1 mg $S\text{-}SO_4^{2-}$ VSS^{-1} d^{-1}. Overall, the SRR and the s-SRR had a similar trend from stages VI to VIII. The TDS concentration was 1998±161 mg TDS L^{-1} in stage VIII.

The pH was 8.10±0.10 and the ORP was -567±16 mV during stages VI to VII. Meanwhile, the pH was 8.20±0.03 and the ORP was -603±11mV for stage VIII; while the former was almost equal to the previous stages, the latter slightly decreased with respect to the previous stages. H_2S-stripping fluctuated along the whole operation. The sulfur mass balance for cycles 42, 46 and 59 was not correct, as TDS accumulation was higher than sulfate consumption, therefore, H_2S-stripping is not plotted for these cycles.

5.3.2. Acetate and COD distribution in the effluent

The results of the acetate concentration in the effluent, in COD-Acetate, along the sequential batch operation, and the COD distribution from cycle 26 to 60, are shown in Figure

5.3. The acetate and TDS concentration were converted to COD as explained in section 5.2.1. Acetate was not produced during the first 14 cycles, but it was largely accumulated in stage V, achieving the highest concentration of 14834 mg COD L^{-1} in cycle 23. After that, it decreased continuously, and it was not detected after cycle 46. In fact, a large quantity of COD-Unidentified was observed in stage VII, 44±10 % of the $COD_{s,dis}$, while the COD-TDS was 42±13 % of the $COD_{s,dis}$.

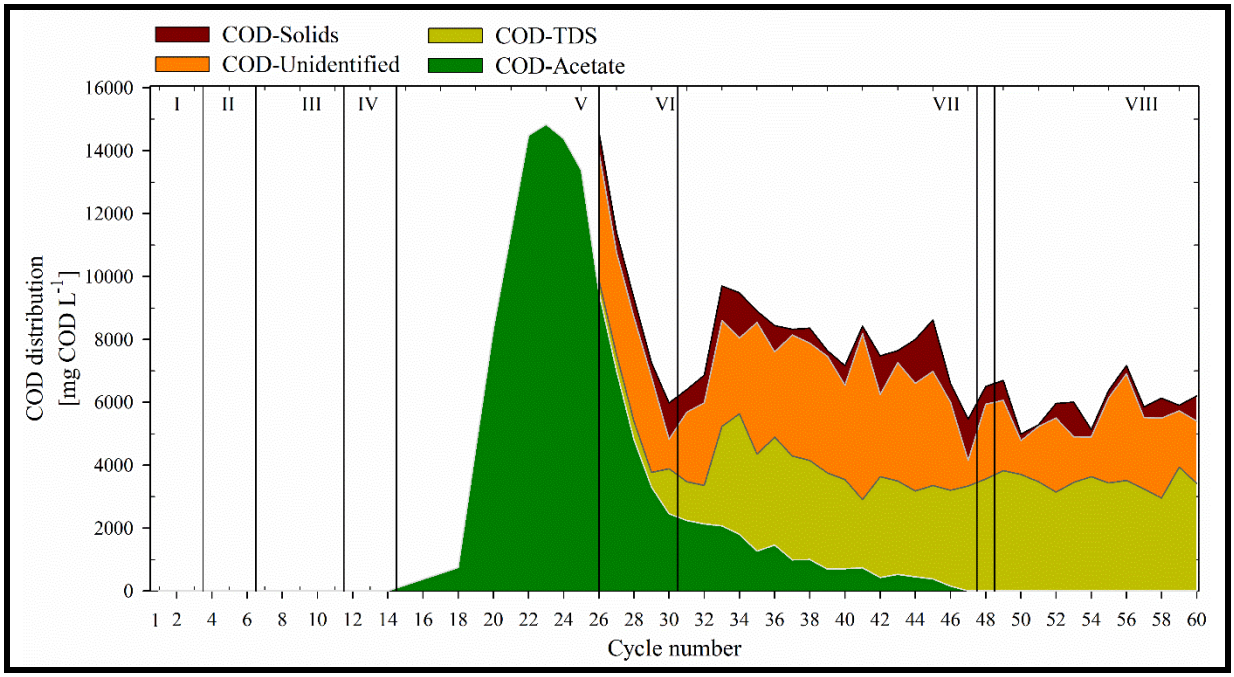

Figure 5.3. Chemical oxygen demand (COD) distribution measured from batch 26 to 60. Total COD and dissolved COD were measured, while TDS- and Acetate- equivalent COD were estimated from their concentrations.

In stage VIII, out of the $COD_{s,dis}$, the COD-Unidentified decreased to 37±8% and the COD-TDS increased to 63±8%. This showed the predominance of the COD-TDS in the effluent, which is the aim of this process. Nevertheless, the fraction of the COD-Unidentified was equivalent to 2068±656 mg COD L^{-1}, representing a high quantity of dissolved COD in the effluent. Finally, the particulate COD (COD-Solids) implied a COD/VSS ratio, based on the VSS concentration in the supernatant, of 1.5±1.0 (mg COD mg^{-1} VSS) for cycles 26 to 60.

5.3.3. Microbial diversity along the sequential batch operation

The sequential batch operation was characterized through Illumina tests as described in section 5.2.1. These results are shown in Figure 5.4, where the taxonomy is displayed in relative abundance (%) at genus level. The distribution is gathered in group A (for sulfur metabolizing microorganisms), group B (for homo-acetogenic microorganisms), group C (for methanogenic microorganisms) for genera of relative abundance larger than 1%; in group O (others), there are gathered genera of other microbial metabolisms (as explained in section 5.2.1) and relative abundance lower than 1 %, while in group U (unclassified), there are gathered unidentified hints in this taxonomy level.

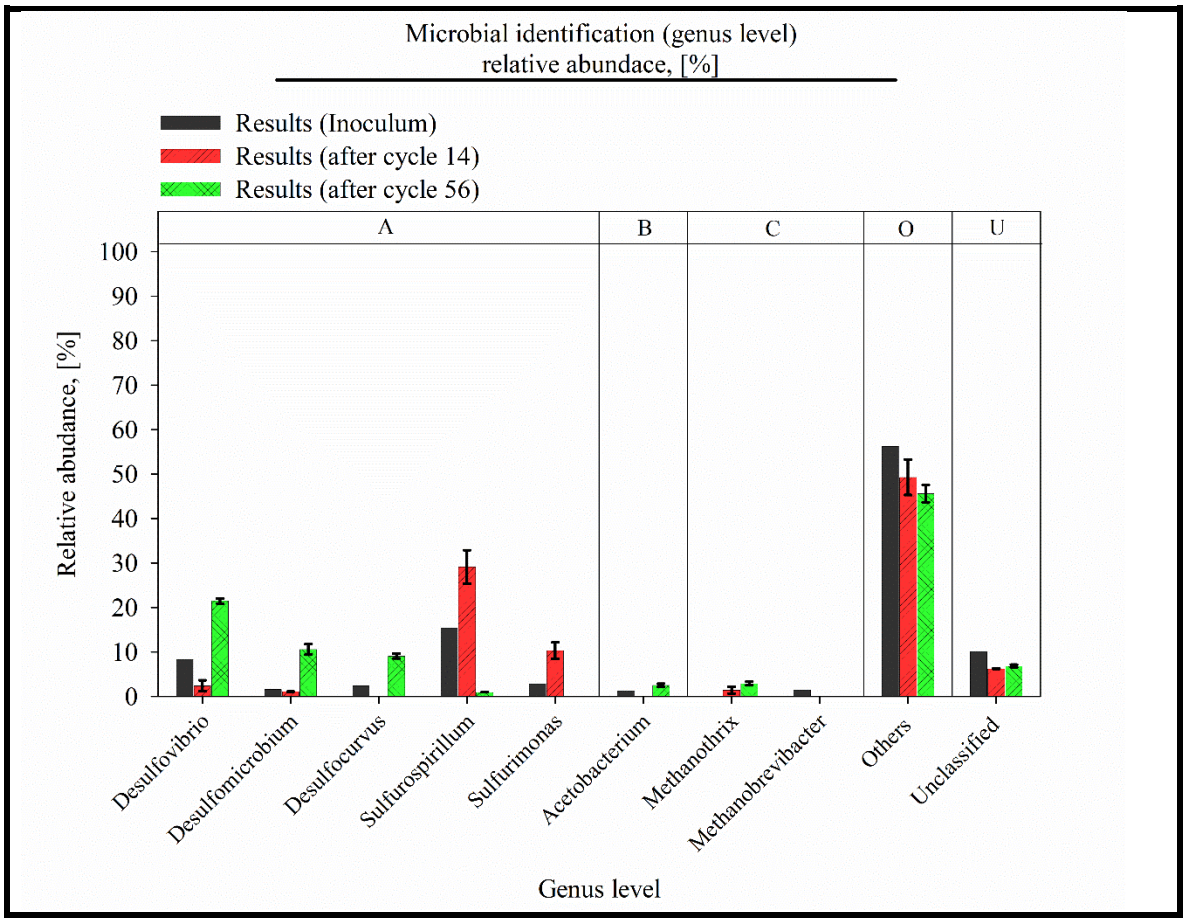

Figure 5.4. Results of the microbial distribution in genus level of the Illumina tests in the inoculum, and the culture medium after cycle 14 and 56. Group A gathered the identified microorganisms that use sulfur in their metabolism. Group B gathered the identified homo-acetogenic microorganisms. Group C gathered the identified methane producing microorganisms. The rest of microorganisms identified in this taxonomic level are gathered in O while the hints that were not identified in this taxonomic level are gathered in U.

From Figure 5.4, the microbial population associated with sulfate reduction partly changed from the inoculum to the culture medium after cycle 14 (end of stage IV), but completely changed from cycle 14 to 56 (from stage IV to VIII). A significant increase was observed for *Desulfovibrio*, *Desulfomicrobium* and *Desulfocurvus* genera that accounted for 21.5, 10.6 and 9.1 %, respectively, in the samples taken after cycle 56. All together were equivalent to 41.1% of the microbial distribution. However, these three genera were equivalent to 12.5 and 3.5% in the microbial distribution in the inoculum and the culture medium after cycle 14, respectively.

Sulfurosporillum was identified in the inoculum, with a relative abundance of 15.4%, and it was predominant among the sulfate reducing microorganisms in cycle 14, but it was dwindled to 1.00±0.02% in cycle 56. *Sulfurimonas* switched from 3% in the inoculum to 10.3±1.8% in cycle 14 and was not identified in cycle 56.

Acetobacterium was identified in the Illumina sequencing, switching from a relative abundance of 1.4% in the inoculum to 2.5±0.4 % in the culture medium in cycle 56, and was not detected in cycle 14.

In terms of methane producing microorganisms, two genera were identified: *Methanobreviabacter* and *Methanothrix*. The former was only identified in the inoculum with a relative abundance of 1.5%, while the latter was not identified in the inoculum, but it was identified in cycle 14 and 56 with relative abundance of 1.4±0.8 % and 2.9±0.4 %, respectively. However, the gas-outlet composition during the whole operation was 85.5±1.5% for H_2 and 9.9±2.5% for CO_2 and methane was not detected.

5.4. DISCUSSION

5.4.1. Analysis of the reactor performance throughout the sequential batch operation

The reactor performance along the sequential batch operation

The system showed a good performance in terms of the SRR until cycle 9, except for cycle 7 that the SRR unexpectedly dropped. As the TSS/VSS measure was missed for cycle 7, it was difficult to relate the drop in the SRR with a possible loss in the VSS concentration. In stage III the high SRR was not reflected in the Sulfate-RE due to the increasing SLR, and thereby the ac-SLR, meaning that the sulfate reduction capacity by then was surpassed by the

sulfate load.

The increase in the TDS concentration from cycle 1 to 9 was large and coupled to a pH raise from 7.40 to 8.00 in the same period. Based on the dissociation constants (pka_1=7.04 and pka_2=11.96),[131] the equivalent increase of H_2S from the TDS concentration was 87 to 108 mg S-H_2S L^{-1} from cycles 1 to 9. H_2S-inhibition concentrations depend on many factors such as the culture type and microbial community.[13] Literature reports H_2S-inhibition constants (k_i) from 57 to 550 mg S-H_2S L^{-1},[4] indicating that the H_2S concentrations in cycles 1 to 9 could have influenced the SRR due to H_2S-inhibition over sulfate reducing microorganisms. This inhibition effect will be studied in the mathematical model of the sequential batch operation (Chapter 7, section 7.5).

The SRR decrease in cycles 10 to 14 could be explained from the decrease in the VSS in the same cycles. Nevertheless, the factors affecting the loss in the VSS concentration in these cycles were undetected. This reduction in the SRR was reflected in the accumulation of sulfate and the loss of TDS by stripping; and, in fact, the sulfate reduction activity and thereby, the TDS concentration showed a strong influence over the pH as this latter dropped to 7.6 in stage IV.

Overall, acetate production was not observed during the first 14 cycles, which could be explained from a H_2-limiting condition that favors sulfate reducing microorganisms as they have higher H_2 affinity over homoacetogens.[44,132] On the contrary, the low SLR during stage V limited the sulfate reducing activity and favored the homo-acetogenesis and thereby the accumulation of acetate in the reactor. Moreover, the absence of reactor partial draining and solid sedimentation in stage V enhanced the accumulation of solids in the reactor, which explained the high VSS concentration in stage VI compared to stage I to IV.

In stage VI, the SRR capacity raised along this stage as the SLR was increased, which showed that the system was able to recover fast after a long period of sulfate-limiting conditions. Also, sulfate reduction activity surpassed homo-acetogenic activity when enough sulfate was available. In fact, acetate was only accumulated in stage V when the SLR and SRR were 324±150 mg S-SO_4^{2-} L^{-1} d^{-1}, and it was washed out in stage VI when sulfate was in excess and the SRR was 652±183 mg S-SO_4^{2-} L^{-1} d^{-1}. Overall, lower H_2 flow rate can be studied in futures research as a strategy to avoid acetate production when SLR is decreased.

During stage VII, the TDS accumulation was much higher than in previous stages,

specifically, from cycle 33 to 47. At the pH in these cycles (8.00±0.10), the equivalent H_2S concentration was 160±29 mg S-H_2S L^{-1}, and for stage VIII (pH = 8.20±0.03), the equivalent H_2S concentration was 138±14 mg S-H_2S L^{-1}. Under these conditions, the sulfate reducing activity may be inhibited to a certain extent. However, the biomass accumulation in the reactor lead to a low impact of such H_2S-inhibition over H2-SRB since a decrease of the SRR was not observed. Then, the sequential batch operation was robust to offset the H_2S-inhibition. The kinetic factors influencing the high resistance of the sulfate reducing microorganisms to H_2S-inhibition will be further discussed and estimated through a mathematical model in Chapter 7

The SLR of 2424 (stage VI) and 1212 (stage VII) mg S-SO_4^{2-} L^{-1} d^{-1} exceeded by far the sulfate reduction capacity of the system, and it was observed from the increasing sulfate accumulation in the reactor. On the contrary, the SLR of 902 mg S-SO_4^{2-} L^{-1} d^{-1} in stage VIII was accompanied by a stable operation regarding SRR and Sulfate-RE, which made it the optimal stage of the whole operation.

With respect to the gas-outlet composition, although the gas chromatography did not detect H_2S, the unidentified gas fraction of 4.6±2.9% could be related to H_2S. The theoretical basis for this assumption is discussed below. Sulfate, H_2 and CO_2 were the sole substrates used, and three biological processes have been reported to take place under these operational conditions: homoacetogenesis, hydrogenotrophic sulfate reduction and hydrogenotrophic methanogenesis.[11] Thus, the expected products would be methane, sulfide and acetate. Methane was not detected in the gas phase as mentioned in section 5.3.3, while H_2S and acetic acid can be found in the gas phase depending on the mass transfer and the chemical equilibrium. For acetate, it was completely dissociated at the pH of the reactor according to its pKa of 4.76,[133] meaning that no acetic acid form was present in the reactor and, therefore, no volatilization of this compound could take place. Consequently, only H_2S could be found in the gas phase, apart from the compounds detected by the GC.

In terms of the COD balance, the large COD-Unidentified observed during stage VII and VIII can be generated from the cell debris. Further studies are suggested to understand the source of the COD-Unidentified and the cell debris composition. In fact, cell debris derived in macromolecules that can be decomposed into soluble organic compounds by hydrolytic bacteria and its microbial activity depends on the substrates. The routes of macromolecules

hydrolysis include carbohydrates degradation to glucose, lipids degradation to glycerol and long fatty acids and proteins degradation to amino acids.[134] Therefore, it is first recommended to identify the type of organic molecules (amino acids, sugars, long chain fatty acids, etc.) that correspond to the COD-Unidentified; then, the degradations routes can be studied through bottle tests as reported in the literature.[135] In our case, microbial activity can be studied separately with each of the most abundant soluble organic molecules found in the COD-Unidentified. This will help to characterize the mechanisms of cell debris hydrolysis to soluble compounds and from there, strategies can be explored to suppress or diminish the hydrolytic activity.

Respecting the COD and VSS, the average value for the COD/VSS ratio obtained from cycle 26 to 60 (1.5±1.0 mg COD mg^{-1} VSS) is in the range of the literature reports that is 1.2 to 1.6 (mg COD mg^{-1} VSS).[136]

The microbial diversity evolution along the sequential batch operation

Regarding the microbial population identified in the Illumina test, the predominant genera after cycle 14 showed an increase in *Sulfurosporillum* and *Sulfurimonas* with respect to the inoculum. These two genera are versatile microorganisms that can use different electron acceptor/donor coupled in their catabolic pathways. *Sulfurosporillum* can use H_2 as electron donor and sulfate, among other sulfur compounds as electron acceptor;[137] while *Sulfurimonas* can use, as electron donor and acceptor, the couple thiosulfate/nitrate or sulfide/oxygen, in the dissimilatory pathway, but it has been reported to grow using reduced sulfur ions as electron acceptors and H_2 as electron donor.[127] These two genera were decreased to less than 4% of relative abundance each one after cycle 56. In fact, after cycle 56, the population showed a predominance of *Desulfovibrio*, *Desulfomicrobium* and *Desulfocurvus*.

Respecting *Desulfovibrio*, which was the most abundant genus amongst the sulfate reducers detected after cycle 56 (21.5% of relative abundance), has been reported to use hydrogen as an essential substrate in its catabolic pathway,[74] and in fact, many species of this genus have been found in H_2-fed reactors and kinetically characterized.[49,138] Species of this genus have also been reported as highly resistant to H_2S inhibition, with complete inhibition of the microbial growth when sulfide concentrations were above 500 mg S-H_2S L^{-1}.[139] For

the latter, even when k_i was not reported, it must be around 250 mg S-H_2S L^{-1} as this parameter refers to the concentration at which the specific growth rate is decreased to the half of its maximum. In fact, *Desulfovibrio* has also been reported in other works with k_i of 250 mg S-H_2S L^{-1}.[4,140]

Similarly, *Desulfomicrobium* (10.6% of relative abundance after cycle 56), has also been reported as the main responsible for the sulfate reduction in a H_2-fed full-scale GLR where methane production also took place.[141] These two genera, *Desulfovibrio* and *Desulfomicrobium,* were also reported by van Houten et al.[53] as the main responsible of the hydrogenotrophic sulfate reduction in a syngas-fed GLR.

Regarding *Desulfocurvus* (9.1% of relative abundance after cycle 56), species from this genus have been reported to use hydrogen as electron donor for the sulfate reduction, but acetate is needed as carbon source.[142] In the GLR, *Desulfocurvus* was not detected previously (inoculum and after cycle 14); indeed, as it was mentioned in Section 5.3.2, acetate was highly accumulated during stage V, which suggests that *Desulfocurvus* proliferation was enhanced by the acetate accumulation. Therefore, further studies are suggested to detect its production mechanisms and its proliferation for longer operations.

Acetobacterium was the homoacetogens identified in the reactor, and it has been reported to grow symbiotically with sulfate reducing bacteria in H_2/CO_2-fed reactors,[49,118] but it was identified in the Illumina results with a low relative abundance (less than 3 % of relative abundance) and only after cycle 56. Consequently, its present is explained from stage V, from where acetate accumulation indicated a high homoacetogenic activity.

In terms of methanogens, two genera were identified: *Methanobreviabacter* and *Methanothrix*. The former was only identified in the inoculum while the latter was not identified in the inoculum, but it was identified in cycle 14 and 56. However, as methane was not detected in any of the preliminary experiments in the GLR (Chapter 4), neither in the sequential batch operation, and based on the low relative abundance, their identifications could be associated to the solid retention in the sedimentation step.

The SRR and the H_2-mass transfer coefficient

The SRR can be estimated based on the abiotic tests reported in Chapter 4, where the K_La_{H2} was estimated (section 4.4.2). Based on K_La_{H2}, the maximum H_2-mass transfer to the

liquid phase was estimated (section 4.4.4). Thus, Equation 2.3 can be used to calculate a theoretical maximum hydrogenotrophic SRR (SRR_{max_th}) assuming that all H_2 transferred is consumed by hydrogenotrophic sulfate reducers. Such SRR_{max_th} was estimated to be 504 mg $S\text{-}SO_4^{2-}$ L^{-1} d^{-1}. The experimental SRR in many cycles of the sequential batch operation was significantly higher than this estimation, meaning that the abiotic tests performed to estimate the K_La_{H2} could not represent the real hydrogen transfer to the liquid phase in the biotic conditions where large solids and dissolved compounds are present. Different factors have been reported in the literature to explain the changes in the mass transfer properties from abiotic to biotic conditions such as microbial activity, reactor type, temperature, inlet/recirculation gas rates, liquid properties and hydrogen partial pressure.[143,144] These parameters affect the gas/liquid mass transfer differently, and some of them could not have a changing effect in the H_2-mass transfer as the experiments, the abiotic and biotic, were performed in the same setup. This is the case of the reactor type, temperature, and inlet/recirculation gas rates.

Moreover, according to the two film theory and the mass transfer equation (Equation 4.1),[102,145] the hydrogen partial pressure (P_{H2}) is mainly associated to the hydrogen liquid saturation[143] . While the abiotic tests were performed only with H_2, i.e., 100% (v/v), the gas H_2 fraction was 85.5±1.5% v/v during the biotic operation of the GLR. Such decrease in the partial pressure would lessen the H_2-mass transfer, meaning that the higher mass transfer observed in the biotic experiments must be attributed to other factors.

Therefore, the increment in the H_2-mass transfer observed in the sequential batch operation must be related to the abovementioned liquid properties and/or microbial activity. On the one hand, it has been reported that mass transfer coefficients (K_La) can be increased or decreased based on the liquid rheological properties. Some works have demonstrated the negative effect of surfactants on K_La,[146,147] others have described the positive effect of ionic salts on the K_La,[143,148] while another report showed that a pH change of 1.6 pH units from 6.7 to 8.3 decreased the O_2-mass transfer coefficient in 30% in a bubble column.[149] In this sense, foam formation was not observed. Thereby the presence of surfactants and their effect was discharged. Meanwhile, ions were present in the reactor, and they could have had a positive influence in the K_La, ergo the pH increase in the reactor could have had an adverse effect on the K_La_{H2}. On the other hand, high solids concentrations could be another concerning pitfall

for the gas/liquid mass transfer as solids increase liquid viscosity and thereby, reduce K_La.[143] The effect of solids over liquid viscosity was studied by Cheng & Li,[150] who found that sludge concentrations of 2 and 10% (w/w) increased the liquid viscosity in 2.7 and 25.7 fold, respectively. Yet, according to the literature review done in this work, and as it has been mentioned in similar works,[143] the direct effect of liquid viscosity over gas/liquid mass transfer has not been reported.

Concerning the microbial activity, it has been reported to affect positively the K_La and different mathematical correlations have been proposed to describe an enhancement factor that have a direct proportionality on the K_La.[143,151,152] In fact, a 10 fold increase in oxygen transfer to the liquid phase was reported in a biotrickling filter due to biomass respiration.[153]

In general, there are many factors that could have affected the H_2-mass transfer, and based on the literature reports, further research is needed to identify the factors influencing the gas/liquid mass transfer in biotic conditions. Herein, two set of experiments are suggested to study the H_2-mass transfer under biotic conditions, a first to estimate the K_La_{H2} under biotic conditions with no sulfate addition, and a second to estimate the K_La_{H2} under biotic conditions with no H_2-consuming microbial activity.

5.4.2. Analysis of the stable conditions for the sulfate reduction: stage VIII

The aim of this section is to discuss the optimal stage (VIII) of the sequential batch operation and to compare it with the literature reports. The most relevant parameters from this stage are summarized in Table 5.2.

One important result of the sequential batch operation of the reactor is the SRR and the Sulfate-RE as these values showed a remarkable improvement compared to the SRR obtained in the preliminary experiments (Chapter 4). The sulfate reducing activity was favored due to the solid recovery step and could have been enhanced by the strong reducing environment (low ORP), mainly caused by the high TDS concentration. The optimal ORP for biological sulfate reduction has not been extensively reported in literature. However, ideal ORP to avoid H_2S-inhibition for an heterotrophic sulfate reducing culture has been reported at -290 mV,[115] and -230 mV,[154] but as this report was focused on avoiding the H_2S-inhibition, it is not possible to know if these ORPs were the real optimal values for the biological sulfate reduction.

A drawback of the operation was the H_2S-stripping that was large under the stable conditions (Table 5.2). The H_2S-stripping was 64±19% of the total sulfide produced (the S-sulfate reduced per cycle); and this fraction of sulfide loss in the gas phase was equivalent to an average mass flow of 3754±1140 mg S-H_2S d^{-1} in stage VIII (determined by mass balance). This high H_2S mass loss in the gas phase implies that a sulfide recovery process from the gas phase is needed to avoid sulfide emissions and for its further conversion to elemental sulfur, as it is the second step of the integrated biological process of the global process under this work was developed: the ENSURE process.

Table 5.2. Remarkable values obtained from the sequential batch operation in stage VIII.

	Units	Value
SRR	[mg S-SO_4^{2-} L^{-1} d^{-1}]	861±56
Sulfate-RE	[%]	93±7
Sulfate in the MM	[mg S-SO_4^{2-} L^{-1} d^{-1}]	5575
pH	-	8.20±0.03
ORP	[mV]	-603±11
TDS	[mg TDS L^{-1}]	1998±160
H_2S in the liquid	[mg S-H_2S L^{-1}]	138±14
H_2S stripping	[%]	64±19
H_2S stripping	[mg S-H_2S d^{-1}]	3754±1140
VSS	[mg VSS L^{-1}]	1054±129
VSS/TSS	-	45±4
$[TSS]_{dis}$	[mg TSS L^{-1}]	928±465
$[VSS]_{dis}$	[mg VSS L^{-1}]	464±165
Unidentified COD_s	[mg COD L^{-1}]	1549±673
Unidentified COD_s	[%]	27±10

Thus, a bioscrubbing process is recommended for the further biological treatment of the sulfide, i.e., its partial oxidation to elemental sulfur (as explained in Chapter 1), as considerable quantities of sulfide concentration are split in the liquid and the gas outlet. Sulfide bioscrubbing, which is a two-step process (a H_2S-absorption and a biological conversion to elemental sulfur), has proven efficiently for the H_2S-capture and biological conversion.[27] A case of successful application of sulfide bioscrubbing is the THIOPAQ process that can capture 99.99 % H_2S from gas stream, and can convert biologically 95%

(w/w) of sulfide to elemental sulfur.[155]

Another pitfall of the process was the high soluble COD (1549±673 mg COD L^{-1}) and the TSS and VSS concentration in the effluent, 928±465 mg L^{-1} and 464±165 mg L^{-1}, respectively. Further studies to identify the factors affecting the cell debris, the large COD concentration in the effluent and to improve the sedimentation steps are suggested. As the sludge sedimentation and return to the reactor is an enhancing factor of the SRR, it also leads to unnecessary solids accumulation that, for the microbial fraction, could lead to cell debris accumulation in the reactor that ends up increasing the dissolved COD. Thus, further experiments could be focused on improving and understanding the sedimentation step to diminish the unnecessary solid accumulation in the reactor. Moreover, the use of coagulants/flocculants can be explored for the discharged supernatant as it has been demonstrated economically and technically feasible for sludge sedimentation.[156]

Overall, the results obtained in this work can be compared with remarkable reports in the literature with respect to systems treating sulfate-rich wastewaters with H_2 as electron donor. Normally, hydrogen is used in biofilm gas-lift reactors for the treatment of wastewaters that lack organic compounds: acid mining streams, toilet flushing, industrial wastewater such as smelting process and flue gases.[36,116,141] GLRs are used to favor H_2-mass transfer and to avoid the growth of heterotrophic microorganisms that are enhanced with the use of organic sources.[4,48,94] Hence, some remarkable results in the literature are gathered in Table 5.3. Most of these reports have used GLRs with temperatures over 30 ºC while different biomass sources were used. In the case of Esposito et al.,[157] a mixed granular sludge from an UASB and suspended sulfidogenic inoculum were used in a GLR with a settler for solid return to the reactor. A Sulfate-RE between 58 to 84 % (w/w) (SRR: 1450 - 2100 mg $S\text{-}SO_4^{2-}$ L^{-1} d^{-1}) with CH_4 production of 10 to 30% (V/V) of the gas fraction were encountered. Also, acetate was used to enhance sulfate reduction and it was possible to decrease the CH_4 concentration from 10% - 30% (V/V) to 2 - 8 % (V/V), although this addition did not raise the Sulfate-RE significantly, as seen in Table 5.3.

Acetate was also used in a full-scale, syngas-fed GLR containing biofilm-type biomass that was setup to treat zinc smelting wastewater. In that case, the SLR was 5000 mg $S\text{-}SO_4^{2-}$ L^{-1} d^{-1} reaching a Sulfate-RE over 90 % (w/w) (SRR over 4500 mg $S\text{-}SO_4^{2-}$ L^{-1} d^{-1}), but CH_4 was produced at a rate of 50 Nm^3 d^{-1}, which was an undesirable product as it demands a

further treatment.[53]

On the contrary, van Houten et al.,[49] used a lab-scale H_2/CO_2 fed GLR with biofilm-type biomass and obtained a SRR between 4000 and 4700 mg $S\text{-}SO_4^{2-}$ L^{-1} d^{-1}. Yet, this high SRR was characterized by large sulfate (2000 - 1300 mg L^{-1}) and acetate (200 mg L^{-1}) concentrations in the effluent.

Table 5.3. Comparison of remarkable literature reports with the results in this work.

Feeding source	pH	T	Sulfate in the influent $\left[\frac{mg\ S\text{-}SO_4^{2-}}{L^{-1}}\right]$	SLR $\left[\frac{mg\ S\text{-}SO_4^{2-}}{L^{-1}\ d^{-1}}\right]$	Sulfate-RE [%, w/w]	Relevant inf.	Reference
H_2/CO_2	7	30	3790	2500	58-84	CH_4	Esposito et al,[157]
H_2/CO_2/ Acetate	7	30	3790	2500	Up to 87	CH_4	Esposito et al,[157]
Syngas/ Acetate	7-7.5	30-35	1700/ 3300	5000	-	CH_4	van Houten et al,[53]
H_2/CO_2	7	30	1120	6000	67-78	Acetate	van Houten et al,[49]
H_2/CO_2	9	35	1600	320	95-100		Sousa et al,[54]
H_2/CO_2	5	30	1500	1600	99		Bijmans et al,[97]
H_2/CO_2	7.5	9		200	17-100		Nevatalo et al,[61]
H_2/CO_2	8.2	20	5575	919±78	93±7		This work

Other works have explored extreme environmental conditions. It is the case of Sousa et al.,[54] who studied the treatment of sulfate-rich wastewater (from the metallurgic sector) with high pH (9.00±0.05) and salinity (33.6 g Na_2CO_3 L^{-1} and 69.3 g $NaHCO_3$ L^{-1}) in a lab-scale GLR with a suspended microbial culture. In this case, a low biomass concentration, lower than 15 mg VSS L^{-1}, was obtained for HRT of 2.5 days while the SRR was 320 mg $S\text{-}SO_4^{2-}$ L^{-1} d^{-1}.

Another case for the treatment of wastewater from the metallurgic sector was reported by Bijmans et al.,[97] who worked with a low pH system in a biofilm-loaded GLR and obtained a 99% Sulfate-RE. In this case, a sulfide removal with $ZnCl_2$ was needed to avoid H_2S-

inhibition.

Finally, a low temperature study (9 ºC) was performed by Nevatalo et al.,[61] in a GLR where pumice particles were used as supporting material for biofilm formation; yet, biofilm formation was not obtained and the microbial culture was suspended resulting in SRR of 198 mg $S\text{-}SO_4^{2-}$ L^{-1} d^{-1}.

Some of these works showed higher SRR than the reported in this work; nevertheless, some of them use acetate as substrate, which in fact is an expensive feedstock. Other works described significant methane/acetate production as mentioned above. Additionally, pH and temperature control were used in all these reports, which in terms of operational cost are also disadvantageous. In the research herein presented, it was observed that the pH was raised from 7.4 to 8.2, but it was stable (as seen in Table 5.2) in the last stage (VIII). Moreover, stage VIII described the most stable results regarding the SRR and the Sulfate-RE, which means that its operational conditions were optimal for the intended goal of this research. This was explained from a balance between the pH-decreasing effect of the CO_2 addition and the pH-increasing effect of the hydrogenotrophic sulfate reduction as seen in Equation 2.3. Therefore, no need of pH control was required, and this represents an advantage, as pH control in a CO_2-bubbled reactor will demand high reactant consumption.

The sulfate feeding concentration is also important, as real wastewaters have sulfate concentration depending on their sources. In the case of flue gases-derived wastewater, typical sulfate concentration have been reported between 3300 to 6700 mg $S\text{-}SO_4^{2-}$ L^{-1},[20] while different processes that were evaluated in the United States reported sulfate concentrations up to 2700 mg $S\text{-}SO_4^{2-}$ L^{-1}.[158] Therefore, the results in this work could be a good alternative for a full-scale implementation considering the sulfate MM concentration evaluated in the optimal condition of the sequential batch operation, 5575 mg $S\text{-}SO_4^{2-}$ L^{-1}, as seen in Table 5.2.

5.5. MAIN CONCLUSIONS

The hydrogenotrophic sulfate reduction was studied in a sequential batch operated GLR where the main results are listed below:

From the environmental conditions in the GLR:

1. The reactor was operated at room temperature (~20ºC). The results suggest that the sulfate reducing activity was comparable to relevant reports in the literature that have been reported at temperatures over 30 ºC.
2. The pH was not controlled and its influence over the SRR was not identified for the pH range where the process was evaluated, from 7.4 to 8.2 from the beginning to the end of the operation. Even though, the pH raise did not show negative influence over the SRR.
3. The pH increase favored the microbial activity by avoiding high H_2S-inhibition as the fraction of H_2S during the optimal stage (VIII), where pH was 8.20±0.03, was only 7.0±0.6 % of the total sulfide concentration (1998±160 mg TDS L^{-1}).

From the microbial competition:

1. The sulfate reducing activity was the predominant hydrogen consumer, since no acetate production took place during the optimal stage, and methane was never identified during the whole operation.
2. Homo-acetogenic activity only took place in a period where the SLR was low (320±158 mg $S\text{-}SO_4^{2-}$ L^{-1} d^{-1}). Therefore, future works must be focused on exploring lower H_2 flow rate to avoid acetate production when SLR decreases.
3. The system showed that the sulfate reducing activity can be recovered fast after long sulfate limiting conditions (53 days) as seen after period V.
4. VSS concentration was not affected during the sequential batch interruption as it increased from 285 to 1315 mg VSS L^{-1} in this period; yet the large biological acetate production also contributed to the VSS increase.

From sulfate treatment capacity and effluent characteristics:

1. The optimal operation was obtained at a SLR of 919±78 mg $S\text{-}SO_4^{2-}$ L^{-1} d^{-1} with a SRR of 861±56 mg $S\text{-}SO_4^{2-}$ L^{-1} d^{-1} and a Sulfate-RE of 93±7%, which are results comparable to some relevant reports in the literature.
2. Results of microbial population identification showed that the most abundant microorganisms were sulfate reducers *Desulfovibrio*, *Desulfomicrobium* and *Desulfocurvus*. These results are according to reports in the literature,which showed that the most abundance microorganisms in H_2-fed GLR were *Desulfovibrio*, *Desulfomicrobium*. Meanwhile, as *Desulfocurvus* has been reported to need acetate for growth, its proliferation was explained from stage V where SLR was decreased and acetate was largely accumulated.
3. Based on the sulfate concentration of the influent, 5575 mg $S\text{-}SO_4^{2-}$ L^{-1}, this process showed a suitable design for the treatment of flue gases-derived wastewaters where similar sulfate concentrations are present. Yet, a scale-up study shall be performed to identify the limitations in terms of large wastewater flowrates.
4. This system showed that at the optimal operation methane was not produced, and the effluent had no acetate. Yet, the production of non-TDS and soluble COD was 1549±673 mg L^{-1} that represented the 27±10% of the total soluble COD present in the effluent, which is a disadvantage of this process.
5. Solid concentration in the effluent was also large as the TSS and VSS values in the optimal operation were 928±465 mg L^{-1} and 464±165 mg L^{-1}, respectively. Further studies are suggested to improve the sedimentation step.
6. As the sulfide produced is split in the liquid and gas effluent, with H_2S-stripping fraction equivalent of 64±19% of the total sulfur conversion, a gas treatment step is needed. A bioscrubbing process is suggested for the further treatment of sulfide and elemental sulfur production.

CHAPTER 6

DEVELOPMENT OF A SULFIDE ONLINE-MONITORING SYSTEM FOR SULFIDOGENIC REACTORS

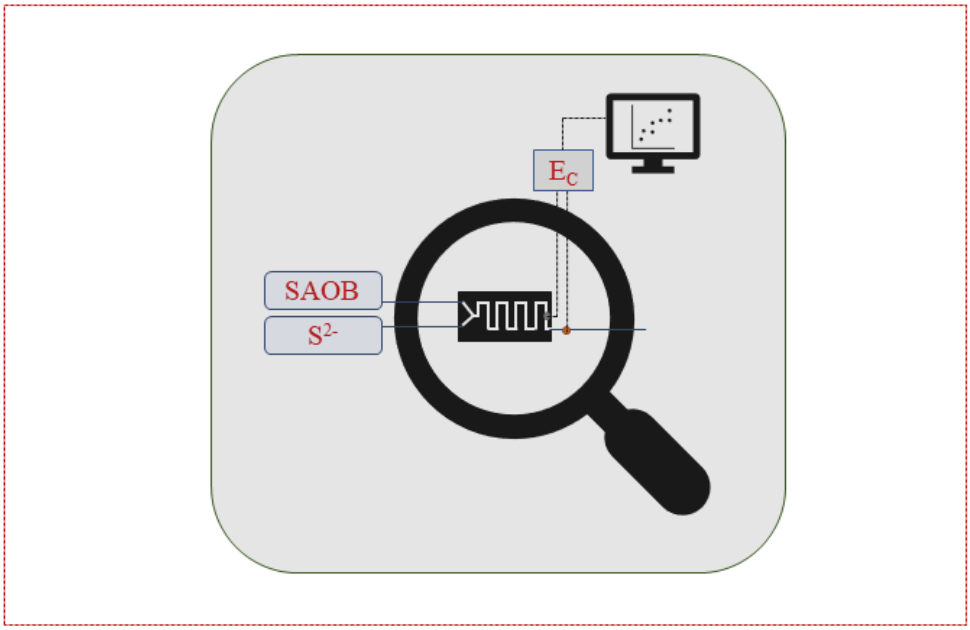

6.1. CHAPTER OUTLINE

This Chapter aims at describing the results obtained from the development and implementation of a sulfide online-monitoring system (S-OMS) for sulfidogenic reactors. This system was based on the lab on a chip (LOC) platform that aims at performing analytical measurements through miniaturized system, and in this case, it was studied through an electrochemical-potentiometric technique with an Ag/Ag_2S-working electrode and an Ag/AgCl-reference electrode. Moreover, the electrochemical cell for the potentiometric measurement was evaluated in a microdevice that was manufactured with 3D-printing technology.

Accordingly, an introduction is carried out in section 6.2, where relevant topics about the type of analytical systems, fabrication of miniaturized analytical systems, electrochemical and potentiometric sulfide measurement in environmental biotechnology are reviewed. Then, the experimental layout is detailed in section 6.3. The results of the S-OMS manufacturing and evaluation of its analytical accuracy are shown in section 6.4 and the results of the S-OMS validation are described in section 6.5. Discussion of the results is examined in section 6.6. Finally, the overall conclusions of this research are laid out in section 6.7.

6.2. INTRODUCTION

Analytical techniques have been widely developed and applied in different scientific fields and economic sectors. They are important to track key components for process behaviors, decision-making, and process control amongst others.[44,66] Analytical methods are based on many different physical principles such as chromatography, spectroscopy, electrophoresis and electrochemistry, among others.[67] Also, these methods have evolved along the years and their usefulness are mainly related to the application field. Yet, different technologies have turned predominantly in recent years due to their easy-to-apply and low application costs. This is the case of LOC platforms that consist of the miniaturization and automation of analytical systems that have been applied mainly in the pharmaceutical and environmental sectors.[68–71] LOC platforms can be developed with the use of various technologies such as inkjet printing and 3D-printing. Both manufacturing methods have been broadly applied for the development of electrochemical sensors,[72,73] and

particularly, 3D-printing has been proven efficiently for the fabrication of microfluidic devices based on assorted analytical techniques.[75,159–162] Additionally, LOCs have been mostly implemented with the use of electrochemical methods as detector, which has been proved ideal for miniaturized analytical system with no loss of analytical accuracy.[68,163]

The basis of electrochemical sensors is the evaluation of electrical variables like electrical current, charges or electrical potential that require an electrochemical cell that must be composed by two electrodes or three electrodes, depending on the required configuration for the measurement techniques used. Then, the electrical variable to be recorded can be related to the present of the ion and/or compound of interest in the aliquot and its concentration could be estimated afterward. Moreover, electrochemical techniques can be primarily classified as potentiometric and voltametric techniques, where the first is electrical current static, i.e., no electrical current flow, and the second is electrical current dynamic, i.e., electrical current flow takes place.[164] Electrochemical cells used for potentiometric measurements are galvanic cells that work in a two-electrode configuration system: a reference electrode with constant electrical potential, and a working electrode that must be in contact with the sample and shall be sensible to an ion of interest. Whereas the electrical current dynamic methods are diverse and complex techniques that vary according to the species under study and detection limits required, the potentiometric methods have been largely applied in multiple technological fields due to the easy-to-apply settings, good reproducibility, fast response, automation capacity and low cost.[165]

As the overall objective of this research is to evaluate the hydrogenotrophic sulfate reduction in a H_2-fed reactor, the sulfide production and monitoring are essential to characterize the biological activity and reactor performance. This is important for operational reasons, as hydrogen sulfide (H_2S) is inhibitory to microbial growth,[11,13,36,74] and also for environmental reasons, as it affects ecosystems by provoking anaerobic conditions in natural water reservoirs that end up lacking oxygen for living beings and by direct toxicity to human and all living beings in its undissociated form, H_2S.[13,25,166]

Evaluation of sulfide in bioreactors is normally made based on iodometric, methylene blue or potentiometric analytical techniques.[44,166] Particularly, the advantage of potentiometric techniques has made predominantly the application of potentiometric sulfide selective electrodes (S^{2-}-ISE) that are fabricated from different types of membrane and has

been applied in the environmental biotechnology field.[44,166,167] However, S^{2-}-ISEs are mainly offline analytical methods, and the need to obtain real-time and *in situ* sulfide data in many processes has led to the development of techniques including novel 3D-printed analytical platforms,[75,162] flow injection analysis (FIA),[168,169] and spectrophotometric detection.[166] From these analytical techniques, the main advantage of potentiometric measurement of sulfide is its fast response time and wide detection range.[170,171] Consequently, its integration as a detector in online monitoring systems is desirable for a more robust performance of bioreactors. Therefore, the S-OMS proposed in this work was based on a LOC platform that was studied through a potentiometric analysis with a Ag/Ag_2S-working electrode and a Ag/AgCl-reference electrode; the latter has been proven as a robust technique to measure sulfide (S^{2-}).[72,75,172]

6.3. EXPERIMENTAL LAYOUT

6.3.1. Experimental setup of the sulfide online-monitoring system

The S-OMS was developed in three global steps: the manufacturing of a microdevice, the evaluation of the analytical parameters, and the validation of the proposed system. The main setup of the system is explained in this section. All measurements were performed at ~20ºC and the system is shown in Figure 6.1; the core of the setup is the microdevice that mixed a sulfide antioxidant buffer (SAOB) with a sulfide-containing sample and contacts the SAOB/sulfide resulting solution with an Ag/Ag_2S-working electrode and an external Ag/AgCl reference-electrode. The SAOB and the sulfide sample were pumped through the microdevice inlets 1 and 2, respectively, and using the microfluidic pump A (Perimax 12 with 4 pumping channels, SPETEC) and the same pumping tube type (1.14 mm inner diameter Tygon tubing, Ismatec) so that both solutions had the same flow rates (1 ml min^{-1}). The microdevice was designed and manufactured following the criteria proposed by Pol et al.,[75] but the integrated pseudo-reference electrode was replaced by an external reference electrode and it was installed outside the microdevice in a methacrylate pre-fabricated piece for sensor placing. This electrode was a commercial double junction Ag/AgCl-reference electrode (Orion™ 900100 Sure-Flow™ Reference Half-Cell Electrode, Thermo Scientific) that uses commercial outer (Orion 900003) and inner (Orion 900002) filling solutions of

0.1 M KNO_3 and 0.1 M KCl, respectively. The working- and reference- electrodes were connected to a potentiostat (Autolab PGSTAT204 potentiostat/galvanostat, Metrohm Autolab B.V.), and this latter was connected to a desktop computer for data acquisition and process setup using the program Nova 2.1 (Build 6159, Copyright 2016, Metrohm Autolab B.V.).

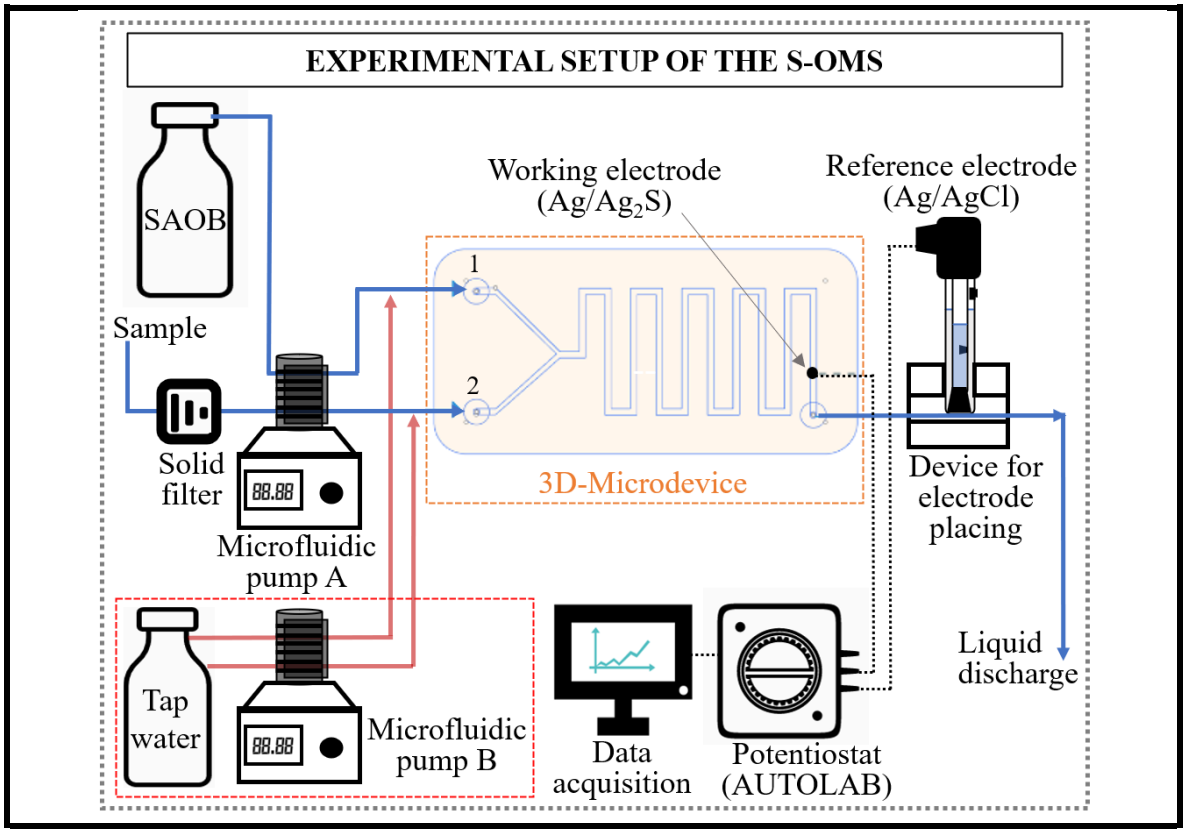

Figure 6.1. The experimental setup of the sulfide online-monitoring system. It consisted of a 3D-microdevice with a working electrode and an external reference electrode, both connected to a potentiostat for data acquisition and processing. The red configuration consisted in a microdevice cleaning and was only used for the system validation in the GLR.

For the S-OMS validation with the GLR samples, the sulfide samples were filtered before pumping through the microdevice with a disposable inline filter (DIF-MN40, Nylon with Borosilicate glass filter, Headline filters) that was used to avoid clogging in case of solids in the sulfide sample. SAOB prescription is presented in Chapter 3 (section 3.2), it was used to preserve sulfide from oxidation and/or precipitation, and to fully dissociate all sulfide forms as the Ag/Ag_2S-working electrode is only sensitive to S^{2-}.[75,164] Thus, as SAOB raised the pH to completely dissociate sulfide species, the measured value is referred to total

dissolved sulfide (TDS) as it is also the case for the commercial S^{2-}-ISE (ISE, Orion™ Silver/Sulfide electrode) that was used in this research to validate the proposed microdevice with the GLR experiments presented in Chapter 5.

The red configuration remarked in Figure 6.1 was set up to clean the channels by flowing tap water through the 3D-microdevice with the microfluidic pump B (LabVI-II, SHENCHEN) after each measurement. This cleaning process was only used for the validation of the S-OMS as the GLR sample matrix could have derived in solid precipitation and thereby clogging the microdevice and/or causing interference in the measurement signal.[173] The Ag/Ag_2S-working electrode was a second-kind electrode and the oxidation-reduction reaction proceeded according to Equation 6.1, while the potentiometric response of the working electrode ($E_{working}$) is related to the sulfide concentration (activity) as defined by the Equation 6.2;[75,91] where $E^0_{Ag2S/Ag}$ is the standard redox potential, R is the universal gas constant equals to $8.314 J \cdot K^{-1} \cdot mol^{-1}$, T is the absolute temperature, F is the Faraday constant equals to $96487 C \cdot mol^{-1}$, n is the number of moles of electron exchange, i.e., equal to 2 according to Equation 6.1, and $\{S^{2-}\}$ is the sulfide activity.

The SAOB-sulfide resulting sample was in contact with the two electrodes and the electrical potential difference of the cell (also known as electromotive force) (E_c in Equation 6.3) was measured with the Autolab potentiostat that was connected to a computer where the software NOVA 2.1.4 was used for data acquisition and process setting (NOVA 2.1.4, Build 6899, Metrohm Autolab B.V). K' in Equation 6.3 represents the constant fraction of the working- and reference- electrode potentials, and $[S^{2-}]$ is the sulfide concentration.

$$Ag_2S_{(s)} + 2e^- \rightarrow 2Ag_{(s)} + S^{2-}{}_{(aq)} \qquad \text{Equation 6.1}$$

$$E_{working} = E^0{}_{Ag2s/Ag} - \frac{2.303 \cdot R \cdot T}{nF} \cdot \log\{S^{2-}\} \qquad \text{Equation 6.2}$$

$$E_c = E_{working} - E_{reference} = K' - \frac{2.303 \cdot R \cdot T}{nF} \cdot \log[S^{2-}] \qquad \text{Equation 6.3}$$

All sulfide-stock solutions used for calibrations and analytical experiments were standardized with the commercial S^{2-}-ISE to determine the real TDS concentration as the sulfide can easily loss through oxidation and evaporation. The standardization procedure is

detailed in Chapter 3 (section 3.2) and in Appendix B.

6.3.2. Design of the 3D-microdevice for sulfide measurement

Microdevice manufacture

The 3D-microdevice was designed in Autodesk Fusion 360, exported as a gcode-file for 3-D printer setting in the software Cura 3.2 (BCN3D Technologies, Inc), and then, it was exported as a stl-file for its manufacture with a 3D printer Sigma R16 (BCN3D Technologies, Inc). As SAOB is a strong alkaline solution that can weaken plastic materials, Co-polyester filament (CPE, colorFabb_XT, AMPHORA) of 2.85 mm diameter was selected to manufacture the microdevice based on its mechanical and chemical stability.[174] Thus, a microdevice was manufactured with CPE and its stability was assessed by pumping SAOB for 24 hours through it.

Ag/Ag_2S-working electrode preparation

The working electrode consisted of a silver wire (diameter: 0.5 mm, purity: 99.99%, AG005150, MicroPlanet) over which sulfide was electrodeposited as reported in similar works.[175] This procedure was done by grabbing a 1.5 cm-length silver wire to the positive source of the Autolab potentiostat, and then partially immersing it, together with the Ag/AgCl-reference electrode, and a platinum counter electrode (Crison Instruments) in 0.05 liters of 0.1 M sulfide solution (prepared on 1 M NaOH solution). Thereupon, sulfide-electrodeposition on the Ag wire was performed with the application of 2.1 V for 30 seconds through the Autolab potentiostat set via NOVA2.1 software. The untreated-Ag wire and the Ag/Ag_2S-working electrode were analyzed through a scanning electron microscopy (SEM) at 5 kV to determine the difference in the morphology and an energy dispersive X-ray spectroscopy (SEM-EDX) at 15 kV to determine the elemental composition of the surface of both wires as suggested by Pol et al,[75]. These measures were performed with a Zeiss Merlin equipment (High resolution SEM with EDZ and EBSD, Oxford LINCA X-max) of the Microscopy Service of the Autonomous University of Barcelona.

6.3.3. Preparation of the analytical measurement system and response evaluation

Preparation of the sulfide online-monitoring system: System calibration

After the microdevice building and the Ag/Ag_2S-working electrode preparation, the analytical system was calibrated as a successive addition method similar to the addition method used for the commercial electrode.[90] In this case the dilutions presented in Table 6.1 were prepared from a sulfide-stock solution and the calibration was done by flowing continuously SAOB through channel 1 (see Figure 6.1) and sequentially the dilutions 5 to 1 (Table 6.1) through channel 2 while E_c was recorded with the Autolab potentiostat. Dilutions lower than number 5 (Table 6.1) were prepared in some cases. The recorded E_c resulted as a stepwise plot of time vs E_c, and the logarithm of TDS concentration shall be linearly related to the E_c as described by Equation 6.3. As all experiments were evaluated at ~20ºC (~293.15K), the slope (m) of the linear regressions in the calibration was used to evaluate the analytical response based on the theoretical slope of -29.09 $mV \cdot decade^{-1}$ (Equation 6.3), which was used as a reference to evaluate the electrochemical response of the electrode as it is also done for the commercial S^{2-}-ISE electrode. Each dilution shown in Table 6.1 and the SAOB were prepared with O_2-free water by bubbling N_2 for 15 min to avoid sulfide oxidation and preserve the buffer solution, respectively.

Table 6.1. Dilutions of sulfide stock solution for the calibration of the S-OMS.

Dilution	Dilution factor respecting sulfide stock solution (TDS)	Preparation	
		From dilution	O_2-free water
1	-	-	-
2	10^{-1}	1 ml of dilution 1	9 ml
3	10^{-2}	1 ml of dilution 2	9 ml
4	10^{-3}	1 ml of dilution 3	9 ml
5	10^{-4}	1 ml of dilution 4	9 ml

Evaluation of the analytical quality parameters

The analytical quality parameters of the S-OMS compelled different experiments that aimed at determining the limit of detection (LOD), the linear range (LR) and the repeatability and reproducibility of the system. LOD and LR were determined for the S-OMS by calibrations of two Ag/Ag_2S-working electrodes before their assembly in the S-OMS. These

calibrations were performed for a sulfide range of 0.02 to 500 mg TDS L^{-1}. The electrodes were assembled to two independent S-OMS that were calibrated for a range of 0.1 to 30400 mg TDS L^{-1}.

The repeatability tests were performed in two sets of experiments. The first set of tests consisted of measuring two sulfide solutions of 10 and 630.7 mg TDS L^{-1} that were measured sequentially three times. The analytical precision was assessed by evaluating the standard deviation (SD) and relative standard deviations (RSD) of the signal for each solution. The second set of experiments consisted of monitoring two sulfide solutions of 2.5 and 86.0 mg TDS L^{-1} with two independent S-OMS settings. This continuous monitoring was carried out by recording the E_c every 0.5 seconds, while samples were taken every 30 minutes to measure the solutions with the commercial S^{2-}-ISE and then comparing the measured values from the two systems for accuracy determination.

Reproducibility tests were evaluated through daily calibration of a unique S-OMS using a sulfide stock solution of 17600 mg TDS L^{-1} and applying the calibration procedure mentioned above. After each calibration, tap water and SAOB were flowed through the S-OMS for 2 hours aiming at mimicking large contact time of the electrodes with a liquid-SAOB matrix. The analytical response, i.e., the sensitivity (*m*) of the calibration curve, was evaluated according to the Nernst Equation (Equation 6.3).

6.3.4. Validation of the sulfide online-monitoring system

The validation of the S-OMS to accuracy evaluation was done with the first 9 experiments of the sequential batch operation explained in Chapter 5. In that sense, the sulfide sample line (Figure 6.1) was connected to the GLR inlet A (Figure 3.1, Chapter 3), and samples were measured every 2 hours. This measurement was done with an automated cycle where microfluid pump A and B were connected to a relay to switch them on and off. The cycles were setup in the custom-made software ADD Control (Labwindows/CVI 2017© National Instruments)[99] as explained in Chapter 4 (section 4.4.1).

The cycles consisted of switching on pump A (Figure 6.1) for 5 minutes to sample the reactor after which it was switched off and pump B (Figure 6.1) was switched on for 2 minutes to flow tap water for tubing and microdevice cleaning. Moreover, a cycle was set up

in the NOVA software that was in pair with the pump cycles and aims at recording the E_c measurement every 2 hours for 2 minutes, the last 2 minutes in which the microfluidic pump A was on as the first 3 minutes of pump A operation were the approximate time for the sulfide samples to flow from the GLR to the S-OMS.

Additionally, TDS was also measured with the commercial S^{2-}-ISE during these experiments, but not with the same sampling frequency. Furthermore, new microdevice with new Ag/Ag_2S-working electrode was used for each batch experiment, and a system calibration was performed before they were used. Finally, a comparison of the validation data to accuracy evaluation with the S-OMS and the commercial S^{2-}-ISE was performed through statistical tests: a liner regression and a *t*-test.

6.4. MANUFACTURE AND CHARACTERIZATION OF THE SULFIDE ONLINE-MONITORING SYSTEM

6.4.1. Microdevice manufacture

The microdevice design was developed similarly to the layout proposed by Pol et al,[75] with some difference regarding the material and the electrodes. Herein, the microdevice is shown in Figure 6.2, in which the design and dimensions of the main microdevice piece, the inlet/outlet connections and the working electrode pieces are detailed. From the three pieces shown in Figure 6.2, the microdevice and the assembly-for-electrode piece were built with the 3-D printer using CPE filaments, while the inlet/outlet were prefabricated-cupper connections. As seen in Figure 6.2, the channels in the microdevice have a square-axial dimension of 1 mm by 1 mm, with a total length of 259 mm that resulted in a liquid residence time of ~8.3 seconds based on the liquid flow rate of 1 ml min^{-1} for each inlet. Also, all pieces were assembled to the main 3D-microdevice piece with fast-drying araldite and in the case of the Ag/Ag_2S-working electrode, the assembly was done after the electrode preparation i.e., the electrodeposition (see section 6.3.2).

The microdevice was built with the main setting shown in Table 6.2, while the extended information of printing layout is detailed in Table A3 of Appendix D; the printing and the plate temperature was set in 255 ºC and 70 ºC according to the filament ideal printing conditions,[176] while the printing layers, the infill density and pattern were set to increase

robustness and reduce liquid leaking. The printing time was 3 hours and 30 minutes and the main piece of the microdevice weighted ~8 grams.

A microdevice was assembled to test liquid leaking and microdevice weakening by flowing SAOB for 24 hours through inlet channels 1 and 2, after which the microdevice did not show any damage or leaking. Therefore, this system was considered robust to proceed with the next step.

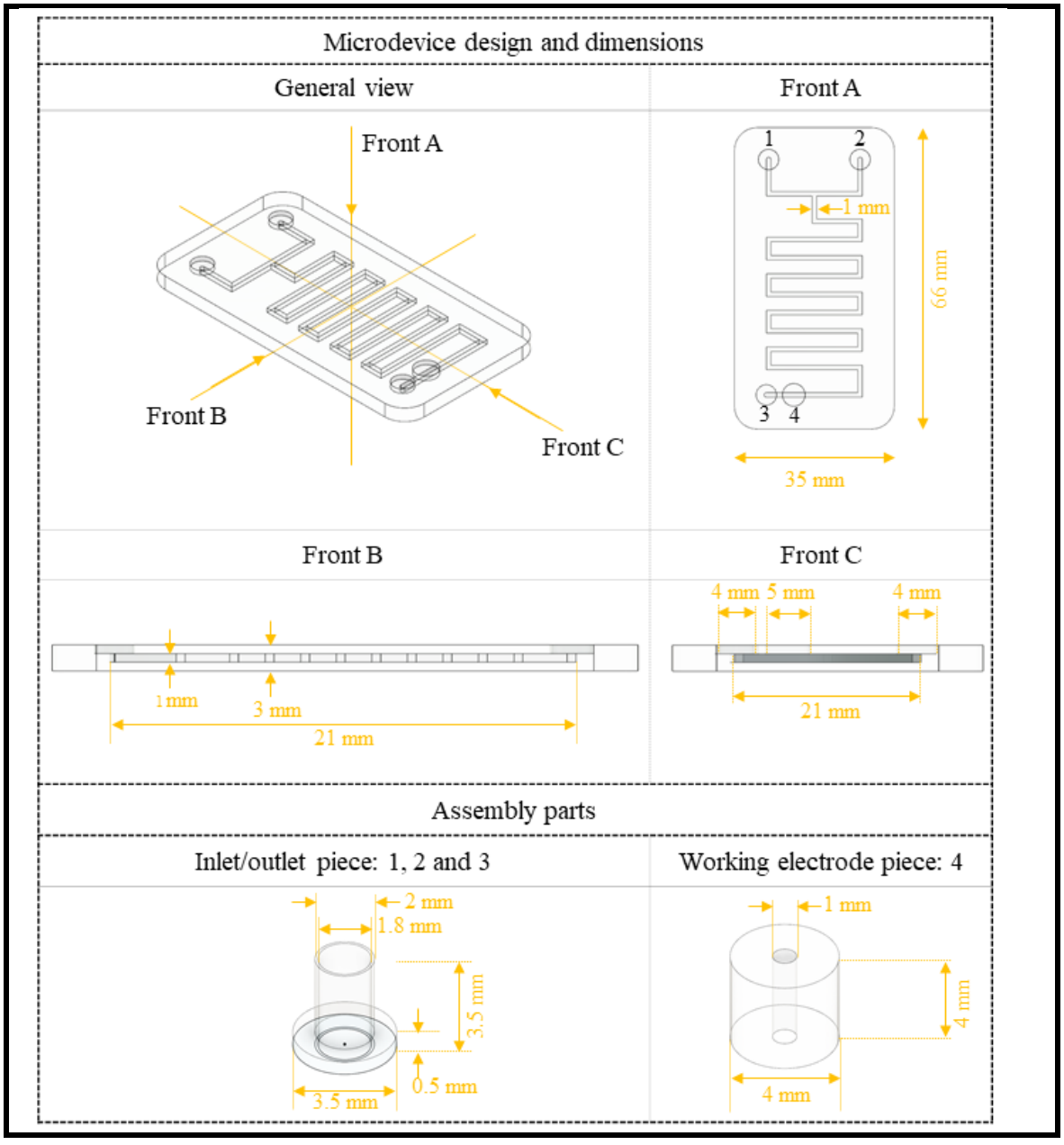

Figure 6.2. Design of the 3D-microdevice. The microdevice and the working electrode piece were designed in Autodesk Fusion 360. The inlet/outlet pieces were prefabricated-cupper connections.

Table 6.2. Main 3-D printer setting for the microdevice manufacture.

Printer	-	Sigma R16 (BCN3D Technologies, Inc)
Hotend	-	e3D-0.4mm-Brass
Printing temperature	[ºC]	255
Plate temperature	[ºC]	70
Infill density	[%]	100
Layer height	[mm]	0.05
Infill pattern	-	Grid
Filament diameter	[mm]	2.85
Total layers	-	58
Printing duration	[hh:mm]	03:30
Microdevice Weight	[g]	~8

6.4.2. Preparation and morphological characterization of the Ag/Ag_2S-working electrode

The Ag/Ag_2S-working electrode was prepared from the electrodeposition process mentioned in section 6.3.2 and then the electrode was analyzed through SEM and SEM-EDX tests. Thus, the results are illustrated in Figure 6.3A and B, where the micrographs, wire diameters and energy dispersive X-ray spectroscopy (EDX) are shown. As seen in Figures 6.3A and B, the untreated-Ag wire had a smooth surface while the Ag/Ag_2S-working electrode surface was harsh, and the diameter difference between them was ~14.8 µm, meaning that the average Ag_2S-wall thickness was ~7.4µm. Meanwhile, EDX confirmed the formation of the Ag_2S layer. The results of energy dispersion (keV) versus relative intensity in arbitrary units (a.u.), showed that the wire was pure Ag while the electrodeposited wire contained Ag and S. The peaks for each element shown in the EDX results are equivalent to 100% (weight) of Ag for the untreated-Ag wire, while the weight fractions were ~12.2% S and ~87.8% Ag for the Ag/Ag_2S wire.

6.4.3. Evaluation of the working range of the sulfide online-monitoring system

After the Ag/Ag_2S-working electrode preparation and morphological characterization, the LOD and the LR of the potentiometric response were evaluated by two consecutive

calibrations of the electrodes before and after assembling.

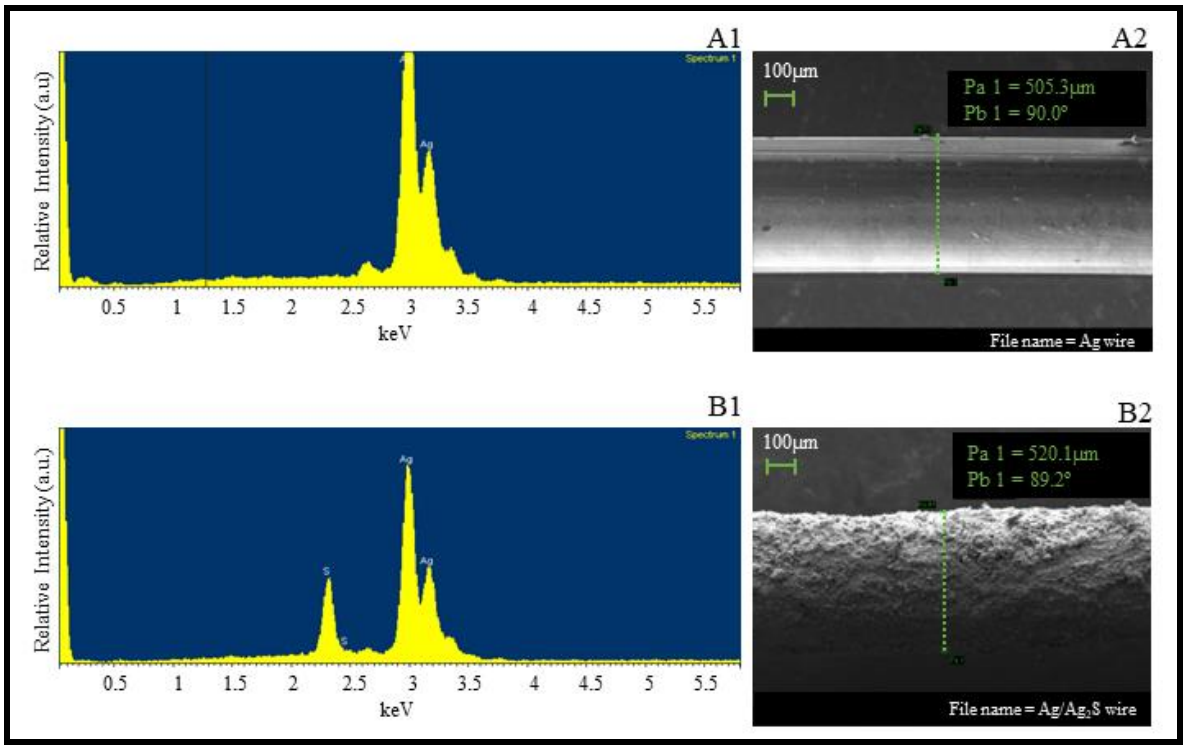

Figure 6.3. Results of SEM and EDX. For the untreated-Ag wire (Figure A) and the Ag/Ag_2S-working electrode (Figure B).

For the first, two Ag/Ag_2S electrodes were subjected to a calibration as shown in Table A4 of Appendix E. These results are shown in Figure 6.4, where logarithm of the TDS concentration versus the E_c in mV are plotted for two Ag/Ag_2S electrodes.

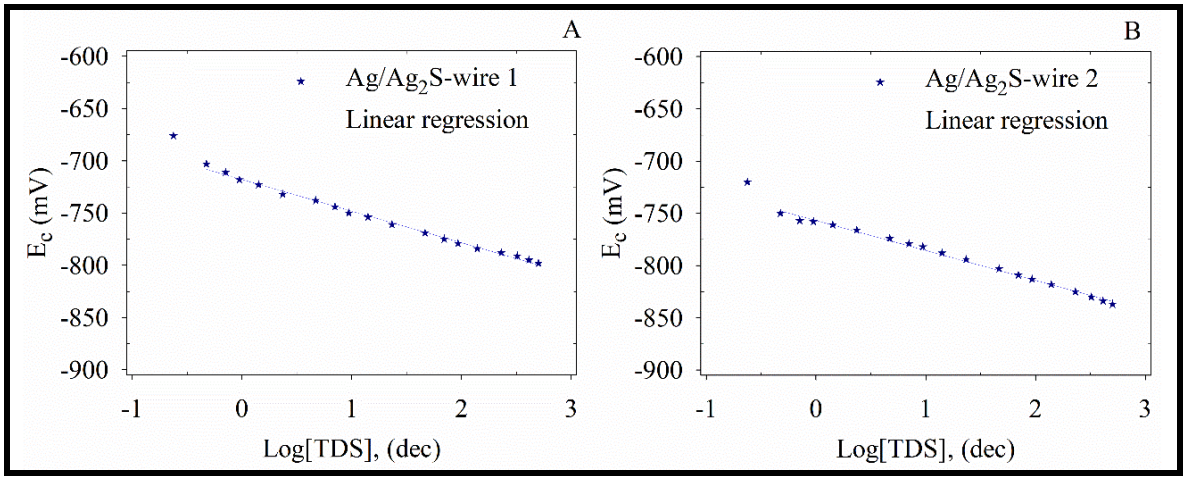

Figure 6.4. Evaluation of the linear range of the Ag/Ag_2S-working electrodes through successive addition method. These calibrations were performed for two Ag/Ag_2S-wires (working electrodes) and are represented in Figures A and B.

The LOD was obtained at 0.2 mg TDS L^{-1} and the low limit of the LR was obtained at 0.5 mg TDS L^{-1} in both cases, i.e., -0.32 in x-axis of Figures A and B, while linearity and stable signal were not achieved for the lower concentrations. The linear regressions for both calibrations were as follows: the slopes (m) were -30.2 and -28.6 mV·dec^{-1}, the y-intercepts (y_0) were -854.1 and -885.8 mV, and the coefficient of determinations (R^2) were 0.995 and 0.995 for wire 1 and 2, respectively.

Consequently, the second set of experiments aimed at determining the linear range of the S-OMS and consisted in calibrating the same Ag/Ag_2S-wires shown in Figure 6.4 but assembled in the S-OMS. Thus, a stock solution was standardized at 30400 mg TDS L^{-1}, and it was used together with dilutions as shown in Table A5 of Appendix E. The results of these calibrations are shown in Figure 6.5, where there are detailed, the same parameters described in Figure 6.4. The results showed that sulfide was not detected for the lowest concentration, i.e., 0.1 mg TDS L^{-1} (data not shown), but it was detected at a concentration of 0.6 mg TDS L^{-1}, which was the LOD. Moreover, a good linear correlation was obtained from concentrations of 1.5 to 30400 mg TDS L^{-1}. The linear regression parameters of the calibration curve were as follows: sensitivities (m) -30 and -29.3 mV·dec^{-1}, y_0 -678.9 and -714.6 mV, and R^2 (n = 6) was 0.99 in both cases, for system 1 and 2, respectively.

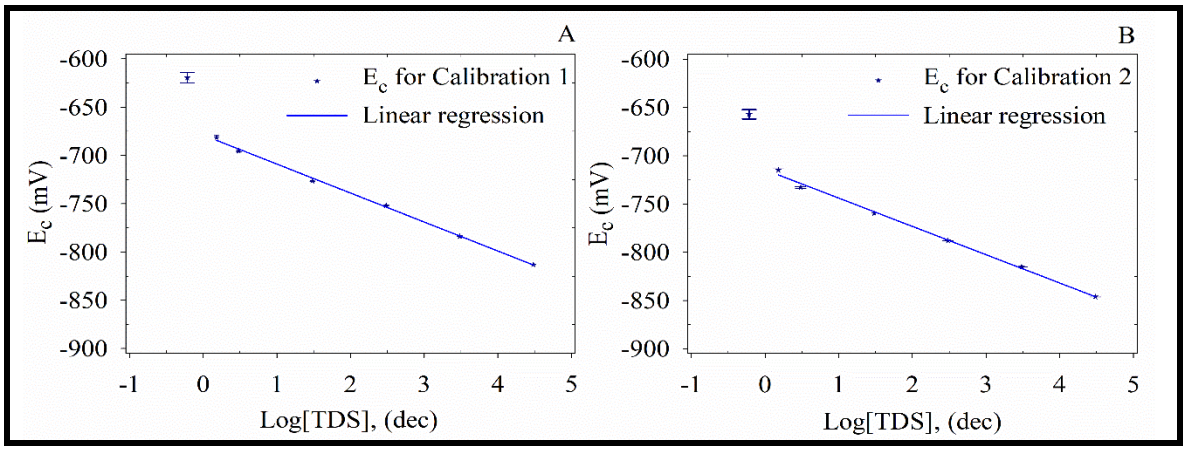

Figure 6.5. Evaluation of the linear range of the sulfide online-monitoring system through the calibration of two S-OMS that were assembled using the Ag/Ag_2S-wires shown in Figure 6.4 A and B, respectively.

6.4.4. Repeatability study of the sulfide online-monitoring system

The analytical robustness of the S-OMS was assessed through measurements over short time periods after different repetitions. The S-OMS calibrations performed in these set of experiments are shown in the Appendix (E). Repeatability tests are shown in Figure 6.6. Figure 6.6A shows the sequential, alternate analysis of two TDS standards (10 and 630.7 mg TDS L^{-1}) in three repetitions. Figure 6.6B shows the continuous evaluation of two standards (2.5 and 86 mg TDS L^{-1}) in two independent S-OMS, as well as the same TDS standards measured with the commercial S^{2-}-ISE.

Results in Figure 6.6A show that E_c required a minimum of about 20 seconds for S2 and about 50 seconds for S1 to reach a stable E_c after switching solutions. Thus, such minimum times to reach a stable E_c were ensured while the last 40 seconds of E_c recorded for each sample were used to analyze the signal variations and the equivalent concentrations. The parameters of the first set of repeatability experiments are detailed in Table 6.3. The recovery percentage was determined by the division of the obtained concentration through the S-OMS by the real concentration of each solution (10.0 mg TDS L^{-1} for standard 1, and 630.7 mg TDS L^{-1} for standard 2). Table 6.3 shows that the maximum RSD for standard 1 was 3.5 % and the average recovery was 103 %; meanwhile, the maximum RSD and the average recovery were 5.3% and 101%, respectively for standard 2.

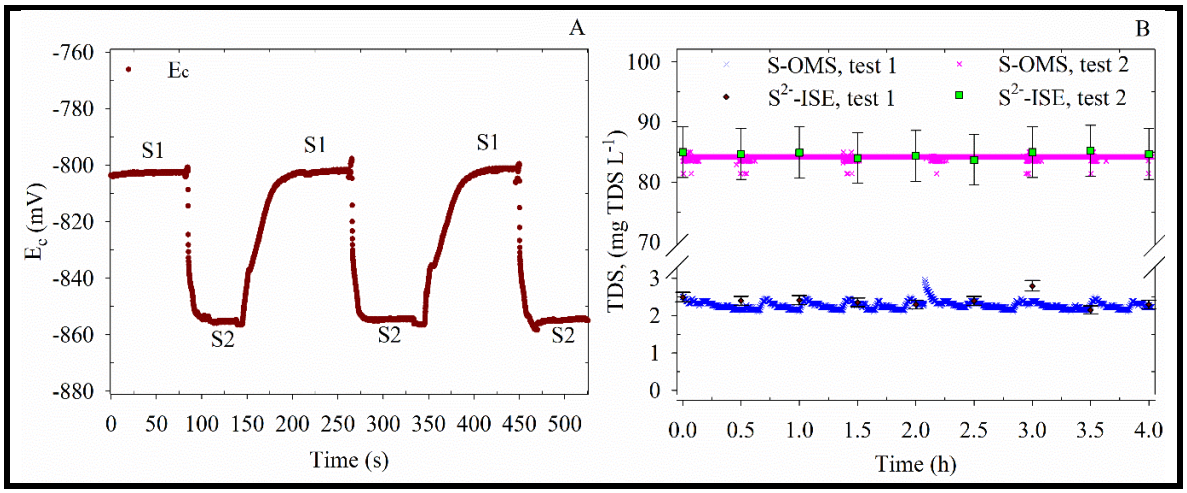

Figure 6.6. Evaluation of the S-OMS repeatability tests. A). E_c was recorded for 10 (S1) and 630.7 (S2) mg TDS L^{-1} in triplicate. B) standards of 2.3 (test 1) and 84.2 (test 2) mg TDS L^{-1} evaluated continuously in independent S-OMS setups and measurements with a commercial S^{2-}-ISE.

Results in Figure 6.6B show that a stable signal and a good matching between the S-OMS and the commercial S^{2-}-ISE were obtained for the two standards assessed. Standard 1 of 2.3 mg TDS L^{-1} lead to an average concentration of 2.3±0.1 mg TDS L^{-1} and an RSD of 4.4% for the S-OMS. A concentration of 2.4±0.2 mg TDS L^{-1} and an RSD of 7.2% were obtained for the commercial S^{2-}-ISE. Standard 2 of 84.2 mg TDS L^{-1} lead to 84.2±0.2 mg TDS L^{-1} and an RSD of 0.3% for the S-OMS, and to 84.3±0.7 mg TDS L^{-1} and an RSD of 0.9% for the S^{2-}-ISE.

Table 6.3. Results of repeatability test. The mean concentration of each measurement (*n* = 3) is detailed with the standard deviation (SD), the relative standard deviation (RSD) and the recovery.

Concentration standard 1 [mg TDS L^{-1}]	SD	RSD (%)	Recovery (%)	Concentration standard 2 [mg TDS L^{-1}]	SD	RSD (%)	Recovery (%)
10.7	0.2	1.8	107	655.8	25.7	3.9	104
10.4	0.3	2.4	104	631.2	33.8	5.3	100.1
9.9	0.3	3.5	99	630.3	15.3	2.4	99.9

6.4.5. Reproducibility study of the sulfide online-monitoring system

Results of the reproducibility test are shown in Figure 6.7. The sensitivity (*m*) of each calibration is represented by the slope of each calibration performed, while the error is determined as a percentage deviation from the theoretical value (-29.09 $mV \cdot dec^{-1}$).

An error threshold of 5 % is plotted to visualize the cutoff defined for a proper calibration. Sensitivity error bars (s_b) were determined from a regression of the set of data using the Excel data solver tool. Individual calibration plots and the other main parameters of the linear regression, i.e., R^2 and y_0, are shown in Figure A6 of Appendix E. Figure 6.7 shows that the daily calibration showed a good Nernst approach for the first 8 days as the confidence interval is low and the errors were always below the 5% threshold. The confidence interval turned large, and the errors increased on days 9 (14 %) and 10 (33%).

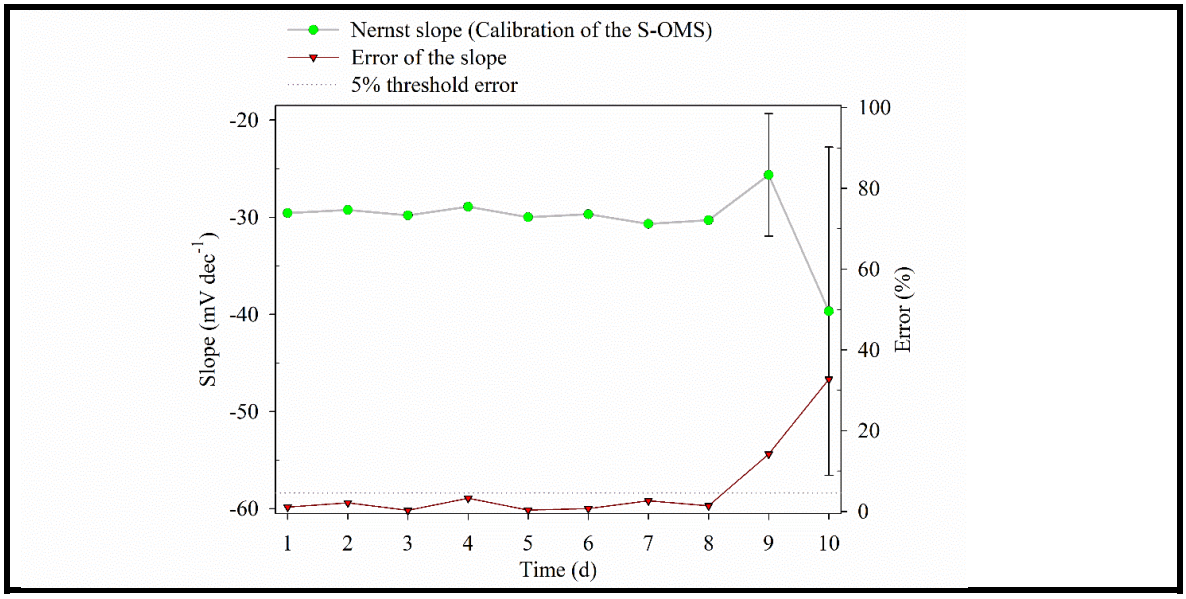

Figure 6.7. Daily calibration of the S-OMS to identify the system reproducibility. The sensitivity (*m*) is represented with green circles with the error bar determined from the linear regression and is plotted on the left y-axis; the error represented with the red-inverse triangles is plotted on the right y-axis where the 5% threshold is also depicted with dotted line.

6.5. VALIDATION OF THE SULFIDE ONLINE-MONITORING SYSTEM WITH THE GLR OPERATION

The validation of the S-OMS was performed with the sequential batch operation of the GLR presented in Chapter 5, where batches 1 to 9, excluding batch 7, were used to monitor the TDS production in each batch and the results are shown in Figure 6.8. The results of the S-OMS and the commercial S^{2-}-ISE are shown in Figure 6.7A. In Figure 6.7B, the correlation of the two analytical systems for the data that were measured at similar time and the linear regression of these two sets of data are depicted; the slope (m), the y-intercept (y_0) and the correlation of determination (R^2) are shown in the legend. Also, for the S-OMS an individual and new S-OMS was implemented for each batch operation, which means that a total of 8 systems were used, and their calibrations and main parameters from the linear regression are detailed in Figure A7 of Appendix E.

Figure 6.8A shows that the two analytical systems have a good matching between them, as the TDS concentrations in both methods showed a similar trend. This matching can be proved by the results in Figure 6.8B, where the linear regression test exhibited a strong relation between the two methods that can be quantitatively analyzed from the linear regression parameters: m (1.03±0.09), y_0 (-27.9±60.5) and R^2 (0.92). Additionally, data

plotted in Figure 6.8B were also compared through a *t*-test for pair samples with two tails and 95% confidence. This test resulted with a *p*-value of 0.643, a *t*-value of -0.477 and a *t*-critical of 2.2, which means that there was no significant statistical difference between the two sets of data.

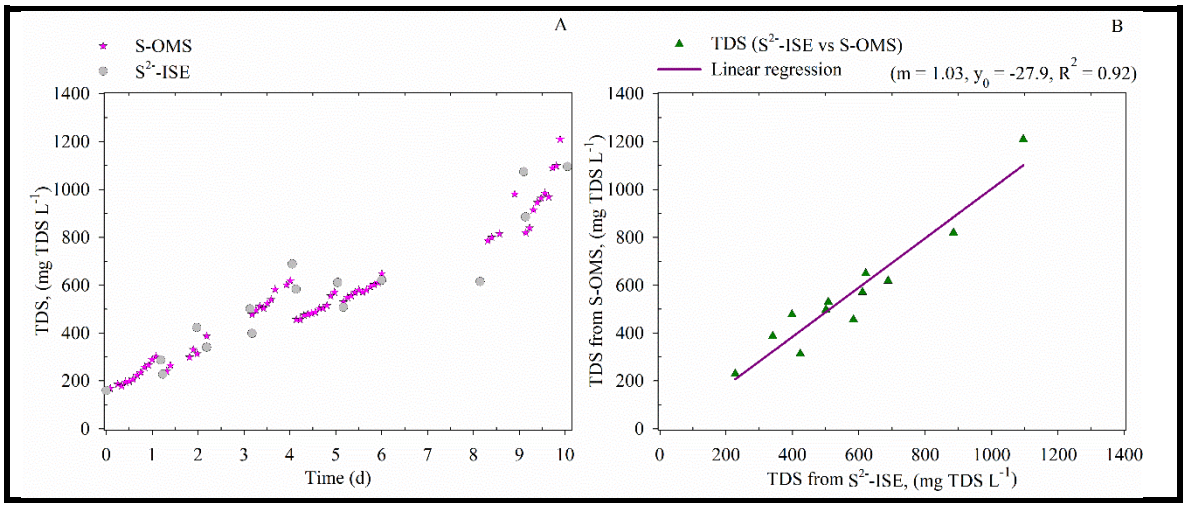

Figure 6.8. Validation of the S-OMS with the experimental data of the GLR sequential batch operation. (A) TDS data from the S-OMS and S^{2-}-ISE. (B) Comparison of the two systems for the sampling time taking at similar time.

6.6. DISCUSSION OF THE ANLAYTICAL RESULTS OF THE NOVEL SULFIDE ONLINE-MONITORING SYSTEM

Regarding the S-OMS fabrication, different observations can be made; from one part, the microdevice manufacturing using CPE-filament showed to be robust as no problem associated with leaking or weaking of the microdevice was observed along the experiments. The electrodeposition resulted with Ag/Ag_2S-working electrode composed mainly by silver sulfide (Ag_2S), which was the composition needed to use it as a potentiometric electrode. From there, it can be concluding that the fabrication process was made successfully.

Regarding the LOD and the LR, the results show that the potentiometric sensitivity of the S-OMS agrees with the theoretical value (m = 29.09 mV dec^{-1}) in the LR. Results can be compared with remarkable results reported in the literature, as seen in Table 6.4. The S-OMS had a low LOD similar to other works,[75,169] but better results were reported by Vallejo et al.,[168] and Li et al.,[166] for FIA systems. The LR was large and similar to the work reported by Pol et al..[75] The reliability of the S-OMS was demonstrated in the repeatability and

reproducibility studies. For the first set of repeatability test, acceptable RSD for repeatability tests are[177] between 4 to 6 % for concentrations of 0.001 to 0.01 % (w/w), which is the case of standard 1, and 3 to 4 % for concentrations of 0.01 to 0.1% (w/w), which is the case of standard 2. The results indicate that a good accuracy in the measurement was observed in five out of six cases. For the second set of repeatability test, even though the means and SDs were similar between the S-OMS and the S^{2-}-ISE, the RSD was higher than 5% for the S^{2-}ISE. Yet, only nine measurements were done with the S^{2-}-ISE, which made the deviation values more influential (as it is for data at 3h). Meanwhile, the E_c measured for the S-OMS was recorded every 0.5 s and resulted in ~28800 data for the 4 hours of monitoring, which made the deviation values less influential for the statistical parameter RSD. Overall, the two analytical measures showed a good agreement between them.

Table 6.4. Literature reports of some remarkable sulfide monitoring systems.

Sulfide analytical system	Limit of detection (LOD) [mg TDS L^{-1}]	Linear range (LR) [mg TDS L^{-1}]	Response time [s]	Reference
3D-printed sulfide electrode (online monitoring)	0.96	3.2 - $3.2 \cdot 10^4$	8	[75]
Sulfide selective electrode (FIA)	0.03	0.1 - 30	240	[168]
Sulfide selective electrode (FIA)	0.32	0.32 - (not reported)	30	[169]
3D-printed fluorescent platform (*in situ*)	-	$3.2 \cdot 10^{-3}$ - 0.16	1200	[162]
Spectrophotometric methylene blue (FIA)	$1.8 \cdot 10^{-5}$	$6.1 \cdot 10^{-5}$ - 4.8	600	[166]
3D-printed microfluidic sulfide-selective sensor (online monitoring)	0.6	1.5 - $3 \cdot 10^4$	20 - 50	This work

The reproducibility test showed that after 8 days, corresponding to a total of 16 hours of electrodes in contact with SAOB-matrix, the Nernst response and the linear regression turned deficient, meaning that the Ag/Ag_2S-working electrode must be replaced or rebuilt with a new electrodeposition of Ag_2S. The decrease in the sensitivity response has been reported in the literature for electroanalytical cells and can be related to different factors such as the sample matrix, microbial cell debris,[173] or formation of silver complexes with EDTA,[178] which means that further studies must focus on these interference factors.

Respecting the validation of the S-OMS, the value of *m* close to 1 indicates a high linear correlation between the two analytical system, which is also the case for R^2; this latter is more sensible to experimental deviations,[179,180] and therefore the deviations from linearity observed in Figure 6.8B have more influence over this parameter. The validation of the S-OMS was also demonstrated from the *t*-test.

Thus, the S-OMS system showed equivalent to the experimental data obtained with the commercial S^{2-}-ISE that was based on a crystalline membrane. Other flow analysis strategies have been applied to the environmental biotechnology field for determination of multiple compounds or ions, with few reports focusing on the detection of sulfide.[181] Sulfide measurement systems have been implemented in online mode on spectrophotometric techniques with detection range of the order of 10^{-1} to 10^{1} mg TDS L^{-1}.[182,183] However, most sulfide flow analysis systems have been reported in the literature with the use of commercial ISEs. Silva et al.,[184] implemented a sequential injection analysis (SIA) system for the detection of sulfide in wastewater and obtained a detection range from 0.17 to 1 mg TDS L^{-1} with a RSD of 5.2%. Potentiometric methods in FIA systems have been explored with commercial ISE,[169] and for in-situ measurement in sulfidogenic reactors.[167]

Thus, the presented S-OMS is a sound approach for future applications as an analytical tool in sulfidogenic reactors where measurements over a wide range of TDS concentrations are required. Also, for the fully validation of this system, further studies are suggested to identify the influence of sample matrix over analytical response and to explore the factors affecting the loss in the potentiometric respond after 16 hours of continuous contact with SAOB.

6.7. MAIN CONCLUSIONS

The S-OMS proposed in this work was manufactured with 3D printing technology and using CPE-filament. The device was fast and easy to manufacture, showing a strong mechanical/chemical stability as no leaking of the microdevice was observed in any of the experiments. The S-OMS showed a good linear correlation between the logarithm of the TDS and the E_c for a working range of 1.5 to 30400 mg TDS L^{-1}. Moreover, the repeatability and reproducibility experiments in the S-OMS showed an RSD in the range 1.8-5.3 % and a

useful lifetime of 16 hours under continuous operation after which the Ag/Ag_2S-working electrode shall be replaced or subjected to a new electrodeposition. The sensitivity of the S-OMS agreed with the theoretical value.

The S-OMS was validated with real samples from a H_2-fed sulfidogenic GLR. The validation consisted in comparing the measurements of S-OMS with a commercial S^{2-}-ISE. The results indicated that the two analytical system were correlated, as it was concluded from a linear regression of the set of data and a *t*-test that showed that there was not significant statistical difference from the two analytical systems. Overall, the S-OMS herein developed is useful as an analytical tool in sulfidogenic reactors where broad range of TDS concentrations are obtained. Nevertheless, further studies are suggested to identify the influence of sample matrix over potentiometric response and to detect the factors affecting the loss Nernst response after 16 hours of continuous operation.

CHAPTER 7

MATHEMATICAL MODELING OF THE BIOLOGICAL SULFATE REDUCTION

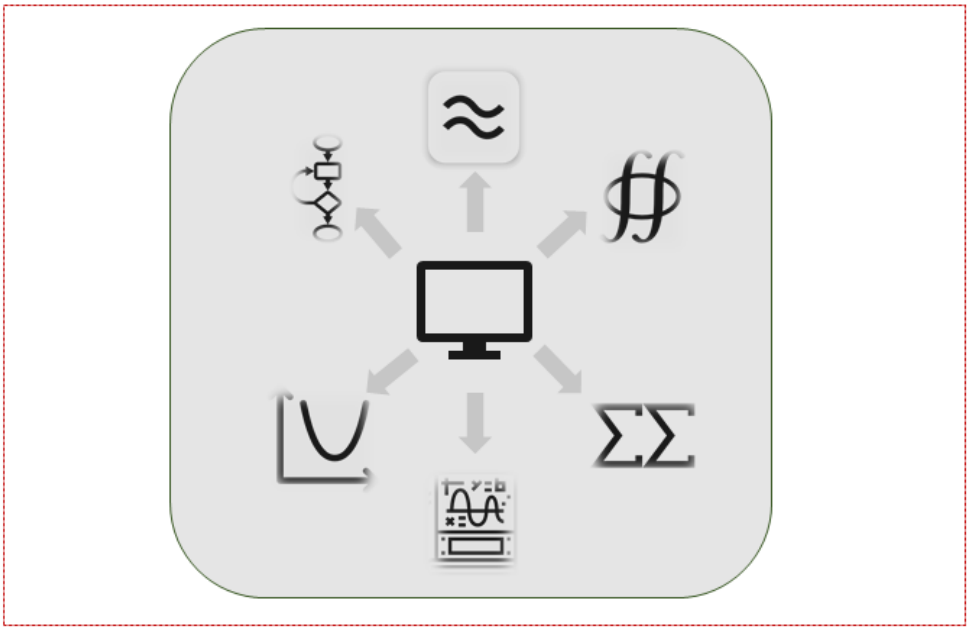

7.1. CHAPTER OUTLINE

Herein, a mathematical model was developed to describe the biological sulfate reduction in the GLR operated in a sequential batch mode that was presented in Chapter 5. The experimental operation of the GLR consisted of 60 batch cycles with a duration of 21 to 22 hours each, where after each cycle part of the culture medium was removed from the reactor for solids sedimentation and extraction of the supernatant, as described in section 5.2.1 of Chapter 5. The sequential batch operation was divided into 8 stages defined from the sulfate loading rates (SLR) as shown in Table 5.1 (section 5.2.2 of Chapter 5).

The mathematical model was defined, calibrated, and validated using the experimental data of the operation mentioned above. After the mathematical model validation, two set of simulations were evaluated for different influent (in terms of sulfate concentrations) and operational conditions. These simulations were developed to demonstrate the usefulness of the model to study the system performance under diverse conditions.

Chapter 7 is organized as follows. A brief presentation in this section 7.1. An introduction of mathematical models and their usefulness is detailed in section 7.2. The mathematical model layout, description, assumptions, and mathematical tools are detailed in section 7.3; the results of the sensitivity analysis are explained in section 7.4; the model calibration and validation are described in section 7.5; the analysis of the parameters calibration in section 7.6; the simulation of different influent and operational conditions in section 7.7; and finally, the main conclusions are detailed in section 7.8.

7.2. INTRODUCTION

7.2.1. Mathematical modeling: an optimization tool for experimental design and process scale-up

Mathematical tools have been implemented worldwide in multiples engineering fields and, in particular, different well-known mathematical models have been developed in the environmental biotechnology area for process design, optimization, scale-up, environmental assessments, process control and scientific research.[44,76,185,186] Overall, the structure of mathematical model implementation includes three global steps: 1) Experimental evaluations; 2) Build-up of mathematical models based on mass balances and microbial kinetics; 3) Mathematical model calibration and validation using experimental data.[76]

One of the first mathematical modeling advances and milestone in the biological treatment of wastewater was led by the International Water Association (IWA), formerly known as the International Association Water Pollution Research and Control (IAWPRC), that developed the activated sludge model (ASM), with its different extensions, aiming at standardizing modeling concepts, enhancing research experimental design and aiding wastewater treatment plant operations.[187]

Thus, through the different extensions of the ASMs, the biological nitrogen, phosphorus and denitrification processes have been described and their applications have been widely proven.[187–189] The IWA has also developed mathematical models for the anerobic treatment of wastewater: the anaerobic digestion model (ADM1), in which the steps of organic-compounds anaerobic biodegradation, i.e., hydrolysis, acidogenesis, acetogenesis and methanogenesis, are described.[79] Indeed, the ADM1 has been extended to include the biological sulfate reduction process as this one normally plays an important role in anaerobic digestion.[77,78,80,83] Nevertheless, anaerobic processes where no organic compounds are largely present and/or fed, e.g., autotrophic sulfate reduction, describe different microbial activities and therefore the biodegradation pathways are diverse. Accordingly, several mathematical models have been proposed to describe the different types of substrate and microbial activity observed in anaerobic systems.[134]

The autotrophic sulfate reduction, where H_2 is used as electron donor, is normally characterized by the proliferation of three main microbial activities: autotrophic (hydrogenotrophic) sulfate reduction, homo-acetogenesis and methanogenesis.[37] These processes have been studied in gas-lift reactors (GLR) to boost the gas-liquid mass transfer, enhance biomass aggregation and mimic a stirred tank reactor (STR) where mixing conditions are favored.[94]

Extensive literature reviews have been done on biological sulfate reducing processes and kinetic parameters estimation by Cassidy et al.[44] and Lens et al.[4] showing that most works have been performed in UASB-type reactors and organic compounds-fed reactors, where the microbial biodegradation of organic compounds mentioned above were accounted for.

Few mathematical models have been reported for hydrogenotrophic sulfate reduction in H_2-fed GLRs. Esposito et al.,[46] proposed a mathematical model using parameters from the literature for GLR design under only-autotrophic and for autotrophic/heterotrophic sulfate

reduction. Similarly, Frunzo et al.[81] also took parameters from the literature and validate a mathematical model for steady-state and dynamic conditions in a GLR under continuous operation.

In terms of estimations of kinetic and stoichiometric parameters for hydrogenotrophic sulfate reducing microorganisms (H2-SRB), they have been reported from mathematical model studies in UASB-type reactors and, in general, based on ADM1. That was the case of Federovich et al.,[78] who developed an extension of ADM1 to describe a long-term operation of a UASB reactor and reported kinetic parameters of H2-SRB. Similar works were described by Kalyuzhnyi et al.,[83,96] where kinetic and stoichiometric parameters for H2-SRB, homo-acetogenic (homo-AC) and methanogenic microorganisms were reported.

Other works have estimated kinetic parameters of H2-SRB for different setup and process conditions. Tang et al.,[95] performed a mathematical model and H2-SRB parameter estimation for a denitrifying membrane biofilm reactor while Noguera et al.,[190] reported a model of lactate- and H_2- substrate for sulfate reducing microorganisms growth. Also, sulfate reducing biofilm has been mathematically modeled to determine process performance in organic compounds-fed reactors.[191]

7.3. MATHEMATICAL MODEL DESCRIPTION

The mathematical model was developed in four main steps that are defined in Figure 7.1: the mathematical model definition, the sensitivity analysis, the model calibration, and the model validation.

For the first step, the model was set up for a single batch cycle based on the mass balances and the microbial growth kinetics, and then the initial conditions in the subsequent sequential batch cycles were stablished from the model assumptions and mass balances. Secondly, a local sensitivity analysis was performed for the same batch cycles used for the model calibration, i.e., the first nine batch cycles were used for this aim. Later, the sensitivity analysis was used to infer which parameters had to be chosen for the calibration. Thirdly, the model calibration consisted in an algorithm set up to minimize an objective function defined as the norm of the arithmetic difference between the experimental and model data. Then, the confidence intervals of the adjusted parameters were determined from the Fisher Information Matrix (FIM) and the residual mean square for the experimental and the model errors were

calculated. As a fourth and final step, the model was validated with the experimental data of batch cycles 10 to 14 and 26 to 60 using the fitted parameters, where different statistical methods were performed to characterize the model accuracy in predicting the experimental values.

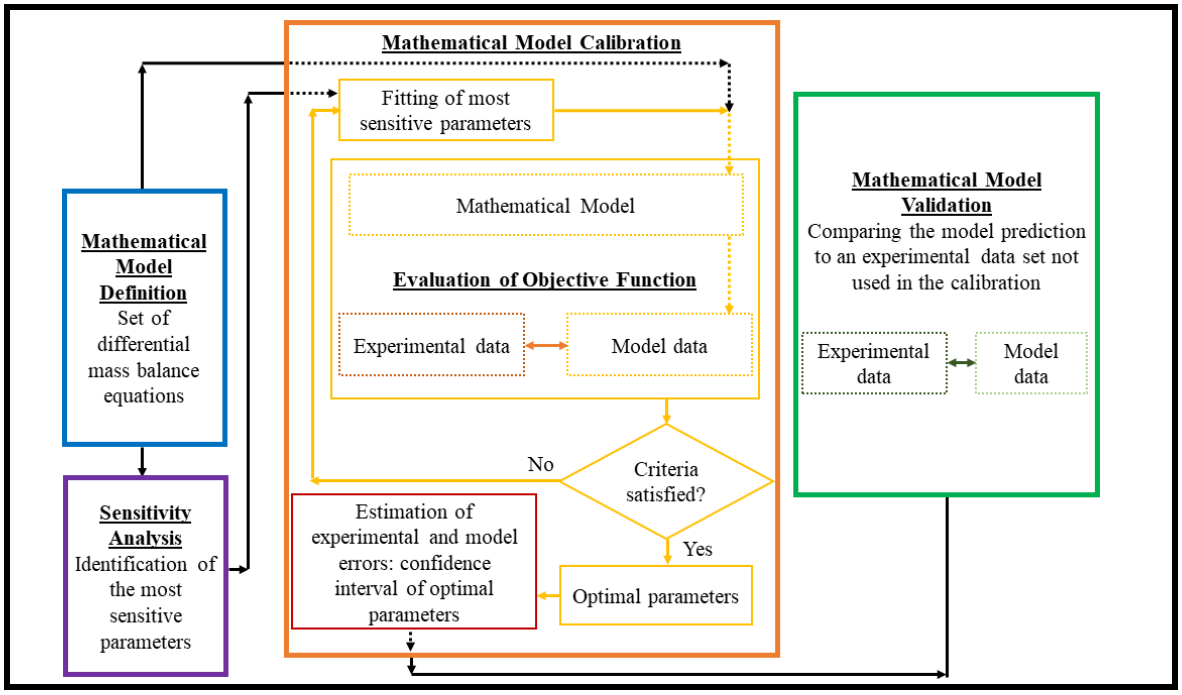

Figure 7.1. Structure of the Mathematical model building. The process was ordered as follows: 1) set of the mass balance equations of all compounds, 2) performance of a sensitivity analysis to identify, 3) model calibration, 4) model validation. This figure is a modification of the algorithm proposed by Dochain et al,[76] and Janssen et al.[192]

7.3.1. Definition of the mathematical model for a single batch in the GLR

The mathematical model was developed to describe the hydrogenotrophic sulfate reduction activity in the GLR based on the results of the sequential batch operation. This mathematical model was set up as a mechanistic model that considered two physicochemical processes, i.e., H_2 and H_2S gas-liquid mass transfer, and two microbial processes, i.e., the hydrogenotrophic sulfate reduction by H2-SRB microorganisms and acetate production by homo-AC microorganisms. Eight components were considered in the model as detailed in Table 7.1. Sulfate, sulfide in the liquid phase (represented as total dissolved sulfide, TDS) and sulfide in the gas phase are herein presented in units of the equivalent sulfur concentration. Inorganic carbon was assumed to be in excess and was not considered as a variable.

Regarding the two physicochemical processes, the H_2- and H_2S- mass transfer rates are defined from the two-film theory,[102,104,143,193] and are described by Equations 7.1 and 7.2, respectively (Table 7.2). For H_2 and H_2S respectively: $r_{t.H2}$ and $r_{t.H2S}$ represent the gas-liquid mass transfer rates, K_La_{H2} and K_La_{H2S} represent the overall mass transfer coefficients, $[H_2]_{sat}$ and $[H_2S]_{sat}$ represent the saturation concentration in the liquid phase at the reactor temperature (~20ºC), and $[H_2]_l$ and $[H_2S]_l$ both represent the concentrations in the liquid phase. In the case of hydrogen sulfide, its concentration in the liquid phase, $[H_2S]_l$, is a pH-dependent fraction of the TDS that depends on the dissociation constants, i.e., pka_1=7.04 and pka_2=11.96,[131] and is calculated using Equation A11 (Appendix B). In both cases, the liquid saturation concentrations, $[H_2]_{sat}$ and $[H_2S]_{sat}$, were determined from the corresponding Henry coefficient[47] (Appendix C) and the concentrations, $[H_2]_g$ and $[H_2S]_g$, in the gas phase determined by the model.

Table 7.1. Components considered in the model mass balances.

Mass balances in the liquid phase		
Sulfate	$[S\text{-}SO_4^{2-}]$	[mg $S\text{-}SO_4^{2-}$ L^{-1}]
Total dissolved sulfide	[TDS]	[mg TDS L^{-1}]
Hydrogen	$[H_2]_l$	[mg H_2 L^{-1}]
Acetate	[AC]	[mg AC L^{-1}]
Hydrogenotrophic sulfate reducing microorganisms	[H2-SRB]	[mg VSS L^{-1}]
Homo-acetogenic microorganisms	[homo-AC]	[mg VSS L^{-1}]
Mass balances in the gas phase		
Hydrogen sulfide	$[S\text{-}H_2S]_g$	[mg $S\text{-}H_2S$ L^{-1}]
Hydrogen	$[H_2]_g$	[mg H_2 L^{-1}]

The K_La_{H2} was previously determined in the GLR (Chapter 4, section 4.4.2) and based on the discussion in Chapter 5 (section 5.4.1), about the estimation of the maximum H_2-mass transfer, a correction factor was applied to the K_La_{H2} for the mathematical model. This was

done as follows: the highest sulfate reduction rate (SRR) achieved along the whole operation was 1144 mg $S\text{-}SO_4^{2-}$ L^{-1} d^{-1} for cycle 48 and, based on the stoichiometric yield in Equation 2.3 (Chapter 2), the equivalent H_2 consumption was 286 mg H_2 L^{-1} d^{-1}, which is a value higher than the theoretical and maximum H_2-mass transfer estimation, i.e., 126 mg H_2 L^{-1} d^{-1} (Chapter 4, section 4.4.4); therefore, a correction factor of 2.3 was applied to the K_La_{H2}, considering that the highest H_2 transfer rate in the reactor was that required to obtain the experimentally observed sulfate reduction rate in batch 48. The H_2S-mass transfer coefficient (K_La_{H2S}) was estimated from the H_2 and H_2S diffusivity coefficients as shown in Equation A12 (Appendix C) as previously reported.[194,195]

Table 7.2. Physicochemical process rates of the sequential batch operation of the GLR.

Gas-liquid mass transfer rates	
$r_{t.H2} = K_La_{H2}\cdot([H_2]_{sat} - [H_2]_l)$	Equation 7.1
$r_{t.H2S} = K_La_{H2S}\cdot([S\text{-}H_2S]_{sat} - [S\text{-}H_2S]_l)$	Equation 7.2

Regarding the microbial growth, kinetics is detailed in Equations 7.3 to 7.6 in Table 7.3. Monod kinetic terms were chosen for microbial growth on hydrogen for H2-SRB and homo-AC, while a non-competitive inhibition term was used to describe the H_2S-inhibition over H2-SRB.[111] The H2-SRB growth rate is represented by a double-Monod expression for hydrogen and sulfate, and a non-competitive inhibition term for the H_2S-inhibition (Equation 7.3), where $r_{H2|SRB}$ is the volumetric growth rate for H2-SRB, $\mu_{max.SRB}$ is the maximum specific growth rate for H2-SRB, $k_{H2.SRB}$ is the H_2 half-saturation constant for H2-SRB, k_{ST} is the sulfate half-saturation constant for H2-SRB, k_i is the H_2S-inhibition constant for H2-SRB, $X_{H2|SRB}$ is the concentration for H2-SRB, $[H_2]_l$ the dissolved H_2 concentration, and $[S\text{-}SO_4^{2-}]$ is the sulfate concentration.

Meanwhile, a single Monod kinetic term was set up for the homo-AC growth rate that was based on hydrogen as described in Equation 7.4, where r_{hAC} is the volumetric growth rate for homo-AC, $\mu_{max.hAC}$ is the maximum specific growth rate for homo-AC, $k_{H2.hAC}$ is the H_2 half-saturation constant for homo-AC; and X_{hAC} is the concentration of homo-AC.

Moreover, a first order kinetic term was stablished for the decay rates of both microorganisms as reported previously;[44,46,81] the volumetric decay rates for H2-SRB and

homo-AC are defined in Equations 7.5 and 7.6 by $d_{H2|SRB}$ and d_{hAC}, respectively, where the specific decay rates are b_{SRB} and b_{hAC}.

The kinetic parameters and the yield coefficients for biomass growth and substrate consumption for H2-SRB and homo-AC were taken from the literature and are detailed in Table 7.4. $Y_{SBR|H2}$ and $Y_{hAC|H2}$ describe mass yield coefficients with H_2 for H2-SRB and homo-AC, respectively, and as the values were reported in equivalent chemical oxygen demand (COD), the conversion factor of 1.45 mg COD mg^{-1} VSS[93,136] was used to express the yield coefficients in volatile suspended solids (VSS), while the H_2 equivalent COD was converted to mass of H_2 similarly to the acetate and TDS conversions to COD explained in Chapter 5 (section 5.2.1).

Table 7.3. Kinetic equations used in the model*.

H2-SRB growth rate	$r_{H2\|SRB} = \mu_{max.SRB} \cdot \frac{[H_2]_l}{[H_2]_l + k_{H2.SRB}} \cdot \frac{[S\text{-}SO_4^{2-}]}{[S\text{-}SO_4^{2-}] + k_{ST}} \cdot \frac{k_i}{k_i + [S\text{-}H_2S]_l} \cdot [X_{H2\|SRB}]$	Equation 7.3
homo-AC growth rate	$r_{hAC} = \mu_{max.hAC} \frac{[H_2]_l}{[H_2]_l + k_{H2.hAC}} \cdot [X_{hAC}]$	Equation 7.4
H2-SRB decay rate	$d_{H2\|SRB} = b_{SRB} \cdot [X_{H2\|SRB}]$	Equation 7.5
homo-AC decay rate	$d_{hAC} = b_{hAC} \cdot [X_{hAC}]$	Equation 7.6

*Units for these rate expressions are mg VSS L^{-1} d^{-1}.

Hence, the mathematical model is shown in Table 7.5 in a Gujer Matrix representation,[129] where the abovementioned 8 components and the 6 processes defined in Table 7.1 and 7.2 are gathered. The generation/consumption term for each component is derived from the multiplication of the component column, i.e., stoichiometric coefficients, by the corresponding process rate specified in the last column. In this case, the $S\text{-}SO_4^{2-}/H_2$ ($Y_{ST|H2}$) and acetate/H_2 ($Y_{AC|H2}$) mass yield coefficients were determined from Equation 2.3 and 2.9 in Chapter 2.

Thus, the generation/consumption term, G_i, derived from the Gujer Matrix of the mathematical model (Table 7.5) is used in the mass balance of each component. For the 6 components in the liquid phase, the mass balances are represented by Equation 7.7, while for the 2 components in the gas phase, the mass balances are represented by Equation 7.8. In

these equations, F_g is the gas-inlet flowrate (86.4 L d^{-1}), V_g is the gas volume (0.94 L), and V is the GLR liquid volume (6.75 L), as defined in Section 4.4.1 of Chapter 4.

Until this point, the mathematical model has been defined for the reaction period during the batch cycle operation. However, the sequential batch operation consisted in two main phases: the reaction and the sedimentation period (section 5.2.1 of Chapter 5). Consequently, the initial concentrations of each component must be defined for a batch cycle operation and for the reactor during the sedimentation time. The latter was considered because during the sedimentation period, that always took place for 2 hours in an external tank with a small fraction extracted from the reactor (V_{sed} = 1.5 - 2.5 L), the rest of the GLR was kept operating with a constant gas flow containing H_2/CO_2. Therefore, microbial activity (sulfate reduction and acetate formation) also took place during that period. Hence, biological activity was not considered in the sedimentation tank, but it was accounted for during the sedimentation time in the GLR. Thus, the model was defined to consider both batch periods of a same cycle. The sequential batch operation is explained in detail in Chapter 5 (section 5.2.1).

Table 7.4. Kinetic, stoichiometric, and physicochemical parameters taken from the literature.

Parameter	Symbol	Units	Value	Source
Parameters of the H2-SRB process				
Maximum specific growth rate for H2-SRB	$\mu_{max.SRB}$	[d^{-1}]	0.30	[44]
H_2 half-saturation constant for H2-SRB	$k_{H2.SRB}$	[mg H_2 L^{-1}]	$6.25 \cdot 10^{-3}$	[44]
Sulfate half-saturation constant for H2-SRB	k_{ST}	[mg S-SO_4^{2-} L^{-1}]	0.15	[44]
Sulfide inhibition constant for H2-SRB	k_i	[mg S-H_2S L^{-1}]	550	[96]
Maximum specific decay rate for H2-SRB	b_{SRB}	[d^{-1}]	0.01	[44]
Mass yield coefficient of H2-SRB and H_2	$Y_{SRB\|H2}$	[mg VSS mg^{-1} H_2]	0.20	[78]
Mass yield coefficient of sulfate and H_2	$Y_{ST\|H2}$	[mg S-SO_4^{2-} mg^{-1} H_2]	4	Eq. 2.3
Parameters of the homo-AC process				
Specific maximum growth rate for homo-AC	$\mu_{max.hAC}$	[d^{-1}]	0.27	[132]
H_2 half-saturation constant for homo-AC	$k_{H2.hAC}$	[mg H_2 L^{-1}]	0.90	[132]
Maximum specific decay rate for homo-AC	b_{hAC}	[d^{-1}]	0.01	[46]
Mass yield coefficient of homo-AC and H_2	$Y_{hAC\|H2}$	[mg VSS mg^{-1} H_2]	0.083	[46]
Mass yield coefficient of acetate and H_2	$Y_{AC\|H2}$	[mg AC mg^{-1} H_2]	7.5	Eq. 2.9

Based on this sequential batch settling, the initial concentrations of all components at the beginning of a batch, $[C]_{to}$, were determined with Equation 7.9 and 7.10, for soluble

([S-SO_4^{2-}], $[H_2]_l$, [TDS], [AC]) and particulate components ([H2-SRB] and [homo-AC]), respectively. In Equation 7.9, $[C]_{added}$ is the concentration of component in the mineral medium (MM), i.e., this only applied to sulfate since the other components in the mathematical model were not added in the MM; VE is the liquid volume exchange, i.e., the volume of liquid replaced per new MM mimicking wastewater; $[C]_{end}$ is the concentration of component at the end of the previous batch; 0.5 [liters] is the settled sludge returned to the reactor; $[C]'_{end}$ represents the concentration of component in the GLR after the sedimentation period; V is the total GLR volume during batch operation (6.75 L); and V' is the reactor liquid volume during the sedimentation period ($V' = V - V_{sed}$).

$$\frac{d[C_i]}{dt} = G_i \qquad \text{Equation 7.7}$$

$$\frac{d[C_i]_g}{dt} = \frac{F_g \cdot \left([C_i]_{g_i} - [C_i]_g\right) + V \cdot G_i}{V_g} \qquad \text{Equation 7.8}$$

The particulate initial concentrations at the beginning of a batch were determined from Equation 7.10, where, besides the parameters defined above, f_{sed} is the particulate fraction loss in the sedimentation step, which was 0.25 and 0.37 when V_{sed} was 1.5 and 2.5 liters, respectively, as explained in Section 5.2.1 (Chapter 5).

$$[C]_{t0} = \frac{[C]_{added} \cdot VE + [C]_{end} \cdot 0.5 + [C]'_{end} \cdot V'}{V} \qquad \text{Equation 7.9}$$

$$[C]_{t0} = \frac{[C]'_{end} \cdot V' + [C]_{end} \cdot V_{sed}(1 - f_{sed})}{V} \qquad \text{Equation 7.10}$$

$$[C]'_{g,t0} = \frac{[C]_{g,end} \cdot V_g + [C]_{g,bag} \cdot V_{sed}}{V_g + V_{sed}} \qquad \text{Equation 7.11}$$

It was assumed that the initial concentrations of gas components at the beginning of a batch cycle did not change during the reactor filling; this assumption was made as the liquid filling process (addition of MM) only implied a decrease in the gas phase volume but not a change in the gas composition.

Table 7.5. Gujer Matrix of the Mathematical Model. The Model consists of 8 components and 6 processes.

Process	Stoichiometry								Process rate
	1	2	3	4	5	6	7	8	
	$[S\text{-}SO_4^{2-}]$	$[H_2]_l$	[TDS]	$[H_2]_g$	$[H_2S]_g$	$[X_{H2\|SRB}]$	$[X_{hAC}]$	[AC]	
1. Growth of H2-SRB	$\frac{-4}{Y_{SRB\|H2}}$	$\frac{-1}{Y_{SRB\|H2}}$	$\frac{+4}{Y_{SRB\|H2}}$			+1			$r_{H2\|SRB}$
2. Decay of H2-SRB						-1			$d_{H2\|SRB}$
3. Growth of homo-AC		$\frac{-1}{Y_{hAC\|H2}}$					+1	$\frac{+7.5}{Y_{hAC\|H2}}$	r_{hAC}
4. Decay of homo-AC							-1		d_{hAC}
5. H_2-mass transfer		+1		-1					$r_{t.H2}$
6. H_2S-mass transfer			+1*		-1				$r_{t.H2S}$

*The fraction of TDS equivalent to $[H_2S]_l$ was used for process number 6, and determined from pH as explained in Appendix B.

The same was also considered for the initial concentrations of the components in the liquid phase of the GLR for the sedimentation period, as the reactor partial draining did not imply liquid dilution; therefore, the concentrations of the components in the liquid phase did not change before and after the partial draining.

On the contrary, the liquid volume removed from the reactor (V_{sed}) was replaced with H_2 during the reactor emptying, which means that the H_2 partial pressure in the gas phase raised and, therefore, $[H_2]_g$ was also increased, while $[H_2S]_g$ was diluted. Hence, the initial concentrations of the gas components in the GLR for the sedimentation period, $[C]'_{g,to}$, were determined with Equation 7.11, where $[C]_{g,end}$ represents the concentrations of the gas component at the end of the batch, and $[C]_{g,bag}$ is the concentration in the bag connected to the reactor to replace the liquid volume removed, i.e., this applied only to H_2 as it was the unique component in the gas bag.

Finally, the following are the general assumptions that were considered for the mathematical model development:

- Ideal mixing in the GLR was assumed.
- Inorganic carbon was in excess.
- Biological activity was not considered in the sedimentation tank, but it was accounted during the sedimentation time in the GLR (as mentioned in Chapter 5, section 5.2.1).
- Methanogenesis was not considered as CH_4 was not detected along the operation.
- Water evaporation was not considered in the model.

7.3.2. Sensitivity analysis to identify the most sensitive parameters of the mathematical model

Sensitivity analysis are mathematical tools developed to identify the influence of model parameters over the process variables that can be useful, among other goals, for further fitting of the most critical model parameters to predict a set of experimental data.[76,196] This process can be applied in two main ways: local or global models; while global sensitivity analysis evaluates the simultaneous influence of a set of parameters over output variables, local sensitivity analysis evaluate the individual influence of each parameter over output variables.[197,198]

Particularly, local sensitivity analysis has been extensively used in modeling of bioreactors to identify effects over variables[76,77]. Based on that, the sensitivity analysis was developed herein to evaluate the individual influence of each parameter over the model outputs for the same period that the calibration was performed, i.e., the first 9 cycles, and using Equation 7.12, where the sensitivity function, $f_{t,j}(\theta_k)$, represents the influence of parameter θ_k with an increase of $\Delta\theta_k$, over component j in time.

The cumulative sensitivity function, $F_j(\theta_k)$, of each parameter θ_k over each component j was determined with Equation 7.13, where the time interval was defined from batch 1 to 9 as mentioned before.

$$f_{t,j}(\theta_k) = \frac{\partial C_{t,j}}{\partial \theta_k} = \frac{C_{t,j}(t,\theta_k + \Delta\theta_k) - C_{t,j}(t,\theta_k - \Delta\theta_k)}{2\,\Delta\theta_k} \qquad \text{Equation 7.12}$$

$$F_j(\theta_k) = \sum_{t_0}^{t_{end}} \left| f_{t,j}(\theta_k) \right| \qquad \text{Equation 7.13}$$

Herein, the sensitivity analysis was evaluated with a 10% increase of parameters over the eight components represented in the Gujer Matrix (Table 7.5). Thus, the following parameters were considered in the sensitivity analysis: the mass transfer coefficients, K_La_{H2} and K_La_{H2S}, the initial biomass active fractions of H2-SRB and homoAC, acf_{SRB} and acf_{hAC}, respectively, and the kinetic/stoichiometric parameters shown in Table 7.4.

Finally, simulations were performed in a custom-made code built in MATLAB (R2021a) that used an *ode15s* function to solve the system of differential equations.

7.3.3. Mathematical model calibration and validation

Experimental periods modelled

After the sensitivity analysis, the model was calibrated and validated. The first 9 cycles were used for model calibration to adjust the most sensitive parameters of the model. Then, the adjusted parameters were used to validate the mathematical model with two sets of data: experiments from cycles 10 to 14 and from 27 to 60, as schematically presented in Figure 7.2. Additionally, and as explained in Chapter 5, the SRR unexpectedly dropped in some

cycles during the sequential batch operation as it was the case of cycles 7, 40 and 46. Therefore, since the sequential batch operation implies the setting of the initial concentrations based on the previous cycle (section 7.3.1) to avoid mathematical model error, i.e., divergence from the experimental values, the calibration was done excluding cycle 7; meanwhile, the sulfate and TDS initial concentrations were set equal to the experimental values for batch cycles 41 and 47.

Also, the active fraction of H2-SRB, acf_{SRB}, was recalibrated in cycle 26 as the SLR was significantly reduced during the sequential batch interruption (stage V), batch cycles 15 to 25, as described in Chapter 5.

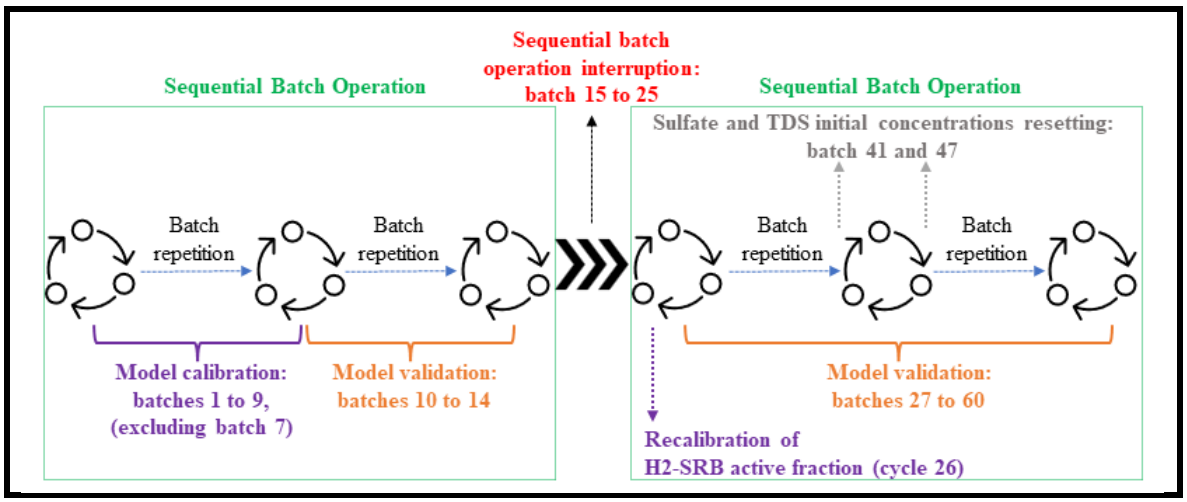

Figure 7.2. Mathematical model calibration and validation with the experimental data. Model calibration was performed with the first 9 cycles (excluding cycle 7); model validation was performed with experiments 10 to 14 and 27 to 60. Cycle 26 was subjected to a recalibration of the H2-SRB active fraction since the SLR was significantly reduced during cycles 15 to 25.

Model calibration

Regarding the calibration procedure, it consisted of three main steps: i) a sensitivity analysis to find the most sensitive parameters, ii) calibration of these parameters to obtain the best model prediction of the experimental values, and iii) determination of the confidence interval of the parameters adjusted.

In the calibration process, sulfate was the unique experimental variable used to fit the parameters and the objective function was defined by the norm of the difference in the experimental and model sulfate concentrations (Equation 7.14) as reported in other works.[186]

Sulfate model concentrations, $[S\text{-}SO_4^{2-}]_{mod}$, were interpolated to the equivalent time of

experimental sulfate values using the MATLAB *pchip* function that is based in a shape-preserving piecewise cubic interpolation,[199] while the objective function, F_{obj}, was minimized with the MATLAB function *fmincon* that finds an optimal local minimum with boundary conditions for nonlinear multivariable functions using an interior-point algorithm.[200] The latter was used to avoid optimization of biomass active fraction higher than 1, which was not possible as the H2-SRB concentration could not be higher than the experimentally measured VSS.

$$F_{obj} = \text{norm}\left([S\text{-}SO_4^{2-}]_{exp} - [S\text{-}SO_4^{2-}]_{mod}\right) \qquad \text{Equation 7.14}$$

As mentioned before, the system of ordinary differential equations was solved using the MATLAB *ode15s* function, which is a variable-step solver based on the numerical differentiation formulas.[201,202]

The parameter estimation errors due to possible error in the experimental values were determined through the Fisher Information Matrix defined in Equation 7.15. In this matrix, N represents the number of experimental data used during the calibration (in this case sulfate), the partial derivative of C with respect to θ is the parameter influence over model sulfate (Equation 7.12) when using the optimal values of parameters, and Q_i is defined as the inverse of the covariance matrix of the experimental error.[76,203] In this case, as sulfate was not measured in duplicate, the experimental error was assumed that of the Ion Chromatography, (5% based on IC calibrates). Thus, the inverse of the FIM is equivalent to the parameters-covariance matrix (*V*), and the approximate parameters standard errors due to experimental error can be determined from the square root of *V*.[76,203]

Similarly, model errors were accounted by assessing the parameters confidence interval. To this aim, the residual error function J(θ) defined in Equation 7.16 was determined first. Then, the residual mean square errors were determined from Equation 7.17. From these Equations, $C_i(\theta)$ is the model sulfate concentration evaluated at the optimal parameters, C_i is the experimental sulfate concentration, p is the number of parameters estimated and N as defined above.

Hence, as suggested by Dochain et al.,[76] the cumulative experimental and model errors to define the parameters standard deviation is defined in Equation 7.18 and the confidence

interval is defined by Equation 7.19, where *t* is the *t*-student determined from a *t*-test that herein was evaluated with a confidence level of 95% (α=0.05).

$$FIM = \sum_{i=1}^{N} \left(\frac{\partial C}{\partial \theta}(t_i) \right)^T Q_i \left(\frac{\partial C}{\partial \theta}(t_i) \right) \quad \text{Equation 7.15}$$

$$J(\theta) = \sum_{i=1}^{N} (C_i(\theta) - C_i)^T Q_i (C_i(\theta) - C_i) \quad \text{Equation 7.16}$$

$$s^2 = \frac{J(\theta)}{N - p} \quad \text{Equation 7.17}$$

$$\sigma(\theta_i) = s\sqrt{V} \quad \text{Equation 7.18}$$

$$CF_{\theta_i} = \pm t_{\alpha;N-p}\sigma(\theta_i) \quad \text{Equation 7.19}$$

Model validation

Model validation was performed to identify the accuracy of the model in predicting the experimental data. For this purpose, three statistical analyses were performed to evaluate the model certainty for the calibration and validation data. The Model Efficiency (ME), the Index of Agreement (IoA) and a linear regression defined in Equations 7.20, 7.21 and 7.22, respectively, were used to compare the model and the experimental data. In these equations, apart from the already defined parameters, $\bar{C}_i$ is the mean of the experimental data, y_i is the y-intercept and *m* is the slope of the linear regression between model and experimental sulfate. The Excel data solver tool was used to determine the errors and the *p*-value of the linear regression parameters. These statistical analyses were used as reported in other works for mathematical model analysis.[76,77,80,81,186,192]

$$ME = 1 - \frac{\sum_{i=1}^{N}(C_i(\theta) - C_i)^2}{\sum_{i=1}^{N}(C_i - \bar{C}_i)^2} \quad \text{Equation 7.20}$$

$$IoA = 1 - \frac{\sum_{i=1}^{N}(C_i(\theta) - C_i)^2}{\sum_{i=1}^{N}(|C_i - \bar{C}_i| + |C_i(\theta) - \bar{C}_i|)^2} \quad \text{Equation 7.21}$$

$$C_i(\theta) = y_i + m \cdot C_i \qquad \text{Equation 7.22}$$

7.3.4. Model simulation under different influent and operational conditions

After the model development, two set of simulations were studied to evaluate the system performance under different sulfate influent concentrations and operational conditions. The simulations were evaluated as shown in Table 7.6. Firstly, the experimental setting shown in Chapter 5 (sequential batch operation) was used to simulate four stages. Secondly, the model was evaluated to predict the performance of the GLR under continuous operation as a continuous stirred-tank reactor (CSTR) with no sludge recovery.

Table 7.6. Evaluation of the model through simulations under different influent and operational conditions

Simulation for a sequential batch operation			
	Cycle duration [d]	VE [L]	Sulfate in the influent [mg $S\text{-}SO_4^{2-}$ L^{-1}]
Stage I	1	1	6000
Stage II	0.5	1	3000
Stage III	1	2	2500
Stage IV	0.5	2	1250
Simulation for a continuous operation			
	HRT [d]	Inlet flowrate [L d^{-1}]	Sulfate in the influent [mg $S\text{-}SO_4^{2-}$ L^{-1}]
Stage I	6	1.1	5000
Stage II	4	1.7	5000
Stage III	4	1.7	3000
Stage IV	2.5	2.7	1000

Mass balance equations for the sequential batch operation were stablished in Equations 7.7 and 7.8. For the CSTR type operation, the mass balances for the liquid phase were defined by Equation 7.23, where $[C_i]_i$ is the concentration of component i in the influent and F_l is the liquid flowrate. The concentrations of validation data at the end of stage VIII were used to

set the initial conditions in both simulations. A pH of 8.2 was used.

$$\frac{d[C_i]}{dt} = \frac{F_l \cdot ([C_i]_{in} - [C_i])}{V} + G_i \qquad \text{Equation 7.23}$$

7.4. RESULTS OF THE SENSITIVITY ANALYSIS: IDENTIFICATION OF THE MOST INFLUENTIAL PARAMETERS OVER MODEL OUTPUTS

The sensitivity analysis was performed using the kinetic and stoichiometric parameters gathered in Table 7.4, and the mass transfer coefficients corrected as explained in section 7.2.1. Meanwhile, for the sensitivity analysis purpose, the active fraction for H2-SRB (acf_{SRB}) and homoAC (acf_{hAC}) were assumed as 30% and 0.5 % of the VSS concentration at the beginning of cycle 1, i.e., 318 mg VSS L^{-1} (section 5.3.1 of Chapter 5); for acf_{SRB}, its approximation was made from the relative abundance of sulfate reducing microorganisms detected in the inoculum (discussed in section 4.4.4, Chapter 4), while acf_{hAC} was set low than 1% as acetate production was not detected during the first 14 cycles. These two parameters were used to set the VSS concentration H2-SRB and homo-AC at the beginning of cycle 1 and the fraction for acf_{hAC} was assumed low due to the absence of acetate during these initial cycles. The sensitivity analyses results are shown in Figure 7.3, where, for each output variable, the cumulative sensitivity function, $F_j(\theta_k)$, for each parameter θ_k is expressed relative to the highest value among them. Thus, Figures 7.3A to 7.3H describe how the model output variables, i.e., components in Table 7.4, change with respect to each parameter i.e., kinetic, stochiometric yield and mass transfer coefficients of the mathematical model. The vertical red dotted line in each Figure represents a 10% threshold above which the relative sensitivity was considered significant.

The results for the components involved in the growth of H2-SRB (i.e., $[S\text{-}SO_4^{2-}]$, $[H_2]_l$, [TDS], $[H_2]_g$, $[H_2S]_g$, $[X_{H2|SRB}]$) showed that the most sensitive parameters were $\mu_{max.SRB}$, k_i, acf_{SRB}, $Y_{SRB|H2}$ and K_La_{H2}. However, large uncertainties were obtained for X_{hAc} and acetate, as 7 and 9 parameters, respectively, showed a large influence over these variables.

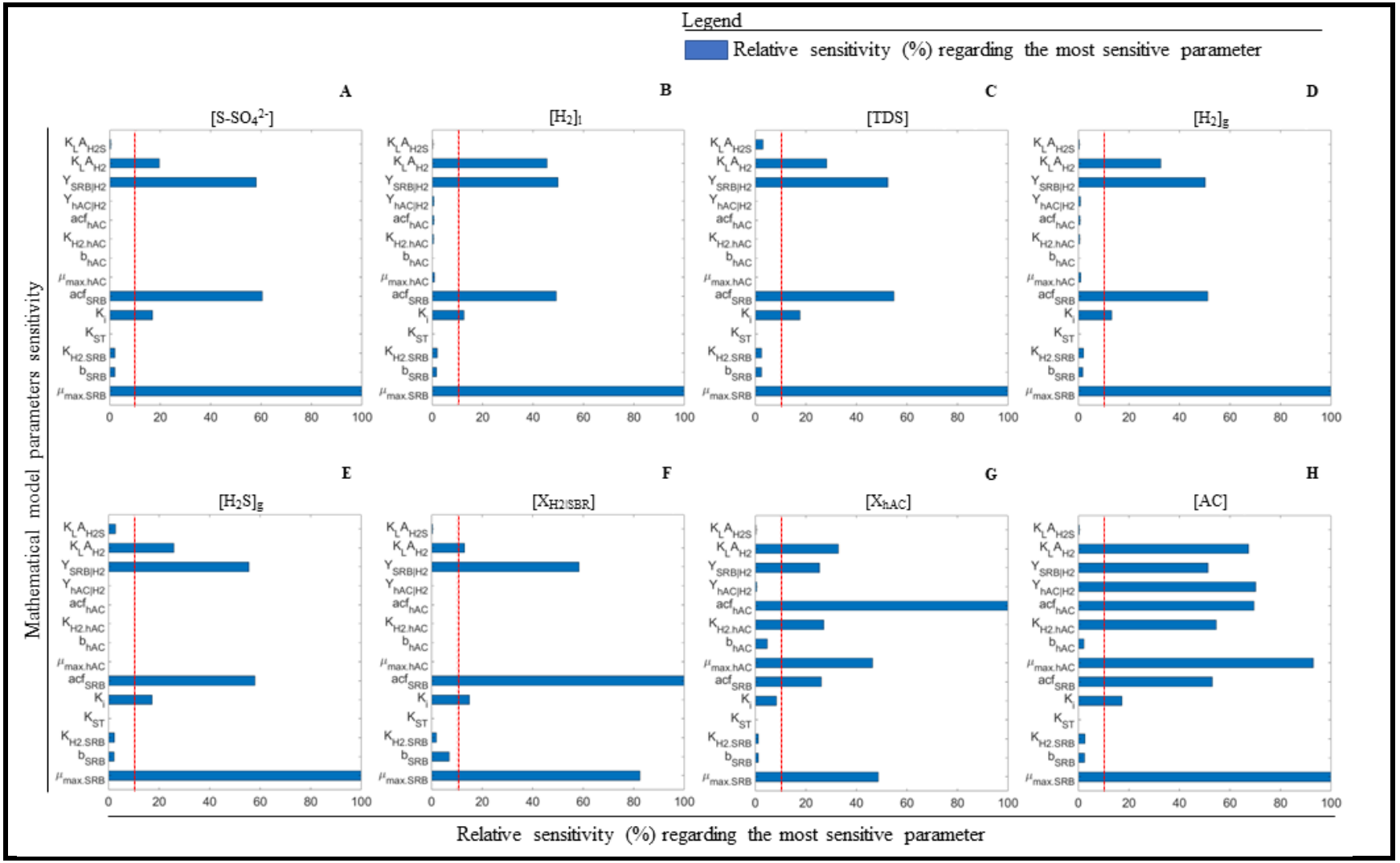

Figure 7.3. Sensitivity analysis of the mathematical model. The relative sensitivity of parameter θ over each component defined as cumulative sensitivity function (F in Equation 7.13) are plotted with respect to the most sensitive parameter. Figures A to H are set for each model component.

The selection of the parameters for model calibration were based on sensitivity analysis results, but other factors were also considered: the experimental data and the nonlinear criterion analyzed by Dochain et al.[76]

The experimental data hinted that homo-AC activity was greatly suppressed as no acetate was observed in the first cycles, which was not the case of H2-SRB activity. Thus, the variables related to the H2-SRB activity were considered over those related to homo-AC for model calibration. Also, in the case of the mass transfer coefficients, the K_La_{H2} was experimentally determined and corrected as explained in section 7.2.1 and, from this value, K_La_{H2S} was also estimated.

Based on the previous discussion, the parameters set was reduced to $\mu_{max.SRB}$, k_i, acf_{SRB} and $Y_{SRB|H2}$, from which $\mu_{max.SRB}$, k_i, and $Y_{SRB|H2}$ are associated to the kinetic growth expression of H2-SRB (Equation 7.3). Since $\mu_{max.SRB}$ and $Y_{SRB|H2}$ are correlated parameters[76], the parameters selected for the calibration were $\mu_{max.SRB}$, k_i, and acf_{SRB}, while $Y_{SRB|H2}$ was set from the literature (Table 7.4).

7.5. RESULTS OF MODEL CALIBRATION AND VALIDATION

7.5.1. Model calibration: optimal parameters and minimization algorithm

As mentioned before, the mathematical model was calibrated with the experimental data of cycles 1 to 9, excluding cycle 7 where SRR dropped significantly. The objective function described in Equation 7.14 was minimized by adjusting the kinetic parameters $\mu_{max.SRB}$, k_i, acf_{SRB}. This process consisted in a multistage estimation to increase the accuracy of the minimization process as it was suggested by Dochain et al.[76] . Both $\mu_{max.SRB}$ and acf_{SRB} were initially estimated with the experimental data from cycles 1 to 6, and the identified optimal values of these two parameters were used to estimate the k_i in a second estimation with the experimental data of cycles 8 and 9.

The two-step estimation resulted in $\mu_{max.SRB}$ = 0.18 d^{-1}, k_i = 158 mg H_2S L^{-1} and acf_{SRB} = 0.20. Then, these three values were used as initial guess for a combined estimation of the three parameters using the set of calibration cycles: 1 to 6 and 8 to 9. This process resulted in the optimal parameters shown in Table 7.7, which also provides the confidence interval of each parameter, the corresponding relative standard deviation (RSD) of the confidence interval and the result of the minimization algorithm.

In the first place, the minimization results show a large value for the F_{obj} that divided by the number of data (37) is equivalent to 33, which is the average error related to each pair of data; this value is equal to 8.4% of the average experimental sulfate concentrations (394 mg $S\text{-}SO_4^{2-}$ L^{-1}) of the data used for the calibration, which means that the error associated to each pair of data is low. Meanwhile, the exit flag value of 2 means that the minimization-stop criteria for the calibration process was due to the change in the x-variable (independent variable) step; in this case the step tolerance was set to 10^{-5} for the independent and dependent variables: time and sulfate concentration. Additionally, the optimal parameters were obtained after 24 iterations.

Table 7.7. Results of the mathematical model calibration. The optimal parameters with the confidence interval and the RSD are detailed; the results of the minimization algorithm for the calibration are also detailed: the objective function value (F_{obj}), the Exit flag that defined the minimization-stop criteria, and the number of iterations.

Optimal values of parameters during calibration and confidence interval			
	$\mu_{max.SRB}$	acf_{SRB}	k_i
Units	[d^{-1}]	-	[mg $S\text{-}H_2S$ L^{-1}]
Value	0.53 ± 0.02	0.200 ± 0.003	100 ± 7
RSD of $CF_{\theta i}$, [%]	3.6	1.3	7
Results of the calibration algorithm in MATLAB			
	F_{obj}	Exit flag	Iterations
Value	1218	2	24

Secondly, the optimal parameters showed a low confidence interval as the RSD was below 5% for $\mu_{max.SRB}$ and acf_{SRB}, and 7% for k_i. The optimal values showed that only 20% of the VSS concentration at the beginning of cycle 1 was due to H2-SRB, the $\mu_{max.SRB}$ was 0.53 d^{-1} indicating that the duplication time for H2-SRB was 1.9 d. Based on the optimized value of k_i (Table 7.7), the H_2S-inhibition was significant along the whole operation, as the equivalent H_2S-concentration raise from cycle 1 to 9 was from 87 to 108 mg H_2S L^{-1} (section 5.3 of Chapter 5), and the average H_2S-concentrations from the other cycles were 102±33 mg $S\text{-}H_2S$ L^{-1} for cycles 10 to 14, 62±7 mg $S\text{-}H_2S$ L^{-1} for cycles 26 to 29, and 148±28 mg $S\text{-}H_2S$

L^{-1} for cycles 30 to 60. These values indicate that the H_2S-concentration was higher than the k_i in many cycles and, therefore, the H_2S-inhibition had a significant impact over the H2-SRB. In fact, Equation 7.3 indicates that when the concentration of H_2S is equal to k_i, the H2-SRB would be reduced to 50% with respect to that at 0 mg S-H_2S L^{-1}. Nevertheless, this H_2S-inhibition was not reflected in the overall performance of the reactor, as no decrease in the SRR was observed.

The optimized kinetic parameters, $\mu_{max.SRB}$ and k_i, will be discussed in detail in section 7.6.

7.5.2. Mathematical model validation and calibration: data comparison and statistical analyses

Sulfate and TDS profile

The mathematical model was run for the whole operation with the optimized parameters. Predicted and experimental concentrations for sulfate and TDS are plotted in Figure 7.4A, while model and experimental TDS concentrations are plotted in Figure 7.4B. The operational stages from which the sequential batch operation was set up (I to VIII) are detailed in both figures, excluding stage V (cycles 15 to 25). These stages were defined, from the sulfate loading rate (SLR) applied along the operation, as follows: cycles 1 to 3 (stage I), cycles 4 to 6 (stage II), cycles 7 to 11 (stage III), cycles 12 to 14 (stage IV), cycles 15 to 25 (stage V), cycles 26 to 30 (stage VI), cycles 31 to 47 (stage VII), cycles 49 to 60 (stage VIII). No sulfate addition was performed for cycle 48 as it was set up to decrease the ongoing sulfate accumulation in the reactor. A detailed description of these stages is provided in Table 5.1 of Chapter 5.

For sulfate, model predictions showed a good fitting for the calibration data. For the second set of validation data, the model was able to correctly describe the sulfate reduction for each batch cycle following the methodology detailed in section 7.2.1 and using the same set of calibrated parameters, thus demonstrating the usefulness of the model for the description of this type of experimental systems. Conversely, the model underestimated the experimental concentration of sulfate in the first set of validation data, cycle 10 to 14, because the experimental rate was lower than the predicted one.

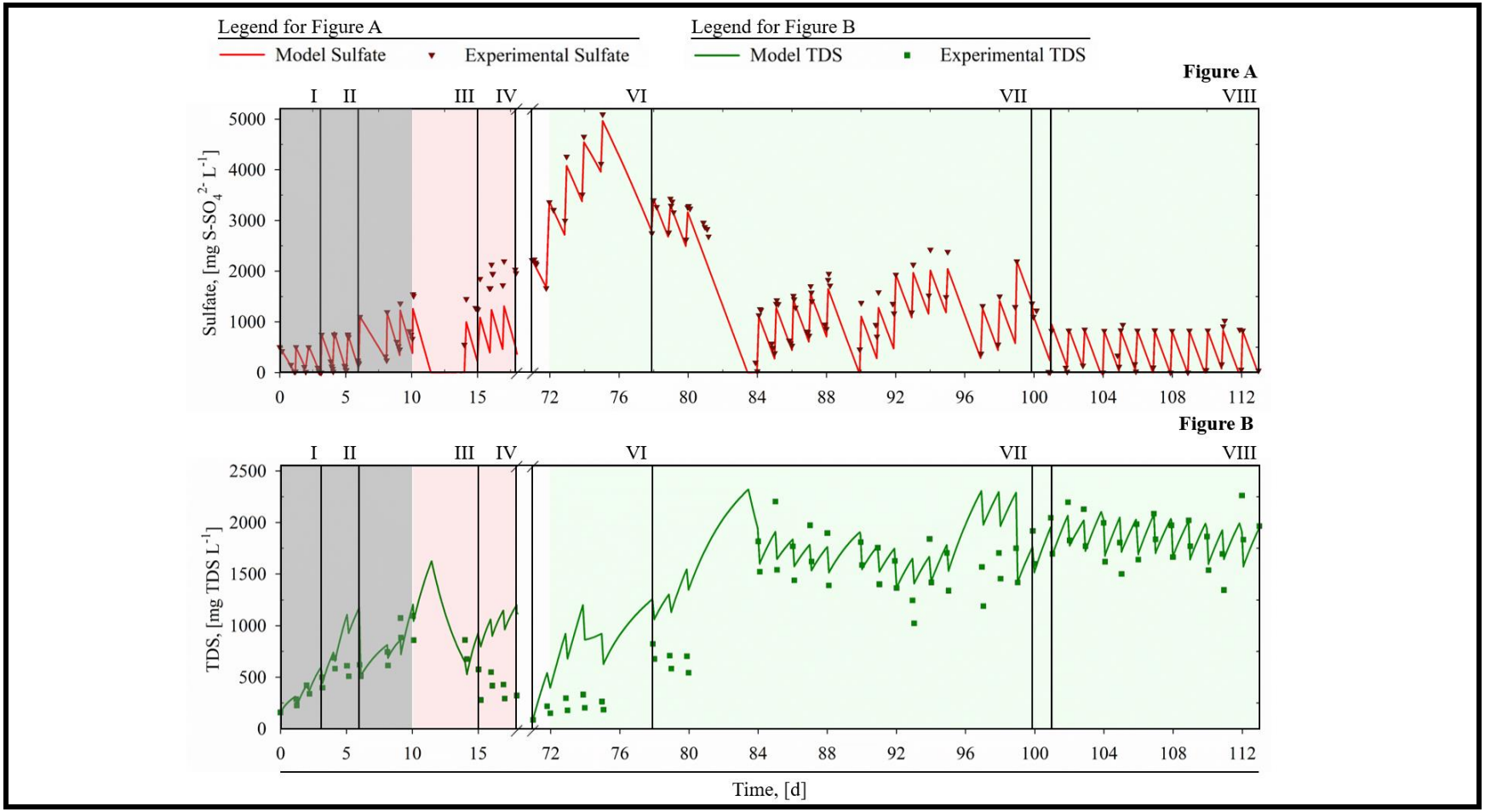

Figure 7.4. Experimental results and model prediction for sulfate and TDS concentrations along the operation (excluding stage V, cycle 15 to 25). In Figure A, model and experimental sulfate are plotted in red-solid line and red-inverted triangles, respectively; in Figure B, model and experimental TDS are plotted in dark green-solid line and green squares, respectively. In both Figures, the color areas in light gray, red and green are equivalent to the calibration, the first and the second set of validation data, respectively. Operation stages, from I to VII, are also detailed.

The significant decrease in the experimental SRR during these cycles was unexpected, as discussed in Chapter 5, and could be explained by operational factors or changes in the microbial community that could not be determined

On the other hand, the predicted profile for TDS had larger deviations from the experimental data for cycle 5 and 6, while from the first set of validation data the unmatched values are explained from the abovementioned loss in the experimental SRR. Regarding the second set of validation data for TDS, the larger differences were observed from cycles 26 to 33 (day 71 to 84) and 44 to 46 (day 95 to 99), albeit a good matching is observed from cycle 34 to 43 (day 84 to 95), 47 (day 99), 48 (100) and all cycles of stage VIII (day 101 to 113). It is worth noting that, although the model reasonably describes the range of TDS concentrations over which the reactor operated, the dynamics was not completely well described, possibly due to variations in the gas-liquid transfer of H_2S, which has an important dependence on pH and temperature.

Acetate and biomass profiles

In this section, model predictions for acetate, H2-SRB and homo-AC are analyzed and compared to experimental data. Results are shown in Figure 7.5. The color areas refer to the same modeling periods mentioned for Figure 7.4; the operational stages and all batch cycles, including stage V, are also shown in both Figures: 7.5A and 7.5B.

Regarding acetate, it was not observed during the first 14 cycles and, when the sulfate loading rate (SLR) was decreased from cycles 15 to 25, acetate accumulated significantly as discussed in Chapter 5. Herein, even when the kinetic parameters for homo-AC were taken from the literature, the model profile follows the experimental data with some errors in its accumulation profile but with a good matching in the washout profile. The fact that $k_{H2.SRB}$ was much lower than $k_{H2.hAC}$ ($6.25 \cdot 10^{-3}$ vs. 0.90 mg H_2 L^{-1}, Table 7.4), means that H2-SRB overcame homo-AC when H_2 was limited; the latter was the case when SLR was high enough (see Table 5.1).

A remarkable result of this work is that the model was able to describe that H2-SRB outcompeted homo-AC activity whenever the SLR was high enough; and in fact, no acetate production was observed during the optimal stage (VIII).

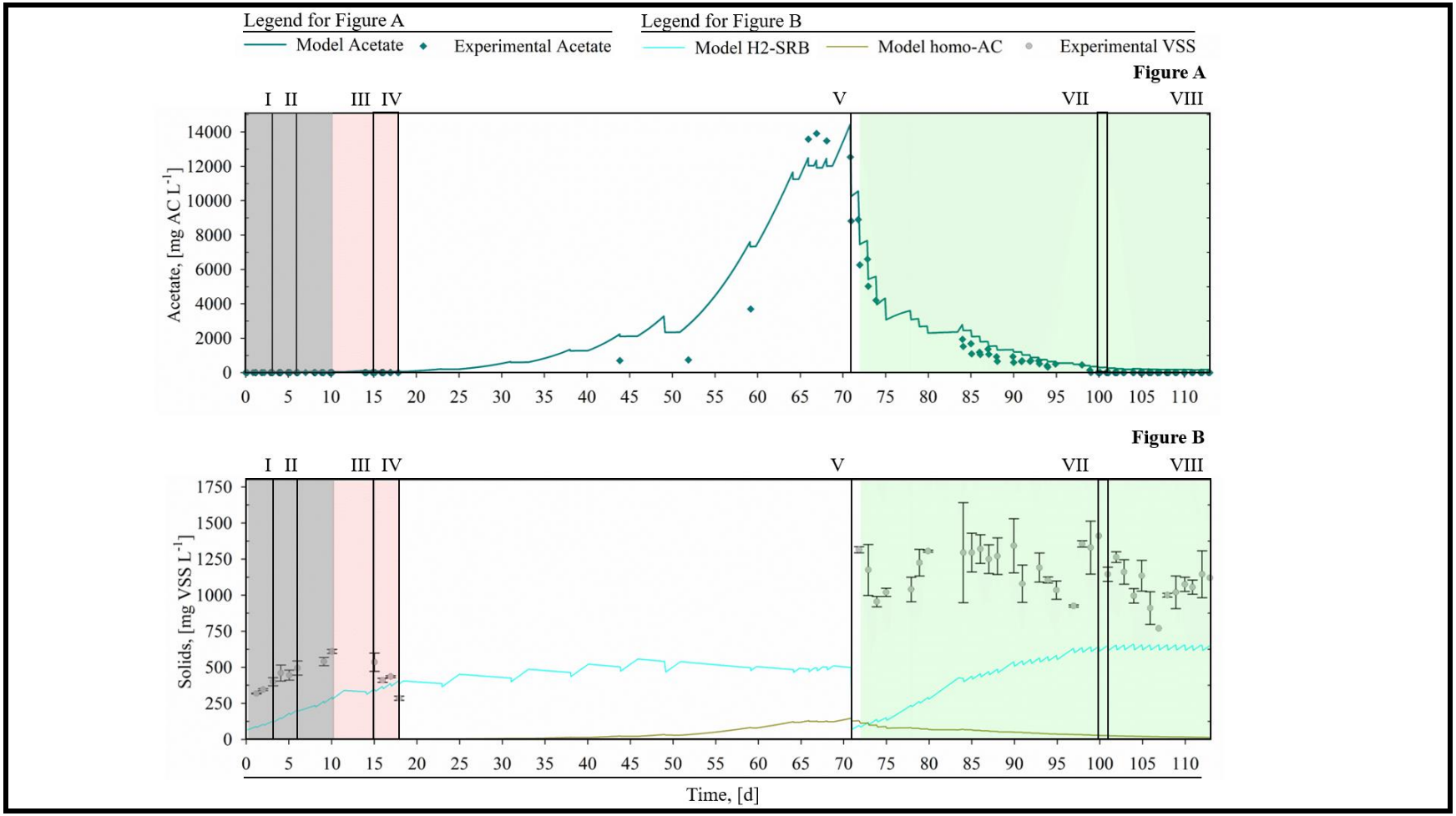

Figure 7.5. Experimental results and model predictions for the acetate and biomass concentrations along the whole operation. In Figure A, model and experimental acetate are plotted in cyan solid line and cyan diamonds, respectively; in Figure B, model H2-SRB, model homo-AC and experimental VSS are plotted in cyan-solid line, dark-yellow solid line, and gray circles, respectively. In both Figures, the color area in light gray, red and green are shaded to distinguish calibration, first and second set of validation data; area in white represents stage V, cycle 15 to 25, from which no validation was studied but it is shown to visualize solids and acetate evolution. Stages from I to VIII are also detailed.

The H2-SRB active fraction showed a continuous increase from 64 to 293 mg VSS L^{-1} from cycle 1 to 9. Later, a moderate increase at a lower rate was predicted from cycle 10 to 14. However, a decrease in the experimental VSS concentration was observed in that period.

In fact, the significant difference between model concentrations of H2-SRB and homo-AC, and the experimental VSS was because the sequential batch operation enhanced solid accumulation that ended up accumulating active H2-SRB, cell debris and other microorganisms may have not been active but were dragged from the inoculum. Additionally, the factors affecting the experimental loss in the VSS from cycles 10 to 14 were undetected, as discussed in Chapter 5 (section 5.4.1).

Then, from cycle 15 to 25, where VSS were not experimentally measured, the H2-SRB had a total increase from 405 to 500 mg VSS L^{-1} and homo-AC achieved a maximum of 145 mg VSS L^{-1}. At this point, as the GLR was kept with a significantly lower SLR during cycles 15 to 25 (days 18 to 68), the acf_{SRB} was recalibrated with the sulfate data of cycle 26, resulting in acf_{SRB} and F_{obj} values of 0.053 and $5 \cdot 10^{-5}$, respectively.

After this recalibration of the acf_{SRB}, the model was run until cycle 60 (day 113) and the results showed that the homo-AC decreased similarly to the acetate concentration and the H2-SRB achieved a stable concentration of 635±16 mg VSS L^{-1} from cycle 48 to the end of the operation.

Statistical analyses

The results of the model for the sulfate, TDS and acetate concentrations were analyzed with the statistical methods mentioned in Section 7.2.3: the ME, IoA and a linear regression with Equations 7.20 to 7.22. For sulfate and TDS, two set of data were analyzed separately: calibration data and second set of validation data (cycles from 27 to 60, days 72 to 113). The first set of validation data was not included in this analysis since the model was not able to correctly describe the results from cycles 10 to 14 (Figure 7.4). On the other hand, only acetate data from its washout curves, which is equivalent to the second set of validation data, were considered in these analyses (cycles 27 to 60, days 72 to 113).

The linear regression is analyzed at first as shown in Figure 7.6, in which experimental and model values are plotted in the x- and y- axis, respectively; the calibration data of sulfate (Figure A) and TDS (Figure B), the second set of validation data of sulfate (Figure C), TDS

(Figure D) and acetate (Figure E) are plotted in Figure 7.6.

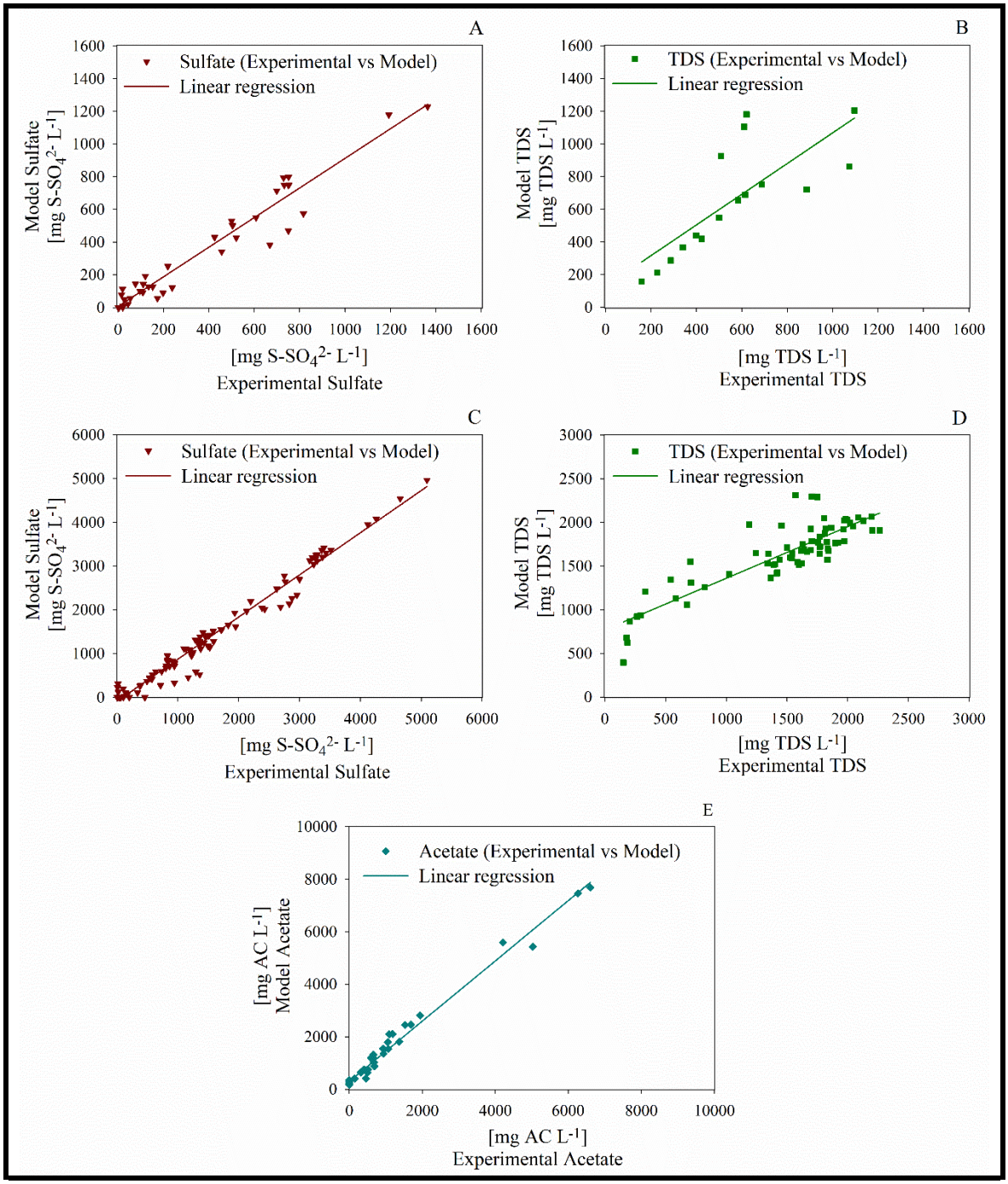

Figure 7.6. Comparison of model and experimental results of sulfate, TDS, and acetate. The calibration data of sulfate and TDS are plotted in Figure A and B; the validation data from batch 27 to 60 of sulfate and TDS are plotted in Figure C and D; the model- vs experimental- acetate data corresponding to the wash-out curve are plotted in Figure E. Solid lines describe the linear regression of the data distribution in each case.

These results show that sulfate data matched the experimental data with more accuracy

than TDS data for the calibration and validation because the objective function for the minimization algorithm was set only to adjust sulfate data but also because of the larger dispersion of TDS data. Regarding acetate, it also describes some deviations but many model data accurately matched the experimental values.

Despite experimental and model data correlated well at a first look, results were also quantitatively analyzed through ME, IoA and linear regression parameters as mentioned above; statistical parameters for sulfate, TDS and acetate data are shown in Table 7.8 for the same set of data shown in Figure 7.6. In this Table, additional parameters from the linear regression are also detailed: the errors of the slope (m) and y-intercept (y_i), and the p-values with a 95% confidence level for these parameters; from the later, a p-value below 0.05 indicates that m and y_i are statistically significant.

The results for the calibration data of sulfate were close to 1 for the ME, IoA and R^2, with small errors for m and y_i; yet, from the p-values, only m was statistically significant. Meanwhile, the validation data for sulfate exhibited even better results for the three statistical parameters, small errors for m and y_i, and the p-values showed that both parameters were statistically significant, meaning that the validation accurately described the experimental data based on the three statistical analyses and the graphical observation.

With respect to TDS, the large deviation of the model and experimental data for the calibration and validation periods is noticed from the ME parameters; nevertheless, the IoA showed much better results indicating a high agreement between the data. TDS results of the linear regressions of the calibration data showed large errors as seen from the y_i and R^2 parameters, with a small improvement for the validation data; the p-values showed that the m parameter was statistically significant for the calibration and validation data while y_i parameter was only statistically significant for the validation data.

Concerning acetate, the ME, IoA are R^2 showed a good agreement between the model and experimental data. From the linear regression, the m value was also close to 1 with minor errors while the y_i value showed significant errors; the p-values for both parameters showed that they were statistically significant.

Overall, the graphical and quantitative analyses of the set of data for sulfate, TDS and acetate demonstrated a good fitting of the mathematical model, especially for sulfate and acetate. Even though, homo-acetogenic kinetics must be quantified to accurately describe its

behavior, while the H_2S-stripping dynamics, and the possible source of experimental deviations shall be identified for a better description of H_2S experimental data.

Table 7.8. Statistical analysis to compare the experimental and model data. Model Efficiency (ME), Index of Agreement (IoA), and linear regression; from the latter, *m* is the slope, y_i is the y-intercept, R^2 is the coefficient of determination, and $p(y_i)$ is the *p*-value for each parameter, *m* and y_i, obtained in the regression 95% confidence.

Statistical analysis for sulfate DATA							
	ME	IoA	Linear regression				
			m	y_i	R^2	*p* (*m*)	*p* (y_i)
Calibration	0.93	0.98	0.91±0.04	6±21	0.94	$4.35\cdot10^{-23}$	0.8
Validation	0.96	0.99	0.96±0.02	-88±30	0.97	$2.26\cdot10^{-82}$	$4.41\cdot10^{-3}$
Statistical analysis for TDS DATA							
	ME	IoA	Linear regression				
			m	y_i	R^2	*p* (*m*)	*p* (y_i)
Calibration	0.26	0.84	0.94±0.21	129±130	0.59	$5.1\cdot10^{-4}$	0.34
Validation	0.64	0.87	0.61±0.04	738±65	0.76	$1.4\cdot10^{-22}$	$2.5\cdot10^{-17}$
Statistical analysis for acetate DATA							
	ME	IoA	Linear regression				
			m	y_i	R^2	*p* (*m*)	*p* (y_i)
Validation	0.82	0.94	1.15±0.02	304±44	0.98	$6.9\cdot10^{-37}$	$2.4\cdot10^{-8}$

7.6. ANALYSIS OF THE OPTIMAL PARAMETERS $\mu_{max.SRB}$ and k_i: COMPARISON WITH LITERAURE REPORTS

In this section, kinetic parameters $\mu_{max.SRB}$ and k_i are compared with other relevant data reported for H2-SRB in literature (Table 7.9). All works found reported $\mu_{max.SRB}$ and k_i estimations at higher temperatures, from 28 to 65 ºC, than in our work (~20ºC); from these works, only Tang et al.,[95,204] reported a lower $\mu_{max.SRB}$, 0.3 d^{-1} at 28ºC, for a denitrifying biofilm membrane reactor where H2-SRB were present.

The other works reported higher $\mu_{max.SRB}$, but they were different from our work in terms of microbial culture and operational conditions. Alphenaar et al.,[82] Kalyuzhnyi et al.,[83] Federovich et al.,[78] and Omil et al.,[84] used granular biomass and organic-fed UASB reactors under mesophilic conditions, while Spanjers et al.,[113] used a methanol-fed EGSB reactor to evaluate the competition between methanogenic microorganisms and H2-SRB under thermophilic conditions. Meanwhile, Robinson et al.,[138] performed bottle tests with H_2 to evaluate methanogenic and H2-SRB activities obtaining a $\mu_{max.SRB}$ similar to the reported by Durán et al.,[195] who ran an AnMBR at thermophilic conditions for a high organic load influent.

Table 7.9. Comparison of remarkable literature reports of H2-SRB kinetic parameters, $\mu_{max.SRB}$ and k_i, with the optimal values obtained in this work.

$\mu_{max.SRB}$	k_i	Temperature	Reference
[d^{-1}]	[mg S-H_2S L^{-1}]	[ºC]	
5.5	550	35	Alphenaar et al.,[82]
2.8	550	35	Kalyuzhnyi et al.,[83]
1.9		65	Spanjers et al.,[113]
1.4		37	Robinson et al.,[138]
1.4	265	65	Durán et al.,[195]
1.1		30	Esposito et al.,[46,157], Frunzo et al.,[81]
0.3		28	Tang et al.,[95,204]
	250	30	Federovich et al.,[78]; Omil et al.,[84]
0.53 ± 0.02	100 ± 7	20	This work

From the results shown in Table 7.9, only Esposito et al.,[46] developed a mathematical model for a H_2-fed GLR using a $\mu_{max.SRB}$ of 1.1 d^{-1} that was validated by Frunzo et al.,[81] for steady and dynamic stages with the experimental data reported by Esposito et al.[157]

The works mentioned above were reported at mesophilic and thermophilic conditions and the higher values for $\mu_{max.SRB}$ are understandable as sulfate reducing microorganisms grow optimally at mesophilic conditions;[36,112] in fact, in our work, the slow growth rate of the microbial culture at ~20ºC and the absence of biofilm/granulated biomass were the cause leading to set up the reactor in a sequential batch operation (Chapter 4).

Regarding k_i, all values reported in Table 7.9 are significantly higher than that found in this work, indicating that the microbial communities developed in other works were more resistant to H_2S-inhbition. Lower k_i of 57 mg S-H_2S L^{-1} has been reported in other works for heterotrophic sulfate reducing microorganisms.[4]

Similarly, $\mu_{max.SRB}$ was lower than most works detailed in Table 7.9, but the reactor performance exhibited an SRR of 919±78 mg S-SO_4^{2-} L^{-1} d^{-1}, and a removal efficiency 93±7%, in stage VII that was comparable to some remarkable results in the literature, as explained in Chapter 5 (section 5.4.2).

Overall, in the optimal condition, when H_2 supply was limited, the operation was able to run with no acetate production. Yet, further studies are recommended for a detail understanding of homo-AC activity as its activity was largely observed when SLR was decreased.

7.7. MODEL EVALUATION FOR DIFFERENT OPERATIONAL CONDITIONS

The mathematical model was used to simulate different operational conditions that could give a perspective on which type of further experiments can be studied in terms of reactor operation and sulfate influent concentrations. These simulations were performed as explained in section 7.3.4 with the operational conditions defined in Table 7.6, where two operational strategies were explored. A first case for a sequential batch operation like the experimental case of Chapter 5, where stages 1 to 4 were evaluated with SLRs of 970, 1067, 873 and 960 mg S-SO_4^{2-} L^{-1} d^{-1}. A second case was simulated for a continuous operation where solid recovery was not considered, and stages 1 to 4 were evaluated with different hydraulic residence times (HRT) and SLRs of 833, 750, 500 and 400 mg S-SO_4^{2-} L^{-1} d^{-1}.

The results for the sequential batch operation are shown in Figure 7.7. Figure 7.7A shows the SLR (determined from Equation 5.5), the SRR (determined from Equation 5.7), the specific sulfate reduction rate (s-SRR, determined from Equation 5.8) and the sulfate removal

efficiency (Sulfate-RE, determined from Equation 5.9). Figure 7.7B shows the VSS concentration at the end of each batch, the VSS concentration in the discharged effluent and the VE.

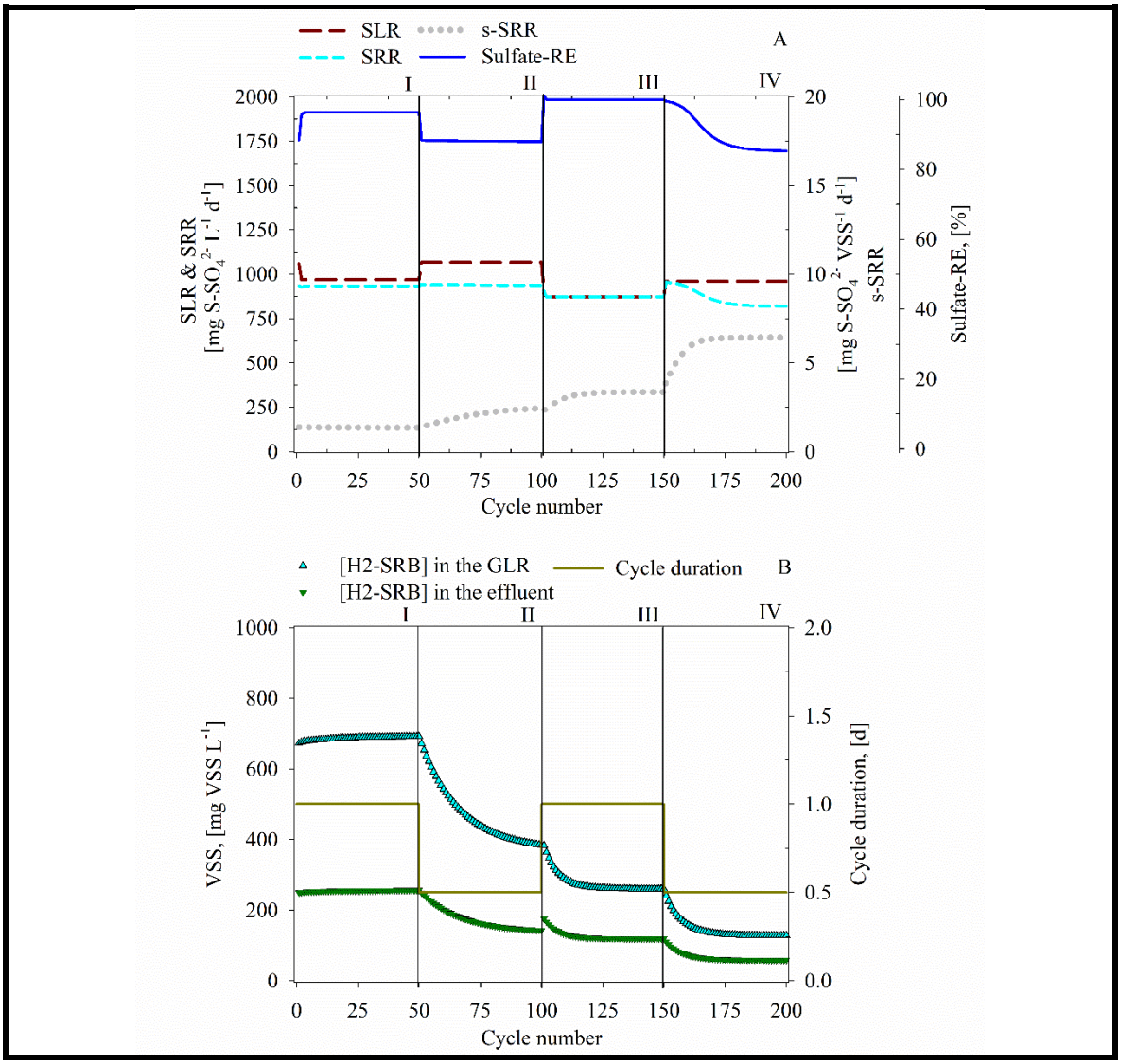

Figure 7.7. Model simulation for a sequential batch operation under different SLR. Figure A shows the SLR, SRR, s-SRR and the Sulfate-RE. Figure B shows H2-SRB concentrations in the GLR at the end of a batch and in the effluent, and the cycle duration.

The results show that the system can achieve Sulfate-RE of 96% (w/w) in stage I, where the cycle duration was 1 day, the VE was 1-L and the sulfate concentration in the influent was 6000 mg $S\text{-}SO_4^{2-}$ L^{-1} (Table 7.6). The H2-SRB concentrations in the GLR at the end of each batch and in the effluent was stable. Cycle II was defined by decreasing the cycle duration to 0.5 days, the SLR was raised with no loss in the SRR as it kept almost equal to

stage I, and therefore the Sulfate-RE decreased to 88% (w/w); nevertheless, the s-SRR increased to 2.4 mg $S\text{-}SO_4^{2-}$ VSS^{-1} d^{-1}, while the H2-SRB in the GLR and in the effluent decreased to 393 and 146 mg VSS L^{-1}, respectively. This increase in the s-SRR with no loss of the SRR was positive as it means that unnecessary solid accumulation in the GLR was decreased. It also happened in stage III and IV. For stage III, the SLR was set at 873 mg $S\text{-}SO_4^{2-}$ L^{-1} d^{-1} by setting the cycle duration to 1 day and VE to 2-L; meanwhile, stage IV was set with a SLR of 960 mg $S\text{-}SO_4^{2-}$ L^{-1} d^{-1} by setting the cycle duration to 0.5 days and the VE in 2-L. SRR achieved stable values at 873 mg $S\text{-}SO_4^{2-}$ L^{-1} d^{-1} (Sulfate-RE of 100% (w/w)) and 820 mg $S\text{-}SO_4^{2-}$ L^{-1} d^{-1} (Sulfate-RE of 86% (w/w)) for stage III and IV, respectively.

In these two last stages, there were neither loss in the SRR but a significant improvement in the s-SRR was observed, which raised to 3.4 (stage III) and 6.4 (stage IV) mg $S\text{-}SO_4^{2-}$ VSS^{-1} d^{-1}. This was reflected in less H2-SRB concentration in the GLR and in the effluent; in fact, the reduction of H2-SRB in the reactor was 82% (w/w) and in the effluent was 77% (w/w) with respect to the concentrations at the end of stage I. This result is remarkable as the large solid production was a problem in the experimental operation because the discharged effluent had large concentrations of TSS (928±465 mg TSS L^{-1}) and VSS (464±165 mg VSS L^{-1}) in stage VIII (Table 5.2 of Chapter 5).

Regarding the continuous operation simulation, the results are shown in Figure 7.8. SLR, SRR, and s-SRR were determined with equations A13 to A15 of Appendix C. The stages were set up for decreasing SLR from stage I to IV. As seen in Figure 7.8A, the SLR was 833 mg $S\text{-}SO_4^{2-}$ L^{-1} d^{-1} in stage I, which achieved stable Sulfate-RE of 100% (w/w), s-SRR of 3.5 mg $S\text{-}SO_4^{2-}$ VSS^{-1} d^{-1} and from Figure 7.8B, H2-SRB concentration achieved a stable value of 239 mg VSS L^{-1} in the effluent. A similar trend was observed from stage I to III as the SLR was decreased to 750 and 500 mg $S\text{-}SO_4^{2-}$ L^{-1} in stage II and III, respectively. The Sulfate-RE was over 98% (w/w) along these stages. Regarding the s-SRR, it increased as the H2-SRB decreased, both achieving stable values of 6.8 mg $S\text{-}SO_4^{2-}$ VSS^{-1} d^{-1} and 72 mg VSS L^{-1}, respectively, at the end of stage III.

In the last stage, the HRT was decreased to 2.5 days, the SLR was 400 mg $S\text{-}SO_4^{2-}$ L^{-1} d^{-1} and the Sulfate-RE decreased until 75% (w/w). The s-SRR increased until 8.1 mg $S\text{-}SO_4^{2-}$ VSS^{-1} d^{-1} while the H2-SRB decreased to 37 mg VSS L^{-1}. This last stage showed that the system can work with a low HRT, which was equivalent to a liquid flow rate of 2.7 L d^{-1}

(reactor volume = 6.75L). Nevertheless, a lower HRT of 2 days resulted in the loss of the SRR and the washout of the H2-SRB culture (data not shown).

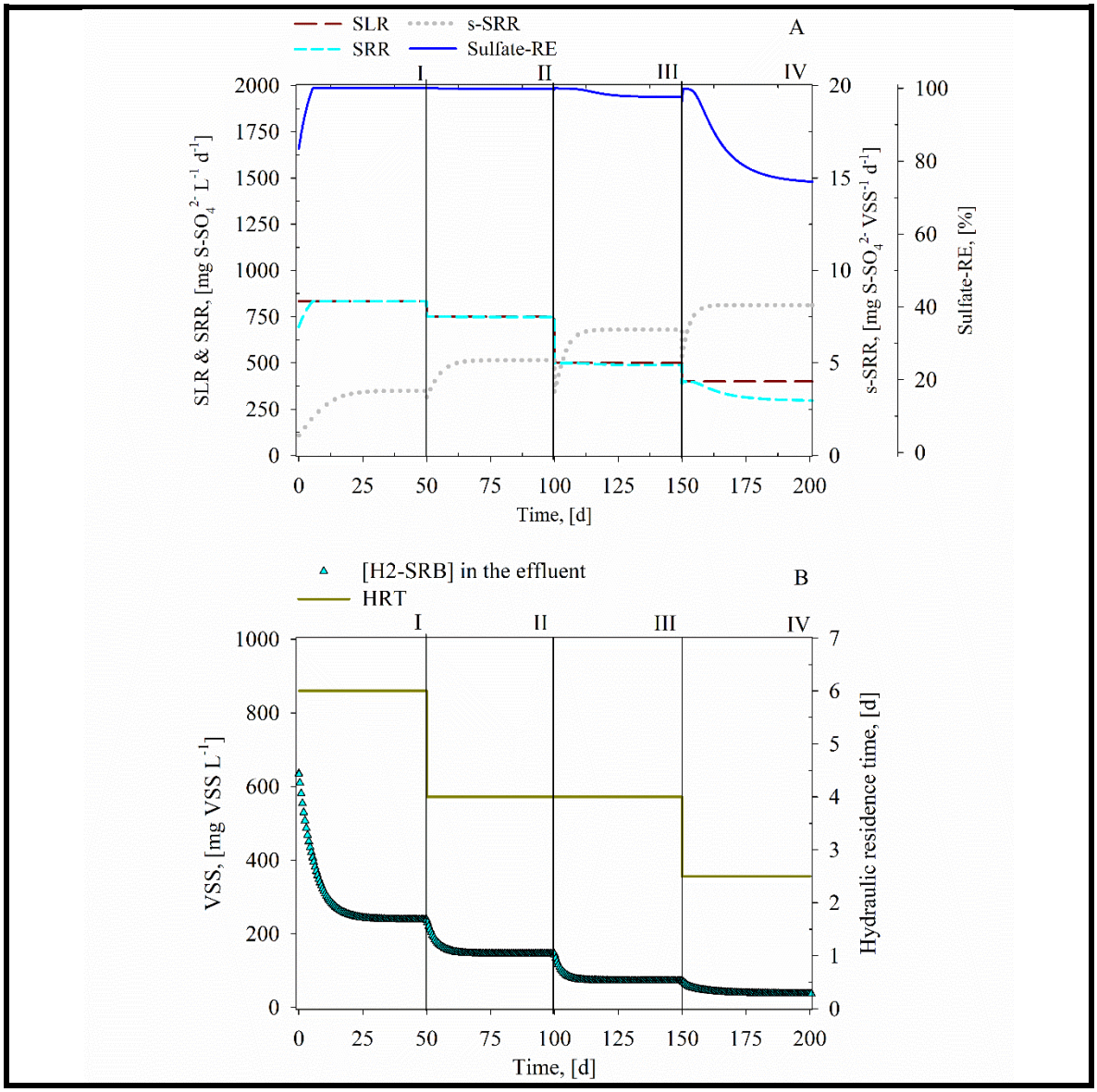

Figure 7.8. Model simulation for a continuous operation under different SLR. Figure A shows the SLR, SRR, s-SRR and the Sulfate-RE. Figure B shows H2-SRB concentrations in the effluent and the HRT.

Also, higher SLRs were evaluated but SRR did not increase (data not shown). Thus, the SRR of 833 mg $S\text{-}SO_4^{2-}$ L^{-1} d^{-1} in stage I was the highest value obtained for the continuous operation, which in fact is comparable with the highest SRR obtained for the sequential batch operation.

Overall, the s-SRR obtained in stages IV of both simulations showed a significant

improvement of this parameter as it was not never higher than 2 during the experimental operation of the GLR (Figure 5.2B, Chapter 5). This means that these conditions could be ideal to reduce the solid concentrations in the effluent as mentioned above.

Regarding acetate, it was not produced along the simulations of both, the sequential and the continuous operations, which demonstrate the useful of this system to avoid acetate production as H_2 was consumed by H2-SRB.

Finally, these simulations show that the system can work in a sequential batch operation or in a continuous operation, opening its applicability to diverse experimental conditions in terms of liquid volume treatment and sulfate concentrations.

7.8. MAIN CONCLUSIONS

A mathematical model was proposed for the sequential batch operation of the GLR to describe the experimental sulfate consumption, obtaining the main conclusions listed below:

From the mathematical model development and sensitivity analysis:

1. A mathematical model was proposed for hydrogenotrophic sulfate reducing reactors, including 6 processes: microbial growth and decay for both hydrogenotrophic sulfate reducing and homo-acetogenic microorganisms, and hydrogen and TDS gas-liquid mass transfer.
2. The model was useful for describing the operation of a sequential batch GLR. A solid removal efficiency (f_{sed}) of 25 and 37 % for 1 and 2 liters of VE that were determined experimentally were used to set up the solid loss in the sedimentation step.
3. A local sensitivity analysis was performed considering the first 9 cycles of the sequential batch operation to identify the most influential parameters of the mathematical model. This analysis was useful to determine the most influential kinetical parameters for describing this system.

From the mathematical model calibration and the confidence interval determination:

1. Modelling results indicated that a correction factor of 2.3 of the experimentally

determined K_La_{H2}, and the K_La_{H2S} was necessary for the proper description of the gas-liquid mass transfer.

2. Model calibration was successfully performed in a three-step calibration process using the experimental sulfate data. Initial estimations of $\mu_{max.SRB}$ and acf_{SRB} were done with cycles 1 to 6, and k_i with cycles 8 to 9. The preliminary estimation of these parameter allowed the model to predict experimental values of cycles 1 to 7 and 8 to 9 with the optimal values of $\mu_{max.SRB}$ = 0.55 d^{-1}, k_i = 100 mg H_2S L^{-1} and acf_{SRB} = 0.20, and the confidence intervals determined from the FIM resulting in 3.6, 7 and 1.3%, respectively.
3. The optimal parameters of $\mu_{max.SRB}$ and k_i evaluated at ~20ºC were lower than some remarkable literatures reports which were mainly evaluated at temperature over 30ºC. These results make sense as it has been previously reported that sulfate reducing microorganisms grow optimally at mesophilic environments.
4. Even when the $\mu_{max.SRB}$ was low, the optimal SRR in stage VIII showed to be comparable with some remarkable results in the literature.
5. Also, based on the k_i, the hydrogenotrophic sulfate reduction seems to be sensitive to H_2S, but even when the H_2S concentrations in the optimal operation were over the k_i value, the SRR did not decrease. Therefore, the sequential batch operation counterbalanced the H_2S-inhibition effect and the low $\mu_{max.SRB}$ by enhancing the solid accumulation.

From the mathematical model validation:

1. The mathematical model was validated with two sets of data: the first from cycle 10 to 14, and the second from cycle 27 to 60. This model was not able to predict the first validation set, which was explained by a decrease in the experimental SRR with an unidentified cause. Meanwhile, the model was able to predict the second set of validation data with a good matching for sulfate, and less accuracy for TDS.
2. The matching accuracy of the experimental and model sulfate data was demonstrated for the calibration and the second set of validation data with three statistical analyses: ME, IoA and linear regression.
3. The model showed less accuracy for TDS based on ME and linear regression, but a good statistical result was disclosed from the IoA. The large experimental deviations for TDS were considered to have significantly influenced the matching.

4. Acetate production was not characterized as not enough data were available during its production, but the model was able to describe properly its washout curve as a good matching was obtained from the three statistical analyses.
   Further study is recommended to understand in detail the acetate formation dynamics.
5. Overall, the results showed a good description of the experimental data, enabling the model to be a useful tool for the description and optimization of similar systems.

From the mathematical model validation:

1. The mathematical model was set up to simulate sequential and continuous operations with different sulfate influent concentrations.
   The simulation showed that the sequential batch operation can work with sulfate influent concentrations of up to 6000 mg $S\text{-}SO_4^{2-}$ L^{-1} achieving Sulfate-RE over 85% (w/w).
   These simulations showed that the maximum SLR for the sequential batch setting was 940 mg $S\text{-}SO_4^{2-}$ L^{-1} d^{-1}.
2. The simulation of the continuous operation showed that the highest SRR was 833 mg $S\text{-}SO_4^{2-}$ L^{-1} d^{-1} and sulfate influent concentrations of up to 5000 mg $S\text{-}SO_4^{2-}$ L^{-1} with Sulfate-RE over 98 % (w/w).
3. The system was able to achieve s-SRR of 6.4 and 8.1 mg $S\text{-}SO_4^{2-}$ VSS^{-1} d^{-1} for the sequential and the continuous operations, respectively, which represents a significant improvement compared to the experimental results.
   These high s-SRR imply that less solids are produced per sulfate reduction and therefore less solids will be in the effluent.
4. Overall, these simulations showed a robust prediction for the treatment of multiple sulfate influent concentrations and work under different operational conditions with high Sulfate-RE performance.

CHAPTER 8
OVERALL CONCLUSIONS

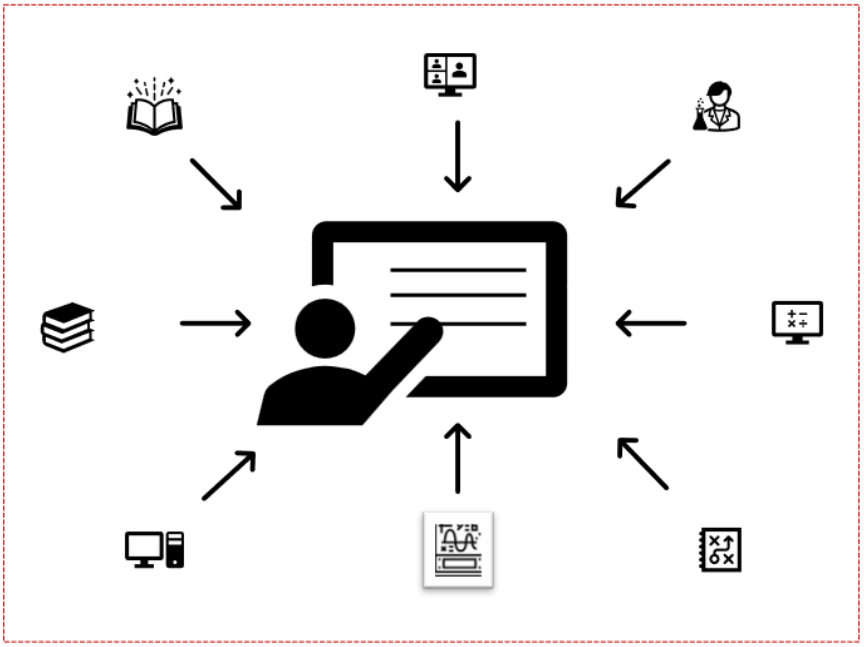

8.1. OVERALL CONCLUSIONS

This work demonstrated that the treatment of sulfate-rich effluents generated in the capture of SO_2 rich streams (flue gases) can be performed autotrophically with a suspended culture in a gas-lift reactor operated in a sequential batch mode. The study was developed in three main facets: 1) experimental evaluation for the biological sulfate reduction, 2) implementation of a sulfide online monitoring system, and 3) mathematical modeling of the biological sulfate reduction.

For the experimental study of the biological sulfate reduction, preliminary experiments that consisted in the operation of two stirred-tank reactors and the GLR demonstrated that hydrogenotrophic methanogenic activity can be completely suppressed. This was attributed to the addition of BES in the first stirred-tank reactor operation. Yet, batch tests in the GLR for kinetic characterization showed that a continuous operation was not feasible as a hydraulic residence time (HRT) over 31 days was needed and the highest sulfate reduction rate (SRR) was only 115±16 mg $S\text{-}SO_4^{2-}$ L^{-1} d^{-1} due to the absence of biofilm or granular biomass.

Nevertheless, it was demonstrated that the GLR could be set up in sequential batch operation to enhance the SRR despite the lack of granular biomass. After 60 cycles it was possible to obtain a maximum and stable SRR of 861±56 mg $S\text{-}SO_4^{2-}$ L^{-1} d^{-1} at a sulfate removal efficiency (Sulfate-RE) of 93±7% (w/w) and a VSS concentration of 1054±129 mg VSS L^{-1}. This was obtained at a temperature of 20 ºC, pH of 8.2±0.03 and at an ORP of -603±11 mV. Moreover, it was concluded that volumetric sulfate loading rate (SLR) higher than 902 mg $S\text{-}SO_4^{2-}$ L^{-1} d^{-1} led to sulfate accumulation in the reactor.

As part of the integrated treatment of flue-gases for biosulfur recovery (SONOVA/ENSURE projects), this research proved that a sulfide H_2S recovery step from the gas outlet was needed for its further conversion to elemental sulfur as a consequence of the high H_2S-stripping (64±19 % w/w of the total TDS production).

The GLR operation showed a robust sulfate reducing activity as no acetate production took place during the optimal stage while methane was never identified during the whole operation, meaning that the hydrogenotrophic sulfate reducing microorganisms (H2-SRB) successfully overcame methanogens and homoacetogens for H_2 competition.

One drawback of the GLR performance was the large soluble COD of unknown source and solid concentrations in the effluent that demand a further treatment before disposal.

In this research, a sulfide online-monitoring system (S-OMS) has also been developed and implemented. The system herein proposed is able to measure sulfide online in a range of 1.5 to 30400 mg TDS L^{-1}. Its analytical efficacy was proven through repeatability and reproducibility tests. Nevertheless, this system showed a short useful lifetime (16 hours) in terms of potentiometric response under continuous operation after which, the working electrode must be replaced or electrodeposited. The validation of the S-OMS was performed in the sulfidogenic GLR, where satisfactory statistical results were obtained when comparing measurements of the proposed analyzer with a commercial sulfide ion selective electrode (S^{2-}-ISE).

The mathematical model developed herein was able to successfully describe the sulfate consumption in the GLR under different operational conditions. The model fit was based on a sensitivity analysis. The best kinetic parameters of H2-SRB allowed a proper description of the experimental data. The validation of the model was proven statistically. The overall gas-liquid H_2-mass transfer coefficient, previously determined experimentally and abiotically in the GLR, was corrected under biological operational conditions. A proper characterization of the gas-liquid mass transfer under the same operational conditions is clearly required to properly describe the overall process.

Also, different operational strategies were simulated with successful results, indicating that this system could work under a wide range of experimental conditions. Thus, this model offers a good tool for further design of reactors for autotrophic sulfate reduction.

8.2. FUTURE WORK

In this work it was possible to successfully enrich H2-SRB and in a suspended culture and a sequential batch operation of a GLR demonstrate high sulfate reduction rates with no acetate and methane production.

However, the results also showed great opportunities for improvement and understanding of the system performance. One difficulty observed from the preliminary experiments of the GLR was the lack of biofilm formation. In this case, futures works can be directed to explore hydrogenotrophic sulfate reducing biofilm of full-scale reactors, which

can be studied from activity tests, microbial identification, detection of extracellular compounds, and the research of operational conditions that enhance biomass aggregation.

Also, it is important to research the factors affecting the gas-liquid H_2-mass transfer under abiotic and biotic conditions. Further experiments must be focused on determining the enhancing influence that the microbial activity may have over the gas-liquid mass transfer coefficients. In the same direction, identification of all operational conditions that can increase the gas-liquid H_2-mass transfer are important to explore, as mass transfer together with biofilm formation are key factors that could boost sulfate reduction capacity.

Respecting the sequential batch operation, the satisfactory results were accompanied by a lack of specific understanding about the dynamics of solid sedimentation, the high COD concentration in the discharge supernatant, the acetate formation, and the variability of hydrogen sulfide stripping. These demand further research as each of these aspects play important roles in the overall performance of the process, in terms of sulfate reduction capacity and its integration in the SONOVA process. These can be researched in pair with the mathematical model herein developed. The simulations performed to discover experimental conditions showed results that can be evaluated experimentally: operation of the GLR with shorter batch duration and higher liquid volume exchange to prove if less solids will be produced and, in that way, if less COD will be present in the effluent. The continuous operation can be explored aiming at proving the same goals, and overall, more simulations scenarios can be evaluated.

The mathematical model can also be improved with the experimental study of the solid sedimentation. Further experiments can be directed to enhance solid sedimentation for a better effluent quality and for its integration in the mathematical model. The latter will be of great importance as it will help to have a mathematical model with more capability of experimental prediction.

The large COD concentration in the effluent can also be researched from the study of microbial cell degradation. Experiments can be focused on determining the routes of cell lysis and the degradation of cell debris that ends up increasing the COD in the effluent. In fact, a proper experimental description of these microbial activities could also be included in the model for its improvement.

In the GLR experiments and model, the homoacetogenic activity was not described in

detail as only a washout curve was studied through the model with kinetics parameters taken from the literature. Even when it was possible to know that acetate formation can be suppressed at high sulfate loading rates, further studies are suggested to describe the homoacetogenic activity and the exploration of other factors, beyond the sulfate loading rate, that can suppress the acetate production.

The high H_2S-striping and its high fluctuations must be studied in future works for two important reasons: 1) it is necessary to recover hydrogen sulfide and fluctuations in the production will difficult the design of sulfide bioscrubbing process, 2) H_2S can inhibit the microbial growth. The large fluctuations in the liquid sulfide concentrations must be coupled with the S-OMS, in which longer monitoring of the reactor and higher sampling frequencies can be evaluated. This must be studied with the monitoring of hydrogen sulfide in the gas phase, and this latter can also be studied with S-OMS. Additionally, it is important to study operational strategies to couple the GLR operation with a sulfide bioscrubbing process so that the sulfate reduction efficiency can be properly quantified. Overall, all futures experiments can be used to improve the mathematical model.

Respecting the S-OMS, the above-mentioned implementation to study the fluctuations in the sulfide stripping must be coupled with the improvement of its analytical accuracy for real samples. As real samples from sulfidogenic reactor are complex and can contain species that can oxidize the sulfide or reduce the silver in the Ag/Ag_2S-working electrode, future works can be focused on the following aspects: 1) the fabrication of more resistant Ag/Ag_2S electrodes to avoid its fast deterioration, 2) the identification of interferences caused by the sample matrix in the potentiometric response, and 3) the replacement of the Ag/Ag_2S electrode by a crystalline membrane electrode in the microfluidic platform to reduce interferences and extend electrode useful lifetime.

REFERENCES

1. Tricker, R. & Tricker, S. Pollutants and contaminants. in *Environmental Requirements for Electromechanical and Electronic Equipment* 158–194 (Newnes, 1999). doi:10.1016/B978-075063902-6.50010-3
2. Dean, S. W. Natural Atmospheres: Corrosion. in *Encyclopedia of Materials: Science and Technology* 5930–5938 (Elsevier, 2001). doi:10.1016/B0-08-043152-6/01033-0
3. Jain, R. K., Cui, Z. "Cindy" & Domen, J. K. Environmental Impacts of Mining. in *Environmental Impact of Mining and Mineral Processing* 53–157 (Elsevier, 2016). doi:10.1016/B978-0-12-804040-9.00004-8
4. Lens, P. N. L. L. *et al.* Biotechnological Treatment of Sulfate-Rich Wastewaters. *Crit. Rev. Environ. Sci. Technol.* **28**, 41–88 (1998).
5. Lettieri, P., Yassin, L. & Simons, S. J. R. Advanced thermal treatment of composite wastes for energy recovery. in *Management, Recycling and Reuse of Waste Composites* 152–191 (Woodhead Publishing, 2010). doi:10.1533/9781845697662.2.152
6. Guimerà, X. *et al.* Optimization of SO2 and NOx sequential wet absorption in a two-stage bioscrubber for elemental sulphur valorisation. *Environ. Sci. Pollut. Res.* **28**, 24605–24617 (2021).
7. Sun, Y., Zwolińska, E. & Chmielewski, A. G. Abatement technologies for high concentrations of NOx and SO2 removal from exhaust gases: A review. *Crit. Rev. Environ. Sci. Technol.* **46**, 119–142 (2016).
8. UNECE. Convention on Long-range Transboundary Air Pollution. *1979* Available at: https://unece.org/convention-and-its-achievements.
9. *Updated Handbook for the 1979 Convention on Long-range Transboundary Air Pollution and its Protocols*. *Updated Handbook for the 1979 Convention on Long-range Transboundary Air Pollution and its Protocols* (UN, 2015). doi:10.18356/4c3fd450-en
10. Miller, B. G. Emissions Control Strategies for Power Plants. in *Coal Energy Systems* 283–392 (Elsevier, 2005). doi:10.1016/B978-012497451-7/50006-1
11. Muyzer, G. & Stams, A. J. M. The ecology and biotechnology of sulphate-reducing bacteria. *Nat. Rev. Microbiol.* **6**, 441–454 (2008).
12. Jones, M. T., Jerram, D. A., Svensen, H. H. & Grove, C. The effects of large igneous

provinces on the global carbon and sulphur cycles. *Palaeogeogr. Palaeoclimatol. Palaeoecol.* **441**, 4–21 (2016).

13. Pokorna, D. & Zabranska, J. Sulfur-oxidizing bacteria in environmental technology. *Biotechnol. Adv.* (2015). doi:10.1016/j.biotechadv.2015.02.007
14. Roth, S. Toxicological and environmental impacts of hydrogen sulfide. in *Signal transduction and the gasotransmitters NO, CO, and H2S in biology and medicine* 293–313 (Humana Totowa, NJ, 2004). doi:10.1007/978-1-59259-806-9_17
15. Lin, S. *et al.* Biological sulfur oxidation in wastewater treatment: A review of emerging opportunities. *Water Res.* **143**, 399–415 (2018).
16. Klimont, Z., Smith, S. J. & Cofala, J. The last decade of global anthropogenic sulfur dioxide: 2000-2011 emissions. *Environ. Res. Lett.* **8**, (2013).
17. International energy agency. Emissions of sulfur dioxide (SO2) by sector and scenario, 2015 and 2040. (2019). Available at: https://www.iea.org/data-and-statistics/charts/emissions-of-sulfur-dioxyde-so2-by-sector-and-scenario-2015-and-2040.
18. Chaudhary, V. *et al.* Low-trace monitoring of airborne sulphur dioxide employing SnO2-CNT hybrids-based energy-efficient chemiresistor. *J. Mater. Res. Technol.* **20**, 2468–2478 (2022).
19. Bhattacharya, J., Das, B. & Dev, S. Geogenic sulfate-rich wastewater: Sources, characteristics, effects and treatment technologies. in *Innovative Exploration Methods for Minerals, Oil, Gas, and Groundwater for Sustainable Development* 249–273 (Elsevier, 2022). doi:10.1016/B978-0-12-823998-8.00095-8
20. Fang, P. *et al.* Removal of High-Concentration Sulfate Ions from the Sodium Alkali FGD Wastewater Using Ettringite Precipitation Method: Factor Assessment, Feasibility, and Prospect. *J. Chem.* **2018**, (2018).
21. National center for biotechnology information. Pub chem compound summary for CID 1119, sulfur dioxide. (2022). Available at: https://pubchem.ncbi.nlm.nih.gov/compound/sulfur-dioxide.
22. Nurhisanah, S. & Hasyim, H. Environmental health risk assessment of sulfur dioxide (SO2) at workers around in combined cycle power plant (CCPP). *Heliyon* **8**, e09388 (2022).

23. Centers for disease control and prevention. Sulfur dioxide immediately dangerous to life or health concnetraionts (IDLH). (1994). Available at: https://www.cdc.gov/niosh/idlh/7446095.html.
24. Cameron, W. D., Bernath, P. & Boone, C. Sulfur dioxide from the atmospheric chemistry experiment (ACE) satellite. *J. Quant. Spectrosc. Radiat. Transf.* **258**, 107341 (2021).
25. PubChem CID. Hydroge sulfide. *National Center for Biotechnology Information* (2022). Available at: https://pubchem.ncbi.nlm.nih.gov/compound/hydrogen-sulfide.
26. Malone Rubright, S. L., Pearce, L. L. & Peterson, J. Environmental toxicology of hydrogen sulfide. *Nitric Oxide* **71**, 1–13 (2017).
27. Pudi, A. *et al.* Hydrogen Sulfide Capture and Removal Technologies: A Comprehensive Review of Recent Developments and Emerging Trends. *Sep. Purif. Technol.* **298**, 121448 (2022).
28. Zhang, P., Luo, Q., Wang, R. & Xu, J. Hydrogen sulfide toxicity inhibits primary root growth through the ROS-NO pathway. *Sci. Rep.* **7**, 1–11 (2017).
29. Sotoodeh, K. Material selection and corrosion. in *Subsea Valves and Actuators for the Oil and Gas Industry* 421–457 (Gulf Professional Publishing, 2021). doi:10.1016/B978-0-323-90605-0.00004-9
30. Córdoba, P. Status of Flue Gas Desulphurisation (FGD) systems from coal-fired power plants: Overview of the physic-chemical control processes of wet limestone FGDs. *Fuel* **144**, 274–286 (2015).
31. Ng, K. H., Lai, S. Y., Jamaludin, N. F. M. & Mohamed, A. R. A review on dry-based and wet-based catalytic sulphur dioxide (SO2) reduction technologies. *J. Hazard. Mater.* **423**, 127061 (2022).
32. Koralegedara, N. H., Pinto, P. X., Dionysiou, D. D. & Al-Abed, S. R. Recent advances in flue gas desulfurization gypsum processes and applications – A review. *J. Environ. Manage.* **251**, 109572 (2019).
33. Butalia, T., Wolfe, W. & Amaya, P. *The utilization of flue-gas desulfurization materials*. *Coal Combustion Products (CCPs): Characteristics, Utilization and Beneficiation* (Elsevier Ltd., 2017). doi:10.1016/B978-0-08-100945-1.00006-X
34. ECOBA. Production and Utilisation of CCPs in 2016 in Europe. 103932 (2016).

35. Gong, Y. & Yang, Z. G. Corrosion evaluation of one wet desulfurization equipment – Flue gas desulfurization unit. *Fuel Process. Technol.* **181**, 279–293 (2018).
36. Hao, T. wei *et al.* A review of biological sulfate conversions in wastewater treatment. *Water Research* (2014). doi:10.1016/j.watres.2014.06.043
37. Liamleam, W. & Annachhatre, A. P. Electron donors for biological sulfate reduction. *Biotechnol. Adv.* **25**, 452–463 (2007).
38. Mora, M. *et al.* Feasibility of S-rich streams valorization through a two-step biosulfur production process. *Chemosphere* **253**, 1–10 (2020).
39. Klotz, M. G., Bryant, D. A. & Hanson, T. E. The microbial sulfur cycle. *Front. Microbiol.* **2**, 3–4 (2011).
40. Dodds, W. K. & Whiles, M. R. Nitrogen, Sulfur, Phosphorus, and Other Nutrients. *Freshw. Ecol.* 345–373 (2010). doi:10.1016/b978-0-12-374724-2.00014-3
41. Zavarzin, G. A. Microbial Cycles. in *Encyclopedia of Ecology, Five-Volume Set* 2335–2341 (Academic Press, 2008). doi:10.1016/B978-008045405-4.00745-X
42. Trudinger, P. A. Chapter 6.1 The Biological Sulfur Cycle. in *Studies in Environmental Science* **3**, 293–313 (Elsevier, 1979).
43. Loka Bharathi, P. A. Sulfur Cycle. *Encycl. Ecol. Five-Volume Set* 3424–3431 (2008). doi:10.1016/B978-008045405-4.00761-8
44. Cassidy, J., Lubberding, H. J., Esposito, G., Keesman, K. J. & Lens, P. N. L. Automated biological sulphate reduction: a review on mathematical models, monitoring and bioprocess control. *FEMS Microbiol. Rev.* **39**, 823–853 (2015).
45. Fernández-Palacios, E., Lafuente, J., Mora, M. & Gabriel, D. Exploring the performance limits of a sulfidogenic UASB during the long-term use of crude glycerol as electron donor. *Sci. Total Environ.* **688**, 1184–1192 (2019).
46. Esposito, G., Lens, P. & Pirozzi, F. User-friendly mathematical model for the design of sulfate reducing H2/CO2 fed bioreactors. *J. Environ. Eng.* (2009). doi:10.1061/(ASCE)0733-9372(2009)135:3(167)
47. Perry, R. H. G., Green, D. W. & Maloney, J. O. *Perry's Chemical Engineers' Handbook (7th Edition). McGraw-Hill* (1997).
48. Lens, P. N. L., Gastesi, R. & Lettinga, G. Use of sulfate reducing cell suspension bioreactors for the treatment of SO2 rich flue gases. *Biodegradation* **14**, 229–240

(2003).

49. Van Houten, R. T., Van Der Spoel, H., Van Aelst, A. C., Hulshoff Pol, L. W. & Lettinga, G. Biological sulfate reduction using synthesis gas as energy and carbon source. *Biotechnol. Bioeng.* **50**, 136–144 (1996).
50. Hao, T. W. *et al.* Characterization of sulfate-reducing granular sludge in the SANI® process. *Water Res.* **47**, 7042–7052 (2013).
51. Hu, Y. *et al.* Effect of influent COD/SO42− ratios on UASB treatment of a synthetic sulfate-containing wastewater. *Chemosphere* **130**, 24–33 (2015).
52. Zhou, X., Fernández-Palacios, E., Dorado, A. D., Gamisans, X. & Gabriel, D. Assessing main process mechanism and rates of sulfate reduction by granular biomass fed with glycerol under sulfidogenic conditions. *Chemosphere* **286**, 131649 (2022).
53. Van Houten, B. H. G. W. *et al.* Long-term performance and microbial community analysis of a full-scale synthesis gas fed reactor treating sulfate- and zinc-rich wastewater. *Appl. Microbiol. Biotechnol.* **84**, 555–563 (2009).
54. Sousa, J. A. B., Plugge, C. M., Stams, A. J. M. & Bijmans, M. F. M. Sulfate reduction in a hydrogen fed bioreactor operated at haloalkaline conditions. *Water Res.* **68**, 67–76 (2015).
55. Vannini, C. *et al.* Sulphide oxidation to elemental sulphur in a membrane bioreactor: Performance and characterization of the selected microbial sulphur-oxidizing community. *Syst. Appl. Microbiol.* **31**, 461–473 (2008).
56. Cueto, D., Mora, M. & Gabriel, D. Evaluating and modeling biological sulfur production in the treatment of sulfide-laden streams containing ammonium. *J. Chem. Technol. Biotechnol.* **96**, 439–447 (2021).
57. United Nacitions. Report of the world comission on environment and development: note / by the secretary-general. *Digital library of the United Nations* (1987). Available at: https://digitallibrary.un.org/record/139811.
58. Velenturf, A. P. M. & Purnell, P. Principles for a sustainable circular economy. *Sustain. Prod. Consum.* **27**, 1437–1457 (2021).
59. United Nations. Cicrcular Economy. *UNECE* (2021). Available at: https://unece.org/trade/CircularEconomy.
60. Arruda, E. H., Melatto, R. A. P. B., Levy, W. & Conti, D. de M. Circular economy: A

brief literature review (2015–2020). *Sustain. Oper. Comput.* **2**, 79–86 (2021).

61. Nevatalo, L. M., Bijmans, M. F. M., Lens, P. N. L., Kaksonen, A. H. & Puhakka, J. A. Hydrogenotrophic sulfate reduction in a gas-lift bioreactor operated at 9°C. *J. Microbiol. Biotechnol.* **20**, 615–621 (2010).
62. Mora, M. *et al.* Respirometric characterization of aerobic sulfide, thiosulfate and elemental sulfur oxidation by S-oxidizing biomass. *Water Res.* (2016). doi:10.1016/j.watres.2015.11.061
63. Mora, M. *et al.* Kinetic and stoichiometric characterization of anoxic sulfide oxidation by SO-NR mixed cultures from anoxic biotrickling filters. *Appl. Microbiol. Biotechnol.* (2014). doi:10.1007/s00253-014-5688-5
64. Fajardo, C. *et al.* Cross effect of temperature, pH and free ammonia on autotrophic denitrification process with sulphide as electron donor. *Chemosphere* **97**, 10–15 (2014).
65. Polizzi, C., Gabriel, D. & Muunz, G. Successful sulphide-driven partial denitrification: efficiency, stability and resilience in SRT-controlled conditions. *Chemosphere* **295**, 133936 (2022).
66. Chen, X., Al, R., Behera, C. R. & Sin, G. *Process Synthesis, Design, and Control of Wastewater Treatment Plants*. *Reference Module in Chemistry, Molecular Sciences and Chemical Engineering* (Elsevier Inc., 2018). doi:10.1016/b978-0-12-409547-2.14345-8
67. Siddiqui, M. R., AlOthman, Z. A. & Rahman, N. Analytical techniques in pharmaceutical analysis: A review. *Arab. J. Chem.* **10**, S1409–S1421 (2017).
68. Fernández-la-Villa, A., Pozo-Ayuso, D. F. & Castaño-Álvarez, M. Microfluidics and electrochemistry: an emerging tandem for next-generation analytical microsystems. *Current Opinion in Electrochemistry* **15**, 175–185 (2019).
69. Francesko, A., Cardoso, V. F. & Lanceros-Méndez, S. *Lab-on-a-chip technology and microfluidics*. *Microfluidics for Pharmaceutical Applications: From Nano/Micro Systems Fabrication to Controlled Drug Delivery* (2018). doi:10.1016/B978-0-12-812659-2.00001-6
70. Jayamohan, H. *et al.* Advances in Microfluidics and Lab-on-a-Chip Technologies. *Mol. Diagnostics Third Ed.* 197–217 (2017). doi:10.1016/B978-0-12-802971-

8.00011-0

71. Büyüktiryaki, S., Sümbelli, Y., Keçili, R. & Hussain, C. M. Lab-on-chip platforms for environmental analysis. *Encycl. Anal. Sci.* 267–273 (2019). doi:10.1016/B978-0-12-409547-2.14489-0
72. Pol, R. *et al.* Inkjet-Printed Sulfide-Selective Electrode. *Anal. Chem.* **89**, 12231–12236 (2017).
73. Kell, A. J. *et al.* Versatile Molecular Silver Ink Platform for Printed Flexible Electronics. *ACS Appl. Mater. Interfaces* **9**, 17226–17237 (2017).
74. Barton, L. L. & Fauque, G. D. *Chapter 2 Biochemistry, Physiology and Biotechnology of Sulfate-Reducing Bacteria*. *Advances in Applied Microbiology* **68**, (2009).
75. Pol, R., Céspedes, F., Gabriel, D. & Baeza, M. Fully integrated screen-printed sulfide-selective sensor on a 3D-printed potentiometric microfluidic platform. *Sensors Actuators, B Chem.* **290**, 364–370 (2019).
76. Dochain, D. & Vanrolleghem, P. A. *Dynamical Modelling and Estimation in Wastewater Treatment Processes*. (IWA, 2001).
77. Barrera, E. L. *et al.* Modeling the anaerobic digestion of cane-molasses vinasse: Extension of the Anaerobic Digestion Model No. 1 (ADM1) with sulfate reduction for a very high strength and sulfate rich wastewater. *Water Res.* **71**, 42–54 (2015).
78. Fedorovich, V., Lens, P. & Kalyuzhnyi, S. Extension of Anaerobic Digestion Model No. 1 with Processes of Sulfate Reduction. *Appl. Biochem. Biotechnol.* **109**, 33–46 (2003).
79. Batstone, D. J. *et al.* The IWA Anaerobic Digestion Model No 1 (ADM1). *Water Sci. Technol.* **45**, 65–73 (2002).
80. Ahammad, S. Z., Gomes, J. & Sreekrishnan, T. R. A Mathematical Model for the Interactive Behavior of Sulfate-Reducing Bacteria and Methanogens During Anaerobic Digestion. *Water Environ. Res.* **83**, 791–801 (2011).
81. Frunzo, L., Esposito, G., Pirozzi, F. & Lens, P. Dynamic mathematical modeling of sulfate reducing gas-lift reactors. *Process Biochem.* (2012). doi:10.1016/j.procbio.2012.08.010
82. Alphenaar, A. *Anaerobic granular sludge: Characterization and Factors Affecting its Functioning*. (1995). doi:edepot.wur.nl/202099

83. Kalyuzhnyi, S., Fedorovich, V., Lens, P., Hulshoff Pol, L. & Lettinga, G. Mathematical modelling as a tool to study population dynamics between sulfate reducing and methanogenic bacteria. *Biodegradation* **9**, 187–199 (1998).
84. Omil, F., Lens, P., Hulshoff Pol, L. W. & Lettinga, G. Characterization of biomass from a sulfidogenic, volatile fatty acid-degrading granular sludge reactor. *Enzyme Microb. Technol.* **20**, 229–236 (1997).
85. Tabiś, B. & Boroń, D. A Simple Analytical Method for Determining Basic Hydrodynamic Characteristics of Hybrid Fluidized-Bed Air-Lift Apparatae. *Chem. Process Eng.* **38**, 121–133 (2017).
86. de Lemos Chernicharo, C. A. *Anaerobic Reactors*. *Water Intelligence Online* **6**, (2015).
87. Nicolella, C., Van Loosdrecht, M. C. M. & Heijnen, J. J. Wastewater treatment with particulate biofilm reactors. *J. Biotechnol.* **80**, 1–33 (2000).
88. Chae, K. J. *et al.* Selective inhibition of methanogens for the improvement of biohydrogen production in microbial electrolysis cells. *Int. J. Hydrogen Energy* **35**, 13379–13386 (2010).
89. GROVE-RASMUSSEN, K. V. Determination of the equivalence point in potentiometric acid-base titrations. *Dan. Tidsskr. Farm.* **35**, 236–242 (1961).
90. Ratzlaff, K. L. Optimizing Precision in Standard Addition Measurement. *Anal. Chem.* **51**, 232–235 (1979).
91. Ciobanu, M., Wilburn, J. P., Krim, M. L., Cliffel, D. E. & Electrochemistry, C. I. N. Fundamentals. (1893). doi:10.1016/B978-0-444-51958-0.50002-1
92. Lovibond. 20 - 1500 mg / l COD b) Instrument specific information. 2–7
93. Metcalf & Eddy. Metcalf & Eddy, Inc. Wastewater Engineering Teatment and Reuse. *Journal of Wastewater Engineering* (2003).
94. Nicolella, C., Van Loosdrecht, M. C. M. & Heijnen, S. J. Particle-based biofilm reactor technology. *Trends Biotechnol.* **18**, 312–320 (2000).
95. Tang, Y. *et al.* A biofilm model to understand the onset of sulfate reduction in denitrifying membrane biofilm reactors. *Biotechnol. Bioeng.* **110**, 763–772 (2013).
96. Kalyuzhnyi, S. V. & Fedorovich, V. V. Mathematical modelling of competition between sulphate reduction and methanogenesis in anaerobic reactors. *Bioresour.*

Technol. **65**, 227–242 (1998).

97. Bijmans, M. F. M., Dopson, M., Ennin, F., Lens, P. N. L. & Buisman, C. J. N. Effect of sulfide removal on sulfate reduction at pH 5 in a hydrogen fed gas-lift bioreactor. *J. Microbiol. Biotechnol.* **18**, 1809–1818 (2008).
98. van Houten, R. T., Pol, L. W. H. & Lettinga, G. Biological sulphate reduction using gas-lift reactors fed with hydrogen and carbon dioxide as energy and carbon source. *Biotechnol. Bioeng.* **44**, 586–594 (1994).
99. Baeza, J. A. ADD Control, Labwindows/CVI 2017© National Instruments.
100. Unisense, A. Hydrogen sensor user manual. 1–17 (2010).
101. Tribe, L. A., Briens, C. L. & Margaritis, A. Determination of the volumetric mass transfer coefficient (kLa) using the dynamic "gas out–gas in" method: Analysis of errors caused by dissolved oxygen probes. *Biotechnology and Bioengineering* (1995). doi:10.1002/bit.260460412
102. Cockx, A., Do-Quang, Z., Audic, J. M., Liné, A. & Roustan, M. Global and local mass transfer coefficients in waste water treatment process by computational fluid dynamics. *Chem. Eng. Process.* **40**, 187–194 (2001).
103. Garcia-Ochoa, F. & Gomez, E. Theoretical prediction of gas-liquid mass transfer coefficient, specific area and hold-up in sparged stirred tanks. *Chem. Eng. Sci.* **59**, 2489–2501 (2004).
104. Rodriguez, G. *et al.* Optimization of oxygen transfer through venturi-based systems applied to the biological sweetening of biogas. *J. Chem. Technol. Biotechnol.* **87**, 854–860 (2012).
105. Van'T Riet, K. Review of Measuring Methods and Results in Nonviscous Gas-Liquid Mass Transfer in Stirred Vessels. *Ind. Eng. Chem. Process Des. Dev.* **18**, 357–364 (1979).
106. Jin, B., Yin, P. & Lant, P. Hydrodynamics and mass transfer coefficient in three-phase air-lift reactors containing activated sludge. *Chem. Eng. Process. Process Intensif.* **45**, 608–617 (2006).
107. Merchuk, J. C. & Gluz, M. Bioreactors, Air-lift Reactors. in *Encyclopedia of Bioprocess Technology* (John Wiley & Sons, Inc., 2002). doi:10.1002/0471250589.ebt029

108. Bu, H., Carvalho, G., Yuan, Z., Bond, P. & Jiang, G. Biotrickling filter for the removal of volatile sulfur compounds from sewers: A review. *Chemosphere* **277**, 130333 (2021).

109. Apilfinez, I., Gutidrrez, A. & Dfaz, M. Eeffet of surface materials on initial biofilm development. **66**, 225–230 (1998).

110. Van Houten, R. T., Yun, S. Y. & Lettinga, G. Thermophilic sulphate and sulphite reduction in lab-scale gas-lift reactors using H2 and CO2 as energy and carbon source. *Biotechnol. Bioeng.* **55**, 807–814 (1997).

111. Doran, M. P. Engineering Principles Second Edition. *Acad. Press* 903 (2013).

112. Colleran, E. & Pender, S. Mesophilic and thermophilic anaerobic digestion of sulphate-containing wastewaters. *Water Sci. Technol.* **45**, 231–235 (2002).

113. Spanjer, H., Weijma, J. & Abusam, A. Modelling the competition between sulphate reducers and methanogens in a thermophilic methanol-fed bioreactor. *Water Sci. Technol.* **45**, 93–98 (2002).

114. Pepper, I. L. & Gentry, T. J. *Earth Environments*. *Environmental Microbiology: Third Edition* (Elsevier Inc., 2015). doi:10.1016/B978-0-12-394626-3.00004-1

115. Khanal, S. K. & Huang, J.-C. Online Oxygen Control for Sulfide Oxidation in Anaerobic Treatment of High-Sulfate Wastewater. *Water Environ. Res.* **78**, 397–408 (2006).

116. van Houten, B. H. G. W. *Microbial aspects of synthesis gas fed bioreactors treating sulfate and metal rich wastewaters*. (2006).

117. Nishio, N. & Nakashimada, Y. *Manufacture of biogas and fertilizer from solid food wastes by means of anaerobic digestion*. *Food Industry Wastes* (Elsevier Inc., 2013). doi:10.1016/B978-0-12-391921-2.00007-X

118. van Houten, R. T. & Lettinga, G. *Biological sulphate reduction with synthesis gas: microbiology and technology*. *Progress in Biotechnology* **11**, (Elsevier Masson SAS, 1996).

119. Grabowski, A., Tindall, B. J., Bardin, V., Blanchet, D. & Jeanthon, C. Petrimonas sulfuriphila gen. nov., sp. nov., a mesophilic fermentative bacterium isolated from a biodegraded oil reservoir. *Int. J. Syst. Evol. Microbiol.* **55**, 1113–1121 (2005).

120. Board, T. E. Petrimonas . *Bergey's Man. Syst. Archaea Bact.* **8**, 1–2 (2015).

121. Bidzhieva, S. K., Sokolova, D. S., Tourova, T. P. & Nazina, T. N. Bacteria of the Genus Sphaerochaeta from Low-Temperature Heavy Oil Reservoirs (Russia). *Microbiol. (Russian Fed.* **87**, 757–765 (2018).
122. Harrns, C., Schleicher, A., Collins, M. D. & Andreesen, J. R. Tissierella creatinophila sp . nov ., a Gram- positive , anaerobic , non-spore-f orming , creatinine-f errnent ing organism. 983–993 (1992).
123. Maspolim, Y., Zhou, Y., Guo, C., Xiao, K. & Ng, W. J. The effect of pH on solubilization of organic matter and microbial community structures in sludge fermentation. *Bioresour. Technol.* **190**, 289–298 (2015).
124. Ezeji, J. C. *et al.* Parabacteroides distasonis: intriguing aerotolerant gut anaerobe with emerging antimicrobial resistance and pathogenic and probiotic roles in human health. *Gut Microbes* **13**, (2021).
125. Liu, Q. Q., Wang, Y., Li, J., Du, Z. J. & Chen, G. J. Saccharicrinis carchari sp. nov., isolated from a shark, and emended descriptions of the genus Saccharicrinis and Saccharicrinis fermentans. *Int. J. Syst. Evol. Microbiol.* **64**, 2204–2209 (2014).
126. Kröger, A. *et al.* Fumarate respiration of Wolinella succinogenes: Enzymology, energetics and coupling mechanism. *Biochim. Biophys. Acta - Bioenerg.* **1553**, 23–38 (2002).
127. Han, Y. & Perner, M. The role of hydrogen for Sulfurimonas denitrificans' metabolism. *PLoS One* **9**, 8–15 (2014).
128. Wesley, I. V. Arcobacter. *Encycl. Food Microbiol. Second Ed.* **1**, 61–68 (2014).
129. Yasui, H. & Goel, R. Application of Mathematical Models to Anaerobic Digestion Process. *Orthod. Treat. Cl. III Malocclusion* 306 (1999).
130. Chan, C. & Farahbakhsh, K. Oxygen Demand of Fresh and Stored Sulfide Solutions and Sulfide-Rich Constructed Wetland Effluent. *Water Environ. Res.* **87**, 721–726 (2015).
131. National Center for Biotechnology Information. PubChem Compound Summary for CID 402, Hydrogen Sulfide. (2004). Available at: https://pubchem.ncbi.nlm.nih.gov/compound/Hydrogen-sulfide.
132. Lokshina, L. Y. & Vavilin, V. A. Kinetic analysis of the key stages of low temperature methanogenesis. *Ecol. Modell.* **117**, 285–303 (1999).

133. National Center for Biotechnology Information. PubChem Compound Summary for CID 176, Acetic Acid. (2022). Available at: https://pubchem.ncbi.nlm.nih.gov/compound/Acetic-Acid. (Accessed: 13th September 2022)

134. Emebu, S., Pecha, J. & Janáčová, D. Review on anaerobic digestion models: Model classification & elaboration of process phenomena. *Renew. Sustain. Energy Rev.* **160**, (2022).

135. Ma, J. *et al.* A simple methodology for rate-limiting step determination for anaerobic digestion of complex substrates and effect of microbial community ratio. *Bioresour. Technol.* **134**, 391–395 (2013).

136. Parker, W. J., Jones, R. M. & Murthy, S. Characterization of the COD/VSS Ratio during Anaerobic Digestion of Waste Activated Sludge: Experimental and Modeling Studies. *Proc. Water Environ. Fed.* **2008**, 524–533 (2012).

137. Adrian, L. & Löffler, F. E. Organohalide-respiring bacteria. *Organohalide-Respiring Bact.* 1–632 (2016). doi:10.1007/978-3-662-49875-0

138. Robinson, J. A. & Tiedje, J. M. Competition between sulfate-reducing and methanogenic bacteria for H2 under resting and growing conditions. *Arch. Microbiol.* **137**, 26–32 (1984).

139. J.W.H., S., Elferink, O., Visser, A., Hulshoff Pol, L. W. & Stams, A. J. M. Sulfate reduction in methanogenic bioreactors. *FEMS Microbiol. Rev.* (1994). doi:10.1111/j.1574-6976.1994.tb00130.x

140. Okabe, S., Nielsen, P. H. & Characklis, W. G. Factors affecting microbial sulfate reduction by Desulfovibrio desulfuricans in continuous culture: Limiting nutrients and sulfide concentration. *Biotechnol. Bioeng.* **40**, 725–734 (1992).

141. Van Houten, B. H. G. W. *et al.* Occurrence of methanogenesis during start-up of a full-scale synthesis gas-fed reactor treating sulfate and metal-rich wastewater. *Water Res.* **40**, 553–560 (2006).

142. Hamdi, O. *et al.* Isolation and characterization of Desulfocurvus thunnarius sp. nov., a sulfate-reducing bacterium isolated from an anaerobic sequencing batch reactor treating cooking wastewater. *Int. J. Syst. Evol. Microbiol.* **63**, 4237–4242 (2013).

143. Jensen, M. B., Ottosen, L. D. M. & Kofoed, M. V. W. H2 gas-liquid mass transfer: A

key element in biological Power-to-Gas methanation. *Renew. Sustain. Energy Rev.* **147**, 111209 (2021).

144. Kraakman, N. J. R., Rocha-Rios, J. & Van Loosdrecht, M. C. M. Review of mass transfer aspects for biological gas treatment. *Appl. Microbiol. Biotechnol.* **91**, 873–886 (2011).
145. Lewis, W. K. & Whitman, W. G. Principles of Gas Absorption. *Ind. Eng. Chem.* **16**, 1215–1220 (1924).
146. Lebrun, G., Xu, F., Le Men, C., Hébrard, G. & Dietrich, N. Gas-liquid mass transfer around a rising bubble: Combined effect of rheology and surfactant. *Fluids* **6**, (2021).
147. Ho, D., Kim, K., Earmme, T. & Kim, C. Enhancing gas–liquid volumetric mass transfer coefficient. *J. Ind. Eng. Chem.* **87**, 1–17 (2020).
148. Baz-Rodríguez, S. A. *et al.* Effect of electrolytes in aqueous solutions on oxygen transfer in gas-liquid bubble columns. *Chem. Eng. Res. Des.* **92**, 2352–2360 (2014).
149. Ferreira, A., Cardoso, P., Teixeira, J. A. & Rocha, F. pH influence on oxygen mass transfer coefficient in a bubble column . Individual characterization of k L and a. *Chem. Eng. Sci.* **100**, 145–152 (2013).
150. Cheng, Y. & Li, H. Rheological behavior of sewage sludge with high solid content. *Water Sci. Technol.* **71**, 1686–1693 (2015).
151. Terjesen, S. G. Mass Transfer with Chemical Reaction. in *Environmental Engineering: A Chemical Engineering Discipline* (eds. Lindner, G. & Nyberg, K.) 67–79 (Springer Netherlands, 1973). doi:10.1007/978-94-010-2608-6_8
152. Merchuk, J. Further Considerations on the Enhancement Factor for Oxygen Absorption into Fermentation Broth. *Biotechnol. Bioeng.* **XIX**, 1885–1889 (1977).
153. Vasel, J. L. & Schrobiltgen, P. Oxygen transfer in trickling filters. *Water Res.* **25**, 53–60 (1991).
154. Khanal, S. K. & Huang, J. C. ORP-based oxygenation for sulfide control in anaerobic treatment of high-sulfate wastewater. *Water Res.* **37**, 2053–2062 (2003).
155. Alex Benschop and Albert Janssen, Alie Hoksberg, Munaf Seriwala, R. A. and C. N. The shell-Paques/THIOPAQ Gas Desulphurisation Process: Successful Start Up First Commercial Unit. - PDF. 1–13 (2015).
156. Wei, H., Gao, B., Ren, J., Li, A. & Yang, H. Coagulation/flocculation in dewatering

of sludge: A review. *Water Res.* **143**, 608–631 (2018).

157. Esposito, G., Weijma, J., Pirozzi, F. & Lens, P. N. L. Effect of the sludge retention time on H2 utilization in a sulphate reducing gas-lift reactor. *Process Biochem.* **39**, 491–498 (2003).
158. Power. Flue Gas Desulfurization Wastewater Treatment Primer. (2009). Available at: https://www.powermag.com/flue-gas-desulfurization-wastewater-treatment-primer/.
159. Gaal, G. *et al.* Simplified fabrication of integrated microfluidic devices using fused deposition modeling 3D printing. *Sensors Actuators, B Chem.* **242**, 35–40 (2017).
160. Au, A. K., Huynh, W., Horowitz, L. F. & Folch, A. 3D-Printed Microfluidics. *Angew. Chemie - Int. Ed.* **55**, 3862–3881 (2016).
161. Manzanares Palenzuela, C. L. & Pumera, M. (Bio)Analytical chemistry enabled by 3D printing: Sensors and biosensors. *TrAC - Trends Anal. Chem.* **103**, 110–118 (2018).
162. Leal, V. G., Batista, A. D. & Petruci, J. F. da S. 3D-printed and fully portable fluorescent-based platform for sulfide determination in waters combining vapor generation extraction and digital images treatment. *Talanta* **222**, (2021).
163. Nesakumar, N., Kesavan, S., Li, C. Z. & Alwarappan, S. Microfluidic Electrochemical Devices for Biosensing. *J. Anal. Test.* **3**, 3–18 (2019).
164. Wang, J. *ANALYTICAL ELECTROCHEMISTRY*. (John Wiley & Sons, Inc., Hoboken, New Jersey, 2006).
165. Lafleur, J. P., Jönsson, A., Senkbeil, S. & Kutter, J. P. Recent advances in lab-on-a-chip for biosensing applications. *Biosens. Bioelectron.* **76**, 213–233 (2016).
166. Li, P., Yuan, D., Huang, Y. & Lin, K. Improving the measurement of total dissolved sulfide in natural waters: A new on-site flow injection analysis method. *Sci. Total Environ.* **829**, 154594 (2022).
167. Villa-Gomez, D. K., Cassidy, J., Keesman, K. J., Sampaio, R. & Lens, P. N. L. Sulfide response analysis for sulfide control using apS electrode in sulfate reducing bioreactors. *Water Res.* **50**, 48–58 (2014).
168. Vallejo, B., Richter, P., Toral, I., Tapia, C. & Luque De Castro, M. D. Determination of sulphide in liquid and solid samples by integrated pervaporation-potentiometric detection. *Anal. Chim. Acta* **436**, 301–307 (2001).
169. Lima, J. L. F. C. & Rocha, L. S. M. Fia tubular potentiometric detectors based on

homogeneous crystalline membranes. Their use in the determination of chloride and sulphide ions in water. *Int. J. Environ. Anal. Chem.* **38**, 127–133 (1990).

170. Sharma, C. & Negi, Y. S. *Methods of inorganic pollutants detection in water*. *Inorganic Pollutants in Water* **1900**, (INC, 2020).
171. Majeed, S., Naqvi, S. T. R., ul Haq, M. N. & Ashiq, M. N. Electroanalytical techniques in biosciences: conductometry, coulometry, voltammetry, and electrochemical sensors. in *Analytical Techniques in Biosciences* 157–178 (INC, 2022). doi:10.1016/b978-0-12-822654-4.00004-x
172. Vivit, D. V., Ball, J. W. & Jenne, E. A. Specific-Ion electrode determinations of sulfide preconcentrated from San Francisco Bay waters. *Environ. Geol. Water Sci.* **6**, 79–90 (1984).
173. Dimeski, G., Badrick, T. & John, A. S. Ion Selective Electrodes (ISEs) and interferences-A review. *Clin. Chim. Acta* **411**, 309–317 (2010).
174. Sastri, V. R. Engineering Thermoplastics: Acrylics, Polycarbonates, Polyurethanes, Polyacetals, Polyesters, and Polyamides. in *Plastics in Medical Devices* 121–172 (2014). doi:dx.doi.org/10.1016/B978-1-4557-3201-2.00007-0
175. Prida, V. M. *et al.* Electrochemical methods for template-assisted synthesis of nanostructured materials. in *Magnetic Nano- and Microwires: Design, Synthesis, Properties and Applications* 3–39 (2015). doi:10.1016/B978-0-08-100164-6.00001-1
176. colorFabb. colorFabb _ XT. **1**, 1 (2020).
177. AOAC International. *AOAC International Guidelines for Laboratories Performing Microbiological and Chemical Analyses of Food and Pharmaceuticals: An Aid to Interpretation of ISO/IEC 17025:2005*. (2010).
178. Fiorucci, A. R., Saran, L. M., Cavalheiro, E. T. G. & Neves, E. A. Thermal stability and bonding in the silver complexes of ethylenediaminetetraacetic acid. *Thermochim. Acta* **356**, 71–78 (2000).
179. Nduka, E. C. & Ogoke, U. P. *Statistical methods and tools in biosciences*. *Analytical Techniques in Biosciences* (INC, 2022). doi:10.1016/b978-0-12-822654-4.00005-1
180. Bisong, E. *Linear Regression*. *Building Machine Learning and Deep Learning Models on Google Cloud Platform* (2019). doi:10.1007/978-1-4842-4470-8_19
181. Mesquita, R. B. R. & Rangel, A. O. S. S. A review on sequential injection methods

for water analysis. *Anal. Chim. Acta* **648**, 7–22 (2009).

182. Ferrer, L., Miro, M., Estela, M. & Cerda, V. Analytical methodologies for reliable sulfide determinations in aqueous matrices exploiting flow-based approaches. **26**, 413–422 (2007).
183. Wang, T., Huang, Y., Xu, J., Guo, W. & Yuan, D. Development and application of a shipboard method for spectrophotometric determination of nanomolar dissolved sulfide in estuarine surface waters using reverse flow injection analysis coupled with a long path length liquid waveguide capillary cell. *Microchem. J.* **168**, (2021).
184. Silva, M. S. P., Galhardo, C. X. & Masini, J. C. Application of sequential injection-monosegmented flow analysis (SI-MSFA) to spectrophotometric determination of sulfide in simulated waters samples. *Talanta* **60**, 45–52 (2003).
185. Beck, M. B., Ravetz, J. R., Mulkey, L. A. & Barnwell, T. O. On the problem of model validation for predictive exposure assessments. *Stoch. Hydrol. Hydraul.* **11**, 229–254 (1997).
186. Solís, B., Guisasola, A., Pijuan, M., Corominas, L. & Baeza, J. A. Systematic calibration of N2O emissions from a full-scale WWTP including a tracer test and a global sensitivity approach. *Chem. Eng. J.* **435**, 134733 (2022).
187. Henze, M., Gujer, W., Mino, T. & Loosdrecht, M. van. *Activated sludge models ASM1, ASM2, ASM2d and ASM3. Scientfic and Technical report* (IWA, 2002). doi:doi.org/10.2166/9781780402369
188. Wichern, M., Gehring, T. & Lübken, M. Modeling of Biological Systems. in *Treatise on Water Science* (2011). doi:10.1016/B978-0-444-53199-5.00086-5
189. Gao, F., Nan, J., Li, S. & Wang, Y. Modeling and simulation of a biological process for treating different COD:N ratio wastewater using an extended ASM1 model. *Chem. Eng. J.* **332**, 671–681 (2018).
190. Noguera, D. R., Brusseau, G. A., Rittmann, B. E. & Stahl, D. A. A unified model describing the role of hydrogen in the growth of Desulfovibrio vulgaris under different environmental conditions. *Biotechnol. Bioeng.* **59**, 732–746 (1998).
191. D'Acunto, B., Esposito, G., Frunzo, L. & Pirozzi, F. Dynamic modeling of sulfate reducing biofilms. *Comput. Math. with Appl.* **62**, 2601–2608 (2011).
192. Janssen, P. H. M. & Heuberger, P. S. C. Calibration of process-oriented models. *Ecol.*

Modell. **83**, 55–66 (1995).

193. Dorado, A. D. *et al.* Evaluation of mass transfer coefficients in biotrickling filters: Experimental determination and comparison to correlations. *Chem. Eng. Technol.* **32**, 1941–1950 (2009).
194. Sáez-Navarrete, C., Rodríguez-Córdova, L., Baraza, X., Gelmi, C. & Herrera, L. Hydrogen kinetics limitation of an autotrophic sulphate reduction reactor. *DYNA* (2012).
195. Durán, F. *et al.* Modeling the anaerobic treatment of sulfate-rich urban wastewater: Application to AnMBR technology. *Water Res.* **184**, (2020).
196. Saltelli, A. *et al. Global sensitivity analysis: The primer*. *Global Sensitivity Analysis: The Primer* (2008). doi:10.1002/9780470725184
197. Ochoa, M. P. & Hoch, P. M. *Global sensitivity analysis in bioreactor networks*. *Computer Aided Chemical Engineering* **29**, (Elsevier B.V., 2011).
198. Ochoa, M. P., Estrada, V., Di Maggio, J. & Hoch, P. M. Dynamic global sensitivity analysis in bioreactor networks for bioethanol production. *Bioresour. Technol.* **200**, 666–679 (2016).
199. MathWorks. pchip. *MathWorks* Available at: https://www.mathworks.com/help/matlab/ref/pchip.html.
200. MathWorks. fmincon. *MathWorks* Available at: https://www.mathworks.com/help/optim/ug/fmincon.html?searchHighlight=fmincon&s_tid=srchtitle_fmincon_1.
201. Shampine, L. F. & Reichelt, M. W. Ode Matlab Solvers. *J. Sci. Comput.* **18**, 1–22 (1997).
202. MathWorks. ode15s. *MathWorks* Available at: https://www.mathworks.com/help/matlab/ref/ode15s.html?searchHighlight=ode15s&s_tid=srchtitle_ode15s_1.
203. Guisasola, A. *et al.* The Influence of Experimental Data Quality and Quantity on Parameter Estimation Accuracy. *Educ. Chem. Eng.* **1**, 139–145 (2006).
204. Tang, Y. *et al.* Bioreduction of nitrate in groundwater using a pilot-scale hydrogen-based membrane biofilm reactor. *Front. Environ. Sci. Eng. China* **4**, 280–285 (2010).

APPENDIX

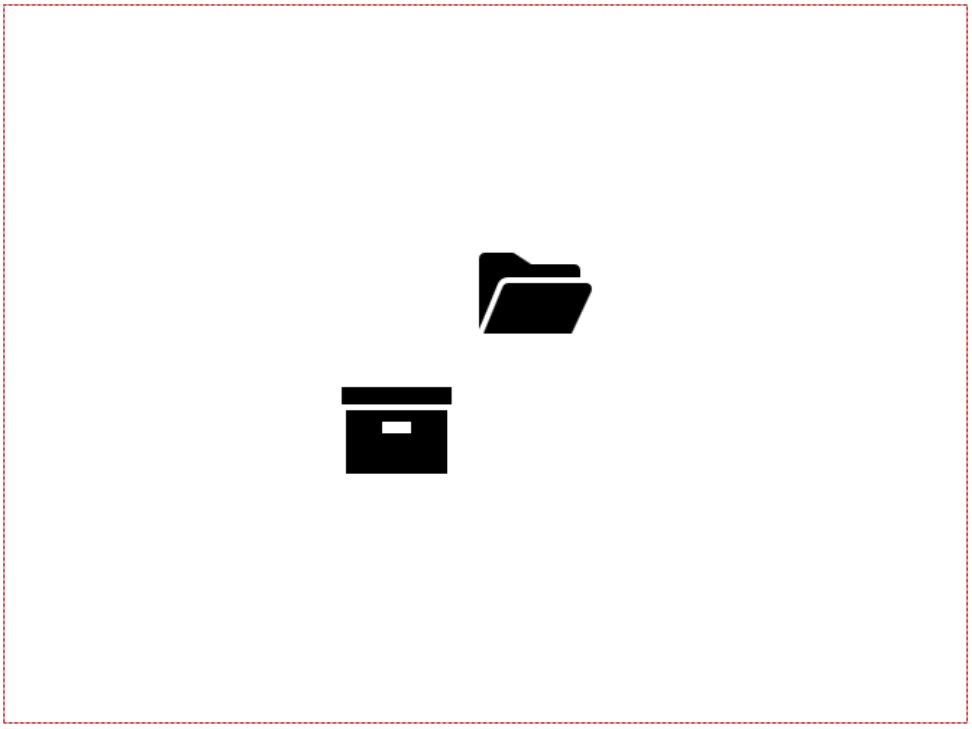

APPENDIX A. TECHNICAL SHEET OF THE GLR DIMENSIONS

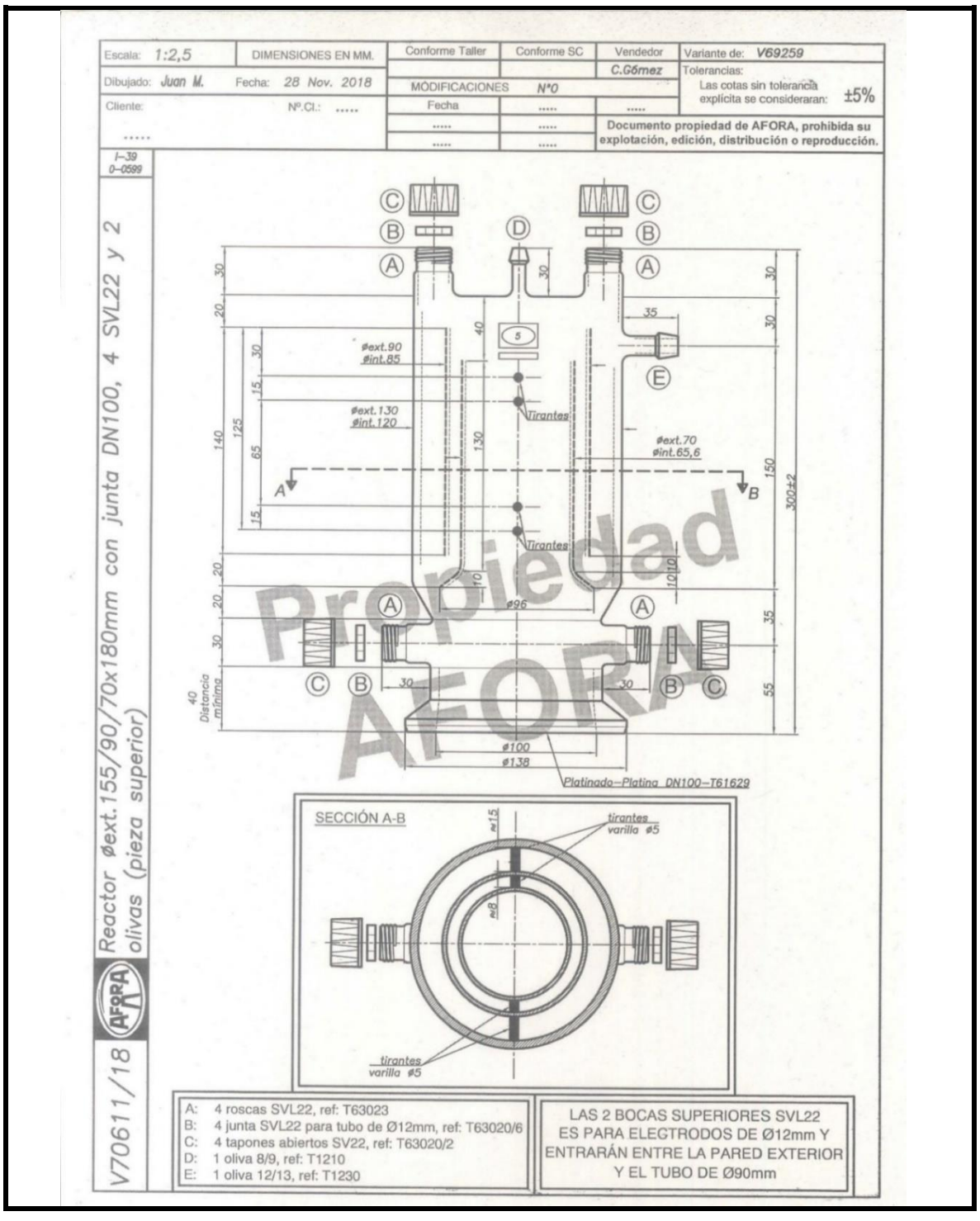

Figure A1. GLR dimensions of the upper part (the three-phase separator).

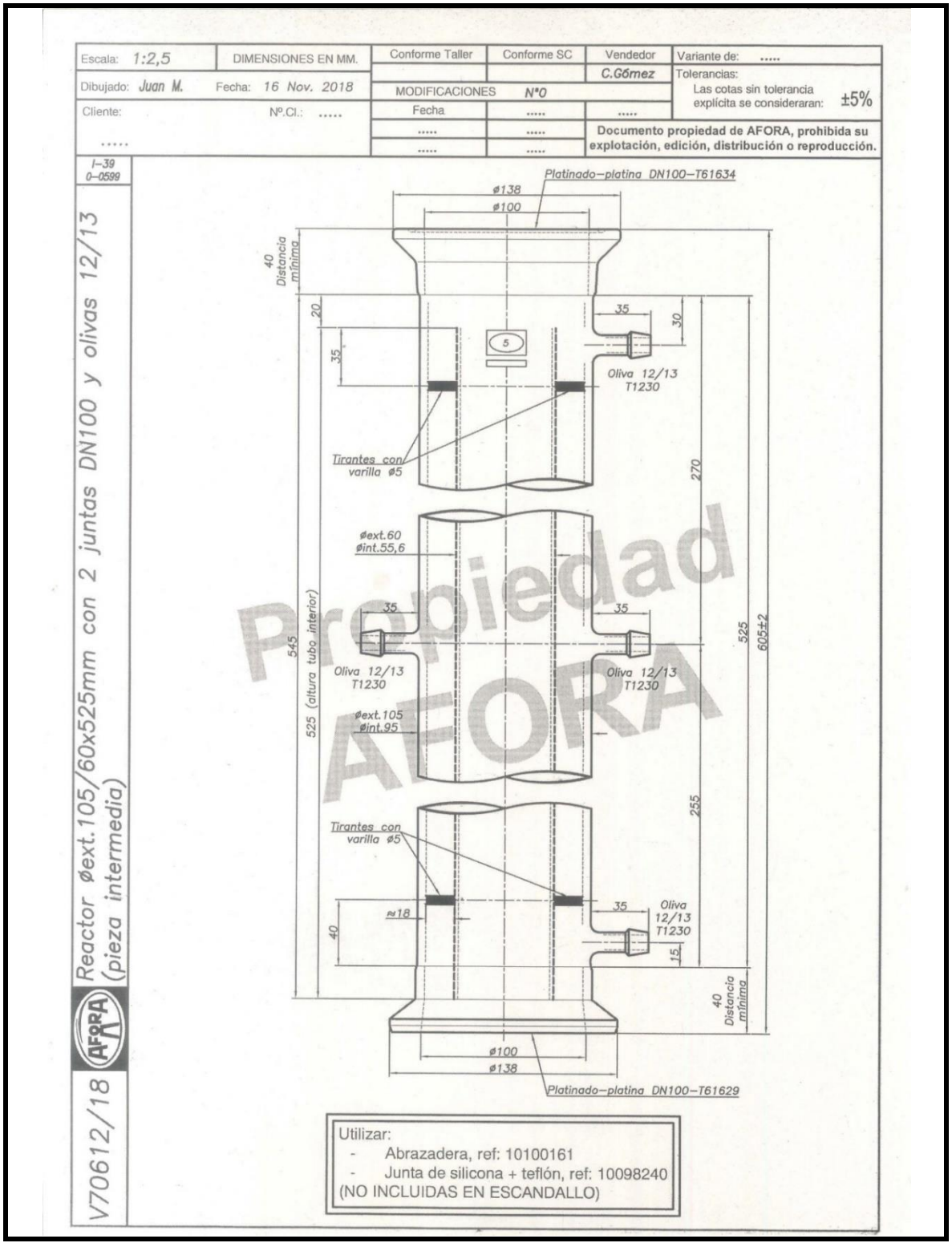

Figure A2. GLR dimensions of the middle part (the mixing zone).

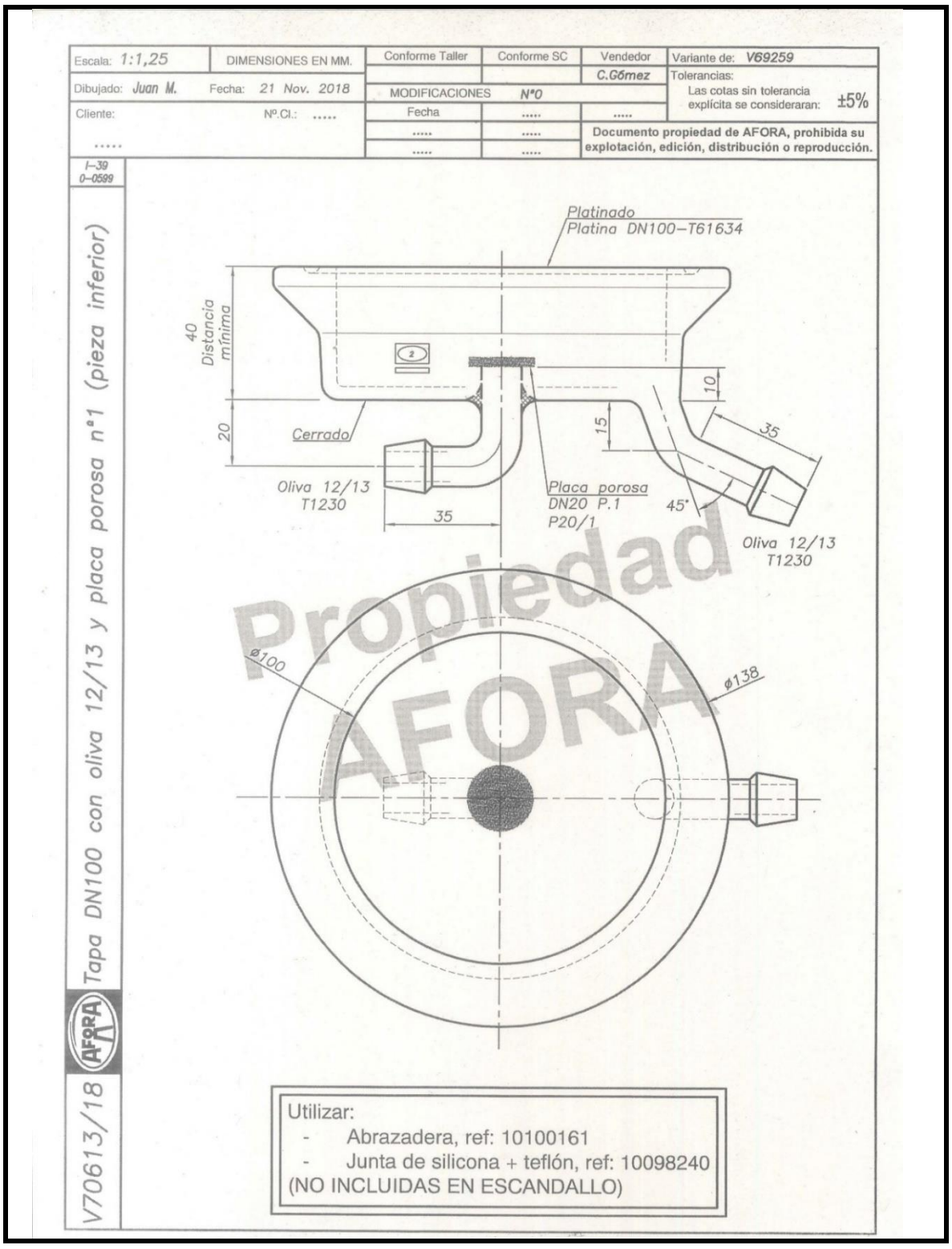

Figure A3. GLR dimensions of the bottom part (the gas diffusion).

APPENDIX B. CALIBRATION OF THE COMMERCIAL S^{2-}-ISE AND SULFIDE DISTRIBUTION

Calibration of the commercial S^{2-}-ISE

This commercial electrode was calibrated by the standard addition method, in which, a known sulfide concentrated solution (determined by a standardization with a Lead solution titration) is added, as shown in Table A1, in a 0.1-liter beaker with 25 ml of distilled water and 25 ml of SAOB where sensor is placed to record E_c (with the Symphony potentiometer) per each of the volume added in the beaker (first column of Table A1).

Table A1. Standard addition method for the commercial S^{2-}-ISE calibration. The addition (first column) of a known sulfide solution (prepared to be 32000 TDS L^{-1}) was added in a 50 ml solution (25 ml distilled water + 25 ml SAOB) and the resulting concentration (column 2) together with the logarithm of this concentration (column 3) are computed. The read E_c is written in column 4 for a further linear regression between the logarithm [TDS] and the E_c.

Volume added of sulfide solution [µL]	[TDS] [mg TDS L^{-1}]	log [TDS]	E_c [mV]
10	6.4	0.81	
10	12.8	1.11	
20	25.6	1.41	
50	57.5	1.76	
100	121.1	2.08	
150	216.1	2.33	
150	310.6	2.49	
200	435.6	2.64	
200	559.6	2.75	
250	713.3	2.85	
250	865.5	2.94	
500	1165.5	3.07	
500	1459.8	3.16	

Sulfide distribution

The sulfide measurement is based on the total dissolved sulfide (TDS), it is important to know the distribution based on the sample pH, as the free H_2S is the sulfide form that can be inhibitory for microbial growth, and it is the form that can be in transfer between gas and liquid phases.

In that way, the sulfide dissociation is according to Equations A1 and A2:

$$H_2S \overset{k1}{\leftrightarrow} HS^- + H^+ \qquad \text{Equation A1}$$

$$HS^- \overset{k2}{\leftrightarrow} S^{2-} + H^+ \qquad \text{Equation A2}$$

While the TDS is equivalent to Equation A3:

$$[TDS] = [H_2S] + [HS^-] + [S^{2-}] \qquad \text{Equation A3}$$

Thus, the corresponding equilibrium constants are defined by Equations A4 and A5:

$$k_1 = \frac{[HS^-][H^+]}{[H_2S]} \qquad \text{Equation A4}$$

$$k_2 = \frac{[S^{2-}][H^+]}{[HS^-]} \qquad \text{Equation A5}$$

Then, based on the logarithm relations of pH, constants k1 and k2 defined by Equations A6, A7 and A8, proper substitution and equation rearrangement will result in Equations A9, A10 and A11:

$$pKa_1 = -\log K_1 \qquad \text{Equation A6}$$

$$pKa_2 = -\log K_2 \qquad \text{Equation A7}$$

$$pH = -\log[H^+] \qquad \text{Equation A8}$$

$$[S^{2-}]=[TDS]\cdot\left[\frac{1}{10^{2pH - pKa_1 - pKa_2}}+10^{pKa_2 - pH}+1\right]^{-1}$$ Equation A9

$$[HS^{-}]=[S^{2-}]\cdot 10^{pKa_2 - pH}$$ Equation A10

$$[H_2S]=[S^{2-}]\cdot\frac{1}{10^{2pH - pKa_1 - pKa_2}}$$ Equation A11

Based on the pH, the TDS concentration, and knowing that the pKa_1 is 7.04 and pKa_2 is 11.96, each of the sulfide forms can be estimated.

APPENDIX C. KINETIC, STOICHIOMETRIC, AND PHYSICOCHEMICAL PARAMETERS

The kinetic and stoichiometric parameters for hydrogenotrophic sulfate reducing microorganisms (H2SRB) and homo-acetogenic microorganisms (homo-AC) are detailed in Table A2, as well as the H_2-mass transfer coefficient and the estimation of the H_2S-mass transfer coefficient and the other physicochemical properties used in along the research.

Whenever the biomass concentration was reported in COD, it was converted to VSS using the factor 1.45 as reported in the literature;[93,136] while for hydrogen and TDS were converted as explained in Chapter 5.

The following correlation was used to determine the K_La_{H2S} from the K_La_{H2}:[194,195]

$$K_La_{H2S} = K_La_{H2} \cdot \sqrt{\frac{D_{H2S}}{D_{H2}}} \qquad \text{Equation A12}$$

Table A2. Kinetic, stoichiometric, and physicochemical parameters.

	Symbol	Units	Value	Reference
Maximum specific growth rate for H2-SRB	$\mu_{max.SRB}$	[d^{-1}]	0.3	[44]
H_2 half-saturation constant for H2-SRB	$k_{H2.SRB}$	[mg H_2 L^{-1}]	$6.25 \cdot 10^{-3}$	[44]
Sulfate half-saturation constant for H2-SRB	k_{ST}	[mg S-SO_4^{2-} L^{-1}]	0.15	[44]
H_2S-inhibition constant for H2-SRB	k_i	[mg S-H_2S L^{-1}]	550	[96]
Decay rate for H2-SRB	b_{SRB}	[d^{-1}]	0.01	[44]
Yield coefficient of H2-SRB and H_2	$Y_{SRB\|H2}$	[mg VSS mg^{-1} H_2]	0.2	[78]
Yield coefficient of sulfate and hydrogen	$Y_{ST\|H2}$	[mg S-SO_4^{2-} mg^{-1} H_2]	4	Eq. 2.3
Maximum specific growth rate for homo-AC	$\mu_{max.hAC}$	[d^{-1}]	0.27	[132]
H_2 half-saturation constant for homo-AC	$k_{H2.hAC}$	[mg H_2 L^{-1}]	0.9	[132]
Decay rate for homo-AC	b_{hAC}	[d^{-1}]	0.01	[46]
Yield coefficient of homo-AC and H_2	$Y_{hAC\|H2}$	[mg VSS mg^{-1} H_2]	0.083	[46]
Yield coefficient of acetate and H_2	$Y_{AC\|H2}$	[mg AC mg^{-1} H_2]	7.5	Eq. 2.9

pka for the H_2S dissociation ($H_2S \leftrightarrow HS^-$)	$pka_{1.H2S}$	-	7.04	[131]
pka for the HS^- dissociation ($HS^- \leftrightarrow S^{2-}$)	$pka_{2.H2S}$	-	11.96	[131]
H_2-diffusivity coefficient in water	D_{H2}	[$cm^2\ s^{-1}$]	$5.85 \cdot 10^{-5}$	[47]
H_2S-diffusivity coefficient in water	D_{H2S}	[$cm^2\ s^{-1}$]	$1.61 \cdot 10^{-5}$	[47]
H_2-Henry coefficient	H_{H2}	[atm L sol mg^{-1} H_2]	$6.15 \cdot 10^{-1}$	[47]
H_2S-Henry coefficient	H_{H2S}	[atm L sol mg^{-1} S-H_2S]	$2.72 \cdot 10^{-4}$	[47]

Determination of SLR, SRR and s-SRR for a continuous operation. This was used for the simulations presented in Chapter 7 (section 7.6).

$$SLR = \frac{\left[S\text{-}SO_4^{2-}\right]_{in} \cdot F_l}{V} \qquad \text{Equation A13}$$

$$SRR = \frac{\left[S\text{-}SO_4^{2-}\right]_{in} - \left[S\text{-}SO_4^{2-}\right]_{out}}{V} \cdot F_l \qquad \text{Equation A14}$$

$$s\text{-}SRR = \frac{SRR}{[VSS]_{out}} \qquad \text{Equation A15}$$

$[S\text{-}SO_4^{2-}]_{in}$ is the sulfate concentration in the influent, $[S\text{-}SO_4^{2-}]_{out}$ is the sulfate concentration in the effluent, $[VSS]_{out}$ is the model H2-SRB concentration in the effluent.

APPENDIX D. 3-D PRINTING SETTING FOR THE MICRODEVICE MANUFACTURE

The 3-D printer setting for the building of the microdevice is detailed in Table A3. The material used was Co-polyester filament (CPE).

Table A3. 3-D printer setting for the microdevice building.

Printer	-	Sigma R16 (BCN3D Technologies, Inc)
Hotend	-	e3D-0.4mm-Brass
Layer height	[mm]	0.05
Shell		
Wall thickness	[mm]	1
Top/Bottom Thickness	[mm]	0.2
Top/Bottom Thickness		Zig Zag
Infill		
Infill density	[%]	100
Infill pattern		Grid
Print infill every	Per layer	1
Material		
Printing temperature	[ºC]	255
Printing temperature, initial layer	[ºC]	235
Plate temperature	[ºC]	70
Filament diameter	[mm]	2.85
Flow	[%]	100
Speed		
Print speed	[mm s^{-1}]	50
Wall speed	[mm s^{-1}]	15
Initial layer speed	[mm s^{-1}]	15
Building plate adhesion		
Type		Skirt
Skirt distance	[mm]	3
Skirt minimum length	[mm]	500
Other information		
Total layers	-	58
Printing duration	[hh:mm]	03:30
Microdevice Weight	[g]	~8

APPENDIX E. CALIBRATION OF THE S-OMS FOR THE DIFFERENT ANALYTICAL AND MONITORING EXPERIMENTS

Table A4. Calibration applied through the standard addition method for two Ag/Ag_2S-wires (electrodes) to determine the linear range and the low limit detection.

Vol added [mL]	Concentration [mg TDS L^{-1}]	Log [TDS]	Wire 1 [mV]	Wire 2 [mV]
0.025	0.02	-1.62	-530	-490
0.025	0.05	-1.32	-595	-560
0.025	0.07	-1.14	-624	-620
0.025	0.10	-1.02	-645	-658
0.05	0.14	-0.84	-669	-700
0.1	0.24	-0.62	-686	-720
0.025	0.47	-0.32	-703	-750
0.025	0.71	-0.15	-711	-757
0.025	0.95	-0.02	-718	-758
0.05	1.42	0.15	-723	-761
0.1	2.36	0.37	-732	-766
0.025	4.71	0.67	-738	-774
0.025	7.05	0.85	-744	-779
0.025	9.39	0.97	-750	-782
0.05	14.1	1.15	-754	-788
0.1	23.3	1.37	-761	-794
0.025	46.6	1.67	-769	-803
0.025	69.9	1.84	-775	-809
0.025	93.1	1.97	-779	-813
0.05	139.4	2.14	-784	-818
0.1	231.4	2.36	-788	-825
0.1	322.8	2.51	-791	-830
0.1	413.4	2.62	-795	-834
0.1	503.3	2.70	-798	-837

Table S5. Sequential sulfide flowing to calibrate the Ag/Ag_2S-working electrodes after setting it up in the S-OMS.

TDS concentration [mg L^{-1}]	Log [TDS]
0.1	-0.92
0.6	-0.22
1.5	0.18
3	0.48
30.4	1.48
304	2.48
3040	3.48
30400	4.48

Calibrations for the repeatability and reproducibility tests:

The calibration performed for the first set of repeatability test is shown in Figure S2, this calibration was performed with a sulfide stock solution of 17600 mg TDS L^{-1}, and 4 consecutive dilutions of the order of 10 prepared from the preceding dilution.

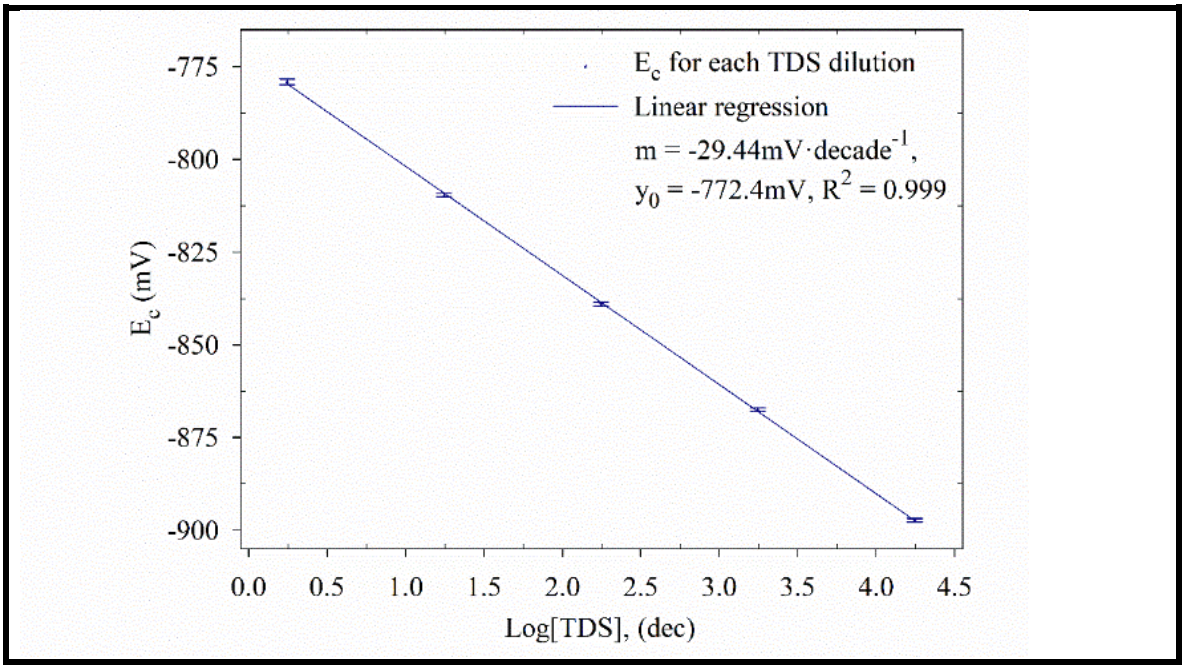

Figure A4. Results of the S-OMS calibration for the first set of repeatability test, where the logarithm of the TDS dilution is plotted against the recorded E_c.

The calibrations performed for the second set of repeatability test are shown in Figure A5. This calibration was performed with a sulfide stock solution of 6880 mg TDS L^{-1}, and 3 consecutive dilutions of the order of 10 prepared from the preceding dilution.

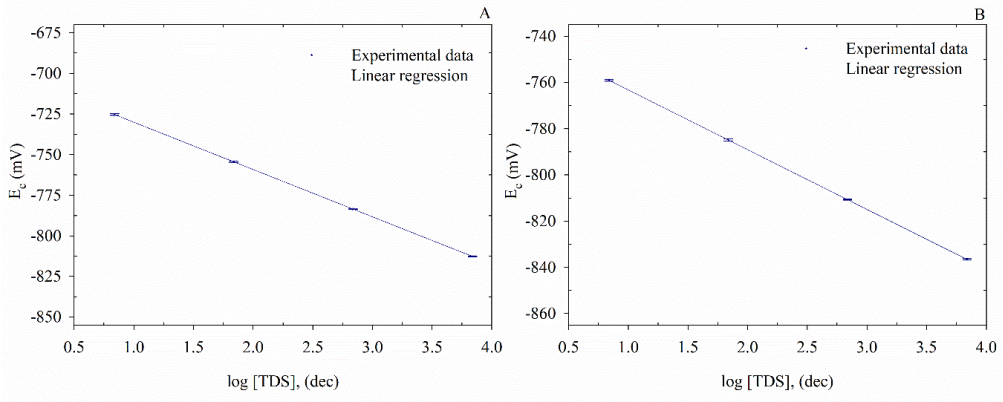

	Linear regression for each calibration	
	CAL1	CAL2
Slope	-29.10	-25.82
y-intercept	-701.0	-737.4
R^2	0.999	0.999

Figure A5. Calibration of the S-OMS for the second set of repeatability experiments. Each calibration was performed for two different microdevice systems. Calibrations 1 and 2 were performed for the S-OMS experiments of solutions of 2.5 and 86 mg TDS L^{-1}. The corresponding parameters for the linear regression are detailed in the Table.

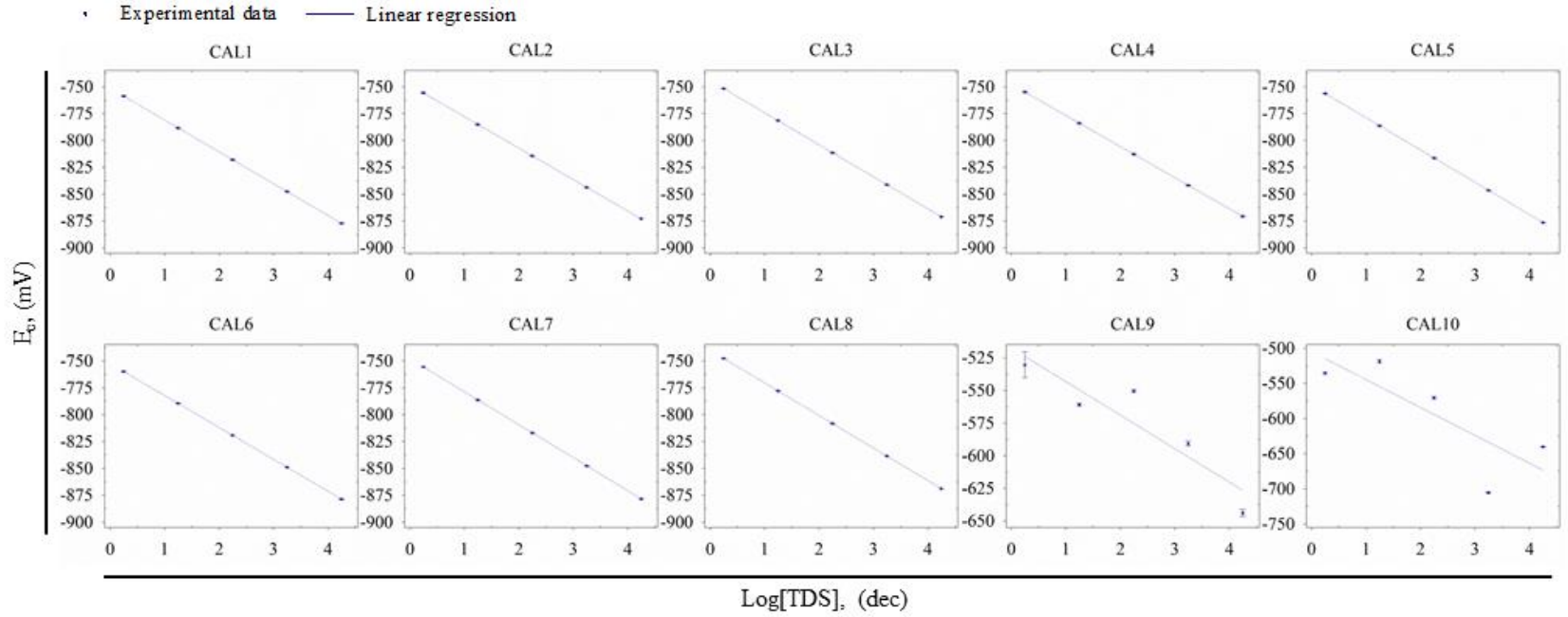

	Linear regression for each calibration									
	CAL1	CAL2	CAL3	CAL4	CAL5	CAL6	CAL7	CAL8	CAL9	CAL10
Slope	-29.58	-29.26	-29.82	-28.92	-30.00	-29.69	-30.69	-30.31	-25.65	-39.68
y-intercept	-751.5	-748.6	-744.4	-747.9	-749.0	-752.5	-748.0	-740.1	-517.6	-504.9
R^2	0.999	0.998	0.997	0.999	0.999	0.989	0.999	0.999	0.847	0.649

Figure A6. Calibration of the S-OMS for the reproducibility experiments. The 10 calibrations are shown in the Figures and the corresponding parameters for the linear regression are detailed in the Table.

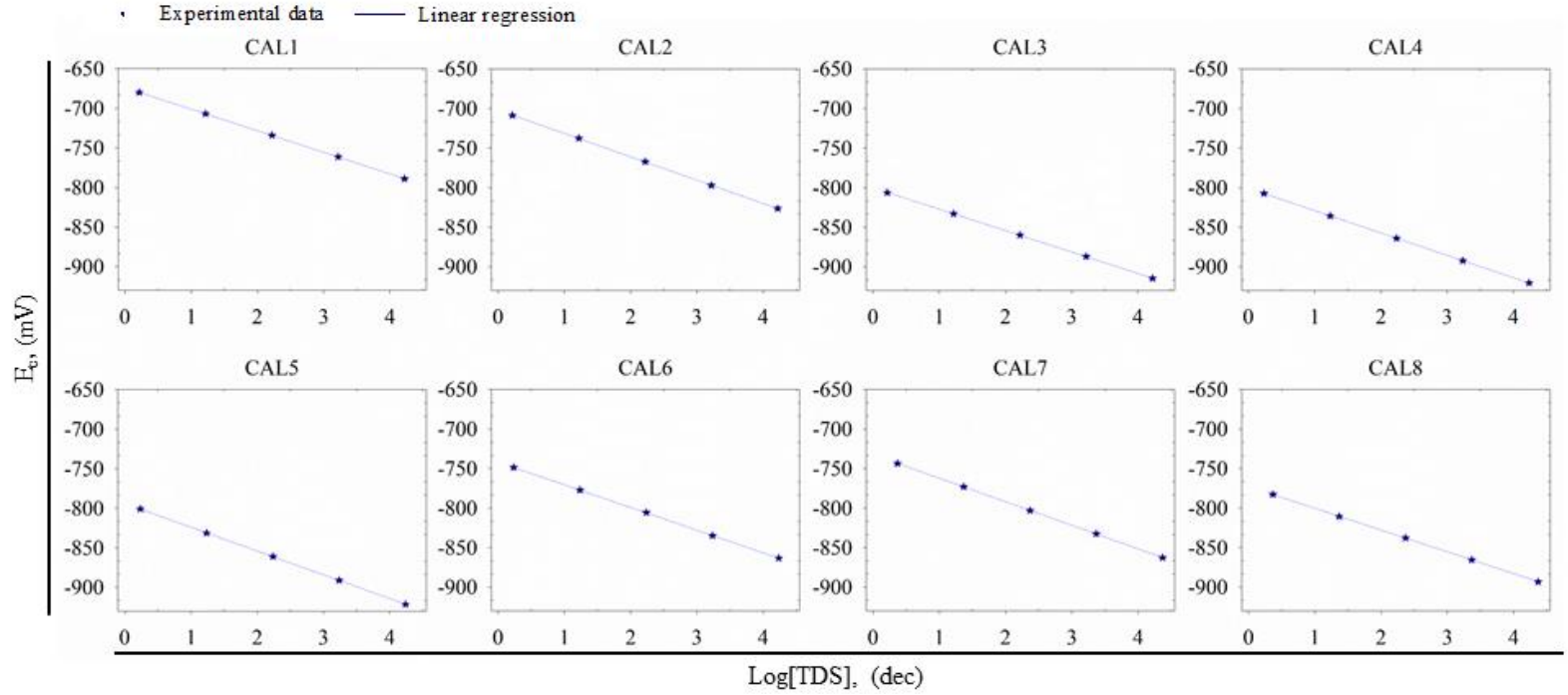

	Linear regression for each calibration							
	CAL1	CAL2	CAL3	CAL4	CAL5	CAL6	CAL7	CAL8
Slope	-27.27	-29.53	-27.09	-28.28	-30.14	-28.64	-29.76	-27.55
y-intercept	-673.7	-701.9	-800.1	-800.7	-793.7	-741.8	-732.3	-772.5
R^2	0.999	0.997	0.995	0.999	0.999	0.998	0.999	0.999

Figure A7. Calibration of the S-OMS for the validation experiments with the GLR operation. Each calibration corresponds to the S-OMS used for each batch of the GLR operation; the 8 calibrations are shown in the Figures and the corresponding parameters for the linear regression are detailed in the Table.